Microwave spectroscopy of glycine and other related molecules. Rotationnal analysis and radioastronomical observations of the interstellar medium.

Marie-Paule Bassez

ORSAY
n° d'ordre : 2498

UNIVERSITE DE PARIS-SUD

CENTRE D'ORSAY

THESE

présentée

Pour obtenir

Le GRADE de DOCTEUR D'ETAT

SPECIALITE : SCIENCES PHYSIQUES (chimie)

PAR

Melle BASSEZ Marie Paule

SUJET : ETUDE SPECTROCHIMIQUE DE LA GLYCINE ET DE QUELQUES MOLECULES CONNEXES. ANALYSE ROTATIONNELLE ET OBSERVATIONS DU MILIEU INTERSTELLAIRE

soutenue le 12 OCTOBRE 1981 devant la Commission d'examen

MM. LEQUEUX James Président

WERTHEIMER Raymond

OMONT Alain

GUELIN Michel

MME MARX Rose

M. FAURE Jean

The Parkes Radiotelescope with its 64m antenna; photo: Marie Paule Bassez, July 1978

AVANT-PROPOS

Cette thèse concerne essentiellement la caractérisation du spectre rotationnel de l'acide aminé glycine et la recherche de ce composé dans des nuages moléculaires de la Galaxie. De plus, de nouvelles transitions de quelques molécules connexes furent détectées et sont analysées. Un plan détaillé est présenté dans l'introduction (p. 1).

Le travail fut effectué entre le 01/03/1976 et le 30/06/1980, dans le laboratoire de spectroscopie microonde du Professeur R.D. Brown, du Département de Chimie de l'Université Monash à Melbourne en Australie. Les observations radioastronomiques furent conduites à Parkes, CSIRO, Australie et Kitt-Peak, NRAO, Etats-Unis, durant des sessions totalisant respectivement soixante deux jours et cinq jours auxquelles je participai. Le radiotélescope d'Onsala, Suède, fut également utilisé.

Les programmes employés sont décrits dans le premier chapitre (p. 6). Certains furent légèrement modifiés afin d'être applicables aux problèmes traités. Tels sont KPRED, STATRED et PDP9-V72/AOS. D'autres furent écrits. Tels sont COCHRAN et deux plus importants qui sont présentés en appendices : WASCAN et SFIT (p. 183).

WASCAN fut écrit avec l'aide considérable de P.D. Godfrey, sauf la partie calculant la structure hyperfine quadrupolaire des composantes Stark (instructions 331 à 656) qui fut écrite par moi-même.

SFIT permet la détermination des moments dipolaires. Il fut adapté du programme Q2FIT, écrit par A. Ottrey, pour obtenir des constantes de couplage quadrupolaire, par superposition sur un écran du spectre expérimental et d'un spectre calculé. Il comprend quatre fragments (OVERLAYS) et une séquence principale qui les lie. Les fragments concernant la recherche des données sur disque ou sur bande magnétique (GETDAT OVERLAY, 71 instructions) et le traçage des courbes sur papier (OVERLAY PLOTTR, 241 instructions) ne furent que très légèrement modifiés. Le fragment permettant la superposition des spectres sur un écran, après variation des composantes du moment dipolaire le long des axes de la molécule et du champ Stark appliqué (OVERLAY RNOBS, 178 instructions), fut largement restructuré sauf la partie concernant le dessin de la courbe lorentzienne (SUBROUTINE LORENT, I-183 à I-284) qui ne le fut que légèrement. Par contre, le fragment qui permet le calcul du spectre

théorique (OVERLAY CSPECT, 536 instructions) fut entièrement changé. Toutefois, il utilise de nombreuses instructions déjà écrites pour WASCAN.

Le deuxième chapitre (p. 14) décrit la caractérisation du spectre microonde de la molécule glycine (p. 14-17), en présentant une étude théorique des différentes conformations et certaines difficultés expérimentales. Il donne les constantes mesurées pour la rotation et la distorsion centrifuge de l'état vibrationnel fondamental (p. 48-55), les vingt-sept fréquences de transitions rotationnelles mesurées dans l'état fondamental de vibration (p. 49-50) et les onze fréquences de transitions mesurées dans des états excités (p. 56). La fréquence de torsion de la liaison C-C (p. 55-60) et les composantes du moment dipolaire (p. 61-75) furent mesurées et sont présentées. Sur la base du moment dipolaire, le spectre observé est attribué (p. 75) à la géométrie (4) de la glycine (p. 18), possédant une liaison hydrogène intramoléculaire entre l'azote et l'hydrogène de l'hydroxyle. L'observation de raies appartenant à une autre conformation est mentionnée (p. 75-77). La structure hyperfine quadrupolaire, due au moment angulaire de spin nucléaire de l'azote, est également analysée (p. 77-80). Les dernières sections de ce chapitre (p. 80-86) décrivent les fabrications d'un système de pompage rapide et de cornets millimétriques qui permirent respectivement une amélioration de la résolution et une extension de la sensibilité de la cellule utilisée.

Cette étude fut en partie publiée avec les coauteurs, R.D. Brown, P.D. Godfrey et J.W.V. Storey (J.C.S. Chem. Comm. 547 (1978). R.D. Brown et P.D. Godfrey sont à l'origine du projet et le suivirent avec intérêt. J.W.V. Storey dessina la cellule. Les travaux sur la glycine commencèrent avec cette cellule peu après mon arrivée. En collaboration avec J.W.V. Storey et tandis qu'il rédigeait sa thèse, j'entrepris les premiers balayages du spectre. Les résultats obtenus sont décrits dans la thèse de J.W.V. Storey. Tous les autres travaux furent menés par moi-même seulement. Des discussions fort profitables furent entretenues, à plusieurs reprises avec P.D. Godfrey et S. Vaccani.

Le troisième chapitre (p. 87) décrit la recherche de la molécule glycine dans des nuages moléculaires interstellaires et l'analyse des résultats obtenus. Des équations tenant compte du transfert de rayonnement et de l'équilibre statistique des transitions collisionnelles et radiatives sont formulées dans le cas d'une molécule asymétrique.

Les observations radioastronomiques sont publiés avec huit coauteurs (Mon. Not. R. astr. Soc., 186, 5P (1979)). R.D. Brown est à l'origine du projet. P.D. Godfrey dirigea les réglages du récepteur, à Parkes, durant les changements nocturnes de fréquence. J.W.V. Storey participa aux observations de Kitt-Peak (cinq jours), pas à celle de Parkes (vingt-trois jours). Il fait toutefois partie de "l'histoire" de la glycine. B.J. Robinson, directeur du CSIRO, apporta son aide et ses conseils durant plusieurs jours d'observation. R.A. Batchelor et M.G. Mc Culloch sont les ingénieurs du CSIRO qui construisirent le mixeur utilisé. O.E.H. Rydbeck et Å.G. Hjalmarson conduisirent les observations à Onsala. Enfin, moi-même je participai à toutes les études traitées dans ce chapitre. Les transitions à observer furent sélectionnées sous la direction de R.D. Brown. Les réglages du récepteur, à Parkes, furent effectués avec P.D. Godfrey. La comparaison des sensibilités des récepteurs, utilisés dans les différents radiotélescopes, fut établie par moi-même, sur la demande de P.D. Godfrey (p. 97-102). Les tests statistiques permettant de déterminer la probabilité de présence d'une raie de forme gaussienne, ainsi que l'intensité du bruit, furent appliqués par moi-même (à l'aide des programmes KPRED et STATRED p. 11-13) sur les spectres obtenus à Parkes et Kitt-Peak (p. 103, colonne 8) et également par R.D. Brown et P.D. Godfrey en ce qui concerne la transition ($J_{K_aK_c} = 10_{3,7} \rightarrow 9_{3,6}$) observée dans la direction de Sagittaire B2 (p. 104). La densité maximale de glycine, dans la direction des nuages moléculaires observés, fut calculée séparément par R.D. Brown et moi-même (p. 103, colonne 11). La section 3.6, concernant l'extension des équations de l'équilibre statistique et du transfert de rayonnement aux molécules asymétriques, fut élaborée par moi-même sur la demande de R.D. Brown et en suivant les conseils de P.D. Godfrey. Il est à noter que cette recherche de la glycine dans le milieu interstellaire fit l'objet de constants échanges d'idées et de calculs entre R.D. Brown, P.D. Godfrey et moi-même.

La publication, relatant ces observations radioastronomiques de la glycine, apparut en Mars 1979. Le 1er Novembre 1980, J.M. Hollis, L.E. Snyder, R.D. Suenram et F.J. Lovas[a] publièrent la recherche d'une deuxième conformation de la glycine que R.D. Suenram et F.J. Lovas[b] avaient indentifiée au laboratoire.

(a) : Ap. J. 241, 1001 (1980)

(b) : J. Am. Chem. Soc. 102, 7180 (1980).

Cette deuxième géométrie est caractérisée par un spectre de type-a, les transitions $^{a}R_{01}$ étant les plus intenses. Trois transitions furent recherchées dans Orion A, Sgr. B2, W51 et IRC + 10216 : (1) $J_{K_aK_c} = 14_{1,14} \rightarrow 13_{1,13}$ à 84217,94 MHz, (2) $J_{K_aK_c} = 14_{0,14} \rightarrow 13_{0,13}$ à 84230,25 MHz et (3) $J_{K_aK_c} = 13_{5,8} \rightarrow 12_{5,7}$ à 90233,73 MHz. La deuxième ne fut pas détectée. La troisième, si présente en émission, fut masquée par la raie du formate de méthyle. A l'emplacement de la première fréquence apparut un pic d'intensité 0,06 K et de largeur à mi-hauteur 30 km s^{-1}. Les auteurs ne réfutent pas la glycine comme composé à l'origine de cette émission, mais ne l'affirment pas non plus. Ils proposent que la conformation recherchée est la conformation de la glycine qui possède la plus faible énergie, et qui se trouve située 490 $\pm$ 150 cm^{-1} au-dessous de la conformation précédemment recherchée par les mêmes auteurs[c] et par nous mêmes. Cette différence d'énergie fut établie à partir de mesures d'intensité des raies ($J_{K_aK_c} = 13_{5,8} \leftarrow 12_{5,7}$) données par les deux conformations et en utilisant 1 debye comme valeur de la composante du moment dipolaire le long de l'axe-a ou axe principal d'une toupie prolate. Du fait de la faible intensité des composantes Stark, ce moment dipolaire ne put être déterminé par la méthode classique, qui consiste à mesurer les déplacements de ces composantes par rapport à la raie d'absorption. Il fut obtenu par la technique moins précise, dite "de croissance", en mesurant la variation d'intensité de la raie ($J_{K_aK_c} = 13_{5,8} \leftarrow 12_{5,7}$) en fonction du champ électrique appliqué. L'erreur ainsi introduite dans la mesure du moment dipolaire explique l'incertitude de 30 % sur l'énergie de séparation des deux conformations.

Cette conformation, nouvellement étudiée, fut attribuée à la géométrie que nous avons numérotée (3) (p. 18-20), qui présente une interaction symétrique des deux hydrogènes de l'amine avec l'oxygène du carbonyle, et qui fut calculée (p. 75-77) comme étant de plus faible énergie que la conformation (4), caractérisée dans ce travail et par F.J. Lovas et R.D. Suenram (p. 51-53).

L'attribution de la géométrie (4) au spectre observé précédemment ne présente pas de controverse, étant donné la forte valeur du moment dipolaire mesuré, μ_a = 5,57 debyes et le fait que seule cette

(c) : L.E. Snyder, J.M. Hollis, R.D. Suenram, F.J. Lovas, L.W. Brown et D. Buhl (1980) en préparation.

géométrie conduise à une valeur élevée (p. 23). Il est à remarquer qu'un moment dipolaire, μ_a = 6,54 debyes, encore plus élevé que celui prédit dans ce travail, fut calculé à partir d'une structure de la glycine optimisée par des méthodes ab-initio[d]. Par contre, plusieurs conformations conduisent à une composante du moment dipolaire, μ_a, d'environ 1 debye, notamment les géométries (3) et (6) (p. 23 et 18). L. Schäfer, H.L. Sellers, F.J. Lovas et R.D. Suenram attribuent toutefois le nouveau spectre observé, à la géométrie (3), en examinant uniquement les constantes rotationnelles[d]. Ils considèrent la variation des constantes lors d'un faible changement des paramètres structuraux et le fait que les données expérimentales soient obtenues pour l'état vibrationnel fondamental et non pour la géométrie d'équilibre et en concluent que les erreurs commises sont seulement de l'ordre de 1 %. Ils comparent les constantes rotationnelles mesurées avec celles calculées pour les conformations (3) et (6) et en déduisent alors que (3) est la géométrie caractéristique du spectre obtenu.

Durant la rédaction de cet avant-propos (30/06/1981), quelques calculs sont effectués à Melbourne, à l'aide du programme WANGP6 (p. 10), afin de déterminer si les raies mesurées par mes soins (p. 76), aux environs de 55 GHz, appartiennent à ce deuxième spectre caractérisé par R.D. Suenram et F.J. Lovas.

En conséquence, à ce jour, aucune détection radioastronomique de la glycine ne peut être avancée avec certitude.

Le quatrième chapitre (P. 116) concerne la détection de nouvelles transitions du méthanol dans plusieurs nuages moléculaires. Les observations furent effectuées à Kitt-Peak et Parkes, entre avril 1978 et mai 1979 (p. 117, 118). D.A. Winkler, P.D. Godfrey et R.D. Brown proposèrent les transitions à observer. Elles furent acceptées par B.J. Robinson et le CSIRO. Les tests statistiques furent appliqués par D.A. Winkler et moi-même, sauf ceux concernant les deux cartes dessinées dans Orion A (p. 125, 126) et celle dessinée dans Sagittaire B2 (p. 130) qui le furent par moi-même (p. 120, colonnes 10 et 11 ; p. 128, 133 et 134, colonnes 8 et 10 ; p. 136, colonne 5). Les analyses présentées dans ce chapitre furent effectuées par moi-même et sur mon initiative, notamment les études d'intensité des raies obtenues par rapport à l'équilibre thermodynamique (les cinq dernières colonnes de tous les tableaux). De nombreuses raies peuvent être expliquées

(d) : L. Schäfer, H.L. Sellers, F.J. Lovas, R.D. Suenram
J. Am. Chem. Soc. 102, 6566 (1980)

avec un simple modèle d'excitation par collisions à la température du nuage moléculaire. Toutefois il serait préférable d'appliquer un modèle d'excitation tenant compte du petit nombre de collisions et des interactions éventuelles des photons émis avec des particules du nuage. Les équations à la base d'un tel modèle furent écrites par moi-même, pour une molécule asymétrique, dans le cas simple d'un nuage de densité uniforme (p. 111-115), d'après un modèle déjà développé pour des molécules diatomiques et suivant des conseils procurés par P.D. Godfrey. Un programme est maintenant écrit à Monash, sur la base de ces équations. L'auteur en est McCray. L'analyse des transitions observées devrait donc être revue.

La publication de ce travail est en préparation. Les auteurs seront vraisemblablement, par ordre alphabétique, M.P. Bassez, R.D. Brown, P.D. Godfrey, McCray, D.A. Winkler.

Le cinquième chapitre (p. 140) traite de la détection de nouvelles transitions du cyanure de méthyle dans des nuages moléculaires. Les observations furent effectuées à Parkes et à Kitt-Peak (p. 141). Ces observations conduisirent à deux publications.

La première publication concerne la transition ($J = 2 \rightarrow 1$) détectée dans la direction de Sagittaire B2 (p. 155-158) (Mon. Not. R. astr. Soc. 180, 1P (1977). Tous les observateurs furent auteurs : G.L. Blackman, R.D. Brown, P.D. Godfrey, M.P. Bassez, A.L. Ottrey, D.A. Winkler et B.J. Robinson. La courbe convolutée autour du spectre expérimental fut tracée par G.L. Blackman (p. 156, fig. 5.4 (b)). L'analyse de l'intensité de la raie fut effectuée par moi-même à une date ultérieure à la publication (p. 157, colonnes 6 à 8).

La deuxième publication est en préparation. Elle concerne la détection des transitions ($J_K = 5_K \rightarrow 4_K$) et ($J_K = 4_K \rightarrow 3_K$) dans la direction d'Orion A. Les intensités de ces transitions ne furent pas concordantes au cours des sessions différentes d'observations (p. 146). Sur la demande de R.D. Brown, j'exploitai la présence de la raie d'émission, H41α, dans tous les spectres observés, pour calibrer les intensités. Toutes les analyses de ces observations du cyanure de méthyle, autres que celles de la transition ($J = 2 \rightarrow 1$) précédemment évoquée, furent effectuées par moi-même et sur mon initiative. Il serait toutefois intéressant d'ajouter à la publication, l'application du modèle d'excitation, proposé précédemment (p. 111-115) et programmé par McCray, à toutes les transitions observées. Un complément d'information sur la détection de la transition dans un état vibrationnellement excité, dans Orion A, serait aussi souhaitable (p. 152).

Les auteurs de la publication seront vraisemblablement par ordre alphabétique, M.P. Bassez, R.D. Brown, P.D. Godfrey et McCray.

Le dernier chapitre (p. 160-165) est un tableau des autres observations auxquelles je participai. Certaines n'aboutirent à aucune détection ; l'analyse de leurs données fut effectuée en collaboration avec d'autres chercheurs et étudiants. Les observations positives ne furent pas analysées par moi-même ; je ne suis donc pas auteur des publications.

Je voudrais très sincèrement exprimer mes remerciements aux membres du jury,

à Monsieur J. Faure, pour son enthousiasme lors de notre entretien,

à Madame R. Marx, pour avoir accepté d'examiner ce travail,

à Monsieur M. Guélin, pour l'intérêt qu'il porte aux résultats obtenus,

à Monsieur A. Omont, qui m'honore en acceptant de juger cette thèse,

à Monsieur R. Wertheimer, qui me fit bénéficier de sa longue expérience microonde. Je luis suis reconnaissante des critiques approfondies qu'il émit envers les analyses spectroscopiques et je suis sensible à l'attention qu'il montre à l'égard de ce travail,

et surtout, à Monsieur J. Lequeux qui m'introduisit dans le laboratoire de R.D. Brown. Je le remercie vivement pour sa confiance, son enthousiasme, sa disponibilité et le soutien qu'il apporta durant le déroulement de ces recherches. Je suis très heureuse qu'il ait accepté de présider cette thèse.

Je voudrais également remercier C. Demuynck et J.L. Destombes pour leur gentillesse et l'aide qu'ils m'apportèrent durant le tirage de cet ouvrage. J'exprime également ma reconnaissance envers le personnel administratif et technique des Universités de Lille I et Paris Sud : Mesdames Doribreux, Dupont, Messieurs Beck, Ghestem, Fauquembergue, Raffaud,...

CONTENTS

FIGURES

TABLES

SUMMARY

This work is essentially concerned with the assignment of the microwave spectrum of the amino acid glycine and with the search for this compound in galactic molecular clouds. In addition, several transitions of related molecules have been newly detected in the interstellar medium and their analyses are presented.

The preliminary chapter is an introduction to the work which has been completed and a presentation of the plan of the thesis.

Chapter one describes the computer programs which have been used and written during the elaboration of the work.

Chapter two presents the assignment of the microwave spectrum of the glycine molecule with measured rotational and centri--fugal distorsion constants of the ground vibrational state. Measured frequencies of rotational transitions in the ground and excited vibrational states and measured values of the C-C torsional frequency and of the dipole moment components are also reported. A theoretical analysis of the nuclear quadrupole hyperfine structure is given. Theoretical considerations on different conformers are also discussed and the assigned geometry is determined. The last sections of this chapter are concerned with experimental modifications of the cell, an improvement in resolution and an extension in the sensitivity range. The fabrications of a pumping system and of horns are described.

Chapter three reports the radioastronomical searches for glycine in molecular clouds, with an analysis of the collected data. Equations of radiative transfer and statistical equilibrium have been formulated in the case of an asymmetric top molecule and are also presented.

Chapter four and five are concerned with the discovery of

several transitions of methanol and methyl cyanide in molecular clouds, and with the analysis of their line intensities.

Chapter six reports other successful discoveries of molecular transitions in the interstellar medium and negative searches.

ACKNOWLEDGEMENTS

I would first like to thank my supervisor, Professor R.D. Brown, for the fascinating projects of research that he suggested. Also, I am most obliged to him for the confidence in me that he displayed during the development of these projects, equally in laboratory work as in radioastronomical observations. His sincere interest in the results that I obtained together with his lucid criticism have been most encouraging.

I would also like to thank Dr P.D. Godfrey for the constructive discussions I enjoyed with him, particularly on microwave spectroscopy and radioastronomy instrumentations I am most grateful to him for his help in programming techniques, and I appreciate his availability when problems arose.

I also thank Dr S. Vaccani for his interest in the glycine work during the later stages of the assignment. The helpful advices of Dr H.I. Gunn and J.G. Crofts are also acknowledged. Dr B. Gatehouse and his staff members in the crystallography department are also thanked for making available their program ORTEP.

The services periodically provided by the various departmental workshops both in modification of existing equipment and in repairs were most appreciated and I especially thank Mr D. Clarke.

I undertook five trips to the radiotelescope at Parkes, with a total of sixty two days of observation. I am grateful to the CSIRO Division of Radiophysics for the opportunity to use their equipment, and in particular to Dr B. Robinson for the stimulating discussions we had during observing sessions. Thanks also are due to the various members of the receiver group who aligned or otherwise modified receivers to suit the proposed searches and in particular to Mr M. Balister who

built the 7 mm cooled mixer receiver and R.A. Batchelor and M.G. McCullech who built an excellent 3 mm mixer. I would like also to thank Messrs D. Winkler, Z. Ninkov and D. McNaughton, who assisted in the observation of interstellar glycine.

I also thank the NRAO for providing time on the Kitt Peak mm-radiotelescope, and again I would like to express appreciation for the way in which the engineers at Kitt Peak maintained the equipment.

Professor O.E.H. Rydbeck and Dr Å.G. Hjalmarson at the Onsala radiotelescope are also most gratefully acknowledged for their unhesitating offer of their facilities and their interest in the glycine search.

The ARGC and Monash University financial assistances are also sincerely acknowledged.

Finally I would like to thank Mrs B. Innes for her care and dedication in typing this thesis.

INTRODUCTION

Hincque etiam colligi facilè potest, non aliam esse materiam coeli quàm terrae ...

We can also readily derive the result that celestial and terrestrial matter do not differ ...

22nd Principle of Material Things

Principles of Philosophy

R. Descartes - 1644 -

Over the last decade, a new class of interstellar objects has been found in the Galaxy - the clouds of gas and dust. Some of them are in the process of condensing into stars and are similar to the original nebula which formed the sun and its planets. By studying these clouds, it is possible to gain a better understanding of the formation of the solar system, of the universe and of life.

During the process of condensation, the molecular chemical composition of the original nebula has been destroyed. But some residues remained cold and chemically unaltered. A great number of these small fragments could have fallen on the early earth, and start a contamination which developed towards biological systems because of favorable conditions of temperature, humidity and asymmetry. Prebiotic molecules which could not have been synthesized in the oxydant atmosphere of the early earth could thus have been formed before the solar system. Observations of the chemical composition of galactic molecular clouds can hence lead to more informations on the origin of life on earth and other planetary systems. Analysis of the radiation emitted or absorbed by the molecules in these clouds provides also knowledge on the physical processes and chemical reactions which occur in the interstellar medium.

In this work, several research problems have been studied. The most substantial project concerns the amino acid glycine, the assignment of its rotational spectrum in the laboratory and the search for this molecule in the interstellar medium. In addition, several transitions of organic molecules have been discovered in molecular clouds.

The assignment of the ground vibrational state of one glycine conformer has been completed and is partly published. It is presented in chapter 2. This project has been very intricate. Since many conformers, vibrational and rotational levels of glycine were populated at the temperature of the work, the pattern of experimental lines was very complex, not only because of superimposed spectra, but also because of the absorption intensity which was spread over a large number of lines and a cell sensitivity which had its maximum at inconveniently low frequencies, making detection and identification difficult. In extra a breakdown occurring at low voltages impeded the modulation of low K lines necessary for the assignment of the spectrum.

A feasibility of the experiment is first described in section 2.1. It is followed in section 2.2 by a theoretical development on the structure of the molecule, still unknown in the gas phase. Several plausible geometries are presented and a complication of the experimental spectrum by internal rotation is considered. A prediction of rotational constants and dipole moments is then given for some selected conformers. Because of too low line intensities it has not been possible to observe low J transitions. Hence a conventional assignment of the spectrum by means of identifications of resolved Stark structures has not been possible. It has been necessary to compare the pattern of experimental lines with expected patterns of the plausible conformers. Line intensities and predicted patterns are presented in the last part of

section 2.2.

The experimental work is described in section 2.3. Most of the observed lines of glycine were very weak. An improvement in signal to noise ratio has been a necessity and is presented at the start of the section. A description of the experimental conditions of work shows how slow and time consuming has been the process of observation of glycine lines. It is followed by tables of measured line frequencies, and the assignment of some lines to a ground vibrational state. Rotational parameters are then given and compared with similar results which appeared in the literature, several months after the publication of this work. Because of the experimental problem of voltage breakdown, the vibrational satellites could not be assigned, but some lines of the first and second excited states have been observed and are listed. A calculation of the C-C torsional frequency is also given. A determination of the dipole moment components along the a- and b-axes is then presented. Because of the experimental impossibility of observing the b-type transitions, it has been necessary to measure μ_b by studying an a-type transition dependent in μ_b. The same method has been applied to determine an upper limit for the dipole moment component along the c-axis. Relying on the dipole moment measurements, a determination of the geometry of the assigned conformer is then given. The study of the isotopic species has been undertaken but not pursued because of a similar work which had started in another laboratory.

To contribute further in the microwave analysis of the glycine molecule, a prediction of the nuclear quadrupole hyperfine structure has been done and has been followed by a design and fabrication of a new pumping system in order to improve the resolution of the cell. This is described in section 2.4. In order to extend the sensitivity of the cell, new millimetre horns have also been built and are presented in section 2.5.

The assignment of the ground vibrational state of the glycine molecule made possible the search for this molecule in the interstellar medium. Chapter 3 describes this project. The observations have been undertaken with the radiotelescopes at Parkes Australia, Kitt Peak U.S.A. and Onsala Sweden and the two clouds known to be the richest in molecules, Orion and Sagittarius B2, have been mostly searched. The transitions have been selected assuming that local thermodynamical equilibrium is realized. Upper limits have been calculated for the column density of glycine molecules towards the observed clouds. An analysis of the presence of this molecule in an extra-terrestrial environment, and possible explanations for the non-detection of glycine together with an analysis of the receiver noise are also presented. In order to predict more precisely the line intensities detected at the telescope it is necessary to solve the equations of radiative transfer and statistical equilibrium. The case of an asymmetric top molecule is also treated in this chapter.

Chapter 4 describes the detection of new transitions of methanol in several interstellar molecular clouds. Five transitions and sixteen molecular clouds have been searched using the radiotelescopes at Parkes and Kitt Peak. An analysis of the line intensities, of their departures from LTE and of the maser emissions are presented. Column densities or lower limits to the column density of methanol in the direction of these clouds are also given. Maps of the $5_{-1}\rightarrow 4_{0}$ E and $4_{-1}\rightarrow 3_{0}$ E emissions have been drawn for the Orion A and Sagittarius B2 molecular clouds, and the position of the sources is discussed.

Several transitions of methyl cyanide have also been detected in Orion A and Sagittarius B2 molecular clouds, and searched in other sources. This project is described in chapter 5. An analysis of the

relative line intensities and a calibration of the antenna temperatures, by means of a hydrogen recombination line, have been completed. The detection of methyl cyanide in a vibrational excited state is also discussed.

The last chapter is a tabulation of negative searches and some other successful molecular observations in the interstellar medium.

In order to perform the calculations and data analyses of the microwave and radioastronomy projects, some computer programs have been used and written. They are presented in chapter 1. The fundamental theoretical concepts necessary for the elaboration of the work can be found in the appendices.

CHAPTER 1

COMPUTER SOFTWARE

This section describes briefly the computer software written and used during the elaboration of this work. Listings and details are given in the Appendices. When programs have been written by other people, their authors are gratefully acknowledged.

TABLE 1.1

Summary of software packages

Rotational spectrum programs:	Authors
CART	Monash group
ORTEP	C.K. Johnson
LSTSQ5	A.L. Ottrey
WANG	A.L. Ottrey
WANGLY/WASCAN	P.D. Godfrey, M.P. Bassez
LSQTAU	R. Champion
WANGP6	A.L. Ottrey
Q2FIT	A.L. Ottrey
SFIT	M.P. Bassez
Laboratory data acquisition and analysis programs:	
CATDIS	J.G. Crofts
CATRED	J.G. Crofts
Radioastronomical programs:	
KPRED	H.I. Gunn, P.D. Godfrey, M.P. Bassez
COCHRAN	M.P. Bassez
STATRED	H.I. Gunn, P.D. Godfrey, J.W. Storey, M.P. Bassez N.S. Witte, D.A. Winkler.
PD9-V72/AOS	H.I. Gunn, M.P. Bassez

1.1 COMPUTER

The calculationsinvolved in ORTEP have been performed on a dual processor Burroughs B-6700. The virtual memory addressing of this computer was complemented by a core memory capacity of 272 K of 48 bit words. Tektronix and Calcomp plotting units have been used to draw glycine structures.

All the other programs have been performed with the Sperry-Univac Varian V72 of the Monash Microwave Spectroscopy Laboratory. The capacity of the mapped core memory was 64 K of 16 bit words and its access time 660 nsec. A hardware floating point processor and 4.6 million words of moving head disc memory were provided. Since 1979 the memory has been extended to 192 K. On-line acquisition of microwave data was achieved through a data bus, deserving up to six spectrometers, at a rate of 15 K words per second.

All the programs described below have been written in Fortran IV.

1.2 ROTATIONAL SPECTRUM PROGRAMS

CART:

Given the structural parameters of the molecule, this program sets the raw cartesian coordinates with x along the first bond, and y in the plane of the first and second bands, and calculates the center of mass of the molecule, the principal moments of inertia, the principal cartesian coordinates and the rotational constants along the principal axes. Different values of the dihedral angle between planes formed by four consecutive atoms, correspond to different conformers of the molecule.

ORTEP:

The Oak Ridge Thermal Ellipsoid Plot program allows stereoscopic illustrations of crystal structures [1]. It has been used in this work for three-dimensional views of the glycine conformers (Fig. 2.2). Using the cartesian coordinates given by CART as input of ORTEP, molecules have been drawn in the principal axes of inertia. The memory capacity of the computer, required for the calculations, is 32 K words.

LSTSQ5:

A least squares fit method is applied on the observed transition frequencies to determine the rotational constants A, B, C and the symmetric top centrifugal distorsion constants D_J, D_{JK}. Standard deviations and correlations between these parameters are derived from the variance-covariance matrix.

WANG:

Upon input of rotational and symmetric top centrifugal distorsion constants and of dipole moment components, this program calculates a symmetric top rotational energy levels, frequencies of transitions formed according to the selection rules, line strengths, and peak fractional absorption coefficients. The Hamiltonian matrix is set up in the symmetric rotor basis functions and transformed into the Wang basis, to reduce the size of the matrices to be diagonalized. The calculation follows R.H. Schwendeman's method [2]. If required a sorting routine lists the transitions frequencies in ascending order.

WANGLY/WASCAN:

It is a suite of five programs written to plot transition line shapes with quadrupole hyperfine and Stark multiplets of an asymmetric top molecule, for given temperature, pressure and applied Stark field. A description of these programs with equations and parameters used, and a brief summary of the molecular rotation theory which supports them is presented in Appendix 1.

WANGLY, the main program, is a special version of WANG for the preparation of a transition catalog. Matrices are dimensionned for $J \leqslant 35$.

WAD1D2, calculates the D-hyperfine parameters used by WASCAN in the determination of the hyperfine constants.

WASTAR, gives the Stark coefficients used by WASCAN in the calculation of the Stark multiplets. The method follows a second order perturbation with one two-level treatment added per transition in cases of near degeneracy.

WASSAD, copies from disc to magnetic tape, the transition data file, in order of J, with reduced Stark coefficients, D-parameters and line strengths recorded for each transition.

WASCAN, uses the file written on tape by WASSAD, as input. It convolves each rotational transition with quadrupole splitting and Stark multiplets to a nominated FWHH for nominated values of dipole moments, quadrupole coupling parameters for one nucleus, temperature, vibrational dilution, mole fraction, voltage and field spacing. In addition when the variance-covariance matrix of the rotational constants is read, the 99% confidence frequency prediction range is calculated. Line profiles are drawn for

each transition defined in a given frequency range, within limits of the total rotational quantum number and above a nominated minimum absorption coefficient.

LSQTAU:

This least-squares program determines asymmetric top centrifugal distorsion constants. The fitted rotational parameters are the Kirchoff's version [3] of Watson's determinable parameters. The Kivelson-Wilson parameters are then derived. Up to 100 rotational transitions may be entered, with a maximum value of 49 for J upper.

WANGP6:

It is a special version of WANG which calculates an asymmetric top spectrum, upon input of the Kivelson-Wilson and Watson's parameters as given by LSQTAU.

Q2FIT:

This program determines quadrupole coupling constants for molecules containing up to two quadrupolar nuclei. Observed and calculated multiplets are displayed on a screen and an interactive fit gives the line hyperfine parameters.

SFIT:

It is a Stark multiplet fitting program, which determines dipole moment components. A calculated Lorentzian Stark structure is matched, using an analog input device, to an experimental multiplet of an individual line displayed on a screen. After adjustment of the centre frequency, width, intensity and base line height of the main line, and of the modulation voltage, dipole moment components are varied until complete superposition of experimental and theoretical Stark

components. A plot of the matched multiplets can be drawn.

The fitting routine is an adapted version of Q2FIT. The calculated Stark pattern is based on the same equations and parameters as those used in the WANGLY/WASCAN suite. This program has been designed to suit the 64 K memory size of the V72 computer and uses overlays.

1.3 LABORATORY DATA ACQUISITION ANALYSIS PROGRAMS

CATDIS:

On-line data acquisition is performed by this program. Individual scans can be stored on disc and submitted to mathematical operations such as averaging, smoothing, sampling tolerance, screen display, plotting and dump on magnetic tape.

CATRED:

This program enables the reduction of the data stored on magnetic tape by CATDIS. Each scan is displayed on a sreeen before selection for addition in a stored average. Determination of centre frequency and width of the line are achieved with a fit of a Lorentzian profile. Linear or quadratic baseline removal, smoothing and plotting are also provided.

1.4 RADIOASTRONOMICAL PROGRAMS

KPRED:

This off-line reduction program of data obtained with the Parkes autocorrelator and Kitt-Peak filter bank receivers, is conformed to the commands of the Sept. 1977 program SPECTRA written by J.M. Hollis [4] for Kitt Peak on-line data reduction.

The averages are time weighted, but can also be weighted in proportion to the inverse square of the system temperature. One section of the spectrum may be shifted by a nominated amount of channels and added or subtracted to the unshifted section. When two uncorrelated polarizations are used, the resulting function divided by 2 represents thus the spectrum observed for twice the amount of time spent on source. Other functions such as tabulation of the average content in scan numbers, removal of some or all scans from the average, baseline subtraction, smoothing, plotting and disc/tape dump are also available.

COCHRAN:

This is a statistical analysis program which has been written to eliminate the subjective method used to tell the presence of a weak signal. It is based on the calculation of the ratio of the largest variance on the sum of all the variances determined during a Gaussian fit of fixed width and frequency [5]. The selection of lines was followed by a Fisher's F test. It has been replaced by STATRD.

STATRD:

This program performs a statistical analysis of weak radioastronomical signals. A linear slope is fitted to the data and the variance of the fit is calculated. Then a second least squares procedure fits this linear slope and a Gaussian profile of nominated width or position. The reduction in the variance of the second fit is converted, by a Fisher's F-test, to a significance level of the presence of the line. This significance is expressed as the odds that the reduction in variance is not due to statistical fluctuations in the noise, e.g. significances of 99.9% and 99% mean that the observed profiles are expected to

originate from a spurious feature only once in 1000 and 100 observations respectively. When this statistical test is applied successively on each channel of the spectrum and then plotted as a function of the channel number, the center frequency of the line can be determined. For strong signals, this program is used to determine peak height, width and position.

PDP9-V72/AOS:

At Parkes, data are written on 9-track tapes via a PDP9-11. After file copying these data on 7-track tapes, with the System DUMPALL of the Monash B-6700, it is necessary to form integer, real, double precision and ASCII variables in V72 compatible form. This program PDP9-V72/AOS has been written to suit the recording format of the A.O.S. spectral line observing program at Parkes.

CHAPTER 2

THE MICROWAVE SPECTRUM OF GLYCINE

The simplest amino acid was first named "sucre de gélatine" by its discoverer Braconnot [1] in 1820. The names glycocoll [2] and glycine [3] were then suggested, but the chemical names are aminoethanoic acid and aminoacetic acid. Twenty seven to thirty grams of glycine are present in a hundred grams of connective tissue proteins. This content may reach forty seven percent in silk fibroin, while the milk components present the lowest protein levels. Glycine is well known in the solid and liquid phases. However, before the elaboration of this work, this molecule was little known in the gas phase. An analysis of the microwave spectrum of this free rotating molecule, of its structure and dipole moment are not only important for radioastronomy observations but could also be of interest for biologists who are studying peptide formation.

2.1 *FEASIBILITY OF THE EXPERIMENT*

Only a few experiments, on mass spectroscopy and vapour pressure, had been attempted on glycine in the gas phase before the start of this work. This is because of the tendency of this molecule to decompose and form diketopiperazine $(O{=}C\text{-}CH_2\text{-}NH\text{-})_2$, when heated [4] and sublimed [5].

To avoid this problem mass spectroscopic studies have been made on methyl [6] and ethyl [7] esters derivatives of glycine. However a sublimation of the free glycine conducted at a temperature of 418 - 423 K and followed by condensation on a cold sleeve set at 7 mm from the sublimation point gave a recovery amount of 99.0% and no formation of

diketopiperazine [8]. Also electron impact (EI) mass spectrometry of the free glycine [9] has been satisfactorily achieved with replacement of the externally heated inlet system [6,7] by a crucible ion source. The energy radiated by the hot filament was sufficient to heat the ion chamber and vaporize the amino acid. No contribution of diketopipe--razine has also been observed in EI [10] and CI (chemical ionisation) [11,12] mass spectra of free amino acids when a direct insertion probe was used. The sample was volatilized directly into the ion source and close to the ionizing electron beam [10], or to the reagent ions [11,12].

Vapour pressure measurements have also been made on the free glycine molecule using Knudsen effusion cell methods. They were conducted either by measurements of mass loss of the vessel containing glycine [13,14] or by measurements of mass gain of a flag, set a few millimeters in front of the sublimation point [15]. In this last experiment the condensation products have also been analysed and shown to be glycine crystals with no diketopiperazine contamination. Figure 2.1 shows the good agreement of these experiments. About 200 μHg of glycine crystals are sublimed at 473 K and only 7 μHg at 433 K.

In all these experiments, the length of path between the sublimation and condensation points was very short, inferior to 1 cm, and no definitive conclusion can be advanced on the decomposition occurring in a microwave cell. However the stability of the glycine molecule in the gas phase seemed sufficient for the experiment to be attempted.

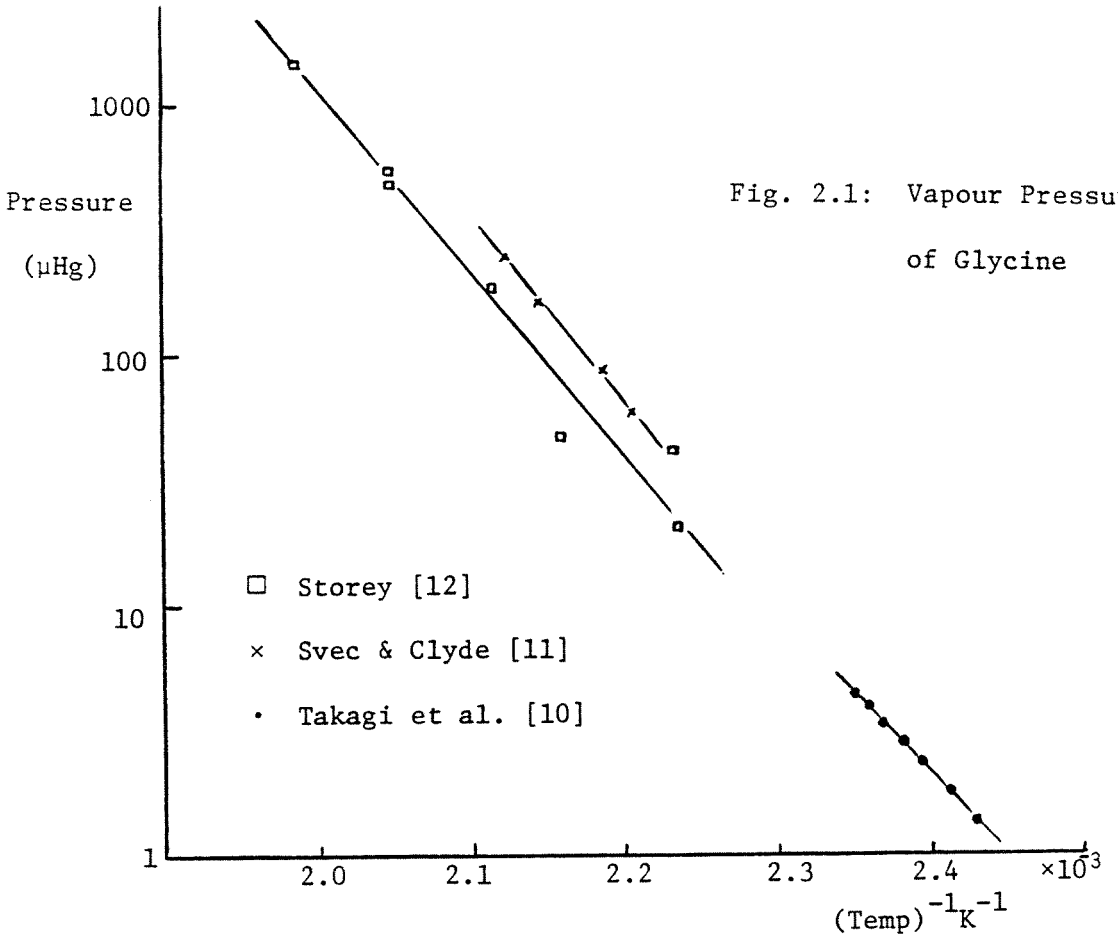

Fig. 2.1: Vapour Pressure of Glycine

2.2 THEORETICAL STUDY OF THE GLYCINE MOLECULE

2.2.1 Conformers

In order to draw a theoretical pattern of the rotational spectrum of glycine, the structure of the free rotating molecule has been predicted.

In solution the zwitterion $^{+}NH_3CH_2COO^{-}$ exists at biological pH and the glycinium ion $^{+}NH_3CH_2COOH$ at low pH, while in the solid state a variety of structures are taken. Bond lengths and angles of the α-crystal have been determined using X-ray [16,17] and neutron diffraction [18] experiments. The electron density distribution of this structure has also been obtained using the X-N Fourier technique [17] and compared with results given by ab initio calculations using an

MO-LCAO SCF method [17]. These data show two bifurcated hydrogen bonds between the oxygens and one hydrogen of the $-CH_2$ and $-NH_3$ groups.

However several studies suggest a neutral form, NH_2CH_2COOH, for the glycine molecule in the gas phase. For instance experiments on EI mass spectra of the free glycine molecule [9] showed that 67.5% of the total ion yield gave a peak at m/e 30, which corresponds to the $(NH_2CH_2-)^+$ fragment and only 1.4% of the ions gave a peak at m/e 31 which represents the $(NH_3CH_2-)^+$ fragment. CNDO calculations [19,20] also favor the neutral form in the isolated state. Informations on the proton transfer from OH to NH_2 are given by experiments on sublimation heat [13] and INDO computations analyze the protonation process of the neutral form [21]. Support for this neutral form is also given by comparison of infra-red spectra of glycine in the solid state and isolated in an argon matrix [22] and the assignment of infra-red bands of glycine isotopic species isolated in an argon or nitrogen matrix [23].

A neutral form has thus been adopted for the gaseous glycine molecule. Several plausible geometries have been selected and are described below.

In the condensed state, the zwitterionic form of the glycine molecule is stabilized by strong electrostatic and polarization interactions with the environment. In the un-ionized form, these effects do not exist and the following free internal rotations may occur:

the amino group around the bond C-N,

the carboxylic group around the bond C-C, and

the hydroxyl group around the bond C-O.

They lead to several conformations of the molecule.

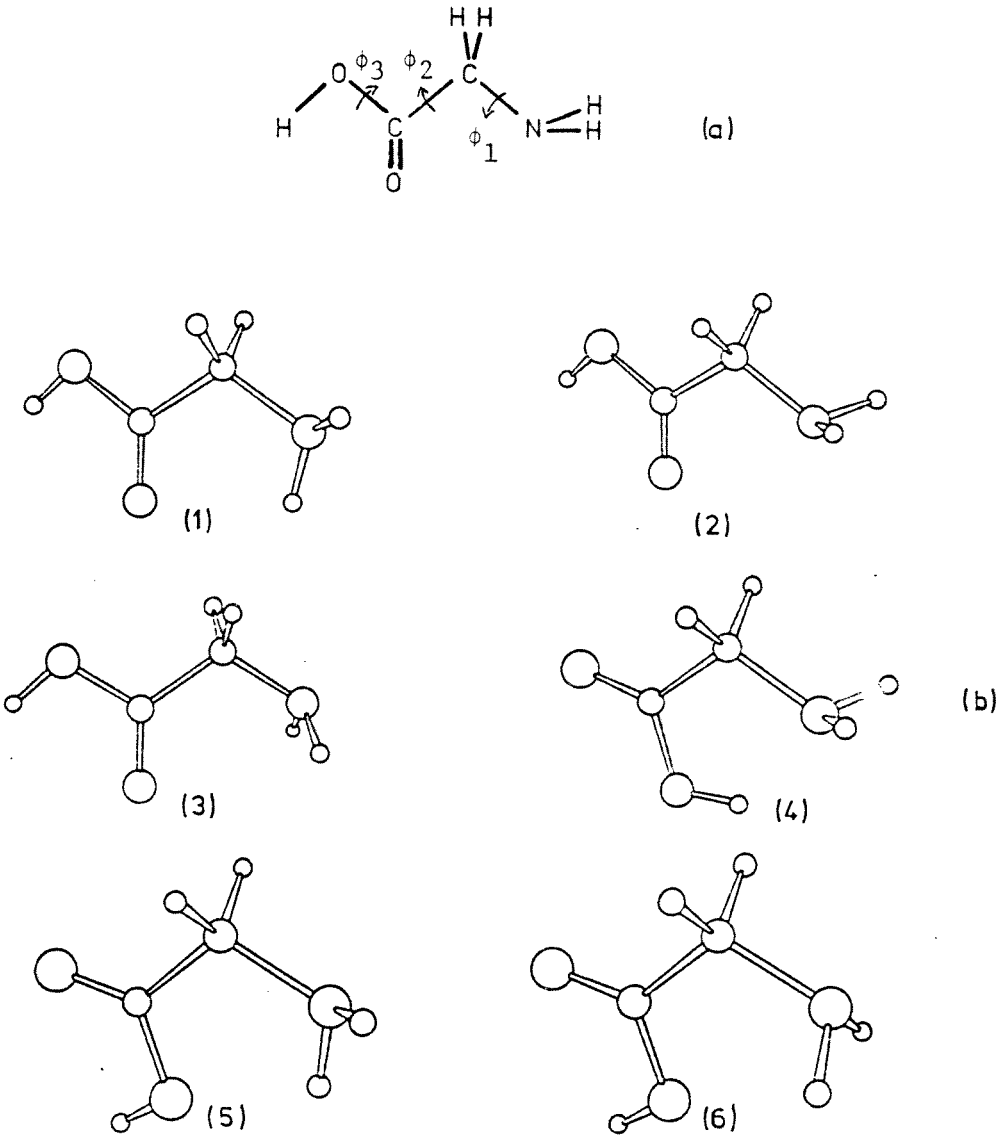

Fig. 2.2 Glycine conformers - (a) the three internal rotational degrees of freedom - (b) the selected conformers.

Six conformations have been selected and are shown on fig. 2.2 (b) above. The heavy atoms are all coplanar and the following differences occur:

Glycine (1), is the minimum energy configuration calculated with CNDO methods [19,20]. Stabilization can occur through hydrogen

bonding between the carbonyl oxygen and one of the amino hydrogens. However repulsive interaction can exist between the other amino hydrogen and the eclipsed methylene hydrogen.

Glycine (2), shows hindrance of the methylene and amino groups and eclipse of the C=O and C-N bonds. This structure seems improbable because of the steric repulsion of the electron lone pairs. However it has been selected in order to compare rotational parameters and dipole moments of a variety of conformers.

Glycine (3), is generated in a 60° rotation of the amino group in (1) and thus shows a symmetric interaction of the amino hydrogens and the carbonyl oxygen. Compared to (2) this structure presents an inversion of the amino group and thus no hindrance of the amino and methylene hydrogens. This conformer was consequently expected to be a good candidate.

Glycine (4), is the geometry which has been assigned in this work. It is the only conformer which presents a trans arrangement of the carboxylic group. Usually the O=C-O-H chain of the carboxylic acids shows a weak hydrogen bond across the group. However a five-membered ring can be stabilized by intramolecular hydrogen bonding such as in the most stable rotamers of methoxyacetic acid [25], glyoxylic acid [26], pyruvic acid [27] and oxalic acid [28]. This conformer has thus the nearest arrangement to the zwitterion form. The choice of this geometry has also been favored by the observations of infra-red spectra [23] where, a weak band at 1785 cm^{-1} was assigned to the ν (C=O) vibration of the trans-carboxyl group, while a strong band at 1770 cm^{-1} was attributed to the cis-form.

Glycine (5), is a transformation of (1) in a 180° rotation of the carboxylic group. Analogy can be made between (5) and the s-trans form of acrylic acid [29], CH_2=CH-COOH, which is

0.16 kcal mol^{-1} less stable than the s-cis form (analog of (1)).

Glycine (6) results from (5) in a 60° rotation of the amino group creating a symmetric interaction of the amino hydrogens with the hydroxy oxygen.

While the experimental microwave study was being pursued, S. Vishreshwara and J.A. Pople were investigating theoretically the six selected conformers, together with fifteen other ones [24]. They carried out ab-initio calculations, using standard restricted Hartree-Fock molecular orbital theory (fig. 2.3). They predicted the conformers (3) and (4) to be the most stable and (2) to be very unstable as expected. (5) and (1) do not appear to be stable conformers as those of acrylic acid and (6) compare to (5) is stabilized by the same amount than (3) with respect to (1).

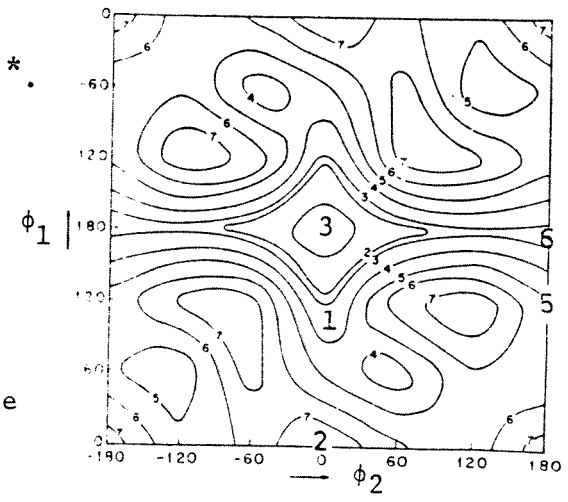

Fig. 2.3: Conformational potential energy map for glycine [24]*. Contour labels refer to energy (kcal mol^{-1}) relative to glycine (3). Glycine (4) is not shown on this map; it is also stable (2.2 kcal mol^{-1} above 3).

2.2.2 *Internal Rotation*

It has been reported that, twenty four vibrational excited states associated with the five lowest normal vibrations of propionic acid [30] have been assigned at room temperature. It is thus likely that, at 473 K, many of the twenty four normal modes of vibration of glycine are populated and that there is interconversion between the rotational conformers.

---

*see footnote p.

Internal rotation effects in microwave spectroscopy are basically rotation - vibration interactions and the higher the barrier above a given vibrational state, the less is observed vibration-rotation interaction within that vibrational state. In methanol there is a strong mixing of the torsional vibration with molecular rotation, and the rotational spectrum is greatly modified. In the most stable conformer of 2-aminoethanol [31], where a hydrogen bond links the hydroxy hydrogen to the nitrogen lone pair, perturbation due to internal rotation is not observed in the ground state. In glycine the two most probable conformers [4] and (3) are probably also stabilized by hydrogen bonding and their interconversion is then limited by a high barrier. Thus the lowest vibrational states should not be perturbed by the fact that the potential energy curve is not harmonic. However some excited torsional states, populated at 473 K, may have energies nearer to the barrier height and show internal rotation effects.

Thus a great number of lines in the microwave spectrum of glycine should originate in different conformers distributed over several vibrational states and, in some cases, these lines could present splitting due to internal rotation coupling. However the two most probable conformers of glycine were not expected to display internal rotation effects in the spectrum of their ground vibrational states.

2.2.3 *Predicted Rotational Constants and Dipole Moment Components*

Geometries of the six selected conformers of glycine have been estimated by combining structural parameters from propionic acid [30] and methylamine [32]. Bond lengths and angles (table 2.1) and appropriate dihedral angles have been computed in the program CART.

The resulting rotational constants are listed in table 2.2.

Variations due to small changes in the values of bond lengths and angles, have been evaluated in the case of the conformer (4). A perturbation of 2° or 1.6% in the angle C-C=O induces a variation of about 1.8% on A and B and 0.8% on C; this second series of rotational constants is listed under $(4)_2$. Bigger variations, 10% on A, 5% on B and 1% on C are seen in the constants of $(4)_3$ for which the structural parameters have been taken from CNDO [20], INDO [21] and molecular orbital calculations [33]. Uncertainties in the predicted rotational constants are thus too big to associate a geometry with the experimental values. The assignment of the observed spectrum to the conformer (4) relied on the dipole moment.

A prediction of the dipole moment components, along the molecular axes, in the principal moments of inertia system has been made for each of the six conformers, using the assumption that dipole moments can be predominantly attributed to electron lone pairs. The lone pair vectors were oriented symmetrically with respect to the bonds, with origin on oxygen and nitrogen atoms, and with values of 1.70, 2.35, 1.31 debyes for the hydroxy oxygen, carbonyl oxygen and amino nitrogen, respectively. The calculated values are reported on table 2.2. This prediction has been useful to evaluate Stark multiplets, and to estimate line intensities and consequently the types of spectra which could be observed (a, b or c).

On table 2.3 are listed the rotational constants of other glycine conformers. They are given for eventual further work.

---

*Other conformational maps of glycine have been published while this work was being typed [58]. They show that theoretical calculations on molecular potential energies have to be accepted with caution.

TABLE 2.1

Structural parameters of glycine borrowed from propionic acid (CH_3CH_2COOH) and methylamine (CH_3NH_2)

bond lengths (Å)	angles (°)
N-H : 1.011	HNH : 105.87
C-N : 1.474	CNH : 112.05
C-H : 1.098	HCH : 109.47
C-C : 1.509	NCC : 112.7
C=O : 1.210	CCH : 107.7
C-O : 1.352	CC=O : 125.8
O-H : 0.970	CC-O : 111.8
	COH : 105.8

TABLE 2.2

Predicted rotational constants and dipole moments of the selected glycine conformations

Conformation	A^a	B^a	C^a	$\mu_a{}^b$	$\mu_b{}^b$	$\mu_c{}^b$
(1)	10.45	3.88	2.91	0.3	0.1	1.1
(2)	10.06	3.76	2.87	0.2	1.9	0.0
(3)	10.36	3.90	2.93	1.0	0.2	0.0
(4)	10.47	4.03	3.01	3.5	1.7	0.0
(5)	10.21	4.12	3.02	0.1	0.6	1.1
(6)	10.11	4.15	3.05	0.6	0.8	0.0
$(4)_2$	10.28	4.10	3.03	3.2	1.2	0.0
$(4)_3$	9.48	4.24	3.03	3.5	1.6	0.0

a : in GHz. b : in D.

TABLE 2.3

Predicted rotational constants of other glycine conformers

Conformer[a]	A[b]	B[b]	C[b]
(60,0,0)	10.55	3.81	2.87
(0,60,0)	9.42	3.79	3.00
(60,60,0)	9.45	3.83	3.01
(120,60,0)	9.35	3.87	3.06
(180,60,0)	9.16	3.92	3.10
(240,60,0)	9.20	3.88	3.08
(300,60,0)	9.36	3.80	3.04
(0,120,0)	9.29	3.90	3.06
(60,120,0)	9.24	3.90	3.10
(300,120,0)	9.32	3.95	3.07
(0,180,0)	10.30	3.98	2.97
(60,180,0)	10.31	4.03	2.98
(180,180,0)	10.11	4.15	3.05

2.2.4 *Expected Pattern of the Spectrum*

As shown in section a below, the lines of glycine have their maximum intensity for high J values. In R band, even though it was the highest sensitivity range of the cell used, no lines of glycine could be observed. The assignment has been done with some lines seen in F band, without any observation of resolved Stark structure, and by comparison of experimental and theoretical stick spectra. It has thus been necessary to understand the type of spectrum that gives each conformer and this is presented in section b.

a : They are labelled by their conformational angle in degree. For instance the conformer (60,0,0) has the geometry with $\phi_1 = 0°$, $\phi_2 = 0°$, $\phi_3 = 0°$, with respect to the conformer (0,0,0) of fig. 2.2a.

b : in GHz.

a) Vibrational and rotational population distributions

At 473 K the intensity of the ground vibrational state is reduced by a factor of 40. This evaluation has been done using the value 104 cm^{-1}, calculated in this work (section 2.3.6), for the C-C torsional vibration, and the eighteen frequency values of fundamental modes of vibration, given by an infra-red analysis [23]. The vibrational partition function [34] was thus calculated to be 40. (Q_v = 60 if $\tau(CC)$ = 60 cm^{-1}).

The relative distribution of population over the rotational levels of a vibrational state has also been calculated using the approximate expressions for the rotational partition function of an asymmetric top [34]. Q_r takes the value of about 1.6 10^5 at 473 K for the six glycine rotamers, four times higher than at room temperature. The rotational fractional population $F_{J,K}$ of the levels of glycine (4) is drawn on fig. 2.4 as a function of J for (K_a=0) and (K_a=J). It is seen that the highly populated levels are those with J around 20 and above, that high K_a transitions are less intense than low K_a ones and that in the range of sensitivity of the R band cell used, the levels are weakly populated.

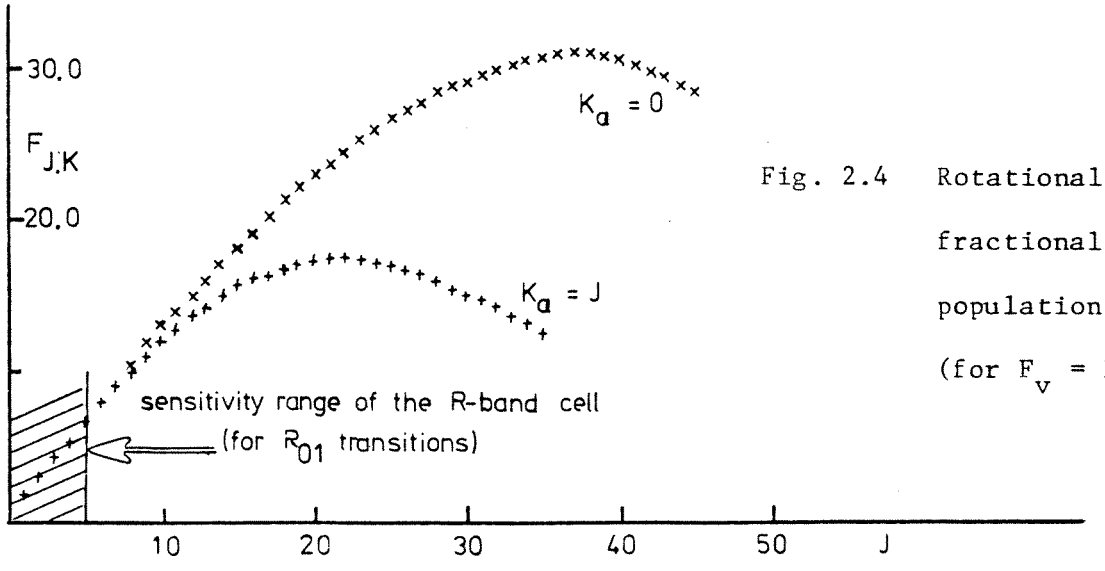

Fig. 2.4 Rotational fractional population - (for F_v = 1).

b) Pattern of lines expected for each conformer

Using the WANGLY-WASCAN program specially written for the purpose of glycine analysis, transition frequencies, line intensities and Stark multiplets have been calculated as a function of the voltage applied for the six conformers.

Each predicted spectrum is a fairly asymmetric top near the prolate type, with Ray's asymmetry parameter around -0.7. Thus when the predominant dipole moment component lies along the a prolate symmetric top axis, the $^aR_{01}$ transitions, the strongest in the spectrum, are grouped in wide ($\Delta J = +1$) bunches. Since, as remembered with the well known energy level diagram of an asymmetric top [35], the highest K_a lines of the ($\Delta J = +1$) series present the strongest symmetric top character, the high K_a $^aR_{01}$ transitions are separated by approximately (B+C). Such are the two most probable conformers (3) and (4). Their two ($K_a = 6$) transitions of the ($J=7\leftarrow6$) branch for instance, may be considered as degenerate (about 10 kHz separate them) and their frequencies are about 300 MHz or 0.6% higher than the frequencies calculated in the symmetric top approximation (B+C)(J+1). Each of these two conformers show an interval of (B+C ≃ 7 GHz) between the highest K_a transitions of their $^aR_{01}$ branches and their spectra are interpenetrated, as shown below:

(3) $5_4\leftarrow4_4$*: 34.4 GHz, $6_5\leftarrow5_5$: 41.3 GHz, $7_6\leftarrow6_6$: 48.2 GHz, $8_7\leftarrow7_7$: 55.0 GHz

(4) 35.4 , 42.5 , 49.6 , 56.7

However the splitting of the low K_a lines is about 13% of the highest K_a transition frequency. The lines of the ($J=7\leftarrow6$) branch of glycine (3) and (4) are thus spread on approximately 7.5 GHz with small mixing in the ($J=6\leftarrow5$) series. This mixing of the low K_a transitions into the main $^aR_{01}$ bunch of the lower J transitions is more important as J increases,

*the transitions are labelled with K_a only, since they exist as a degenerate pair.

creating complications in the assignment of the lines. The next strongest lines of these two conformers, ten, twenty times weaker than the $^{a}R_{01}$, are the $^{a}Q_{2-1}$, $^{a}Q_{0-1}$ and $^{a}R_{2-1}$ branches, which in the case of glycine (4) are also overlapped by the ^{b}R series.

The configuration (1) presents a c-type spectrum with $^{c}R_{10}$, $^{c}Q_{10}$ and $^{c}Q_{1-2}$ as predominant transitions. The $^{c}R_{10}$ line frequencies are always higher than the frequencies of the $^{a}R_{01}$ transitions occurring from the same lower state, as also seen from the energy level diagrams of an asymmetric top [35]. For instance, the $3_{1,2} \leftarrow 2_{1,1}$ is predicted to occur at 21.76 GHz and the $3_{2,1} \leftarrow 2_{1,1}$ at 40.57 GHz. With the cell used, the only observable R branch transitions of this conformer belong to the (J=2←1) and (J=3←2) series. However a great number of Q branch lines fall into the 20-60 GHz range and could be used for the assignment of the spectrum. For instance the head of the $^{c}Q_{10}$ and $^{c}Q_{1-2}$ series for (K_a = 2←1), is expected at 19.27 GHz and at 34.84 GHz for the (K_a = 3←2).

The configuration (5) presents also a c-type spectrum with b-type overlapping. It could also be assigned with Q branches. The head of the $^{c}Q_{10}$ and $^{c}Q_{1-2}$ series occurs at 21.70 GHz for the (K_a = 2←1) transitions and at 32.61 GHz for the (K_a = 3←2).

The conformer (6) gives rise to a mixed b and a-type spectrum with the ($J_{K_a} = 7_6 \leftarrow 6_6$) at 50.79 GHz. Finally the most improbable of the six conformers, glycine (2), presents a pure irregular b-type spectrum.

Fig. 2.5 The Spectrometer.

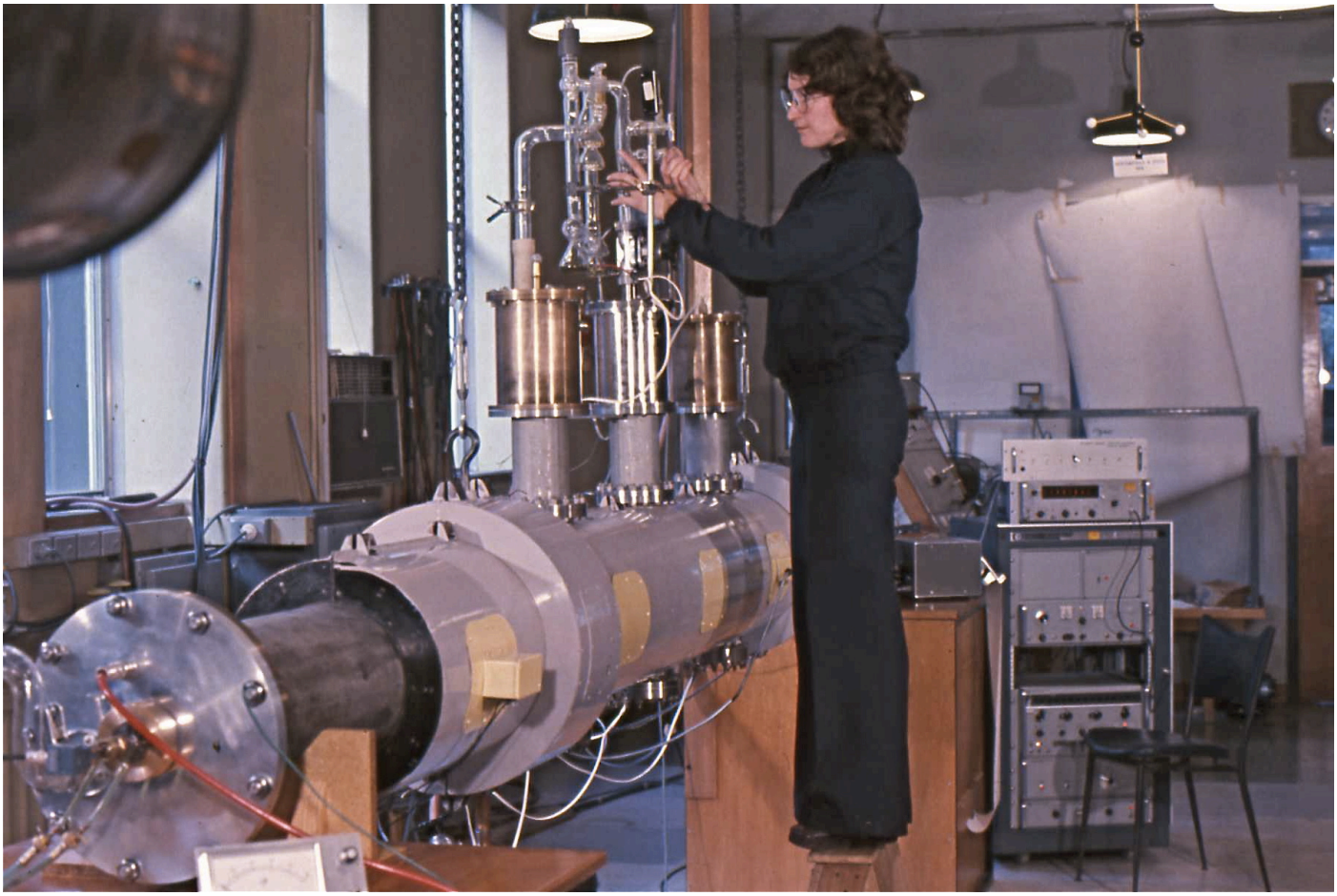

Marie Paule Bassez with the glycine cell
Monash University, march 1976, photo John Storey

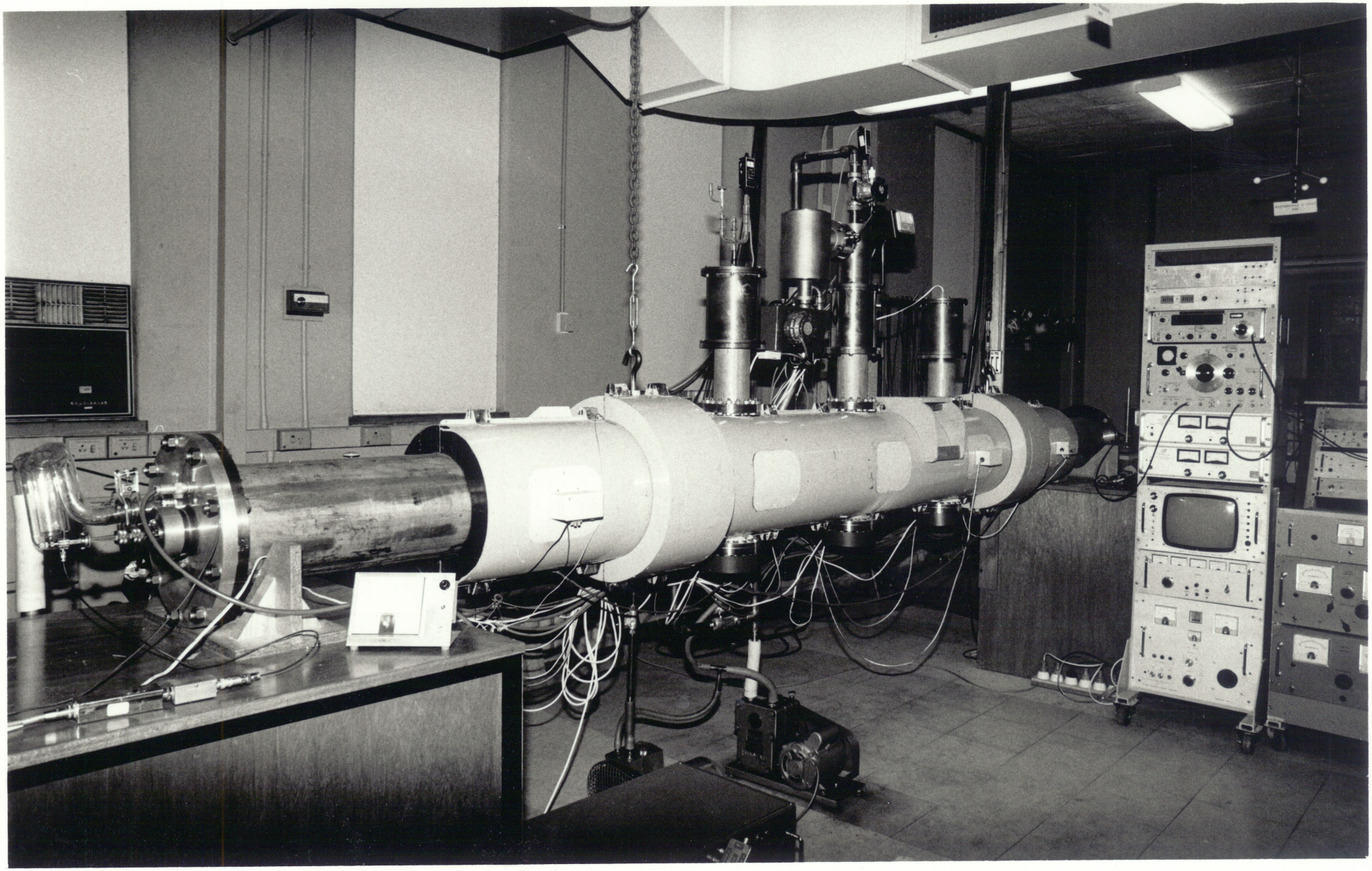

The glycine cell with the improved pumping system and the temperature controller. The newly build horns which increase the sensitivity of the cell in the millimeter-wave range are located inside. photo: Marie Paule Bassez 1977

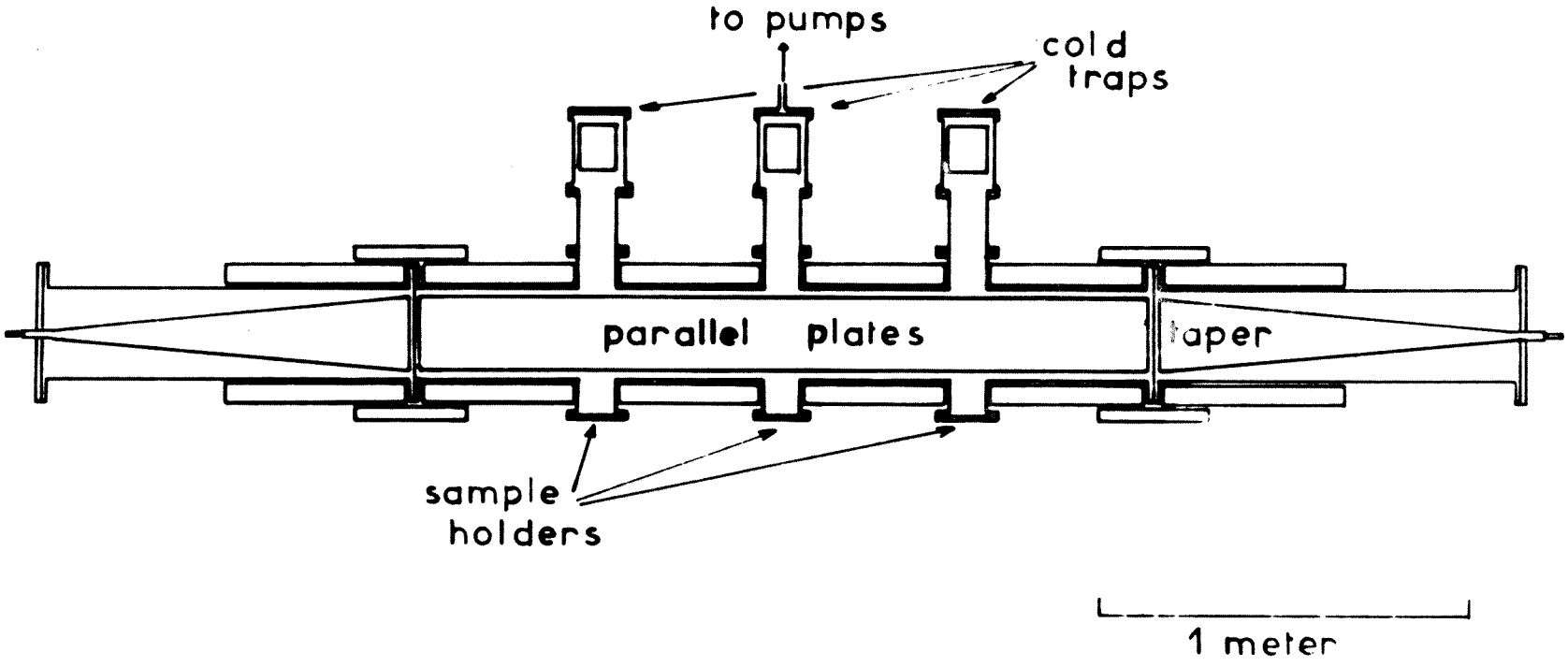
to pumps
cold traps
parallel plates
taper
sample holders
1 meter

Fig. 2.6 Spectrometer components

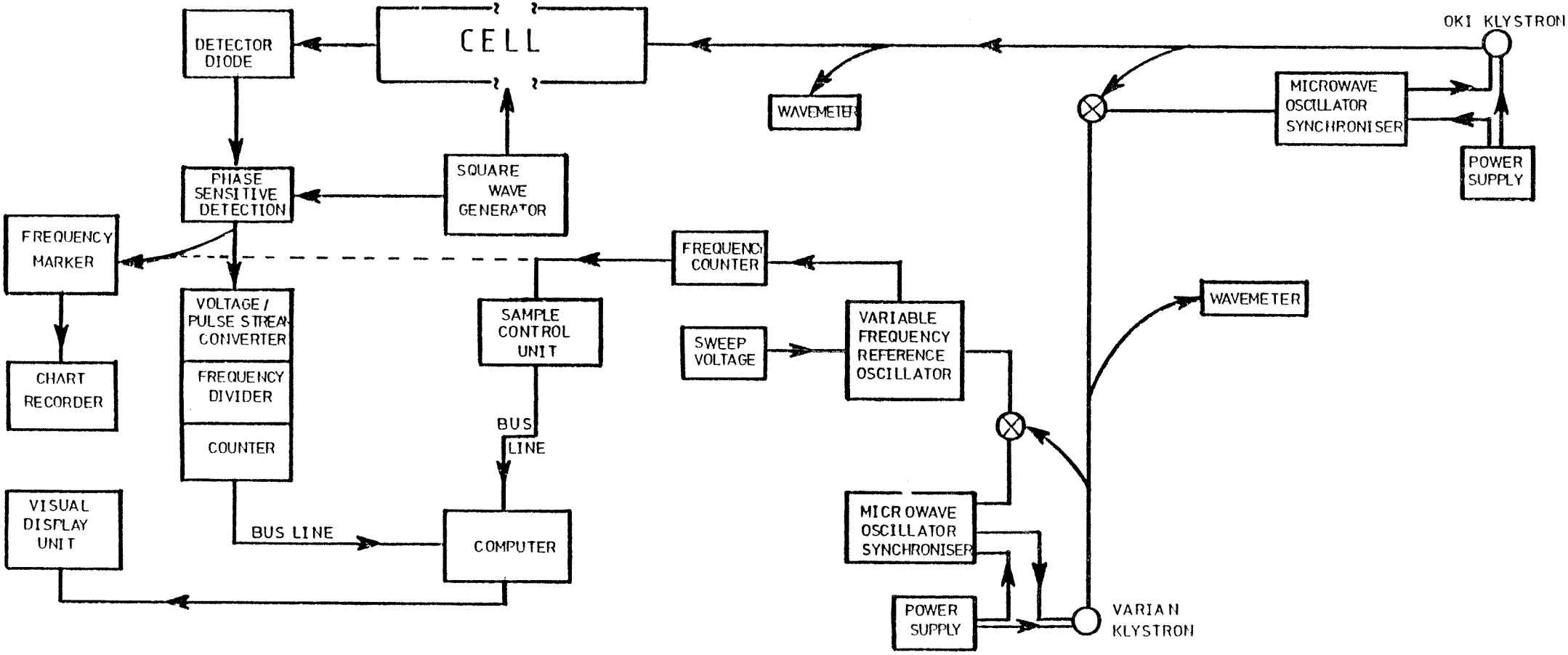
DETECTOR DIODE
CELL
OKI KLYSTRON
WAVEMETER
MICROWAVE OSCILLATOR SYNCHRONISER
POWER SUPPLY
PHASE SENSITIVE DETECTION
SQUARE WAVE GENERATOR
FREQUENCY MARKER
FREQUENCY COUNTER
VOLTAGE / PULSE STREAM CONVERTER
SAMPLE CONTROL UNIT
SWEEP VOLTAGE
VARIABLE FREQUENCY REFERENCE OSCILLATOR
WAVEMETER
CHART RECORDER
FREQUENCY DIVIDER
BUS LINE
COUNTER
VISUAL DISPLAY UNIT
BUS LINE
COMPUTER
MICROWAVE OSCILLATOR SYNCHRONISER
POWER SUPPLY
VARIAN KLYSTRON

2.3 EXPERIMENTAL STUDY OF THE GLYCINE MOLECULE

2.3.1 Spectrometer components and noise

In the spectrometer used (fig. 2.5 and 2.6), the signal was recovered from the noise through a conventional Stark modulation of the absorption line, followed by synchronous detection using a phase sensitive detector, referenced to the modulator, followed by a low-pass filter. Phase stabilized klystrons were mostly used as generators of microwave power.

The 0.15 m^3 heated cell was made of stainless steel, contained internally silvered parallel glass plates and was terminated in a waveguide of 21.1 GHz cut-off frequency. It is fully described in J. Storey's thesis [15]. During the elaboration of this work, regular measurements of the microwave transmission were taken with TRG precision attenuators. With freshly silvered plates the cell attenuation was only 3 dB in R band, below 35 GHz, but increased to 11 dB at 59 GHz and 17 dB at 85 GHz. In order to increase the sensitivity, a new trans-mission line has been built during this work and is described in section 2.5. Improvement of the resolution has also been achieved by designing and using a new pumping system (section 2.4.2). For fail-safety of the heating system, a temperature controller has also been built and is presented in section 2.3.2.c. An increase in the signal to noise ratio has been a necessity and the ways of achieving this goal are described below.

The main sources of noise in a microwave spectrometer are: random noise caused by the movement of electrons, 1/f noise, noise due to vibrations and modulation pick up.

"Flicker noise" or 1/f noise is the most difficult to eliminate since its cause is not well understood. It is commonly

regarded as independent of temperature and considered as a stationary Gaussian random process [36]. Since f is the modulation frequency, 1/f noise has been reduced by choosing the square-wave generator with the highest modulation frequency available in the laboratory, 33 kHz.

In addition to the random inherent shot noise of its electron beam and 1/f noise, a klystron shows variations due to thermal changes and mechanical vibrations, which result in amplitude and frequency modulated noise. High improvement in the klystron stability has been achieved with a change in the cooling method, and the use of electronic stabilization. A ventilation of air has been replaced by a water-cooled heat sink surrounding the tube, more convenient than an oil bath. High frequency klystrons have been phase stabilized [37] in a double lock referenced to a fundamental oscillator. A Micro-Now variable quartz crystal oscillator with very good stability, 1 ppm per 24 hours, has been chosen in the early scans. The frequency multiplier chain of this apparatus can be drawn as follows:

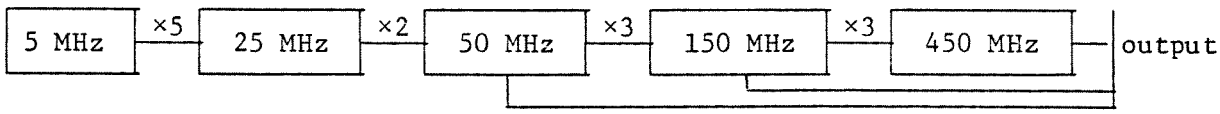

The strongest locks were obtained with the 450 MHz output. However harmonics of the 150, 50 even 25 MHz and also spurious combinations of harmonics, were strong enough to lock on. This often led in F band, to a jump from one lock to another during the scan. For this reason a Hewlett-Packard transfer oscillator has been preferred even though its noise level and frequency stability were not as performant as the Micro-Now system.

When a Hewlett-Packard BWO has been used, the ΔF mode has been chosen. It corresponds to an electronic tuning of a varactor and

thus gives a more stable frequency than the start/stop mode where a tank capacitor is driven by a servo control motor.

Noise in the detector system originates in the semi-conductor diode, transformer, preamplifier, A.C. and D.C. amplifiers.
The noise present in the signal at the detector diode output has been increased so as to exceed the level of the A.C. amplifier noise, by means of a transformer followed by a field effect transistor (F.E.T.) preamplifier. The 1 KΩ transformer used was a low noise ferrite type and proper impedance matching minimized the noise contributed by the preamplifier. However the D.C. amplifier at the output of the phase-sensitive detector showed a stronger 1/f component than the A.C. amplifier and its gain has always been kept very low during the scans.
A semi-conductor diode produces thermal noise in its spreading ohmic resistance [38], shot noise at the p-n junction and a dominant 1/f noise. Since point contact diodes have higher 1/f noise than Schottky barrier diodes and that tunnel diodes, otherwise quiet, cannot be used above R band because of their high junction capacitance, Schottky diodes have been used in F and V bands.
The output noise power of the detecting system is expressed as:

$$P = (kT + cI^2/f)\Delta f \qquad [39]$$

where I is the D.C. crystal current, and Δf the frequency bandwidth of the D.C. amplifier. The signal to noise ratio has thus been improved by a decrease of Δf. This filtering, ultimately limited by the frequency drift of the source, has been used with a stabilized klystron.
However it required an increase in time constant τ and consequently a high time of scan t, in order to observe an undistorted absorption line.
Computer averaging has thus been used very often and is described in appendix 3. Without this method, the $4_{3,2} \leftarrow 3_{3,1}$ line at 28 GHz could

never have been observed with the available equipment.

Noise arising from vibrations external to the cell can be eliminated in the future by cushioning and installing away from the cell the six vacuum pumps of 120 lmn^{-1} average capacity which are now in the vicinity of the spectrometer. The flaky silver parts of the plates, which fluctuated either with the external vibrations or at the modulation frequency, were an important source of noise. Regular resilvering of the plates has eliminated this problem. Finally modulation pick-up, which is the detection at the modulation frequency of a signal radiated by the square wave generator, has been reduced by choosing short interconnecting coaxial cables.

Tests on the amplifier noise were done regularly with hot-cold loads. Typical values are the following: 80 K of system temperature, 1.278 of integration time factor and 1.066 dB of noise figure.

2.3.2 *Experimental Conditions*

The observations of glycine lines have been a time consuming process, not only because of a cell sensitivity which was at inconven--iently low frequencies but also because of long, non-efficient hours spent for heating, cooling opening, cleaning the cell, making of aluminium o-rings and regular resilvering of the plates. This was accompanied by the short period of time during which the sample was available for observations, and a breakdown occurring at low voltages. These conditions of work are presented here.

a) Sample:

Glycine crystals were deposited by dropping them into the two end sample holders through a funnel placed in the two end upper

pumping ports. Approximately 2 × 50 g of BDH "chromatographically homogeneous" glycine was used for a typical four hours experiment. During sublimation glycine was transferred from the lower sample holders to the upper cold traps while the volatile decomposition products were evacuated through the central port. After about one hundred hours of experiments the condensed solid was scratched off the cold trap walls. It was essentially white but contained a few yellow contaminating materials. An infra-red spectrum of this sublimated glycine showed the bands of absorption the α-crystals [22]. This solid was then grounded into powder and recycled in further experiments. After complete sublimation, the sample holders were left with a black decomposition product, the amount of which increased with the temperature of sublimation.

b) Pressure:

To avoid a higher rate of consumption than one hundred grams of glycine per four hours of experiments, the upper pumping ports were blanked off with steel baffles. The central port remained with a hole of 2.5 cm in diameter, decreasing in size as the glycine deposited on the walls of the cold traps. One end port had a circular opening of 1 mm leaving passage to the thermocouple connected to a glass plate. This thermocouple was then continuously centrally positioned to avoid its trapping in the sublimated glycine crystals. In these conditions a vacuum of 50 μ was achieved in 15 mn with a PVD ULVAC rotary pump working at a flow rate of 180 lmn^{-1} through a 1.25" line out of the upper central port. The pressure decreased to a few microns in the next 15 mn through a two stage 1" diffusion pump made of glass and filled with Apiezon C hydrocarbon oil. During heating of the cell,

degazing up to 30 μ occurred. At a cell temperature of 473 K and an external temperature of the sample holders of 493 K, the linewidths obtained for glycine with this vacuum system were about 2.5 MHz.

Only the pressure of volatile decomposition products was known by reading a Pirani gauge. At these temperatures, it was always inferior or equal to 1 μ. Thus, considering a line broadening of 30 kHz per μ the pressure of glycine inside the cell could be estimated at about 80 μ. Measurements of pressure have been necessary when the cell was hot and the sample containers not heated. A test gas has thus been introduced, acetaldehyde, and its line broadening has been observed as a function of the cell temperature. The selected line was $3_{1,2} \leftarrow 2_{1,1}$ at 59379.59 MHz. No significant increase in linewidth has been observed, thus applying that the pressure inside the hot cell was certainly inferior to 1 μ.

With the pumping system described in section 2.5.2, methanol linewidths of 130 kHz have been observed.

c) Heating controller

The temperatures of the cell and sample holders were stabilized with an electronic temperature controller regulated with chromel-alumel thermocouples. To counter any malfunctioning of this apparatus a heating controller has been built. It uses a bimetallic switch which cuts off the heater current when the temperature reaches a nominated value. At the same time,a signal is sent to the computer in order to facilitate the reduction of stored data. With this piece of equipment, overnight heating of the cell has been made possible.

d) Heating time:

Since the behaviour of the glass is not well known above 473 K [40], the internal temperature of the cell has been kept at 473 K. Three hours were required for the temperature to be increased from 333 K and stabilized at 473 K. However eighteen hours were necessary for the cell to return to 333 K by convection cooling. In order to avoid breakage of the hot glass plates when in contact with the cool conditioned air, the cell has never been opened when its temperature was higher than 333 K.

The temperature of sublimation was not directly measureable, but with a thermocouple set between the heater and the sample holder. About forty five minutes were necessary to stabilize the sample temperature and see the lines of glycine appear, when the surrounding temperature of the sample holders was 493 K.

Thus four hours of scanning required more than twenty one hours of experiment.

e) Glycine condensation:

The brass horns were assembled with soft solder of 443 K melting point. Water-cooling was preventing their deformation. For best microwave transmission, they were positioned as nearest as possible to the glass plates, touching the separating mica windows and cooling them down. This was followed by a condensation of glycine crystals on the windows, a decrease in transmission and in some cases a power saturation of the line or a total attenuation of the microwaves. Every ten to twelve hours of scanning, the cell was opened and the glycine crystals were removed under water. New aluminium o-rings were placed

in order to form the vacuum seal between end and center chambers, and the cell was ready for the next experiment. This deposit could be highly eliminated by sliding the horns about 3 cm away from the windows. However the coupling between horns and plates in these relative positions corresponded to a loss of transmission of about 50%.

f) Silver decomposition:

The silver coating of the plates had to be very smooth and uniform to avoid any impedance discontinuities leading to reflexion of microwaves. Since the silver was easily destroyed in contact of glycine, decomposition products and air, the cell was always kept under vacuum with short exposures to air during glycine refills. However regular resilvering has been necessary. The method followed was the Brashear's process [41] used for telescope mirrors.

g) Voltage breakdown:

A breakdown occured at a field of 200-300 V cm^{-1}, and was followed by total decomposition of glycine. This happened when the cell was hot and the sample heated or not. A study of this phenomenon is given in fig. 2.7.

It is not exactly repetitive but a critical point seems to appear around 393 K and a weaker one around 433 K. They could correspond to the transition points of the glass since devitrification occurs at 393 K and 423 K when the heating rate is faster than 4 K mn^{-1} [42]. However the maximum rate reached in this experiment was 1.7 K mn^{-1} A surprising fact is that the cell generated current with an electromotrice force which could attain 1.80 V above 413 K

Fig. 2.7 Voltage breakdown analysis.

(a) The cell resistance as a function of the cell temperature - (measured with an insulation tester).

(b) The voltage breakdown as a function of the cell temperature - (measured with the applied field either positif or negatif).

(c) The voltage generated by the cell as a function of the cell temperature.

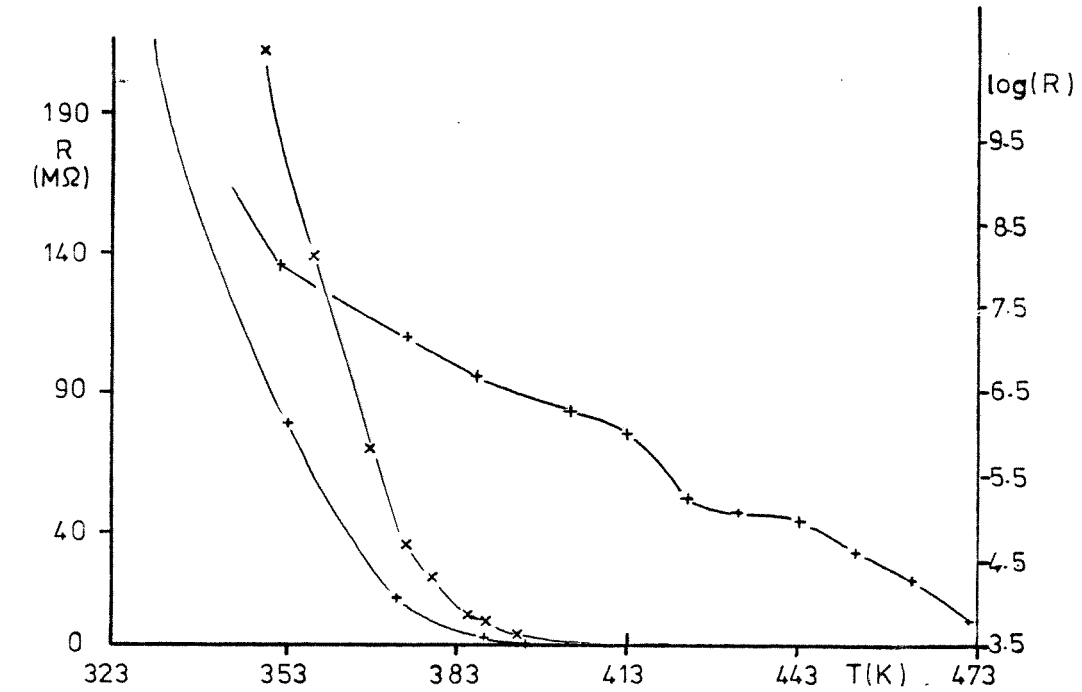
190
R
(MΩ)
140
90
40
0
323
353
383
413
443
T(K)
473
log(R)
9.5
8.5
7.5
6.5
5.5
4.5
3.5

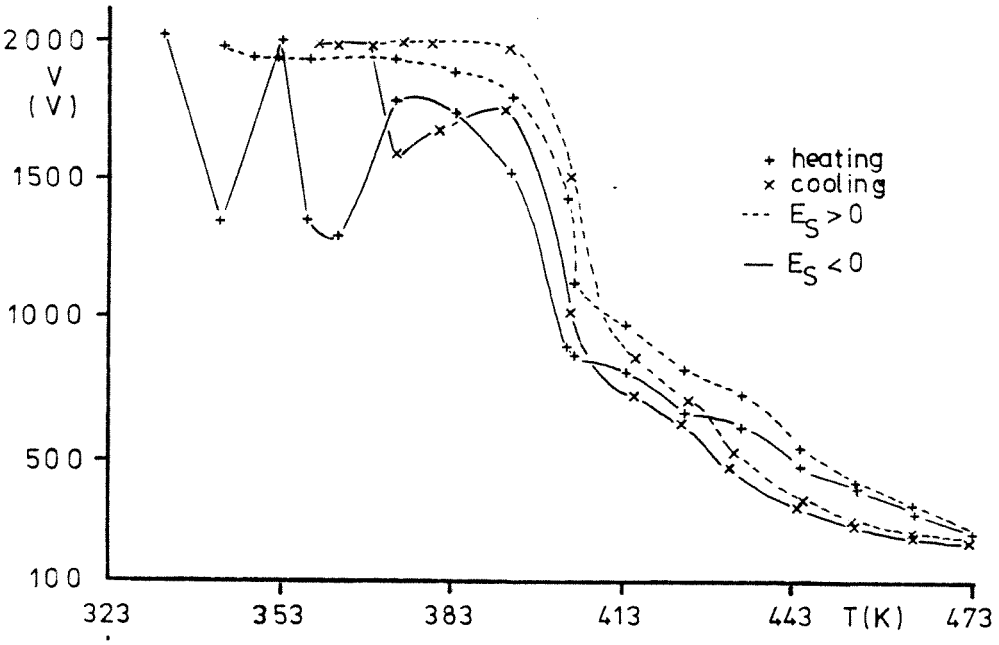
2000
V
(V)
1500
1000
500
100
323
353
383
413
443
T(K)
473
+ heating
× cooling
--- $E_S > 0$
— $E_S < 0$

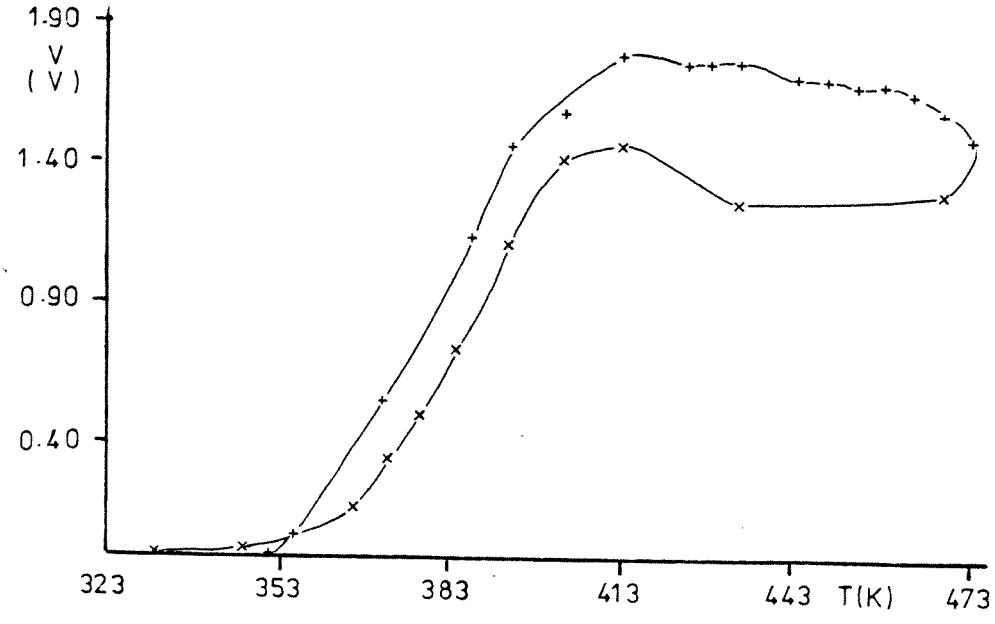
1.90
V
(V)
1.40
0.90
0.40
323
353
383
413
443
T(K)
473

(e.m.f. (Ag/Ag^{+}) = -0.8 V). This discharge was not due to a breakdown inside the mica [43] nor to a conduction through the 0.5" glass spacers, nor to the Stark lid. A current explanation would be a glow discharge [44]. However an addition of 10 or 20 μ of air or acetalde--hyde did not change the value of the breakdown voltage, and no glow or arc was visible. An important observation was that the Stark field could be increased to 700-800 V cm^{-1} after heating of the sample holders at 673 K for a day and of the cell at 473 K for about a week.

A possible conclusion may be that a discharge of glycine or decomposition products occurred at very low pressures, less than 1 μ. When the voltage increased, ionization increased and when the ion pressure was high enough, the breakdown occurred. When the cell had been heated for long hours, contaminating products were evacuated and the Stark voltage could be higher.

h) Tuning of the horns:

Another process which has been very time consuming has been the narrow range of coupling between plates and horns. In low R band frequencies, the tuning could be achieved on 200 MHz but only about 80 MHz could be achieved at 57 GHz.

2.3.3 *Observed Spectrum*

R band has been searched from 26.5 to 29.0 GHz and from 33.5 to 37.5 GHz, with Stark field of 80 and 315 V cm^{-1}. A Hewlett-Packard BWO, model KO3 8690 A was used. It has been phase-locked with a 30 MHz IF to a reference transistor VFO oscillator, the frequency of which may vary between 240 and 400 MHz. The crystal detector was a Hewlett-Packard R 422 A. Broadband scans were swept with a width of 150 MHz, a time constant of 1 s and a chart recorder speed of 1" mn^{-1}. In these conditions, a line of 2 MHz wide was visible. Table 2.4 lists the observed lines. Only two correspond to transitions of the assigned conformer (4). For the purpose of future work informations are given on signal to noise ratios.

These lines may originate from glycine or from non identified decomposition products. Numerous transitionsof ammonia and methylamine have been found. They are not mentioned. Two procedures have been adopted to decide if a line belongs to the glycine spectrum: several plausible volatile decomposition products were introduced in the cell at 473 K and their spectra were observed; also the complete isolation of the cell from the pumps by closing a tap, was followed by a rapid increase in intensity of the decomposition product lines and some broadening of the glycine lines.

In F band the search has been carried out from 49 to 63 GHz, using the 50 V11, 55 V11 and 60 V12 OKI klystrons, by driving reflector voltage potentiometers with a synchronous motor, at a rate of 5 MHz cm^{-1}. Numerous lines were detected using a time constant of 1 s and Stark fields between 1.5 and 315 V cm^{-1}. Their density was bigger around 50 and 57 GHz where were expected the high K_a transitions of the series (J=7←6) and (J=8←7) of the conformer (4) (cf. section 2.2.4). Examples of lines are shown on fig. 2.8. The spectra b and c have been

Some observed F-band lines[a]

frequency[b] (MHz)	V[c] (V)	S/N	frequency[b] (MHz)	V[c] (V)	S/N	frequency[b] (MHz)	V[c] (V)	S/N	frequency[b] (MHz)	V[c] (V)	S/N	frequency[b] (MHz)	V[c] (V)	S/N	frequency (MHz)	V[c] (V)	S/N
44384.32	400	2	50949.52	850	2	52990.00	400	2	57213.096	25		57481.41	2	2.5	57613.43	100	3.5
44393.90	400	2	50951.57	850	2	53078.16	400	2	57219.674	25		57483.70	2	2	57642.48	10	2
44398.59	400	2	50954.14	850	2.5	53088.81	400	3	57225.50	400	3	57492.67	2	2	57651.60	25	3
44400.40	400	2	50956.70	850	2	53124.24	400	3	57232.00	2.5	5	57496.87	2	2	57654.80	25	2
44406.10	400	3	50993.08	700	2	55105.208	500		57240.22	2.5	2.5	57510.30	2	1.5	57657.60	25	2
44420.40	400	2	50996.16	700	2	55108.956	400		57263.00	2	3	57512.50	2	2	57666.40	25	3
44465.90	400	2	51000.77	700	2	57004.39	2.5	2	57308.18	2	3	57517.50	400	3	57829.00	25	3
49964.57	25	2	51013.07	700	2	57010.00	2.5	2	57311.75	2	2	57521.50	400	6	57836.05	25	3
44983.87	25	2	51015.12	700	2	57031.12	200	5	57314.75	2	3	57525.59	400	4	57866.40	25	4
50085.05	25	1.5	51018.20	700	2.5	57040.21	200	10	57330.58	100	2	57527.50	400	3	57919.13	110	2
50098.58	110	2	51021.27	700	3.0	57048.73	200	2	57333.78	100	2	57531.79	2	2.5	57923.20	110	2
50104.627	100		51022.81	700	2	57096.45	7	4	57342.08[a]	100	3	57529.60	400	3	57938.93	110	2
50110.497	100		51051.51	700	2	57099.88	100	5	57347.23	400	4	57537.40	400	2	58414.80	400	2
50113.861	400		51085.64	700	3	57101.48	7	1.5	57350.31	400	1.5	57539.50	400	2	58461.23	400	2
50114.975	100		51086.85	700	3	57104.35	106	1.5	57360.00	100	3.5	57541.87	100	2	59045.39	400	3
50125.35	110	2	51095.79	700	2	57105.61	100	10	57364.56	100	3.5	57543.12	2	3.5	59111.17	100	1.2
50137.47	110	3	51106.44	700	2.5	57112.99	100	8	57428.57	100	3	57547.59	100	2.5	59131.00	110	4
50140.00	110	3	51108.98	700	2.5	57117.00	5	1.5	57437.20	100	3	57551.30	100	3	59168.84	110	2
50142.02	110	1.5	51165.23	100	3	57119.30	106	3	57440.472	15		57552.70	100	3	59174.32	110	4
50145.05	110	1.5	51168.80	25	2	57123.90	11	2	57442.097	15		57554.23	110	7	59179.82	400	2
50147.87	110	1.5	51188.40	400	2	57125.55	15	3	57446.82	25	2	57560.19	25	2	59268.55	400	4
50153.13	100	2	51191.50	400	2	57127.35	5	2	57448.495	15		57564.77	25	3	59273.27	400	3
50175.35	100	2	51207.90	400	2	57130.80	15	2	57451.67	100	3	57568.20	25	2	59279.05	400	5
50217.07	150	3	51212.10	400	2	57132.52	5	2	57456.033	15		57570.49	25	2	59290.97	400	2
50218.59[a]	150	4	51213.60	400	2	57134.36	14	2	57459.41	400	4.5	57577.13	24	3	59325.78	400	3
50219.60	150	5	51242.80	400	2.5	57138.85	14	1.5	57462.829	15		57585.50	25	1.5	59392.98	400	3
50223.64	150	2	51248.80	400	2	57142.07	5.5	3	57466.30	400	2.5	57593.60	25	1.5	59418.68	150	3
50230.50	150	3	51268.70	400	3	57148.97	5.5	2	57470.20	400	5	57595.68	25	2.5	59426.95	400	4
50237.10	150	4	52900.48	100	2.5	57165.07	2	2	57471.88	2	2	57599.98	25	1.5	59435.31	400	1.5
50422.339	300		52906.18	100	3	57168.17	106	5	57473.39	2	2.5	57603.13	25	2	59443.60	400	2
50724.80	700	2	52958.525	350		57174.50	104	3	57475.11	2	1.5	57605.42	25	2	59491.47	400	3
50941.83	500	3	52977.775	500		57187.15	106	5	57478.55	2	1.5	57607.93	25	2	59872.41	107	4
50947.68	850	2	52979.390	500													

a : Only two of the listed lines are known to belong to the spectrum of the assigned conformer (whose lines are listed in tables 2.6 and 2.9): The ($v = 1$ $J = 7_{3,5} \leftarrow 6_{3,4}$) at 50218.59 MHz and the ($v = 1$ $J = 8_{3,6} \leftarrow 7_{3,5}$ at 57342.08 MHz). The other lines probably originate from other glycine conformers in the ground and excited states or from non-identified decomposition products. They are listed for the purpose of further work.

b : The listed frequencies have been measured with a stabilized klystron. When three decimals are given, the measurement has been made with a time constant of 8s and with up-and down-scans. The other ones have been measured with a time constant of 1s.

c : The voltage, V, was applied on plates spaced by 0.5".

TABLE 2.4

Observed R-band lines

frequency (MHz)	V^a (V)	S/N	frequency (MHz)	V^a (V)	S/N	frequency (MHz)	V^a (V)	S/N	frequency (MHz)	V^a (V)	S/N	frequency (MHz)	V^a (V)	S/N	frequency (MHz)	V^a (V)	S/N
26542	100	2	28832	400	1.5	28919	400	2	35037	700	2	35565	100	1.3	35898	100	1.5
26558	100	1.5	28834	400	1.5	28926	400	1.1	35044	700	2	35669	100	1.3	35904	100	1.8
26568	100	1.5	28841	400	1.5	33514	230	2	35195	700	2	35680	400	2	35925	100	1.5
26915	100	1.5	28843	400	2	33818	230	1.5	35231	500	2.5	35695	100	1.3	35940[c]	150	2.0
27164.5	100	1.5	28845	400	1.5	33835	230	1.5	35232	700	2	35730.5	100	2	35960	100	1.5
27175	100	1.5	28847	400	1.1	33846	230	1.5	35247	700	2	35732.5	200	2	35994	400	1.5
27208	100	1.5	28858	400	2	34128	230	1.5	35268	500	1.5	35742.5[b]	200	2.5	36020	400	1.5
27224.5	100	1.5	28865	400	1.5	34159.5	230	1.5	35290	700	2	35748	200	4	36022	100	2
27231	100	2	28867	400	1.8	34316.5	230	2	35306	700	2	35758	100	2	36059.	400	2
27296	100	1.3	28880	400	1.1	34534	700	1.5	35308	500	2	35779.5	100	2	36100	100	1.5
28728	400	2	28886	400	1.5	34620	700	1.5	35328.5	400	1.5	35798	100	2	36164	100	1.8
28749	400	1.2	28887	400	1.1	34712	700	1.5	35333.5	400	1.5	35800	100	2	36352	400	1.5
28770	400	1.5	28895.5	400	1.5	34866	700	1.5	35336	400	2	35805	100	2	36388	100	1.3
28781	400	1.2	28898	400	1.5	34870	700	1.5	35363	400	1.5	35822	400	3	36460	100	1.3
28789	210	1.5	28901	400	1.5	34910	230	1.5	35394	400	1.5	35858	400	2.5	36477	100	1.3
28795	210	2	28907.5	400	1.5	35002	700	2	35405	400	1.5	35862	100	2	37143	100	1.3
28800	400	1.5	28915	400	1.1	35024	700	2	35527	400	1.5	35885	100	1.5			

a : The voltage, V, was applied on plates spaced by 0.5".

b : The ($v = 0$ $J = 5_{3,3} \leftarrow 4_{3,2}$) of glycine (4).

c : The ($v = 0$ $J = 5_{3,2} \leftarrow 4_{3,1}$) of glycine (4).

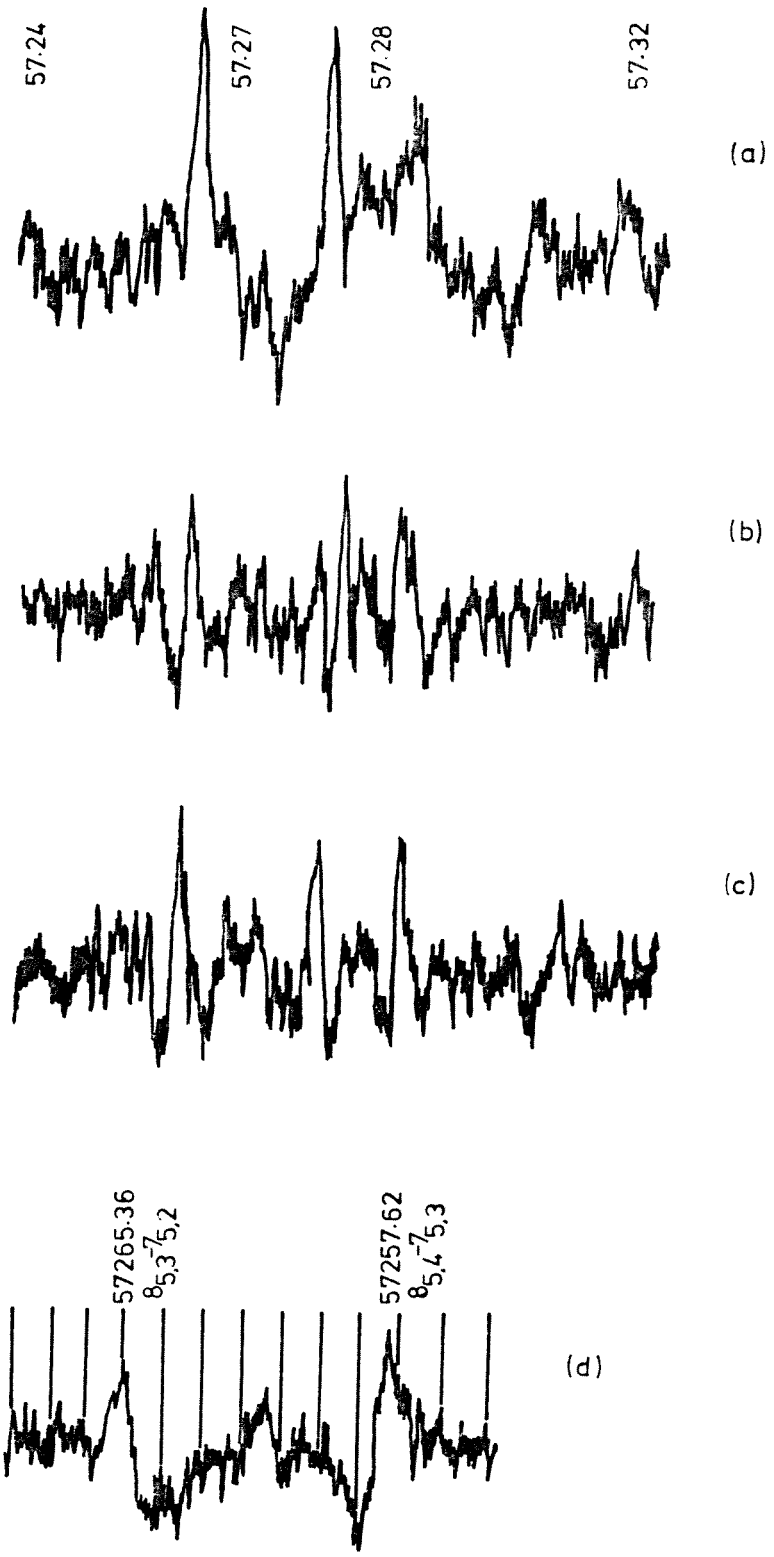

Fig. 2.8 Some observed lines.

The spectrum (d) has been recorded with a phase-stabilized klystron. The applied modulation field was 79 V cm^{-1} for (a) and 2 V cm^{-1} for the other ones. In all cases, the time constant was 1 s.

recorded consecutively without any external change in the experimental conditions. Phase-locked klystrons offered more reproducibility (fig. 2.8d) and precise measurements of frequencies. They have been used systematically over the main regions of lines which had been observed without klystron stabilization. Most of the observed lines have been detected with F and E band klystrons, operated in a double lock system, referenced to a 50 MHz Micro-Now model 101 D and with 60 MHz phase lock IF signals. The problem of jump between locks has been eliminated, first by recording spectra of the same frequency range for different series of locking frequencies and then by using a transfer oscillator (cf. section 2.3.1). Table 2.5 lists some measured line frequencies.

2.3.4 *Assignment of the ground vibrational state of one conformer*

The starting point of the assignment has been the observation at 2.0 V cm^{-1} of two lines separated by 8 MHz around 57261 MHz (see Fig. 2.8d). These lines were predicted from the glycine (4) model, to appear about 400 MHz lower in frequency, with a separation of 4 MHz and a fast Stark effect. The transitions involved are the $8_{5,4} \leftarrow 7_{5,3}$ and $8_{5,3} \leftarrow 7_{5,2}$. The lower and upper levels are respectively 2.3 and 9.8 MHz apart (as calculated from the rotational constants experimentally determined). This is a case of near degeneracy, where the interaction matrix elements $\langle 8_{5,4}|\mathcal{H}_E|8_{5,3}\rangle$ and $\langle 7_{5,3}|\mathcal{H}_E|7_{5,2}\rangle$ cause the strongest contributions to the Stark shifts. ($\mathcal{H}_E$ is the Hamiltonian for the interaction between the Stark field and the molecular dipole moment.)

Fig. 2.9 gives a schematic view of the energy levels involved in the (J=8←7) $^aR_{01}$ series of transitions, with the Stark effect of one M component drawn as a function of the applied electric field. The numbers indicate the experimental values. As expected for a fairly near

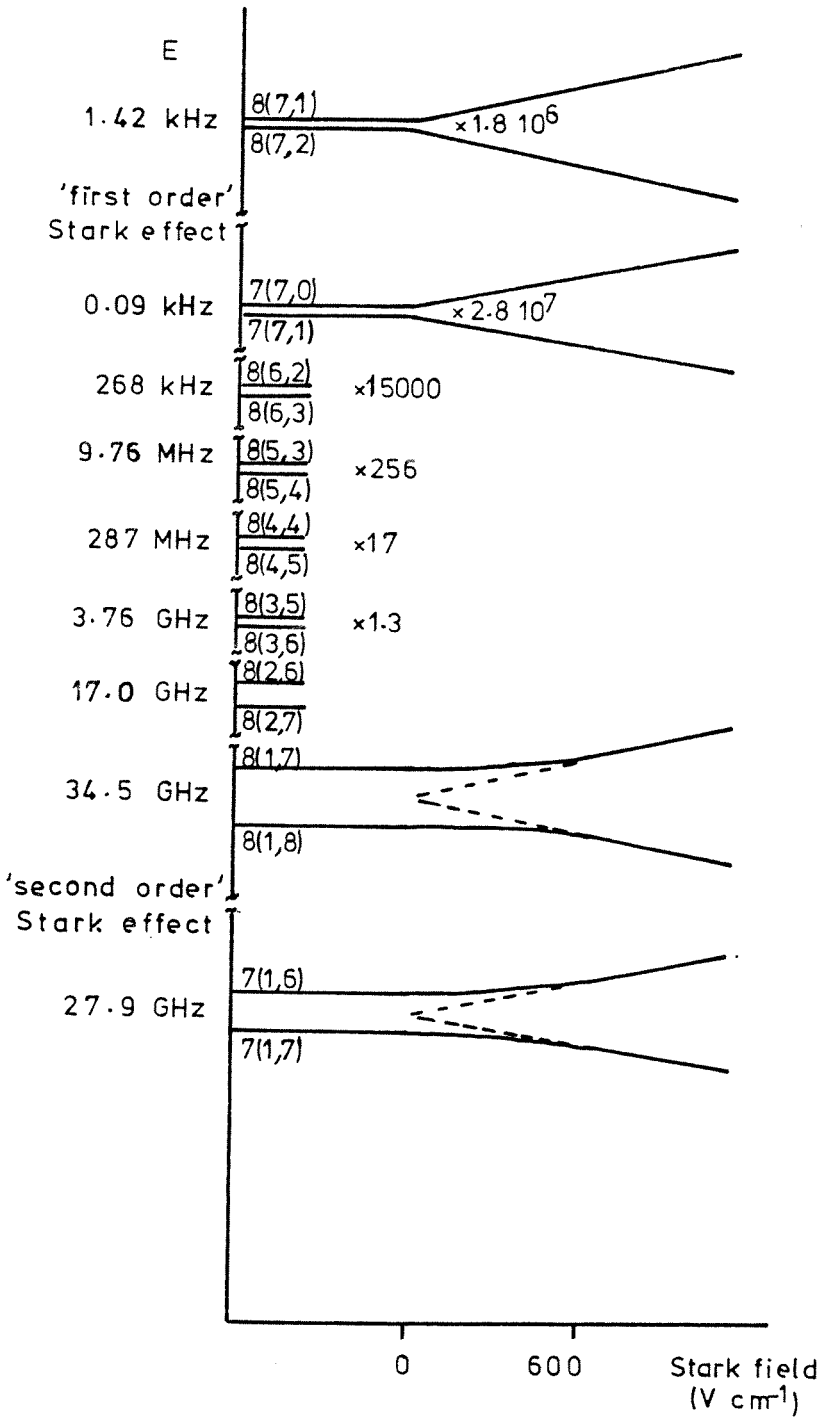

Fig. 2.9 A schematic view of the Stark energy levels of glycine.

For clarity the J = 7 levels are not drawn between $J_{K_a} = 7_7$ and $J_{K_a} = 7_1$ and only one M component is represented.

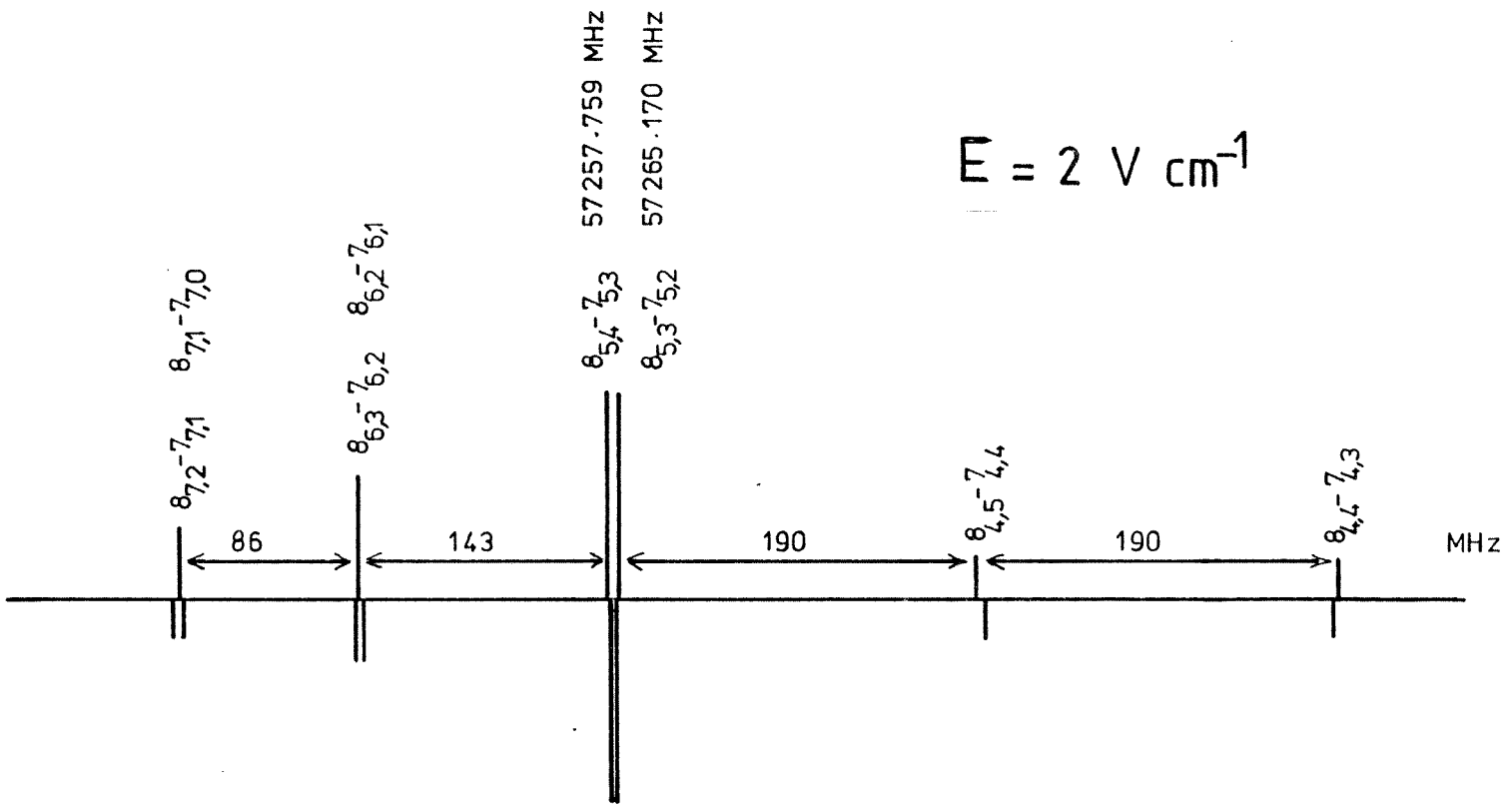

Fig. 2.10 The pattern of high K_a lines of glycine.

prolate symmetric top, the low K_a doublet levels are much further apart than the high K_a ones. Consequently the Stark energies of the low K_a levels can be calculated with the conventional perturbation method, and are proportional to E^2, but the Stark energies of the high K_a levels are obtained by solving the two by two matrix for two nearby levels. A smooth transition is thus observed from a "second-order" to a linear "first-order" type of Stark effect. At 2.0 V cm^{-1} the transitions involving the (K_a = 7, 6, 5 and 4) doublets are already modulated. However the (K_a = 4) transitions connect states which are not so degenerate and they are only partially modulated. Consequently as seen on fig. 2.10, their intensities are lower than those of the (K_a = 7, 6 and 5) doublets which show the expected progression.

A similar pattern of high K_a lines has been recognized around 50 GHz, at 300 MHz higher than the frequency predicted from the glycine (4) model. These two series of high K_a lines were not sufficient to obtain the three rotational constants. Only the value of (B+C) could be determined. In order to obtain B and C independently it has been necessary to observe the remaining lines of the series. The asymmetry splitting being wider for low K_a levels, the A constant could also be determined from low K_a transitions and essentially from the (K_a = 2). With an experimental linewidth of 2 to 3 MHz a detectable intensity of the (K_a = 2 and 1) lines required a minimum modulation which was higher than the voltage breakdown, about 400 and 600 V cm^{-1}. The (K_a = 0) levels which, in any case, exhibit a "second-order" type of Stark effect were connected in a transition which necessitated about 1000 V cm^{-1} to be observable. More than a hundred least squares fit calculations of the rotational parameters have been attempted before a sufficient Stark voltage could be applied. The Q branch lines, which would have

improved the value of the rotational constant A, were too weak to be observed.

2.3.5 *Rotational Parameters*

Frequencies of the lines included in the least squares fit calculations are listed in table 2.6. Most of them are averaged measurements of lines observed with a chart recorder during increasing and decreasing frequency scans. The time constant was 8 s. The standard deviation includes effects of both random measurements and tracking errors. Where "c.av." is written in comments, the lines have been observed by computer averaging with a time constant of 0.2 s and during the indicated time t. Their frequencies have been measured with a Lorentzian fit procured by the program CATRED. In this case, the standard deviation has been determined from the scatter of results produced by repetitive attempts to measure the frequency with the interactive curve fitting program. Nineteen of these lines (marked with an a) have been used in the program LSTSQ5 for the determination of the rotational constants A, B, C and of the symmetric top centrifugal distorsion constants D_J and $D_{J,K}$ (table 2.7)*. Subsequently, following the development of the program LSQTAU, all twenty seven lines, including those observed at a later stage during the analysis of the dipole moment, have been used to determine the asymmetric top rotational parameters (table 2.8).

Two months after the publication of this work, a similar work on glycine has been published by R.D. Suenram and F.J. Lovas. As seen in table 2.7 and 2.8, their rotational parameters are in perfect agreement with those obtained in this work. An LSQTAU calculation on their forty three selected lines gave a standard deviation of the fit

---

* In tables 2.7, 2.8 and 2.10, the standard deviation of κ has been calculated from the standard deviations and covariances of A, B and C.

TABLE 2.6

Transitions included in the least squares analyses

transition[b]	measured frequency MHz	measured standard deviation MHz	Freq. calc. with asymm. top parameters MHz	$\Delta\nu$(meas-calc) MHz	comments
$^{a}8_{7} \leftarrow 7_{7}$	57028.055	.171	57027.940	.115	
$^{a}8_{6} \leftarrow 7_{6}$	57114.496	.130	57114.660	-.164	
$^{a}8_{5,4} \leftarrow 7_{5,3}$	57257.759	.068	57257.719	.040	
$^{a}8_{5,3} \leftarrow 7_{5,2}$	57265.170	.150	57265.222	-.052	
$^{a}8_{4,5} \leftarrow 7_{4,4}$	57454.737	.208	57454.838	-.101	
$^{a}8_{4,4} \leftarrow 7_{4,3}$	57644.535	.163	57644.381	.154	
$^{a}8_{3,6} \leftarrow 7_{3,5}$	57216.630	.150	57216.514	.116	
$^{a}8_{3,5} \leftarrow 7_{3,4}$	59137.375	.375	59137.370	.005	
$^{a}8_{2,7} \leftarrow 7_{2,6}$	55133.355	.041	55133.384	-.029	
$^{8}2_{,6} \leftarrow 7_{2,5}$	60539.526	.015	60539.549	-.023	c.av., t = 12 mn
$^{a}8_{1,8} \leftarrow 7_{1,7}$	50757.260	.122	50757.236	.024	
$^{a}8_{1,7} \leftarrow 7_{1,6}$	57341.017	.132	57340.948	.069	
$^{8}0_{,8} \leftarrow 7_{0,7}$	51035.100	.100	51035.049	.051	

TABLE 2.6 (cont'd)

transition[b]	measured frequency MHz	measured standard deviation MHz	Freq. calc. with asymm. top parameters MHz	$\Delta\nu$(meas-calc) MHz	comments
$^{7}_{6}\ \leftarrow {}^{6}_{6}$	49910.831	.019	49910.708	.123	
[a] $^{7}_{5,3} \leftarrow {}^{6}_{5,2}$	50007.857	.092	50007.715	.142	
[a] $^{7}_{5,2} \leftarrow {}^{6}_{5,1}$	50009.365	.080	50009.614	-.241	
[a] $^{7}_{4,4} \leftarrow {}^{6}_{4,3}$	50162.255	.014	50162.477	-.221	
[a] $^{7}_{4,3} \leftarrow {}^{6}_{4,2}$	50233.425	.070	50233.487	-.062	
[a] $^{7}_{3,5} \leftarrow {}^{6}_{3,4}$	50107.640	.160	50107.539	.101	
[a] $^{7}_{3,4} \leftarrow {}^{6}_{3,3}$	51177.070	.140	51177.026	.044	
$^{7}_{2,6} \leftarrow {}^{6}_{2,5}$	48578.603	.034	48578.667	-.064	
[a] $^{7}_{2,5} \leftarrow {}^{6}_{2,4}$	52945.856	.019	52945.853	.003	
[a] $^{7}_{1,6} \leftarrow {}^{6}_{1,5}$	51027.741	.134	51027.793	-.052	
$^{9}_{0,9} \leftarrow {}^{8}_{0,8}$	56984.731	.015	56984.794	-.063	c.av., t = 4 mn
$^{10}_{0,10} \leftarrow {}^{9}_{0,9}$	62 959.128	.015	62959.114	.014	c.av., t = 5 mn
$^{4}_{2,3} \leftarrow {}^{3}_{2,2}$	28215.508	.015	28215.508	.049	c.av., t = 2093 mn
$^{4}_{2,2} \leftarrow {}^{3}_{2,1}$	29398.600	.015	29398.544	.055	c.av., t = 1020 mn

a : transitions included in the least-squares fit of symmetric top centrifugal distorsion constants.
b : when K_c is omitted, the transition exists as a degenerate pair.

TABLE 2.7

Experimentally determined rotational and symmetric top centrifugal distorsion constants of glycine

A	10129.20 (24)	MHz
B	4071.449 (18)	MHz
C	3007.511 (25)	MHz
D_J	.00052 (16)	MHz
D_{JK}	.00548 (18)	MHz
κ	-.7012 (48)	

Standard deviation of the fit = .140 MHz

Correlation matrix

	A	B	C	D_J	D_{JK}
A	1.000	.320	-.402	-.062	-.222
B		1.000	.526	.823	-.034
C			1.000	.888	-.080
D_J				1.000	-.216
D_{JK}					1.000

Publication: J.C.S. Chem. Comm. p 547, 05 July 1978,
received by the journal on 21 February 1978

TABLE 2.8

Experimentally determined asymmetric top rotational parameters of glycine

Watson's determinable parameters (MHz)

	This work		NBS [a]	
A''	10131.09	(49)	10130.47	(62)
B''	4071.488	(26)	4071.473	(36)
C''	3007.484	(24)	3007.538	(44)
τ_{aaaa}	-.93	(31)	-.094	(100)
τ_{bbbb}	-.00144	(93)	-.00298	(52)
τ_{cccc}	-.00158	(51)	-.00175	(51)
τ_1	-.0288	(15)	.02852	(64)
τ_2	-.0049	(11)	.00689	(44)
τ_3 [b]	-.149	(65)	.033	(36)

Kivelson-Wilson parameters (MHz)

A'	10131.09	(49)
B'	4071.473	(26)
C'	3007.483	(24)
τ'_{aabb}	-.0027	(56)
τ'_{bbcc}	.0051	(17)
τ'_{ccaa}	-.0312	(47)

Standard deviation of the fit (MHz)

.121	.390

TABLE 2.8 (cont'd)

Correlation matrix

	A"	B"	C"	τ_{aaaa}	τ_{bbbb}	τ_{cccc}	τ_1	τ_2
A"	1.00	.57	-.54	-.83	-.11	.15	-.12	.48
B"		1.00	-.71	-.32	-.81	.58	-.18	.19
C"			1.00	.35	.58	-.79	-.41	-.51
τ_{aaaa}				1.00	.02	.19	-.10	-.77
τ_{bbbb}					1.00	-.50	-.13	-.23
τ_{cccc}						1.00	.13	-.06
τ_1							1.00	.68
τ_2								1.00

Inertia defect (amu Å^2)

$$\Delta = I_c - I_a - I_b = -5.9760 \quad (40)$$

Ray asymmetry parameter

$$\kappa = -.701 \ (23)$$

a : Publication: J. Mol. Spectrosc. 72, 372, Sept. 1978,
received by the journal on 22 May 1978.

b : τ_3 is fixed by the planarity conditions.

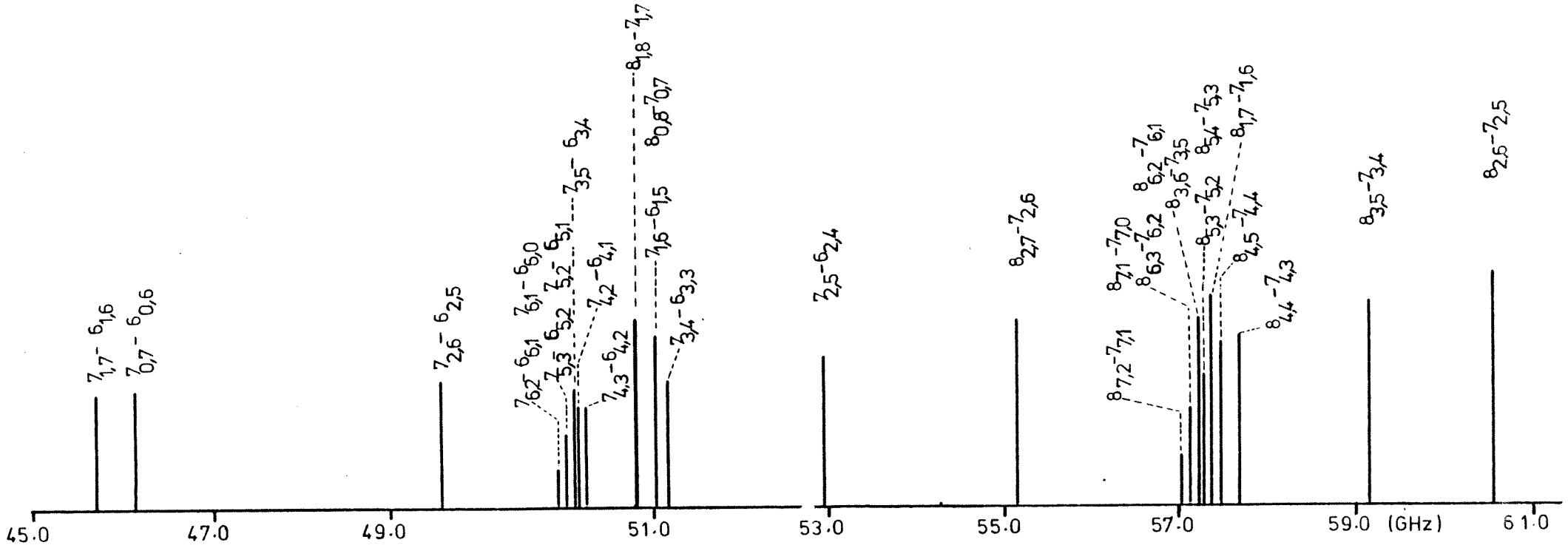

Fig. 2.11 Stick spectrum of the measured (J = 8←7) and (J = 7←6) lines of glycine.

three times higher than which one calculated in this work. This is due to the fact that the NBS lines are much wider. The centrifugal distorsion constants are more precisely determined by the NBS analysis, because they have been calculated from measurements of higher frequency lines.

Fig. 2.11 represents the stick spectrum of the (J=8←7) and (J=7←6) $^aR_{01}$ branches. It shows how the lines are distributed along the microwave frequency range, and the steady increase in intensity from low to high K_a transitions. The asymmetry is seen in the mixing of the low K_a (J=8←7) transitions into the (J=7←6) bunch of lines.

2.3.6 *Frequency of the C-C Torsional Vibration*

As expected, line splitting due to internal rotation of the amino and carboxyl groups have not been observed in the spectrum of the ground state. However the torsional vibration around the bond C-C has been detected in two excited vibrational states. These vibrational satellites have been recognized at higher frequencies with respect to the ground state transitions, via the doublet ($J_{K_a} = 8_5 \leftarrow 7_5$), which was modulated at 2.0 V cm^{-1} with converging Stark lobes and a separation of around 7.5 MHz. Because of the voltage breakdown, observation of the complete series could not be done. Table 2.9 lists the observed frequencies of these two states. In the case of the first excited state, a comparison is done with values predicted from the assignment reported by R.D. Suenram and F.J. Lovas [45]. An LSQTAU fit on the thirty four selected NBS lines gave the Kivelson-Wilson parameters required by the spectral program prediction WANGP6. They are listed in table 2.10. These satellite lines fit a rigid rotor spectrum corrected for small centrifugal distorsion. However two transitions at 86.45 GHz

TABLE 2.9

Measured and calculated frequencies of glycine transitions in vibrationally excited states

transition	measured frequency v=0 MHz	measured frequency v=1 MHz	calculated frequency[a] v=1 MHz	measured frequency v=2 MHz
$8_7 \leftarrow 7_7$	57028.055 (171)	57157.917 (15)	57157.94	
$8_6 \leftarrow 7_6$	57114.496 (130)	57243.971 (15)	57244.25	57364.169 (15)
$8_{5,4} \leftarrow 7_{5,3}$	57257.759 (68)	57386.729 (15)	57386.94	57510.006 (15)
$8_{5,3} \leftarrow 7_{5,2}$	57265.170 (150)	57394.434 (15)	57394.53	57517.979 (15)
$8_{4,5} \leftarrow 7_{4,4}$	57454.737 (208)	57583.137 (15)	57583.23	
$8_{4,4} \leftarrow 7_{4,3}$	57644.535 (163)	57774.947 (15)	57774.25	
$7_{5,3} \leftarrow 6_{5,2}$	50007.857 (92)	50120.945 (95)	50120.74	
$7_{5,2} \leftarrow 6_{5,1}$	50009.365 (80)	50122.437 (85)	50122.66	

a : calculated from transitions observed at higher frequencies [45].

TABLE 2.10

Experimentally determined rotational parameters of the first vibrationally excited state of glycine[a]

Watson's determinable parameters (MHz)

A"	10080.5	(11)
B"	4077.247	(89)
C"	3017.79	(11)
τ''_{aaaa}	-.18	(21)
τ''_{bbbb}	-.0021	(13)
τ''_{cccc}	-.0033	(12)
τ_1	-.0212	(12)
τ_2	-.00499	(92)
τ_3	-.003	(42)

Kivelson-Wilson parameters (MHz)

A'	10080.5	(11)
B'	4071.240	(89)
C'	3017.79	(11)
τ'_{aabb}	-.0066	(41)
τ'_{bbcc}	-.0011	(13)
τ'_{ccaa}	-.0135	(37)

Standard deviation of the fit (MHz)

.395

TABLE 2.10 (continu'd)

Correlation matrix

	A"	B"	C"	τ''_{aaaa}	τ''_{bbbb}	τ''_{cccc}	τ_1	τ_2
A"	1.00	.81	-.80	-.82	-.57	.75	.29	.63
B"		1.00	-.98	-.56	-.93	.96	.65	.75
C"			1.00	.55	.91	-.98	-.71	-.78
τ''_{aaaa}				1.00	.37	-.43	-.26	-.72
τ''_{bbbb}					1.00	-.89	-.83	-.79
τ''_{cccc}						1.00	.65	.67
τ_1							1.00	.85
τ_2								1.00

Inertia defect (amu Å^2)

$\Delta = I_c - I_a - I_b = -6.6176$ (86)

Ray asymmetry parameter

$\kappa = -.700$ (31)

a : These parameters have been calculated from the frequencies of thirty four lines measured, between 75 and 115 GHz, by R.D. Suenram and F.J. Lovas [45]. These authors reported the Watson's parameters solely.

TABLE 2.11

Frequency of the C-C torsional vibration in some acids and in glycine

Molecule	Intensity method cm^{-1}	Inertia defect method cm^{-1}	Divers methods cm^{-1}	Ref.
pyruvic acid $CH_3COCOOH$	101 ± 9	89		27
glyoxylic acid HCOCOOH	167 ± 12	112	122[b]	49
s-cis acrylic acid CH_2=CHCOOH	105 ± 20	88		29
s-trans acrylic acid CH_2=CHCOOH	95 ± 20	90		29
cis propionic acid CH_3CH_2COOH		74[a]	64 ± 3[c]	30
methoxyacetic acid CH_3OCH_2COOH		91 or 86		25
glycine NH_2CH_2COOH	114 ± 20	104		this work
chloroacetic acid $CH_2ClCOOH$		62		50

a : value calculated in this work.

b : deduced from an I.R. combination mode.

c : based on variation of rotational constants, relative intensities and inertia defect.

have not been identified because of perturbation and could suggest some internal rotation effects.

The value of the lowest vibrational frequency could be approximately determined by the intensity method and by means of inertia defects considerations (table 2.11). A comparison with similar calculations for other molecules show that these methods are reliable within 20%. The intensity measurements of the same transition, in two different vibrational states, present some difficulties of reproducibility because of reflections of microwave in the transition line, variation of detector efficiency with frequency, variation of sample pressure or saturation of lines [46]. Because of the too small intensity variation, within experimental errors, between the ground and the first excited states, measurements have been carried out between the ground and the second excited states. Energy differences between these states have been derived by assuming that relative intensities are proportional to the Boltzmann factor.

The calculation from the observed change in inertia defect [47,48,49] seems more accurate. $\omega(cm^{-1}) = - 67.5/(\Delta_{1exc.} - \Delta_{gr.})$. Considering the negative change in the inertia defect ($\Delta_{1exc} - \Delta_{gr} = - 0.65 \cup \AA^2$), this vibration has been assigned to the lowest out-of-plane mode [48], i.e. the torsional vibration around the C-C bond. Further support for this interpretation may be obtained from a comparison with the frequency of the C-C torsional vibration of other acids. This value appears to lie within 20% around 90 cm^{-1}, for most acids listed in table 2.11. Thus the lowest vibration frequency of glycine has been assigned to the C-C torsional vibration with the value

$$\omega = 104 \pm 20 \text{ cm}^{-1} .$$

2.3.7 *Dipole moment component along the a-axis*

The dipole moment component along the a limiting prolate rotor axis of the assigned conformer was predicted to be much higher than the components along the two other axes. It has been confirmed by the detection of a-type transitions solely. Because a parallel plate transmission line procures homogeneous Stark fields, precise measure--ments of the (ΔM_J=0) Stark components have been made and accurate values of the dipole moments have been determined.

Since the individual Stark components of the species (J=8←7) and (J=7←6) were not observable, the rate of growth technique [51] could have been applied. It consists in the observation of the change in line shape, as a function of the amplitude of the modulation field. However preference has been given to the observation, by computer averaging, of a low J transition, even if the intensity of the main line was much lower. The frequencies of the $^aR_{01}$ (J=4←3) branch lie just above the cell cut-off frequency (21.1 GHz). The two most intense transitions of this series are first the $4_{1,3}\leftarrow 3_{1,2}$ and second the $4_{0,4}\leftarrow 3_{0,3}$. However, even with 300 V cm^{-1} of modulation and 700 kHz of linewidth, their Stark structure is not resolved. The transition $4_{2,3}\leftarrow 3_{2,2}$ is 0.7 times less intense than the $4_{1,3}\leftarrow 3_{1,2}$, when fully modulated, but requires only a modulation of 63 V cm^{-1} to show a spectrum with three Stark components resolved on a width of 13 MHz. Consequently this transition has been chosen. Its observed spectrum is shown in fig. 2.12. Thirty five hours have been necessary to obtain a resolution of the Stark components (M_J=1) and (M_J=2), and a suggestion of the (M_J=3). The modulation of the (M_J=0) component would have increased the intensity of the main line by 35% and reduce the integration time by a factor of 1.8. Unfortunately a shift of 600 kHz only, required 315 V cm^{-1} which was the value of the breakdown field.

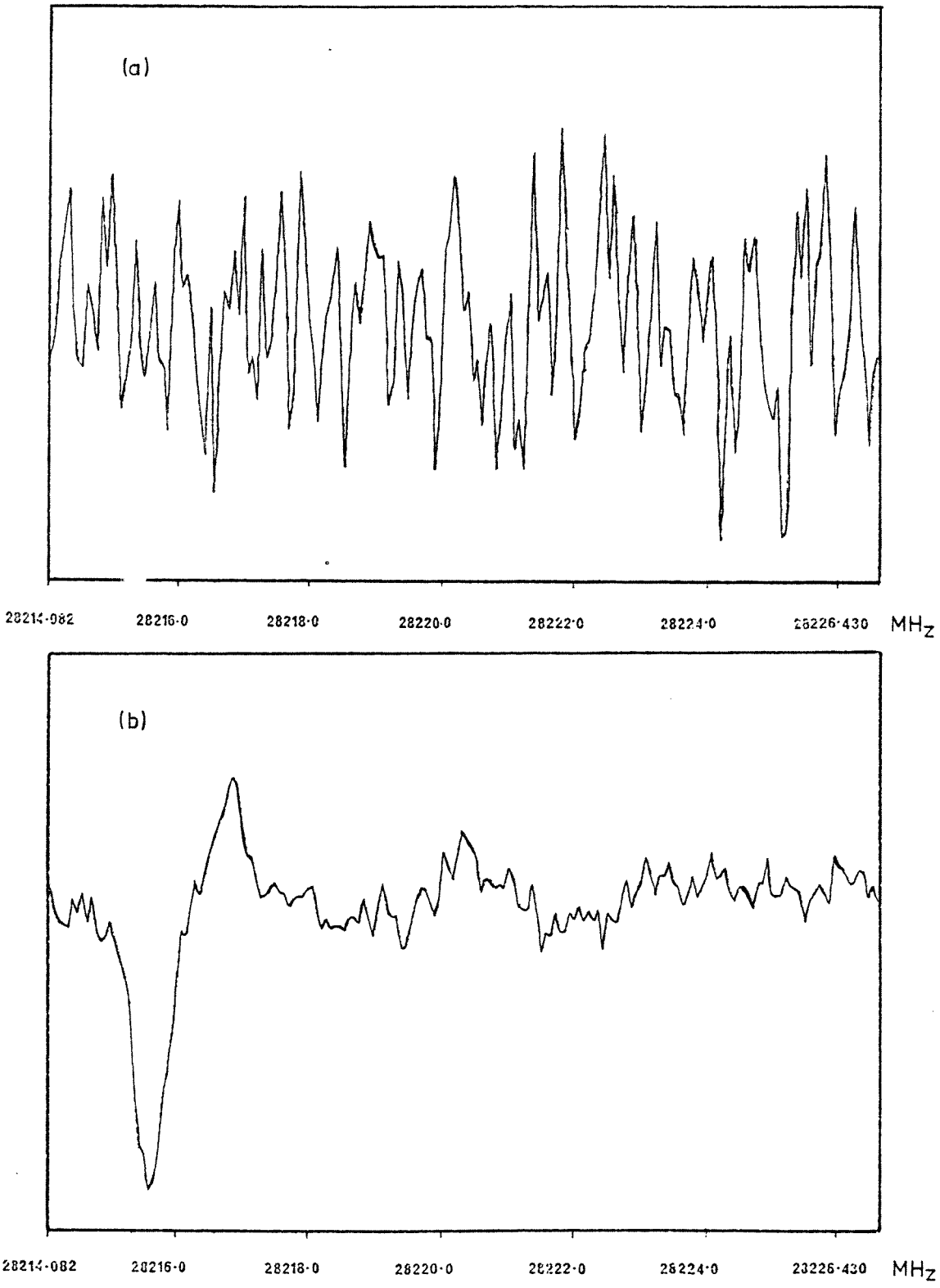

Fig. 2.12 The ($J_{K_aK_c} = 4_{2,3} \leftarrow 3_{2,2}$) transition of glycine.

(a) spectrum from one scan.

(b) spectrum from an average of 1820 scans of 1.15 mn each.

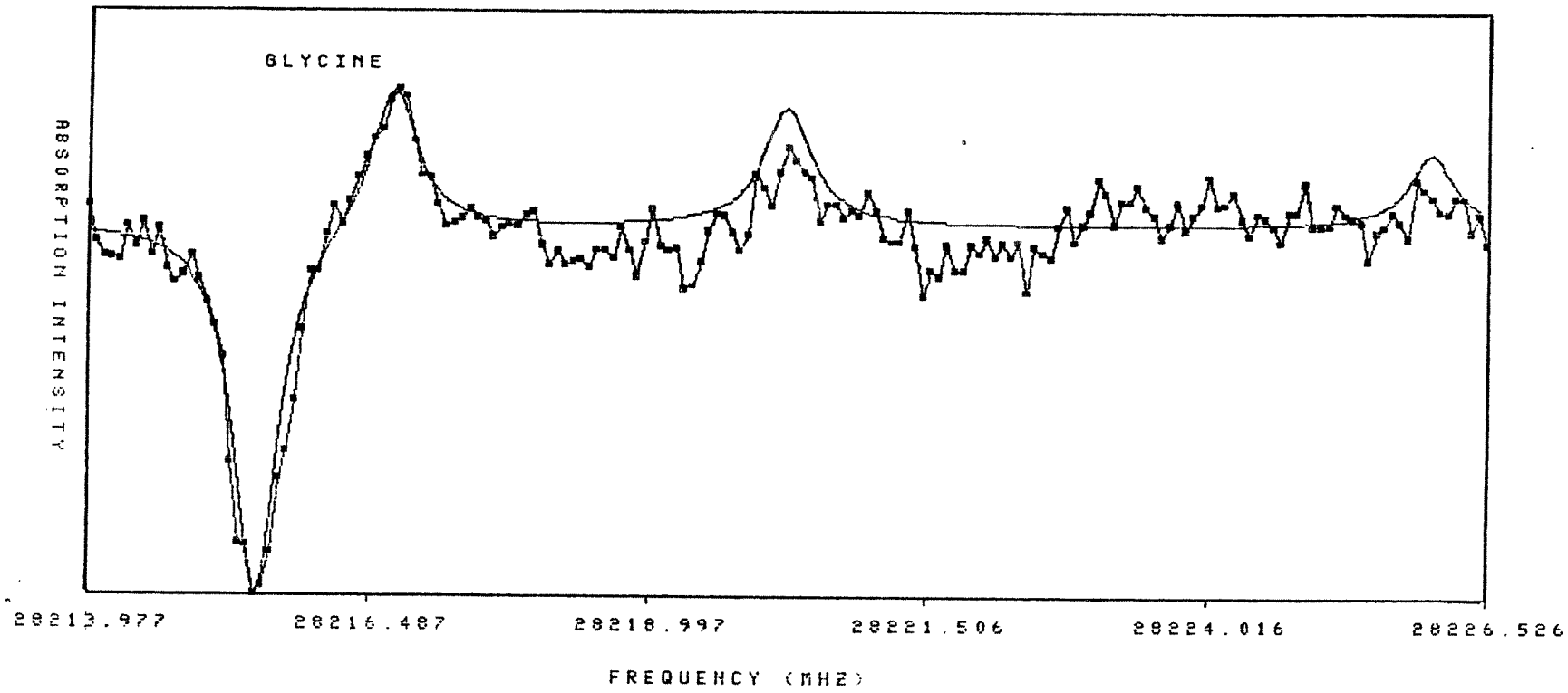

Fig. 2.13 Determination of the μ_a dipole moment component with the transition ($J_{K_aK_c} = 4_{2,3} \leftarrow 3_{2,2}$). Plots of calculated and experimental spectra.

The equipment consisted of a 30V10 OKI klystron set in a double phase-lock. Because of the inconsistent stability of the lock, one bit of the analog to digital converter has been used as a flag to recognize, during the data reduction, the spectra which were recorded with an out-of-lock klystron. By lowering the sublimation temperature (the surrounding temperature of the sample holders was 453 K) the linewidth could be narrower than in earlier scans, and the frequencies of the Stark components have been measured more precisely. The Hewlett-Packard square wave generator had a stabilized power supply.

The component μ_a has been measured by means of the program SFIT, written especially for the determination of the dipole moment components of glycine. Fig. 2.13 is a duplicate of the superposed experimental and calculated spectra, drawn by the plotting option.

$$\mu_a = 5.57 \pm .01 \text{ debyes}$$

The standard deviation has been determined from the scatter of results produced by repetitive attempts to measure the dipole moment with the interactive curve fitting SFIT program.

2.3.8 *Dipole moment component along the b-axis. An indirect analysis.*

It has not been possible to observe pure b-type transitions. The determination of the dipole moment component μ_b has been achieved with the analysis of a R branch a-type transition dependent in μ_b, i.e. a $^aR_{01}$ transition which has one level in common with a near degenerate pure b-type transition.

Table 2.12 gives a list of pure b-type transitions, with frequencies below 5.0 GHz. These transitions link a rotational level J_K to the rotational level $(J+1)_{(K-1)}$. Thirteen transitions of the table

TABLE 2.12

Pure b--type transitions

transition	frequency (MHz)
$^{9}_{1,9} \leftarrow {}^{8}_{2,6}$	5.667
$^{10}_{5,6} \leftarrow {}^{9}_{6,3}$	133.201
$^{10}_{5,5} \leftarrow {}^{9}_{6,4}$	232.917
$^{7}_{5,3} \leftarrow {}^{8}_{4,4}$	1038.052
$^{7}_{5,2} \leftarrow {}^{8}_{4,5}$	1327.787
$^{12}_{6,7} \leftarrow {}^{11}_{7,4}$	1543.318
$^{12}_{6,6} \leftarrow {}^{11}_{7,5}$	1576.087
$^{5}_{2,4} \leftarrow {}^{4}_{3,1}$	1688.437
$^{2}_{2,0} \leftarrow {}^{3}_{1,3}$	1928.114
$^{14}_{3,11} \leftarrow {}^{15}_{2,14}$	2106.550
$^{5}_{4,2} \leftarrow {}^{6}_{3,3}$	2144.569
$^{4}_{1,4} \leftarrow {}^{3}_{2,1}$	2292.283
$^{5}_{4,1} \leftarrow {}^{6}_{3,4}$	2924.774
$^{14}_{7,8} \leftarrow {}^{13}_{8,5}$	2937.846
$^{14}_{7,7} \leftarrow {}^{13}_{8,6}$	2948.285
$^{3}_{3,1} \leftarrow {}^{4}_{2,6}$	2996.360
$^{14}_{9,6} \leftarrow {}^{15}_{8,7}$	3273.315
$^{14}_{9,5} \leftarrow {}^{15}_{8,8}$	3274.415
$^{8}_{1,8} \leftarrow {}^{7}_{2,5}$	3718.450
$^{7}_{3,5} \leftarrow {}^{6}_{4,2}$	4259.699
$^{3}_{1,2} \leftarrow {}^{2}_{2,1}$	4573.981
$^{12}_{8,5} \leftarrow {}^{13}_{7,6}$	4648.090
$^{12}_{8,4} \leftarrow {}^{13}_{7,7}$	4651.624
$^{14}_{2,13} \leftarrow {}^{13}_{3,10}$	4800.565
$^{3}_{3,0} \leftarrow {}^{4}_{2,3}$	4818.378
$^{9}_{2,7} \leftarrow {}^{10}_{1,10}$	4979.224

present the energy level configuration described in (a) below and thirteen other transitions show the (b) configuration.

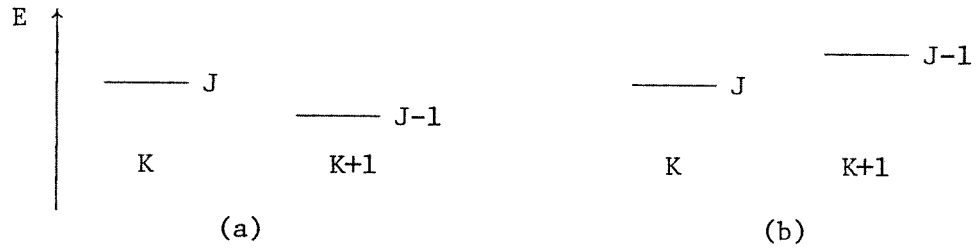

The value of J for which the near degeneracy occurs can be calculated by finding the minimum value of $(E(J)_K - E(J-1)_{(K+1)})$. Using the energy expression for a symmetric top, the lowest J transitions showing this type of degeneracy are found for $J = \frac{A - (B+C)/2}{B + C}$. However the glycine molecule is too far from a symmetric top to obtain accurate J values with this formula and precise solutions of the Hamiltonian for an asymmetric top have to be calculated.

Fortunately the two near degenerate states $9_{1,9}$, $8_{2,6}$ are involved in a-type transitions which were observable with an R band cell. The two $^aR_{01}$ transitions from and to the state $9_{1,9}$ are slightly dependent in μ_c since the two states $9_{1,9}$ and $9_{0,9}$, connected by a pure c-type transition, are only 180 MHz apart (fig. 2.17). This case of Stark effect calculation, where one level is involved in two near degeneracies, requires the solution of a 3×3 matrix and is not considered in WANGLY. Hence the transitions out and into the level $9_{1,9}$ could not be studied.

The transition $9_{2,7} \leftarrow 8_{2,6}$, at 67857.266 MHz, was not observable with the R band cell, only the transition $8_{2,6} \leftarrow 7_{2,5}$ could be studied. Fields up to 315 V cm^{-1} could be applied. This was not sufficient to resolve the Stark components and only a global shift has been observed. However this global Stark shift was quite μ_b dependent

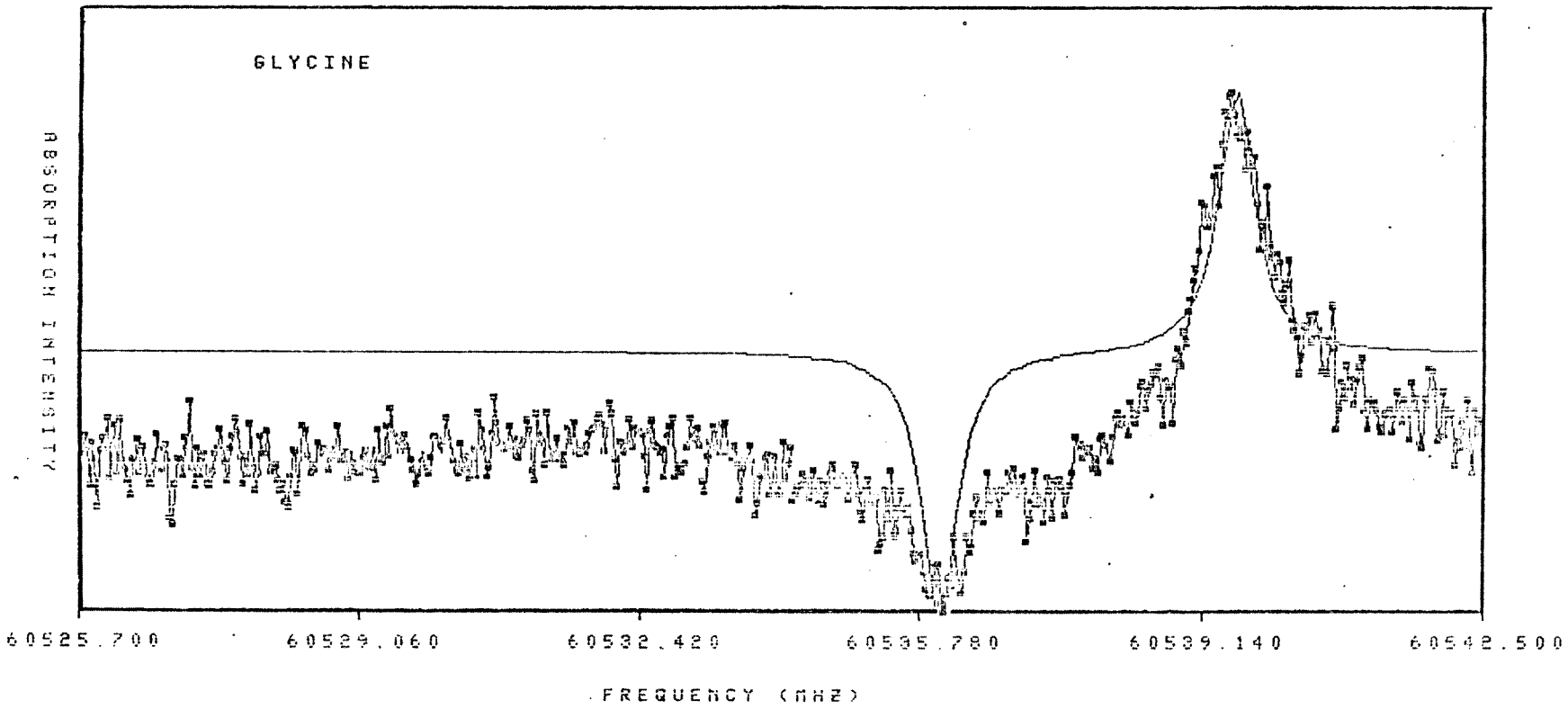

Fig. 2.14 Determination of the μ_b dipole moment component with the transition ($J_{K_aK_c} = 8_{2,6} \leftarrow 7_{2,5}$). Plots of calculated and experimental spectra.

and the value of the dipole moment component along the b-axis could be measured. Experimental spectra taken at 236, 295 and 315 V cm^{-1} led to the following results:

$$\mu_b = 0.32 \pm .01 \text{ debyes} .$$

Fig. 2.14 shows the spectrum observed at 295 V cm^{-1} with a surrounding temperature of the sample holders of 478 K. The width of the spectrum is 17 MHz and the FWHH of the line has easily been narrowed to 495 kHz using the improved pumping system described in section 2.4.2. No smoothing function has been applied to the spectrum.

2.3.9 *Dipole moment component along the c-axis. A systematic degeneracy.*

No pure c-type transition was expected to be detected. As in the determination of μ_b, a search for an observable $^aR_{01}$ transition that is dependent in μ_c has been undertaken, i.e. a search for a $^aR_{01}$ transition which has one level in common with a near degenerate pure c-type transition.

A list of pure c-type transitions with frequencies between 0.009 MHz and 1000 MHz is shown in table 2.13. In the contrary to the b-type transitions, the near degeneracies of the energy levels are not always accidental but are due to the fact that the glycine rotor is not far from a prolate symmetric top. As remembered by the asymmetric-symmetric top correlation diagram of energy levels [35], a first-order a-type transition connects a pair of levels which are split by asymmetry, and a first-order c-type transition connects states which would be degenerate if the molecule was an oblate rotor. As expected for an asymmetric top not far from the prolate case, these c-type transitions have the following particularities: their frequencies decrease with J

TABLE 2.13

Pure c-type transitions

transition	frequency(MHz)
$^{16}_{1,16} \leftarrow {}^{16}_{0,16}$	.009
$^{15}_{1,15} \leftarrow {}^{15}_{0,15}$	1.715
$^{14}_{1,14} \leftarrow {}^{14}_{0,14}$	5.004
$^{13}_{1,13} \leftarrow {}^{13}_{0,13}$	11.400
$^{12}_{1,12} \leftarrow {}^{12}_{0,12}$	23.878
$^{11}_{1,11} \leftarrow {}^{11}_{0,11}$	48.054
$^{10}_{1,10} \leftarrow {}^{10}_{0,10}$	94.247
$^{15}_{2,14} \leftarrow {}^{15}_{1,14}$	124.077
$^{10}_{5,6} \leftarrow {}^{9}_{6,4}$	134.033
$^{9}_{1,9} \leftarrow {}^{9}_{0,9}$	180.890
$^{10}_{5,5} \leftarrow {}^{9}_{6,3}$	232.085
$^{14}_{2,13} \leftarrow {}^{14}_{1,13}$	233.722
$^{8}_{1,8} \leftarrow {}^{8}_{0,8}$	338.932
$^{13}_{2,12} \leftarrow {}^{13}_{1,12}$	428.434
$^{7}_{1,7} \leftarrow {}^{7}_{0,7}$	616.685
$^{12}_{2,11} \leftarrow {}^{12}_{1,11}$	764.847

TABLE 2.14

Progression in the frequencies of the c-type transitions

(MHz)

	$16_{1,16} \leftarrow 16_{0,16}$	0.0090				
	$15_{1,15} \leftarrow 15_{0,15}$	1.7150				
	$14_{1,14} \leftarrow 14_{0,14}$	5.0037			$5_{3,3} \leftarrow 5_{2,3}$	30033
J ↑	⋮		$4_{2,3} \leftarrow 4_{1,3}$	14722	$4_{3,2} \leftarrow 4_{2,2}$	31515
	$3_{1,3} \leftarrow 3_{0,3}$	3951.2	$3_{2,2} \leftarrow 3_{1,2}$	16663	$3_{3,1} \leftarrow 3_{2,1}$	32395
	$2_{1,2} \leftarrow 2_{0,2}$	5122.0	$2_{2,1} \leftarrow 2_{1,1}$	18173		
	$1_{1,1} \leftarrow 1_{0,1}$	6057.7				
			←			
			K_c			

TABLE 2.15

Progression in the frequencies of the a-type transitions

(MHz)

	$8_{8,0} \leftarrow 8_{8,1}$	0.00001				
	$7_{7,0} \leftarrow 7_{7,1}$	0.00009				
	$6_{6,0} \leftarrow 6_{6,1}$	0.00186			$5_{3,2} \leftarrow 5_{3,3}$	266.00
J ↑	⋮		$4_{3,1} \leftarrow 4_{3,2}$	67.625	$4_{2,2} \leftarrow 4_{2,3}$	1812.3
	$3_{3,0} \leftarrow 3_{3,1}$	9.7412	$3_{2,1} \leftarrow 3_{2,2}$	629.15	$3_{1,2} \leftarrow 3_{1,3}$	6373.9
	$2_{2,0} \leftarrow 2_{2,1}$	128.20	$2_{1,1} \leftarrow 2_{1,2}$	3191.8		
	$1_{1,0} \leftarrow 1_{1,1}$	1063.9				
			←			
			K_a			

for a given K_c and decrease, for a given J, with increasing values of K_c, as shown on table 2.14. Thus the highest K_c transition of a Q branch series has the smallest frequency of the series. Also these highest K_c transition frequencies are decreasing while J is increasing. A systematic near degeneracy is thus observed in the Q branch of the c-type transitions. It becomes very small when J attains 15 and decreases indefinitely without however vanishing since asymmetric levels of a given J never cross.

The same type of degeneracy is observed in a-type transitions as shown in table 2.15. However since in Q branches, an a-type transition has a smaller frequency than the consecutive c-type one, the near degeneracy occurs at a lower value of J. Some levels with J as low as 8 and 7 are nearly degenerate and contribute in the fast Stark effect observed during the assignment of the spectrum. Such is each J_{K_a} doublet 8_7, 8_6, 8_5, 7_6, 7_5 and 7_4 (cf. section 2.3.4).

Table 2.13 shows also two accidental near degeneracies in R branch transitions. Since these transitions have levels involved also in pure b-type transitions, they have not been considered in the study of the μ_c dipole moment, for the reasons explained in the precedent section.

Two transitions could be observed with R band horns. Their spectra are shown in fig. 2.15 a and b. The surrounding temperature of the sample holders was 503 K. The phase-locked klystrons were the 55 V11 and 60 V12. The spectrum widths are 16 MHz and 17 MHz for the $9_{0,9} \leftarrow 8_{0,8}$ and $10_{0,10} \leftarrow 9_{0,9}$ respectively. No smoothing function has been applied to the data.

The maximum modulation field which could be applied without breakdown was 236 and 382 V cm^{-1} for the $9_{0,9} \leftarrow 8_{0,8}$ and the $10_{0,10} \leftarrow 9_{0,9}$ respectively. It is surprising that these two lines showed an

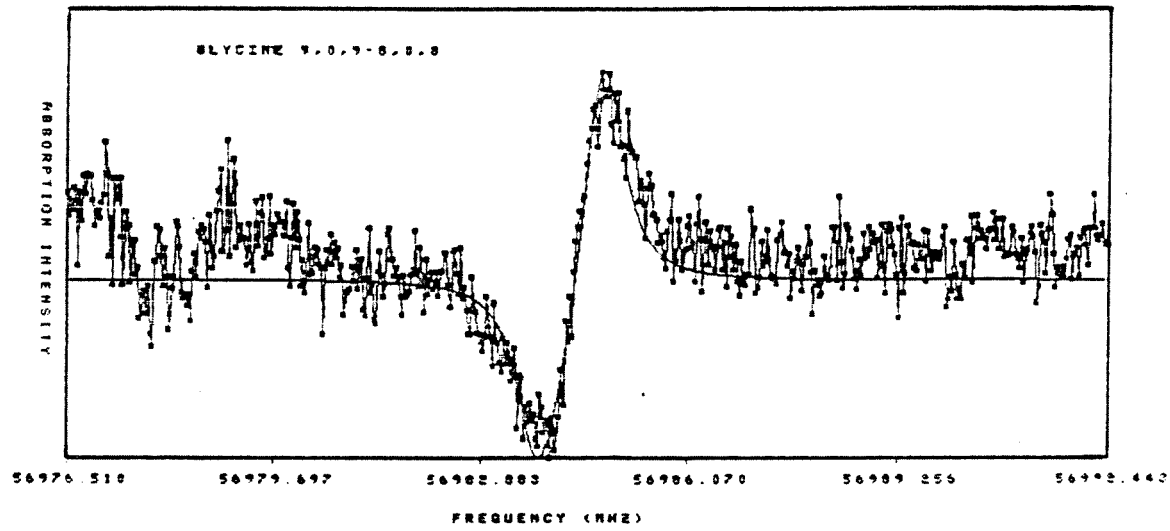

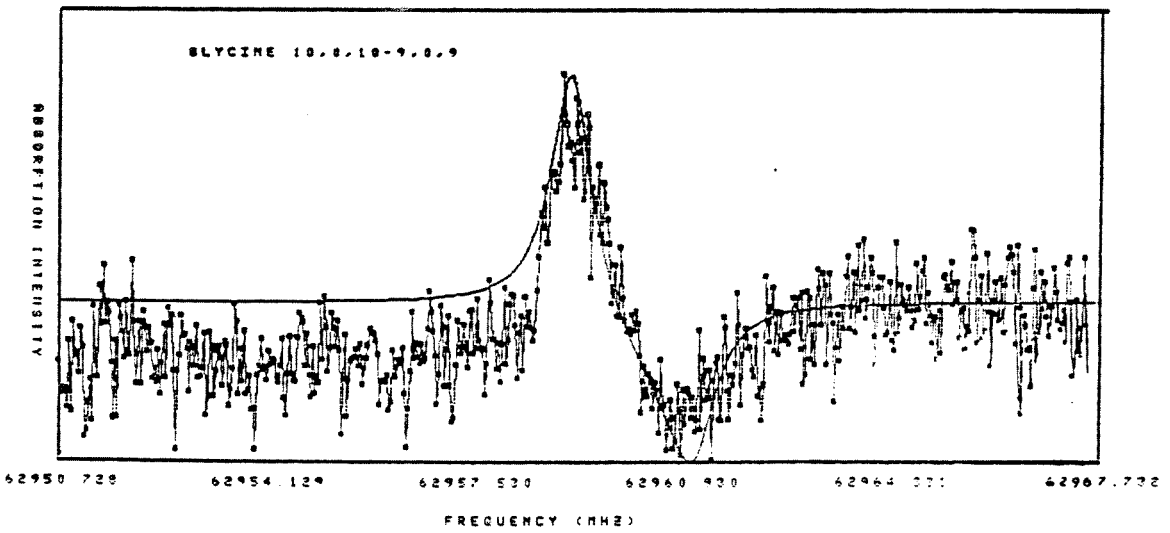

Fig. 2.15 Determination of an upper limit to the μ_c dipole moment component with

(a) the ($J_{K_aK_c} = 9_{0,9} \leftarrow 8_{0,8}$) transition.

(b) the ($J_{K_aK_c} = 10_{0,10} \leftarrow 9_{0,9}$) transition.

Plots of calculated and experimental spectra.

Fig. 2.16 Schematic view of the Stark energy levels involved in the transitions selectionned for the determination of the dipole moment components μ_b and μ_c.

Only one M component is represented. The transitions marked 'b' and 'c' have been observed for the analyses of μ_b and μ_c respectively.

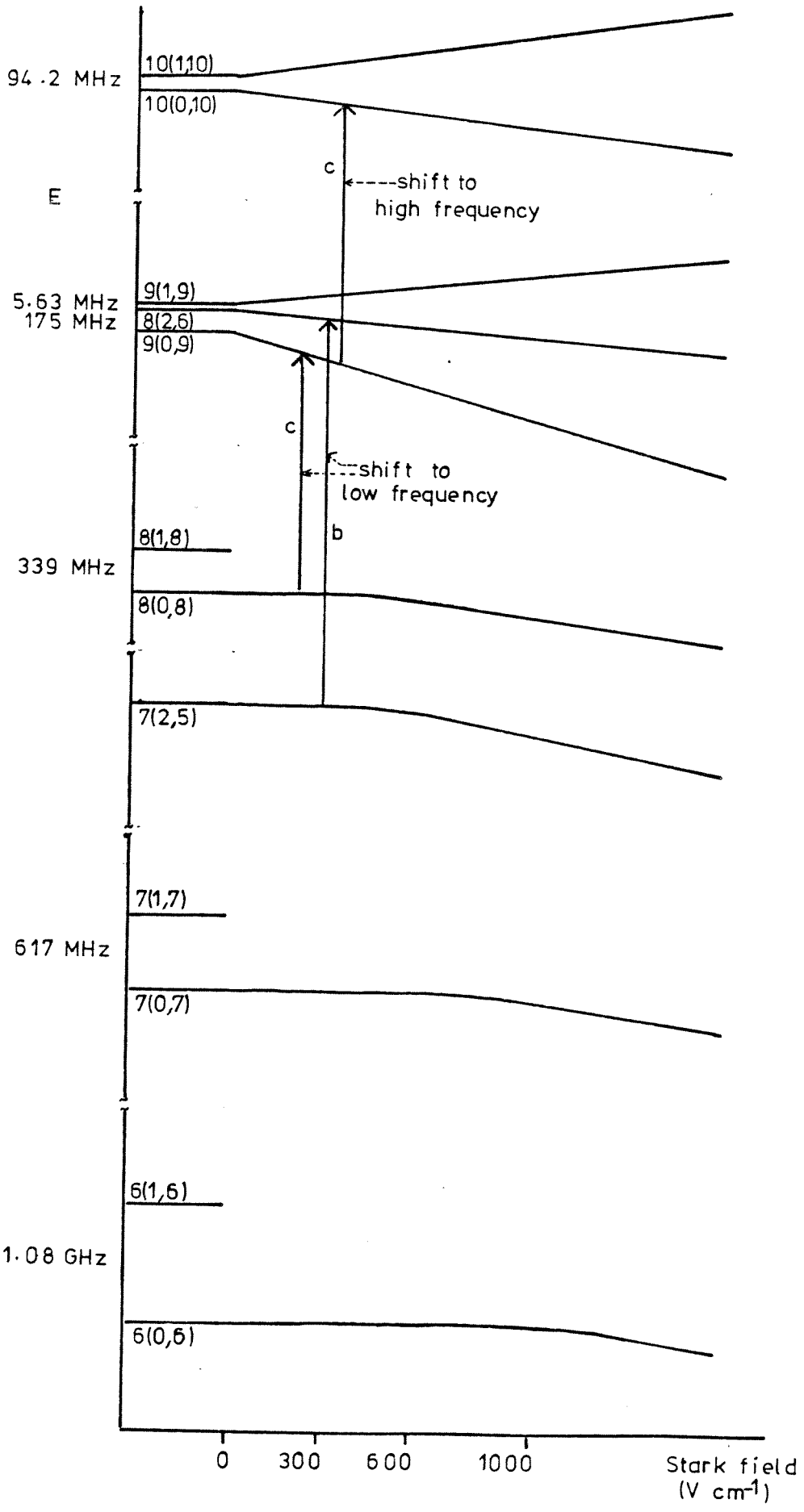
94.2 MHz
10(1,10)
10(0,10)
c
shift to
high frequency
E
5.63 MHz
175 MHz
9(1,9)
8(2,6)
9(0,9)
c
shift to
low frequency
b
8(1,8)
339 MHz
8(0,8)
7(2,5)
7(1,7)
617 MHz
7(0,7)
6(1,6)
1.08 GHz
6(0,6)
0
300
600
1000
Stark field
(V cm-1)

observable intensity at so low voltages compare to the $7_{0,7}\leftarrow 6_{0,6}$ and $8_{0,8}\leftarrow 7_{0,7}$ transitions which required about 1000 V cm^{-1} to be detected. This is due to the fact (fig. 2.16) that a $^aR_{2-3}$ transition, $8_{2,6}\leftarrow 9_{0,9}$, not far from a near degenerate type, is strongly involved in the Stark effect of the $9_{0,9}$ level, pushing it far more to lower frequencies than are the levels $8_{0,8}$, $7_{0,7}$ and $6_{0,6}$. These three last levels are not involved in near degeneracies and their Stark effect is of a 'second order' type. Their components are shifted towards low frequencies since each upper level of the transitions is pushed a little more downwards as pictured on fig. 2.16. The transitions $10_{0,10}\leftarrow 9_{0,9}$ and $9_{0,9}\leftarrow 8_{0,8}$ in the opposite, have a faster Stark effect with components shifted respectively towards high and low frequencies. They thus show a sufficient intensity to be observable at low voltages. However more than 1000 V cm^{-1} is required to resolve the components. Consequently only a global shift has been detected. This shift is sensitive to the value of μ_c, since the two transitions have levels involved in c-type transitions not far from near degenerate type. However since the levels $10_{1,10}$, $10_{0,10}$ and $9_{1,9}$, $9_{0,9}$ are not very degenerate and μ_c is very small, the levels $10_{0,10}$ and $9_{0,9}$ are not strongly perturbed and the μ_c dependence of the transitions $10_{0,10}\leftarrow 9_{0,9}$ and $9_{0,9}\leftarrow 8_{0,8}$ is relatively small. Only an upper limit of the μ_c dipole moment component could be obtained:

$$\mu_c < 0.1 \text{ debye}$$

This determination has been of interest for the search of glycine in space. Indeed the rate of emission from an upper level of a molecule, in an interstellar cloud, is governed by the A-Einstein coefficient, in the same way that the rate of absorption of radiation in the laboratory is governed by the B-Einstein coefficient. These coefficients are proportional to the square of the dipole moment. With

the low value of μ_c it has been justifiable not to take into account the pure c-type transitions, in the calculations of the total rate of emission from an upper level.

In order to obtain a precise value of the dipole moment component along the c axis, the transition to study would be the $16_{0,16} \leftarrow 15_{0,15}$ at 98989.761 MHz. The levels $16_{0,16}$ and $16_{1,16}$ are separated by 9 kHz only, and no nearby near degenerate levels are connected in a b-type transition similar to the $9_{1,9} \leftarrow 8_{2,6}$. Their Stark effect are thus only dependent in μ_a and μ_c. This transition can in the future be studied with the newly built millimeter horns described in section 2.5.

2.3.10 *Structure of the free rotating glycine molecule. Measured lines of another conformer.*

By means of a comparison between expected and observed patterns of lines and between the measured and predicted dipole moment component along the a-axis, the observed spectrum has been assigned to the conformer (4). R.D. Suenram and F.J. Lovas [45] have not measured the dipole moment, but in view of the fact that high J K_a=0 and K_a=1 transitions require high modulation fields (up to 3500 V cm^{-1}), they estimated a minimum value of 3.0 D. for μ_a. On this basis they also proposed glycine (4) as geometry for the assigned conformer.

The isotopic species study had started when R.D. Suenram and F.J. Lovas reported a work in progress on the deuterated forms. Since their millimetre wave cell allowed observations of very strong lines (S/N $\sim$ 10 with τ = 0.3 s) and Stark modulations up to 3500 V cm^{-1} the project has been abandonned in the Monash laboratory.

The alternative configuration (3), predicted to be more stable

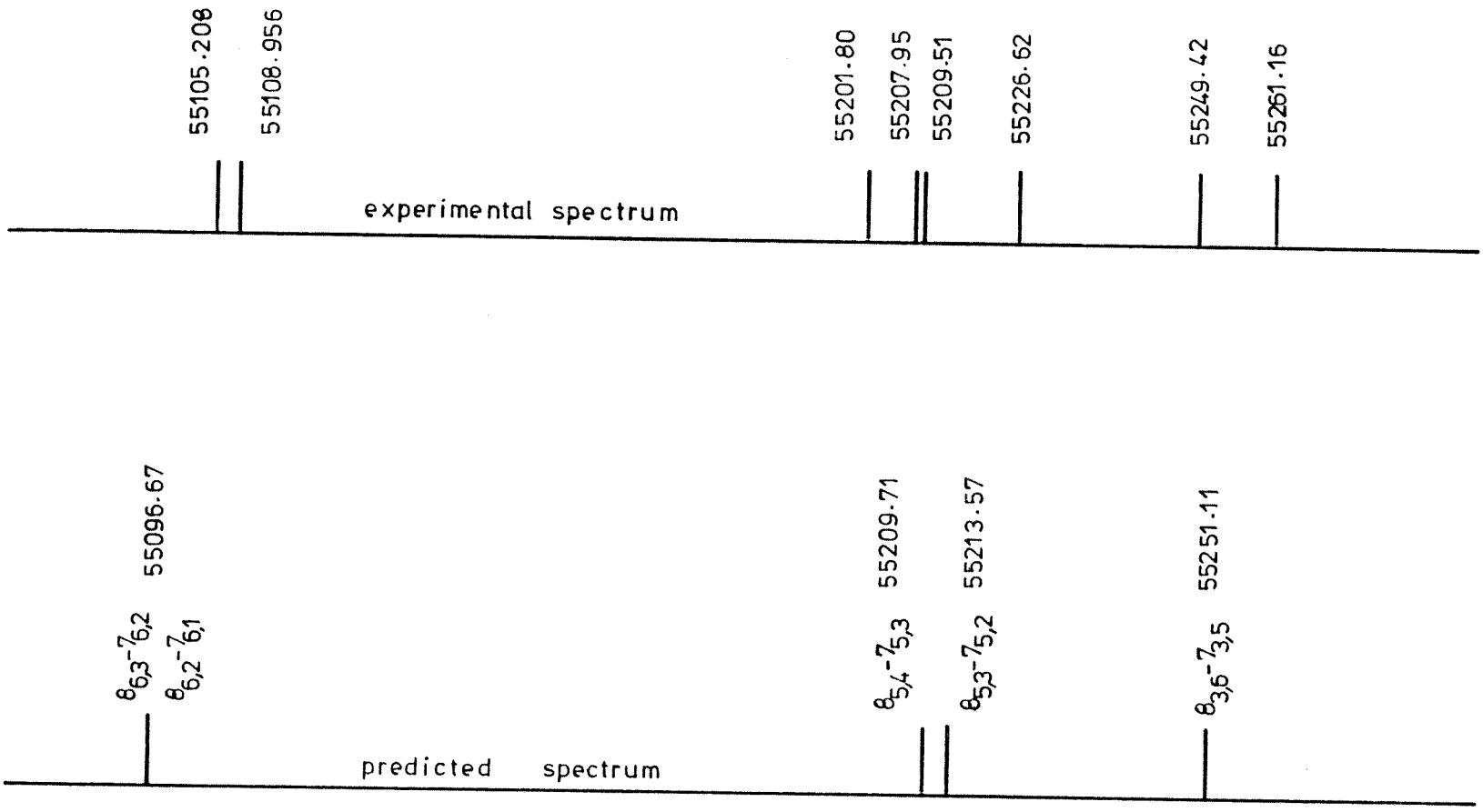

Fig. 2.17 Stick spectra of calculated and measured lines of another conformer of glycine.

than (4) on the basis of ab initio calculations [24,52], has a too low predicted value of the μ_a dipole moment component (1.0) to be at the origin of the observed spectrum. For the same reasons the conformers (1) favored by a CNDO calculation [19,20] has been eliminated. However glycine (4) is not necessarily the lowest energy conformation of glycine. Glycine (3) with its low μ_a dipole moment is expected to present a weak spectrum unless its rotational levels are much more populated than those of (4). Some lines have been found in the predicted frequency range of the conformer (3). They are shown on fig. 2.17 together with the calculated transition frequencies. If these lines belong to the spectrum of glycine (3), it is surprising how small is the error between the predicted and measured frequencies. Since the voltage breakdown can now be avoided, a search for low K_a lines of this conformer would be of interest.

2.4 HIGH RESOLUTION SPECTROMETER AND NUCLEAR QUADRUPOLE COUPLING CONSTANTS

2.4.1 Nuclear quadrupole coupling constants

Three series of prediction of the nuclear quadrupole coupling constants have been made by rotating the nuclear coupling tensors of ammonia, methylamine and 2 aminoethanol into the principal inertia frame of glycine (4) (table 2.16).

The following method has been followed. First the known molecule is drawn in its principal inertia axes with the aid of the program CART. Then raw coordinates of glycine are determined so that the amino group orientation is the same than which one of the known molecule in its inertia system of reference. CART gives then the transformation matrix from these coordinates to the principal inertia

TABLE 2.16

Nuclear quadrupole coupling constants of glycine derived from measured constants of other molecules

molecule	χ_{aa}	χ_{bb}	χ_{cc}	comments	ref
ammonia NH_3	2.04	2.04	-4.08	measured	53
2-aminoethanol $NH_2CH_2CH_2OH$	-3.1 (2)	0.9 (5)	2.2 (4)	measured	31
methylamine CH_3NH_2	2.30	2.02	-4.32	measured	32
glycine NH_2CH_2COOH	2.04	1.91	-3.95	calculated with ammonia constants	this work
glycine NH_2CH_2COOH	0.58	0.98	-1.56	calculated with 2-aminoethanol constants	this work
glycine NH_2CH_2COOH	2.20	2.10	-4.30	calculated with methylamine constants	this work

Fig. 2.18 The high resolution spectrum of the ($J_{K_aK_c} = 4_{3,1} \leftarrow 3_{3,0}$) transition of glycine.

A possible hyperfine structure.

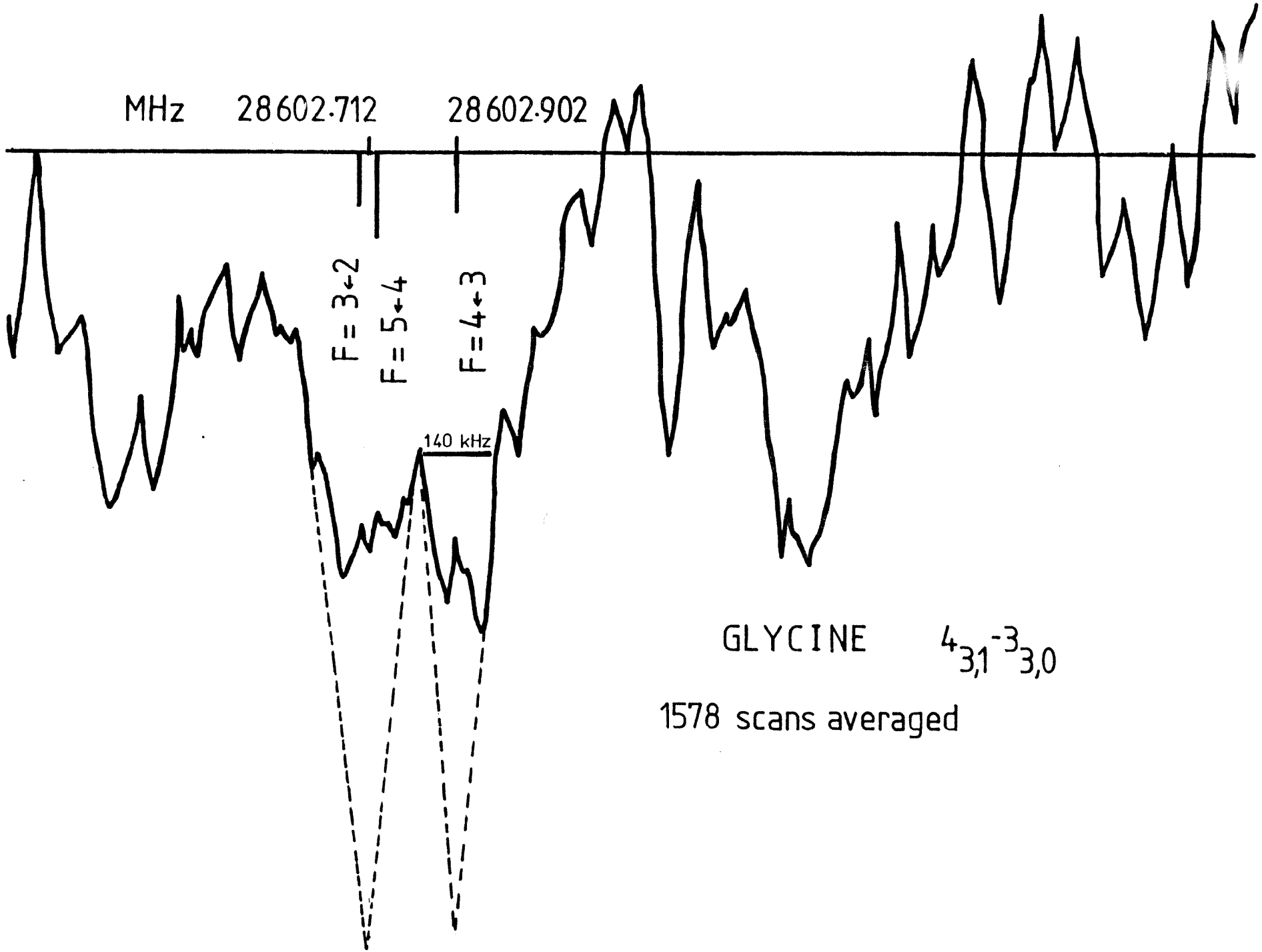
MHz
28602·712
28602·902
F= 3←2
F= 5←4
F=4←3
140 kHz
GLYCINE $4_{3,1}-3_{3,0}$
1578 scans averaged

axes coordinates of glycine, which is in fact the transformation matrix for the amino group from the inertia system of the known molecule to the glycine inertia axes. When the electronic environment of the nitrogen atom is similar for both glycine and the known molecule, predictions of the coupling constants may be very accurate. A prediction has been evaluated with ammonia and methylamine. The molecule 2-aminoethanol has also been chosen because it shows an intramolecular hydrogen bond -OH...N- similar to that of glycine (4).

Following the setting up of the new pumping system, the transition $4_{3,1} \leftarrow 3_{3,0}$ has been observed. Fig. 2.18 shows an average of 1578 scans of 3 mn 24 s each. The study of the hyperfine structure requires more experiments but it can already be advanced that the coupling constants determined from 2-aminoethanol seem to explain better the observed spectrum. This implies an intramolecular hydrogen bond in the structure of glycine and confirms the assignment of the conformer (4) to the measured spectrum.

2.4.2 *Improved pumping system*

The Doppler width is the narrowest line shape which can be achieved in microwave spectroscopy. In the case of glycine, at 473 K, the Doppler FWHH is 50 kHz at 28 GHz and 102 kHz at 57 GHz. The 2-3 MHz linewidth which has been observed in this work are due essentially to intermolecular collisions. Each pressure of 1 Pascal (10 μHg) contributes 300 kHz broadening. The fast pumping system described here has increased the mean free path of the molecules and has enabled observations of

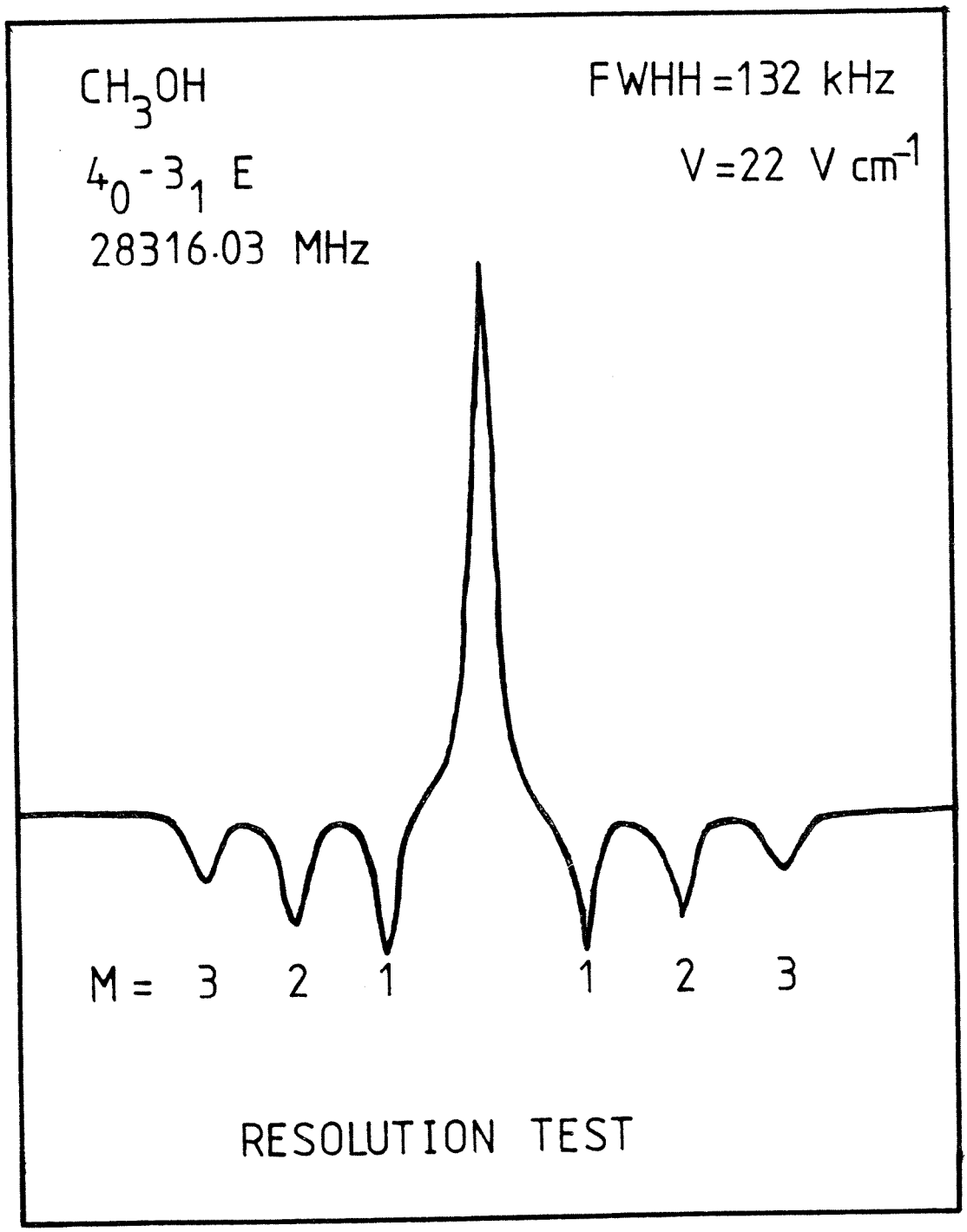

Fig. 2.19 The ($J_K = 4_0 \leftarrow 3_1$ E) transition of methanol observed with the improved pumping system.

TABLE 2.17

Conductances of tubes and liquid nitrogen traps

Tubes	Conductance calculated at 298 K ($1s^{-1}$)
tube above the pump	92
liquid nitrogen trap above the pump	1083
tube centered on the valve	201
tube above the cell nitrogen trap	889
cell nitrogen trap	422
tubing above cell	582

methanol lines of 130 kHz FWHH (fig. 2.19).

The 2.3 MHz lines have been observed when air and gaseous samples were evacuated out of the cell using a two-stage fractionating oil diffusion pump made of Pyrex and backed by a rotary mechanical pump. The high velocity working fluid was an Apiezon C hydrocarbon oil and the throat diameter was 1". A new diffusion pump has been set up. It has been filled with a Dow-Corning Silicone 704 oil. Its low vapour pressure (4.10^{-8} μ at 298 K) allows a larger clearance between nozzle and condensing wall and consequently generates a faster speed of exhaust than hydrocarbon oil. This pump is air-cooled and the diameter of the throat is 1.5".

A new exhausting system has been built and is viewed on fig. 2.5. It has been designed in a way to minimize speed losses. The conductances of tubes and liquid nitrogen traps have been calculated using the theory on flow of gases [54], and are listed in table 2.17. The cylindrical tube above the pump, contributes the biggest reduction in pumping speed. Its size has been constrained by the exit diameter of the pump and the neighborhood of the gas exit tube. When the pump is attached to this vacuum line, the 80 ls^{-1} speed is reduced to 29 ls^{-1}.

2.5 MILLIMETRE-WAVE SPECTROMETER

In order to increase the sensitivity of the cell in the millimetre range, new horns have been built. Their shape has been designed to suit the length of the end chamber and the dimensions of the glass plates. They are 1 m long with a flare angle of 0.64° in the E plane, to match the 0.5" plate spacing to the 1.55 mm width of the E band waveguide into which they terminate. In the H plane the flare angle is 9.78° in order to match the 7" plate height to the 3.10 mm height of the

waveguide. A full treatment of horn design may be found in reference [55].

The manufacture of the horns has to be very accurate. Any rough internal surface of the walls would increase the resistance and thus the attenuation of the transmission line. Because of the difficulty of machining very accurately small dimension waveguides, it has been necessary to copper electroform an 18 cm taper (4 cm waveguide and 14 cm horn) and extend it with brass plates to the required size. A complete electroforming system has been set up, following advices given by B. Macke [56]. Some details are given in appendix 4. Informations on electroforming can also be found in reference [57].

The clean aluminium mandrel has been immersed in an acidic copper sulfate solution, at a temperature of 294 K, and submitted to an anodic oxydation during an hour, under a current of 120 mA dm^{-2}. The alumine layer prevented aluminium from being attacked by alkaline ions, and thus preserved the polish of the inner surface of the horn. Using the same bath, after reversal of the polarities, and adjustment of the current at 1.5 A dm^{-2}, copper deposited during 384 h, to a thickness of 2.13 mm. Since the solution was in a glass bucket insulated from the outside with polystyrene foam, the temperature has been kept very stable during the total operation. After removing the copper growths at the narrow end (due to higher current density), aluminium was dissolved, during a week, in a caustic soda bath at 388 K. Concentrated hydrochloric acid provided the final cleaning.

One of the pair of manufactured horns is shown on fig. 2.20.

Fig. 2.20 One millimetre-wave horn

The tubing along the horn is for water-cooling.

One milimeter-wave horn photo Marie Paule Bassez 1977

CHAPTER 3

A SEARCH FOR INTERSTELLAR GLYCINE

A search has been made for the simplest amino acid - glycine - in Sgr. B2, Ori. A and seven other molecular clouds. Six different lines were sought ranging from 83.4 GHz down to 22.7 GHz and radio--telescopes at Parkes, N.S.W., Kitt Peak, Arizona and Onsala, Sweden were used. On the assumption of reasonable values for T_{ex} and Boltzmann distributions over rotational energy states, upper limits of column densities for glycine of a few times 10^{13} cm^{-2} were typically established in the sources surveyed. Glycine appears to be less abundant than ethanol or ethyl cyanide in molecular clouds such as Sgr. B2 and Ori. A.

3.1 *SELECTED TRANSITIONS OF GLYCINE*

The rate of transitions from an upper to a lower level involves the product of level populations and Einstein A-coefficients. Its calculation requires a knowledge of the populations and hence a full solution of the statistical rate equations. Because of unknown quantities, such as collision cross-sections for neutral particles upon glycine, and uncertainties about the physical conditions prevailing in the clouds, an elaborate modelling of the excitation conditions did not seem justifiable. Using the approximate model of local thermodynamical equilibrium, the first criterion for selection was the following:

In order for the upper level of a transition to be populated, the energy of the level must be at the most equal to the kinetic energy of the molecular cloud.

TABLE 3.1

Transitions selected for the glycine search

transition*	frequency (MHz)	A (s^{-1})	$A/\Sigma A_{ul}$	E_{ul}/k (K)	line label
$11_{10,2}\rightarrow 10_{10,1}$	78379.51	$1.44\ 10^{-5}$	.159		
$11_{10,1}\rightarrow 10_{10,0}$	78379.51	$1.44\ 10^{-5}$	.175		
$11_{9,2}\rightarrow 10_{9,1}$	78450.58	$2.76\ 10^{-5}$	.343		
$11_{9,3}\rightarrow 10_{9,2}$	78450.58	$2.76\ 10^{-5}$	.297		
$11_{8,3}\rightarrow 10_{8,2}$	78549.58	$3.95\ 10^{-5}$	.493		
$11_{8,4}\rightarrow 10_{8,3}$	78549.58	$3.95\ 10^{-5}$	.416		
$11_{7,4}\rightarrow 10_{7,3}$	78694.84	$5.02\ 10^{-5}$	.623		
$11_{7,5}\rightarrow 10_{7,4}$	78694.62	$5.02\ 10^{-5}$	.520		
$11_{6,5}\rightarrow 10_{6,4}$	78926.70	$5.97\ 10^{-5}$	.725		
$11_{6,6}\rightarrow 10_{6,5}$	78918.96	$5.97\ 10^{-5}$	.626		
$11_{5,6}\rightarrow 10_{5,5}$	79401.02	$6.87\ 10^{-5}$	.804		
$11_{5,7}\rightarrow 10_{5,6}$	79243.58	$6.83\ 10^{-5}$	.723		
$11_{4,7}\rightarrow 10_{4,6}$	80923.93	$7.95\ 10^{-5}$	.114		
$11_{4,8}\rightarrow 10_{4,7}$	79332.62	$7.48\ 10^{-5}$	.785		
$11_{3,8}\rightarrow 10_{3,7}$	83356.02	$9.32\ 10^{-5}$	.924	26.2	1
$11_{3,9}\rightarrow 10_{3,8}$	77916.68	$7.51\ 10^{-5}$	.819	25.5	3
$11_{2,9}\rightarrow 10_{2,8}$	81438.77	$8.88\ 10^{-5}$	.959	24.9	2
$11_{2,10}\rightarrow 10_{2,9}$	74121.82	$6.70\ 10^{-5}$	.957	23.1	
$11_{1,10}\rightarrow 10_{1,9}$	75009.90	$6.97\ 10^{-5}$	.957	23.0	5
$11_{1,11}\rightarrow 10_{1,10}$	68903.57	$5.56\ 10^{-5}$			
$12_{11,2}\rightarrow 11_{11,1}$	85495.84	$1.73\ 10^{-5}$		64.8	
$12_{4,8}\rightarrow 11_{4,7}$	89125.45	$1.09\ 10^{-4}$		32.2	
$12_{2,12}\rightarrow 11_{2,11}$	81603.18	$8.58\ 10^{-5}$		26.9	
$12_{1,11}\rightarrow 11_{1,10}$	80838.33	$8.78\ 10^{-5}$		26.9	
$12_{1,12}\rightarrow 11_{1,11}$	74926.41	$7.18\ 10^{-5}$		24.1	
$12_{0,11}\rightarrow 11_{0,10}$	74950.58	$7.19\ 10^{-5}$		24.1	
$10_{9,1}\rightarrow 9_{9,0}$	71262.60	$1.18\ 10^{-5}$			
$10_{3,7}\rightarrow 9_{3,6}$	75379.48	$6.74\ 10^{-5}$	.945	22.2	4
$10_{2,8}\rightarrow 9_{2,7}$	74838.99	$6.87\ 10^{-5}$	.789	21.0	
$3_{1,2}\rightarrow 2_{1,1}$	22747.14	$1.62\ 10^{-6}$	.905	2.4	6
$3_{2,1}\rightarrow 2_{2,0}$	21737.60	$8.84\ 10^{-7}$	.128	3.3	

*the transitions which have been sought are underlined and labelled.

The number of molecules undergoing a transition from this level is proportional to the A-coefficient. The second criterion for selection has thus been chosen to be:

The transition has a large Einstein-A coefficient.

Since this coefficient involves the frequency elevated at the power three, the highest the frequency of the transition the more molecules are seen in emission, as far as the upper levels are populated. This led to the observation of relatively high J transitions ($J_{upper} \simeq 11$).

The depopulation of an upper level is distributed over several lower ones and the most intense transition from this level has to be compared with the most intense transition from other levels to gain knowledge about the most intense emission. Consequently the third criterion for selection was:

The transition is the fastest radiative exit channel from the upper level.

Table 3.1 lists some transitions of glycine with the energy of the upper level, E_{ul}, the Einstein A-coefficient and its relative value with respect to the sum of the A-coefficients of all transitions out of the upper level. The transitions selected for the search are underlined, the others are listed for comparison. Only the $^{a}R_{01}$ type of transitions have been considered. Indeed the dipole moment component along the a-axis, the strongest of the three components ($\mu_a = 5.57$ D., $\mu_b = 0.32$ D., $\mu_c < 0.1$ D.) contributes the most to the value of the A-coefficient. The $^{a}Q_{0-1}$ and $^{a}Q_{2-1}$ transitions, with same J_{upper} or J_{lower}, have smaller line strengths and occur at lower frequencies, hence their A-coefficients are smaller. When levels with (J = 12) form the

upper states of the transitions, the A-coefficients are slightly bigger, but in some cases these levels lie too high in frequency to be thermally populated in other clouds than Ori. A(OH). Also since most of the levels (J = 13) have still higher energies above ground, their popula--tions are insignificant and will not contribute, by their own deexcitation, to the populations of the (J = 12) levels. Thus the only considered transitions have been those with ($J_{upper} \leq 11$).

Within these transitions only those with a fast exit rate from the upper levels have been retained. This criterion has been satisfied by comparing, for each above selected transition, the ratios of their A-value on the sum of the A-values of all transitions out of the upper level. For instance, the level $11_{2,9}$ is depopulated at 96% into the level $10_{2,8}$, while only 11% of the level $11_{4,7}$ is depopulated into the level $11_{4,6}$. The transition $11_{2,9} \rightarrow 10_{2,8}$ has thus been selected for the glycine search. The calculations of the sums of the A-coefficients has been carried out without taking into account the weakly allowed transitions of the type ($\Delta K_a \gtrsim \pm 3$), neither the pure c-type transitions. The $3_{1,2} \rightarrow 2_{1,1}$ transition was the only one at the frequency of the maser receiver (22.0 to 24.5 GHz) and has thus been selected. By chance this transition presents a high exit rate from the upper level.

3.2 OBSERVATIONS

Observations were conducted using radiotelescopes at Parkes ANRAO*, Kitt Peak NRAO** and the Onsala Space Observatory***. Some

* The Australian National Radio Astronomy Observatory is operated by the CSIRO, division of Radiophysics, Epping, N.S.W. Australia.

** This National Radio Astronomy Observatory near Tucson, Arizona, is operated by Associated Universities Inc., under contract with the National Science Foundation, U.S.A.

***The Onsala Space Observatory is operated by the Chalmers University of Technology, Göteborg, Sweden.

TABLE 3.2

Telescope specifications

telescope	exposure	ϕ (m)	HPBW	tel.ef.[a] (%)	front end	back end	receiver configuration	T_{sys} SSB (K)
Parkes	open	16.7	57" at 75 GHz	20	cooled mixer and parametric amplifier	AOS/ one-bit correlator	beam-switching/ total power	680
Kitt Peak	radome	11.0	87" at 75 GHz	70	cooled mixer and parametric amplifier	filter banks	position-switching	1700
Onsala	radome	20.1	2'18" at 23 GHz	75	traveling wave maser	one-bit correlator	total power	130

abbreviations: ϕ = diameter of the antenna

tel.ef. = telescope efficiency

a : These values have been assumed in the calculations.

specifications of these telescopes are listed in table 3.2.

3.2.1 *Observations conducted at Parkes*

The Parkes observations have been conducted on 23 days, from the 28 June to the 19 July 1978, in collaboration with R.D. Brown, P.D. Godfrey, B.J. Robinson, R.A. Batchelor and M.G. McCulloch. The telescope, located at 33°S latitude, is a prime focus instrument. The central 16.7 m aluminium panelled surface [1] of the 64 m welded steel paraboloidal antenna was illuminated with 10 dB taper at the edge, leading to a 57" half power beamwidth (HPBW) at 75 GHz.

A schematic view of the receiver used is drawn on fig. 3.1. This receiver [2] covers two bands, 33.50 GHz (7.5 mm) and 75-110 GHz (3.3 mm). Each band is set with separate feed horns and mixers which are cooled at 70 K. Only the 3.3 mm section has been involved in the glycine search.

The receiver front end consisted of a klystron local oscillator (1^{rst}LO) phase-locked, with a 200-800 MHz variable frequency IF, to a suitable harmonic of a value or a comb of frequencies, ν_{comb}, which was itself a multiple (17, 18, 19, 20) of a 100.000 MHz or 102.777 MHz crystal oscillator. This LO was fed into the 70 K mixer which converted the signal into a lower intermediate frequency (1^{rst}IF). A 3-stage 4.5-5.0 GHz Comtech parametric amplifier, helium cryogenically cooled at 20 K, was used as 1^{rst}IF amplifier. A further ambient temperature mixer provided the 2^{nd} IF at 100-600 MHz, which was amplified by $\sim$ 60 dB before transmission in the control room.

Mixers were used to create frequency down-conversion. Their operation depends on the non-linear resistance of metal-to-semiconductor contacts and for low noise output they require a low junction capacitance

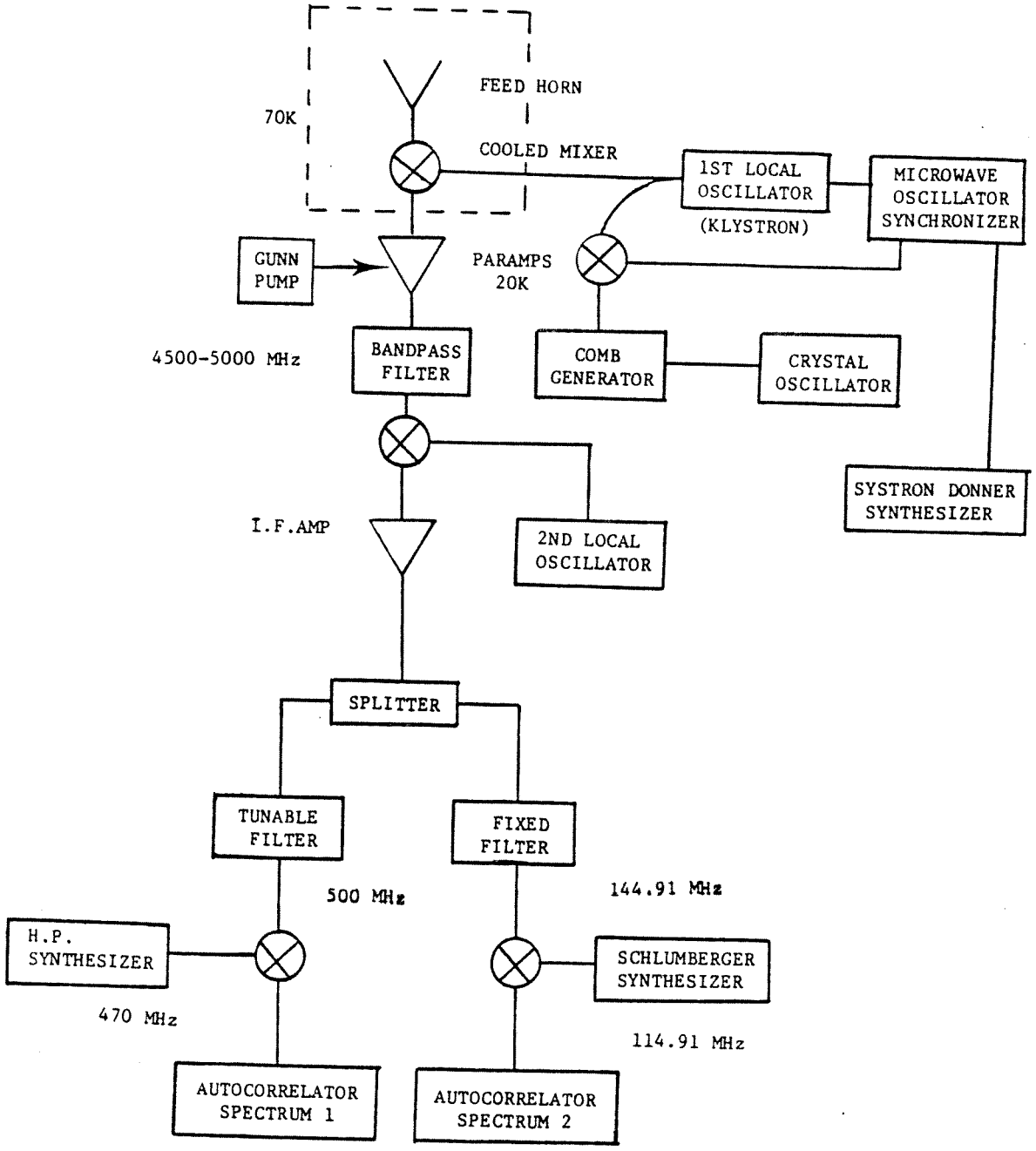

Fig. 3.1 The Parkes 7 and 3 mm receiver

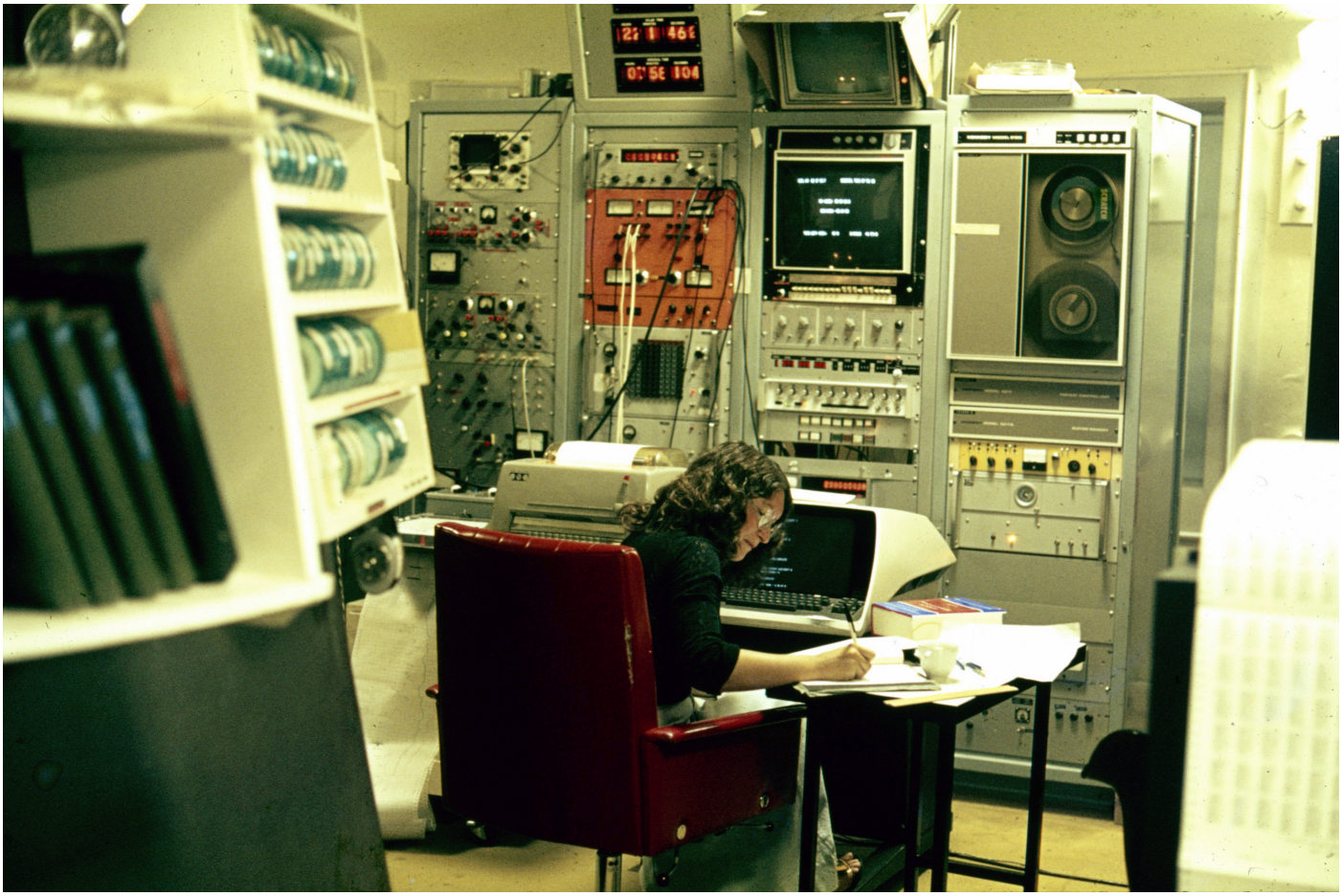

Marie Paule Bassez in the Control Room of the Parkes Radiotelescope (July 1978)
photo: Peter Godfrey

and low series resistance. Each mixer of this receiver consisted of a GaAs chip (0.25 × 0.25 × 0.125 mm), on one broad face of which was an ohmic contact and on the other a matrix of ∿ 3 μm diameter Schottky diodes. A whisker was used to make contact with a Schottky diode in the matrix. The mixer diodes had a junction capacitance of ∿ 30 femtofarads and a series resistance of ∿ 5Ω, with a resulting cut-off frequency of ∿ 1500 GHz.

The calibration of the receiver front end was performed with microwave absorbers at ambient and liquid nitrogen temperatures, placed in front of the feed horn. The system noise temperature was measured to be only 340 K double sideband (DSB) at 75.0 GHz.

The IF signal arriving in the back end was split in two channels and further down-converted to 30 MHz, before being fed into a one-bit digital autocorrelator [3], with 1024 channels and a maximum sampling rate of 20 MHz allowing bandwidths up to 10 MHz. Most of the search for glycine was made in the direction of Sgr. B2, a large velocity width cloud. In this case, the signals were analysed by an accousto-optical spectrometer (AOS)* [4] installed in one channel of the back end.

---

*The autocorrelation function $\rho_x(\tau)$ of a function x(t) is a measure of the correlation between the values that this function takes at values of the variable differing by an amount τ:

$$\text{with} \quad x(t) = 2\int_0^\infty a(\nu)\cos(2\pi\nu t)\,d\nu \ ,$$

$$\rho_x(\tau) = \langle x(t)x(t+\tau)\rangle = 4\int_0^\infty A(\nu)\cos(2\pi\nu\tau)\,d\nu \quad [5]$$

The Fourier transform of this autocorrelation function gives the power spectrum $A(\nu)$ of the frequency ν. In a digital autocorrelator the autocorrelation function is formed in successive channels of a

footnote cont'd on next page.....

With the AOS, the observations were made in the beam-switching mode with on and off-source positions alternating at a rate of 0.5 Hz. The total power mode was used with the autocorrelator. In both cases, a reference spectrum was subtracted. More informations on receiver components can be found in reference [8].

3.2.2 *Observations conducted at Kitt Peak*

The Kitt Peak observations were conducted on five days between the 16 and the 21 of April 1978, in collaboration with R.D. Brown, P.D. Godfrey and J.W. Storey. The 36-ft one-piece aluminium surfaced antenna is located at the latitude 31°57'12.10" N. With an rms surface accuracy of 0.14 mm this telescope can be used at frequencies above 200 GHz. The focal system was a Cassegrain type. Thermal expansion of the legs, which support the secondary reflector, was monitored by temperature sensors followed by a computer control.

As in Parkes, the receiver included a cooled mixer in the front end [9]. But, in this case, two channels were sampling orthogonally

---

footnote cont'd from previous page....

multichannel accumulator, by summing the product of the signal $x(t)$ with the delayed signal $x(t + \tau)$. In the case of the Parkes autocorrelator, at the end of the 2s averaging period, the contents of the accumulator is transferred to a PDP-9 computer where the Fourier transform is performed. The bandwidth is governed by the sampling rate.

In the AOS, the IF signal induces an accoustic wave in a modulator which is traversed by a laser beam. The phonon-photon interaction produces a diffracted beam whose angular distribution reflects the frequency distribution of the IF signal. The Fourier transform, performed by a lens [6], is in this case relating frequency and space instead of frequency and time as above [7]. The light modulator acts as a delay line.

Receiver of the 36 feet (12 m) Radiotelescope at Kitt-Peak, Arizona
photo: Marie Paule Bassez (April 1978)

polarized radiations from the feed horn and were thus providing uncorrelated noise. The output signals from both channels could hence be averaged to improve the signal to noise ratio by $\sqrt{2}$. Calibrations of the signal intensities were accomplished with frequent use (once or twice per hour) of an absorbing chopper vane. Hot and cold loads were also used and led to a single sideband (SSB) system temperature measure-ment of 1700 K at frequencies between 73 and 85 GHz.

The back end consisted of two 256-channels filter banks with 250 kHz and 100 kHz filters during the Ori. A(OH) observations and with 1 MHz and 500 kHz filters during the observations of the high dispersion source Sgr. B2. The available Fabry-Perot image rejection filter [10] has not been used. Data were obtained for all transitions in a position-switching mode, with a reference position of 30' west in azimuth.

3.2.3 *Observations conducted at Onsala*

The observations were conducted at Onsala in April 1978, by R.D. Brown, P.D. Godfrey, D.E.H. Rydbeck and Å.G. Hjalmarson. The 66-ft antenna of the Cassegrain telescope is mounted with aluminium panels of 0.16 mm rms surface accuracy [11] and is enclosed in a translucent radome which transmits 80 to 95 percent of radiations at millimetre wavelengths. The pointing error was less than 12" rms.

The telescope was equipped with a traveling-wave maser (TWM) receiver [12], with iron-doped rutile (TiO_2) as active material. Masers are known to be low noise microwave amplifiers [13], showing greater stability than parametric amplifiers. A disadvantage for radio astronomy is their narrow bandwidths, rending them unsuitable for observations of large velocity clouds. This maser was a dielectric image line type and could achieve more gain than waveguide masers. The instantaneous 3-dB

bandwidth was 60 MHz and the tunable range was 22.0 - 24.5 GHz. Liquid helium allowed cooling to 2 K and a superconducting magnet provided the required magnetic field, 6.5 kG. With this maser receiver, 130 K SSB system temperature was achieved at 22 GHz.

The local oscillator was phase-locked to the observatory hydrogen maser frequency standard. A 512 channel one-bit autocorrelator was used as back end and position-switching was the adopted mode.

3.2.4 *Comparison of the receivers*

A comparison of the receivers used at Kitt Peak and Parkes has been possible since the same frequency range has been observed with both telescopes.

The sensitivity constant K_s of a receiver is determined as: $K_s = ((\Delta T_{rms}(\Delta\nu t)^{\frac{1}{2}})/T_{sys}$ [14], where ΔT_{rms} is the r . system temperature, $\Delta\nu$ the resolution bandwidth, t the on-source integration time and T_{sys} the system temperature. Using this expression with the line characteristics listed in table 3.5 and assuming that beam filling was achieved, some ratios of receiver sensitivity constants have been calculated for lines observed at Parkes and Kitt Peak and are listed on table 3.3. A second series of ratios has been calculated with the sensitivity constant theoretically determined from the mode of observation. In these calculations, the rms system temperature, which is the intrinsic noise of the receivers, takes the values of the antenna temperature non corrected for telescope efficiency. The theoretical sensitivity constant of the receivers and the on-source integration times have been determined as described below.

A one-bit correlator has 64% ($2/\pi$) of the signal to noise ratio of a continuously multiplying correlator. This loss in sensitivity can be represented by a constant K_s of $\pi/2$. The Parkes correlator has

TABLE 3.3

Experimentally and theoretically determined sensitivity constants of the receivers

line	label	frequency GHz	receiver*	source	experimentally determined ratios of sensitivity constants	theoretically determined ratios of sensitivity constants
	1	83.3	KP-FB	Sgr B2		
	2	81.4	KP-FB	Sgr B2	$K_S(1)/K_S(2)$ = 0.78	1.00
	3	77.9	KP-FB	Sgr B2		
	5	75.0	KP-FB	Sgr B2	$K_S(3)/K_S(5)$ = 1.15	1.00
a	1	83.3	KP-FB	Ori A		
	2	81.4	KP-FB	Ori A	$K_S(1)/K_S(2)$ = 0.86	1.00
	3	77.9	KP-FB	Ori A		
	5	75.0	KP-FB	Ori A	$K_S(3)/K_S(5)$ = 1.08	1.00
	4	75.4	P-AOS	Sgr B2		
	5	75.0	P-AOS	Sgr B2	$K_S(4)/K_S(5)$ = 0.74	1.00
	4	75.4	P-AOS	Sgr B2		
b	5	75.0	KP-FB	Sgr B2	$K_S(AOS)/K_S(FB)$ = 4.06	1.41
	5	75.0	P-AOS	Sgr B2		
	5	75.0	KP-FB	Sgr B2	$K_S(AOS)/K_S(FB)$ = 5.43	1.41
	5	75.0	P-AOS	Sgr B2		
c	4	75.4	P-Cor	Ori A	$K_S(AOS)/K_S(Co\cdot)$ = 2.34	1.27
	4	75.4	P-AOS	Sgr B2		
	4	75.4	P-Cor	Ori A	$K_S(AOS)/K_S(Cor)$ = 1.75	1.27
d	4	75.4	P-Cor	Ori A		
	5	75.0	KP-FB	Ori A	$K_S(Cor)/K_S(FB)$ = 4.10	1.11

*abbreviations: KP = Kitt Peak, FB = Filter Bank, P = Parkes, AOS = accousto-optical spectrograph, Cor = one-bit correlator

been used in the total power mode with a reference spectrum. In this mode, the noise which is added to the on-source spectrum by the reference spectrum contributes a factor of $\sqrt{2}$ to K_S, when the on-source integration time is defined as the time spent on-source solely. Hence theoretically the sensitivity constant of the one-bit correlator receiver can be expressed as:

$$K_S(\text{Cor}) = (\pi/2) \times \sqrt{2} = \pi/\sqrt{2} \quad .$$

At Kitt Peak, the filter bank receiver has been used in a position-switching mode and the on-source integration time has been defined as the time spent on-source and on the reference position. In this case, another factor of $\sqrt{2}$ has to be taken into account in the loss of sensitivity of the receiver, because half the time of observation is spent on the reference position. Thus the sensitivity constant of the filter bank receiver can be expressed as:

$$K_S(\text{FB}) = 2 \quad .$$

The AOS has been used in the beam-switching mode. In this case, the standing wave pattern of the antenna, the atmospheric emission, and the spurious features of the receiver have been eliminated with a reference spectrum, as in the case of observations with the correlator and filter bank receivers. But the AOS showed a supplementary component of noise, the intensity of which was inversely proportional to the noise frequency and which did not average to zero as the white Gaussian fluctuations do. This flicker noise, encountered in most microwave laboratory components, does not vary very much during a short period of time. By quickly (in this case every two seconds) switching the beam from the source to a comparison position and subtracting the two spectra, it is possible to decrease considerably its intensity. However this mode of observation contributes a factor of 2 in excess to the noise observed

in the position-switching mode, because of the noise added to the spectrum by the off-source spectrum and because, during the on-source observation, half the time only is spent with the beam on-source. Hence if the on-source time of integration is defined to be solely the time spent by the telescope pointing on-source with the beam on-source and on the comparison point, the sensitivity constant of the AOS receiver can be expressed as:

$$K_S = 2\sqrt{2}$$

It is now possible to compare these theoretical constants with the experimentally determined ones. In the a-series of calculations of the table 3.3, the experimentally determined ratios of sensitivity constants have been obtained from data on pair of lines of similar frequencies, and observed with the same telescope and the same receiver. As expected, the ratios are within 25% of unity.

The c-series of calculations concerns also observations effectuated with the same telescope, but with different receivers. The K_S ratios of AOS versus correlator is measured to be within 30% of 2. Considering that K_S can be represented by a product of partial sensitivity constants related to the front end, the back end and the mode of observations:

$$K_S = \overline{K}_S(FE)\overline{K}_S(BE)\overline{K}_S(MO) \ ,$$

the partial sensitivity constants of the AOS and the correlator are found to be equal ($\overline{K}_S(AOS) = (2 \times \overline{K}_S(Cor) \times \sqrt{2})/2\sqrt{2}$). Thus is appears that the AOS entails the same loss of sensitivity as the one-bit correlator relative to a continuous or many-bit correlator, and that it is the mode of observation which decreases its sensitivity by a factor of 2. In any case it is necessary to integrate four times longer with the AOS, to obtain the same rms temperature as with the one-bit correlator. If the position-switching mode had been used, a gain of 50% ((2-4)/4) in sensitivity would have been achieved over the beam-switching

mode (with the on-source time of integration defined for both modes as the time spent on-source and on the reference position). However the position-switching mode of observations requires a fast settling time of the telescope antenna and a computer control. The antenna settling time at Parkes was about 10 seconds while the mirror settling time was about 50 milliseconds.

The b- and d-series of calculations are not so easily interpreted, because they involve different radiotelescopes and hence the calibration errors may be different. Also, in this case, the system temperatures of the front end are different (the sensitivity of the Kitt Peak front end is reduced by 2.5 with respect to the Parkes front end). From "b", the AOS appears to produce an output which has a noise contribution eight times greater than that in the corresponding output from the filter banks for an equivalent input $(\overline{K}_S(\text{AOS}) = (4.74 \times 2.5) \times 2/2\sqrt{2})$. From "d" the noise contribution at the output of the correlator seems to be fourteen times greater than at the output of the filter banks.

Even if the above comparison of receivers in different telescopes is very approximate, it appears that, despite its noisy front end, the Kitt Peak receiver achieved, in a much shorter time, an rms temperature equivalent to that achieved with the Parkes receivers. Of course the Parkes latitude is more suitable for observations of the galactic center. With 74° of maximum zenith angle achieved by the Kitt Peak antenna and 60° by the Parkes one, the times available for the observations on Sgr. B2 were $\sim$ 4 h.15mn. at Kitt Peak and $\sim$ 6 h. at Parkes. It is possible to represent the loss of the Kitt Peak signal to noise ratio, due to a shorter time of integration, by a fourth "partial sensitivity constant", $\overline{K}_S(L)$, arising from the latitude and not from the receiver. These constants are summarized in the table below. The

sensitivity constant K_S^* includes the receiver noise and the time available for observations. The partial constant related to the mode of observations has been defined as a function of the indicated on-source time of integration.

TABLE 3.4

Partial sensitivity constants of the receivers

receiver	$\overline{K}_S$(FE)	$\overline{K}_S$(BE)	$\overline{K}_S$(MO)	K_S	$\overline{K}_S$(L)	K_S^*	on-source time of integration
Kitt Peak (filter banks)	2.5	1	2	1.0	1.2	1.0	on-s + ref
Parkes (one-bit correlator)	1.0	8[ab]	$\sqrt{2}$	2.2	1.0	1.8	on-s
Parkes (AOS)	1.0	8[a]	$2\sqrt{2}$	4.5	1.0	3.7	on-s (beam on-s + beam off-s)

a : this factor varies as a function of calibration errors.

b : this factor can be decomposed in the product, $5 \times (\pi/2)$, which shows the excess contribution of noise.

3.3 *UPPER LIMITS OF GLYCINE COLUMN DENSITY*

Since any interstellar molecular lines from glycine was expected to be very weak, substantial integration times were used. Details of the searches are given in table 3.5. Fig. 3.2 shows an average of 33600 seconds of integration on the transition $10_{3,7} \rightarrow 9_{3,6}$ at 75379.5 GHz observed at Parkes, in the direction of Sgr. B2. A smoothing function has been applied on five channels and the base line has been removed by linear regression. At the position of the arrow, the frequency of the

TABLE 3.5

Upper limits of glycine column density

Source	α(1950) h m s	δ(1950) ° ' "	Telescope	Line	Frequency resolution	On-source time (s)	ΔT_a (rms)	Source parameters T_{ex} (K)	ΔV(km/s)	Upper limit nL (cm^{-2})
Sgr B2 (OH)	17 44 11	-28 22 30	Kitt Peak	(1)	1 MHz	8160	0.02*	35	25	7×10^{13}
			Kitt Peak	(2)	1 MHz	6000	0.03*	35	25	9×10^{13}
			Kitt Peak	(3)	1 MHz	7440	0.03*	35	25	9×10^{13}
		-28 22 42	Parkes	(4)	1 MHz	33600	0.014	35	25	3×10^{14}†
			Parkes	(5)	1 MHz	29700	0.02	35	25	2×10^{14}†
		-28 22 30	Kitt Peak	(5)	1 MHz	12720	0.02*	35	25	8×10^{13}
Ori A (OH)	5 32 47	-5 24 21	Kitt Peak	(1)	250 kHz	7200	0.03*	90	3	3×10^{13}
			Kitt Peak	(2)	250 kHz	9600	0.03*	90	3	3×10^{13}
			Kitt Peak	(3)	250 kHz	4800	0.04*	90	3	4×10^{13}
			Parkes	(4)	250 kHz	9600	0.03	90	3	2×10^{14}†
			Kitt Peak	(5)	250 kHz	16400	0.02*	90	3	3×10^{13}
			Onsala	(6)	240 kHz	34500	0.02*	90	3	2×10^{14}
DR21 (OH)	20 37 14	42 12 00	Onsala	(6)	240 kHz	28500	0.02*	40	2.5	6×10^{13}
Heiles 2	4 38 39	25 35 00	Onsala	(6)	120 kHz	10600	0.04*	7	0.5	2×10^{12}
NGC 2264	6 38 24	9 32 12	Onsala	(6)	60 kHz	3800	0.12*	40	3	4×10^{14}
W51	19 21 27	14 24 30	Onsala	(6)	240 kHz	15700	0.02*	45	15	4×10^{14}
NGC 7538	23 11 37	61 11 48	Onsala	(6)	240 kHz	2900	0.06*	40	5	4×10^{14}
W3 (OH)	2 23 17	61 39 00	Onsala	(6)	240 kHz	12200	0.03*	33	7	2×10^{14}
L134N	15 51 30	-2 43 31	Onsala	(6)	60 kHz	5000	0.06*	7	0.5	3×10^{12}

*T_a corrected for telescope efficiency of 70 per cent (Kitt Peak) and 75 per cent (Onsala).

†Assumes telescope efficiency of 20 per cent.

Fig. 3.2 The ($J_{K_a K_c} = 10_{3,7} \rightarrow 9_{3,6}$) transition of glycine observed in the direction of the Sgr B2 molecular cloud.

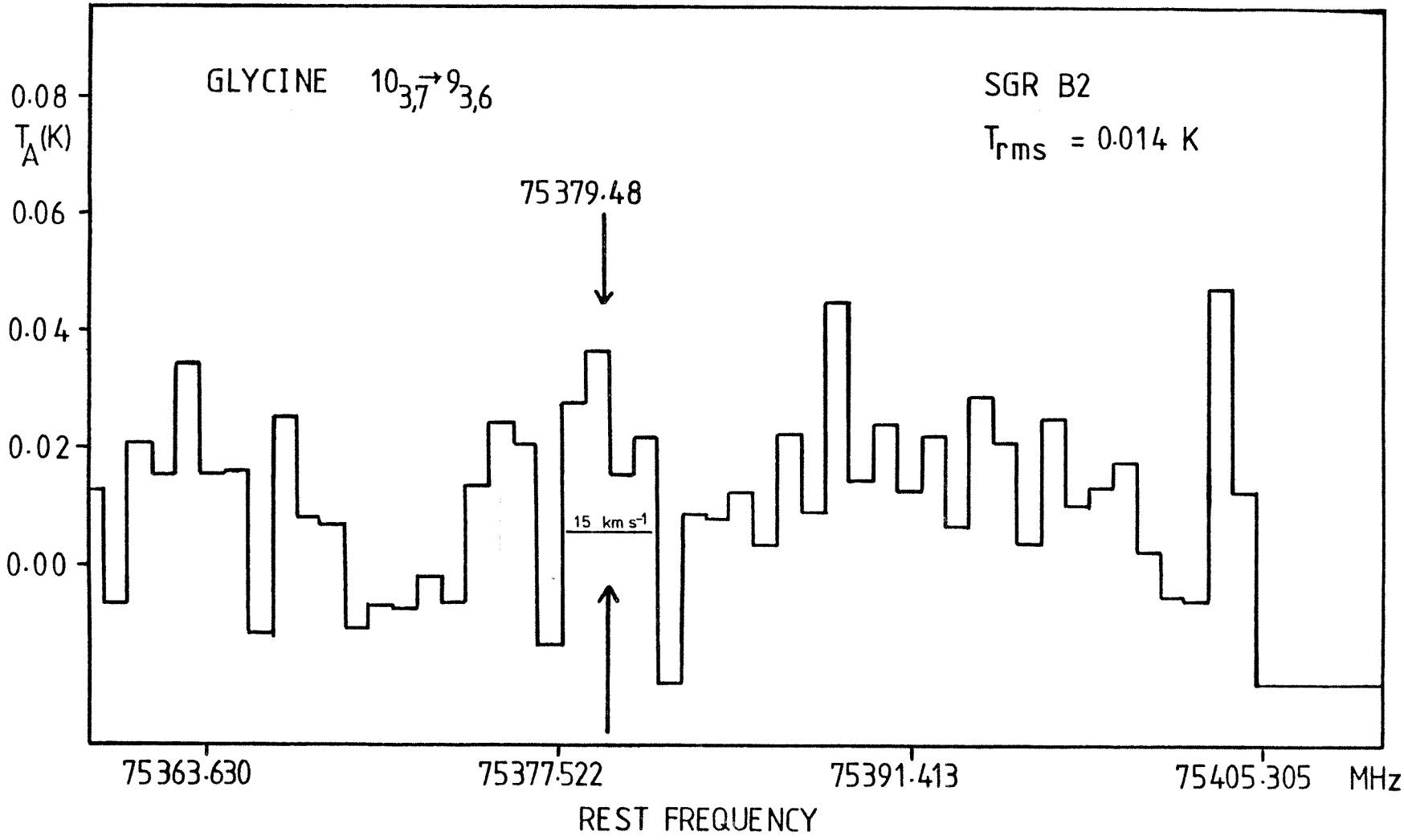
GLYCINE $10_{3,7} \rightarrow 9_{3,6}$
SGR B2
T_{rms} = 0.014 K
75379.48
0.08
T_A(K)
0.06
0.04
0.02
0.00
15 km s^{-1}
75363.630
75377.522
75391.413
75405.305
MHz
REST FREQUENCY

glycine transition has been corrected for a velocity with respect to the local standard of rest (lsr) of 62 km s^{-1} a value typical of other molecules which are most likely related to glycine, methylamine CH_3NH_2 [15,16], cyanamide NH_2CN [17], methyl cyanide CH_3CN [18] and ethyl cyanide CH_3CH_2CN [19]. The signals emitted by these molecules show a velocity width which is spread between 16 and 21.4 km s^{-1} (CH_3NH_2: 20 km s^{-1}, NH_2CN: 17.9 and 21.4 km s^{-1}, CH_3CN: 16 km s^{-1} and CH_3CH_2CN: 18 km s^{-1}). A Fisher F-test applied at the position of the glycine signal, with a Gaussian profile of 18 km s^{-1} FWHH gave a probability of presence of the line of 92%. This probability means that the observed line is expected to originate from a spurious feature only eight times in hundred observations. This probability is not high enough to conclude from these observations in the presence of glycine in the molecular cloud Sgr B2.

However upper limits for the column density of glycine in the various sources can be derived and has been calculated, using the values listed in table 3.4 and assuming that a signal of intensity twice the rms noise might just be perceived. As in the process of selection of transitions, a Boltzmann distribution over the lower energy states has been assumed. The values of the excitation temperature, T_{ex}, are thus estimated kinetic temperatures of molecular clouds. A similar LTE model accounted within a factor of two for observed intensities of a considerable number of lines of the relatively large molecule ethyl cyanide in Ori. A. Details on the calculations can be found in appendix 5.

In most of the listed sources, glycine, if present has a column density no greater than a few times 10^{13} cm^{-2}. A tighter limit is set for several cold clouds. In the case of Sgr. B2 and Ori. A, where most molecules have been found, this implies that, if glycine is

present, it is less abundant than some of relatively large molecules such as ethanol, CH_3CH_2OH, [20] ($N \simeq 10^{15}$ cm^{-2} with T_{ex} = 20 K) and ethyl cyanide [19] ($N = 0.9 \times 10^{14}$ cm^{-2} with T_{ex} = 20 K).

3.4 EVIDENCE FOR AN EXTRATERRESTRIAL GLYCINE

There is evidence that extraterrestrial glycine exists, in view of the analysis of meteorites and lunar rocks and in view also of the presence in molecular clouds of organic molecules which could, by association, form glycine.

Of course the study of extraterrestrial specimens is subject to the problem of biological contamination [21]. When necessary care has been taken to eliminate handling impurities [22], the amplitude of this problem can still be decreased by considering the structures and the relative amounts of the amino acids, and the distribution of their enantiomers. Since the value of these results is slightly reduced by the racemization processes [23] and the presence of D-amino acids in some contaminating micro-organisms [24], the isotopic ratio $^{13}C/^{12}C$ is also taken into account.

Table 3.6 gives some examples of meteorites and lunar rocks, with their contents in glycine. All the meteorites which are mentioned are of carbonaceous chondrites type [25]. It is the Murchinson fall which presents the most convincing result. This meteorite has been treated with contamination-proof technique and showed the presence of an almost equal amount of D- and L-enamtiomers of amino acids found in terrestrial proteins. Several non proteins amino acids have also been detected [26]. The carbon isotopic ratio differs appreciably from the ratio observable on earth to confirm an extraterrestrial origin ($\delta^{13}C$ = + 4.4 to + 5.9‰ against - 8 to - 29‰ on earth).

Lunar rocks supplied by the Apollo expeditions have also shown

TABLE 3.6

Some examples of extraterrestrial specimens and their glycine contents

Meteorites	date of fall	glycine content $\mu g/g_{sample}$	total amino acid content $\mu g/g_{carbon}$	ref.
Cold Bokkeveld (S^{th} Africa)	13/10/1838	6.1		[34]
Orgueil (France)	14/05/1864	13.1		[34]
Warrenton (Missouri USA)	3/01/1877	10.9		[34]
Mighei (USSR)	18/06/1889	5.4		[34]
Felix (Alabama USA)	15/05/1900	7.6		[34]
Mokoia (N. Zealand)	26/11/1908	12.3		[34]
Murray (Kentucky USA)	20/09/1950	3.0	400	[26c,27]
Murchison (Australia)	28/09/1969	6.1	600	[26c,27]

Lunar samples	glycine content $\mu g/g_{sample}$		ref.
Apollo 12	$< 10^{-3}$	510	[27,35]
Apollo 14	$3\ 10^{-3}$	250	[27,35]
Apollo 15	$10\ 10^{-3}$	65	[27,35]
Apollo 16	$5\ 10^{-3}$	70	[27,35]

the presence of extraterrestrial glycine. Since the amino acids to carbon ratios and the relative amounts of amino acids are comparable for both meteorites and lunar samples, it is suggested that common chemical processes have been operative [27]. In view of its low concentration, glycine could have been deposited on the moon by meteorites, in a similar way than the earth could have been contaminated.

It is interesting to note that all the protein and non-protein amino acids, found in the Murchison meteorite, were synthesized by action of electric discharges on a mixture of methane, nitrogen and water with traces of ammonia [28] and that the amino acids to glycine ratios in the meteorite were close to the ratios obtained with the electric discharges. Some heterocyclic amino acids, which cannot be formed in a conventional Miller-Urey experiment (CH_4, H_2O, NH_3) [29], have also been synthesized in a Fischer-Tropsch reaction [30].

Since meteorites are expected to be condensates from the solar nebula [31], which is only an advanced stage of the gas and dust clouds which have been observed in this work, it is reasonable to think that amino acids are present in these clouds. However, even without the support of the meteorites, it is predictable that glycine is formed in these molecular clouds, in view of the great number of organic molecules which have already been detected [32] ($\sim$ 700 transitions distributed over $\sim$ 50 molecular species). Numerous calculations on the chemical evolution of these molecular clouds are currently being developed [33]. Two series of processes are favored: catalytic reactions on the surface of grains and gas phase reactions with ion-molecule schemes. No model has yet predicted the formation of glycine. This is due to the enormous number of reactions which has to be taken into account for the formation of a ten atoms molecule. Also, uncertainties on parameters such as collisional excitation rates, adsorption energies, products distribution

of ion-molecule reactions, temperature density and velocity distributions of the clouds make these models too approximate, as far as the complex molecules are concerned. This imprecision is also emphasized by the different mechanisms of formation and destruction which occur as a result of the physical conditions inside or in the environment of the molecular cloud: ultraviolet radiation, X ray, cosmic ray and shock waves initiated by stellar winds, expanding HII regions and supernova remnants. The pathways to the formation of glycine, as for any polyatomic molecule, have to be exothermic (because of the low kinetic temperature of the clouds) and should proceed without activation energy (in order to increase the rates of the reactions). Exothermic gas phase ion-molecule reactions should hence contribute for a major part. This is supported by the fact that catalytic associations produce in general chain-type of molecules and no asymmetric conformations.

Hence glycine of extraterrestrial origin could have been deposited on the earth and the moon by meteorites which had been formed in the original nebula. By searching for glycine in clouds similar to the original nebula, a positive detection should have been obtained. Reasons for the non-detection are given in the next section.

3.5 *POSSIBLE EXPLANATIONS FOR THE NON-DETECTION OF GLYCINE*

Three possible explanations can be advanced for the non-detection of interstellar glycine: the noise produced by the receivers is too high, the choice of the transitions should have been determined by solving the equations of statistical equilibrium or the searched conformer is not the lowest energy conformation present in the clouds.

As seen from the study of section 3.2.3, a telescope set in Parkes with the Kitt Peak antenna and back end receiver and the Parkes front end would have been more suitable for the search of weak signals.

A maser front end could be used. Maser receivers have very low noise and some have been built for use at high frequencies. Unfortunately they show a too narrow instantaneous bandwidth for molecular line observations (5.5 MHz, for a F-band push-pull cavity maser of 30 dB gain, operated at 2.1 K and 2800 Gauss [36]). However 140 MHz bandwidth has been achieved, at the Five College Observatory, between 85 and 90 GHz, with a traveling-wave maser of 15 dB gain and 100 K SSB noise temperature including the atmosphere [37]. The trend nowadays in the aim of decreasing the front end detector noise, is the use of superconductor-insulator-superconductor (SIS) (Josephson) tunnel junctions in heterodyne mixing [38], instead of the point-contact Schottky diodes. Mixer noise temperatures as low as the photon noise limit, 1.5 K DSB can be achieved. But to gain full advantage of this low figure, a noiseless amplifier has to be developed.

Despite the cases for which local thermodynamical equilibrium explain the behaviour of observed emission lines, this theory may not prevail for glycine in the searched molecular clouds. A full study of the radiative transfer, with solutions of the equations of statistical equilibrium may be a necessity to predict the intensities of the glycine emitted lines. For the purpose of future observations on glycine and other complex molecules, this theory has been developed in the case of an asymmetric top and is presented in the next section.

It would also be advisable to search for other conformers of glycine.

3.6 RADIATIVE TRANSFER AND STATISTICAL EQUILIBRIUM IN THE ROTATIONAL TRANSITIONS OF AN ASYMMETRIC TOP MOLECULE

As mentioned earlier, simple LTE models accounted satisfact--orily for observed intensities of detected molecules. In these cases, line shapes can be explained by the fact, that molecules are excited to the local kinetic temperature (T) solely by collisions occurring in any direction with any velocity. However, in many interstellar clouds, the material densities are too low for collisions to populate the molecular energy levels involved in the detected transitions, and radiation trapping accounts as a component for the observed line intensities. Hence radiative transfer and statistical equilibrium equations have been solved for different types of clouds [39]. Two velocity models are mainly considered: gravitational collapse with systematic velocity gradients and turbulence. R.E. White [39] showed that, within the geometrical and physical uncertainties of the molecular cloud, the velocity gradient model may be used confidently. Consequently the gravitational collapse model of P. Goldreich and J. Kwan [39] has been the basis of this work. This model is applicable to diatomic molecules. In the following section, the equations of radiative transfer and statistical equilibrium, derived by P. Goldreich and J. Kwan, are extended to asymmetric top molecules.

The model assumes that the cloud is a uniform density, pressure free sphere which has collapsed from infinite radius and consequently has an infall velocity:

$$v(r) = \left(\frac{2GM}{R^3}\right)^{1/2} r = \frac{V}{R} r$$

where M is the mass of the cloud,

R its outer radius,

G the gravitational constant and

r the distance from the cloud center.

Considering that the collapse velocity is much bigger than the thermal velocity, the equations of radiative transfer are treated in the approximation developed by J.I. Castor [40], and the solutions are used in the equations of statistical equilibrium. In this treatment, the mean radiation intensity at any point in the cloud, J_ν (which is the specific intensity, I_ν, integrated over the line profile and averaged over angle), depends only upon the local value of the source function, S_ν ($S_\nu = \varepsilon_\nu/\kappa_\nu$ ratio of emission and absorption coefficients of the medium), and upon the escape probability, β, that a photon emitted at that point will escape from the cloud without further interaction.

In a gaseous atmosphere of a molecular species, transitions occur between rotational levels, due to collisional and radiative processes. The equilibrium distribution of populations is expressed by the solution of the statistical equilibrium equations:

$$\sum_j P_{ij}\, n_i = \sum_j P_{ji}\, n_j \quad (j \neq i)$$

with $$\sum_j n_j = N \quad \text{and} \quad P_{ij} = R_{ij} + C_{ij} \ .$$

N is the total number of molecules, per unit volume, of the species whose excitation is to be studied, and P_{ij} is the transition rate from the level i to the level j; it consists of two terms, a collisional rate C_{ij} and a radiative rate R_{ij}.

The equations of P. Goldreich and J. Kwan are based on a three level consideration:

—— J+1
—— J
—— J-1

But for the asymmetric molecule, levels with different values of J may interpenetrate, such as:

—— J-1	—— J-1	—— J	—— J	—— J+1
—— J	—— J	—— J	—— J	—— J
—— J	—— J-1	—— J	—— J-1	—— J

Consequently several different cases have to be considered in the formulation of the transition rates. Considering a level J in between an upper level, J_u, and a lower level, J_l, the equations of statistical equilibrium for an asymmetric top molecule can be expressed as:

$$\frac{dn_J}{dt} = \beta_{J_u,J} A_{J_u,J} \frac{g_{J_u}}{g_J} \left(n_j - \frac{(n_J - n_{J_u})}{[\exp(E_J - E_{J_u})/kT_{BB} - 1]} \right)$$

$$- \beta_{J,J_l} A_{J,J_l} \left(n_J - \frac{(n_{J_l} - n_J)}{[\exp(E_{J_l} - E_J)/kT_{BB} - 1]} \right) \qquad (1)$$

$$+ C\left\{ \sum_{L=J_u}^{\infty} g_L \left(n_L - n_J \exp \frac{(E_J - E_L)}{kT} \right) \right\}$$

$$- C\left\{ \sum_{L=0}^{J_l} g_L \left(n_J - n_L \exp \frac{(E_L - E_J)}{kT} \right) \right\}$$

The first term is the rate of radiative filling of the J level, the second is the rate of radiative decay of the J level, the third is the rate of filling of the J level by collisional de-excitation of the levels above J and the last term is the rate of collisional de-population of the J level to lower levels.

The term $\beta_{J_u,J}$ is the average escape probability for a photon emitted in the transition ($J_u \rightarrow J$). Following P. Goldreich and J. Kwan in the modification of J.I. Castor's results, β can be expressed as:

$$\beta_{J_u,J} = [1 - \exp(-\tau_{J_u,J})]/\tau_{J_u,J}$$

where the optical depth is:

$$\tau_{J_u,J} = N \frac{hcR}{4\pi V} B_{J_u \rightarrow J} g_{J_u} (n_J - n_{J_u}) \ .$$

For an asymmetric top, the coefficient for stimulated emission is expressed as (appendix 6):

$$B_{J_u \to J} = (g_J/g_{J_u}) B_{J_u \leftarrow J}$$

$$B_{J_u \to J} = (g_J/g_{J_u}) \frac{8\pi^3}{3h^2} \frac{1}{4\pi\varepsilon_0} \frac{\mu^2 S}{g_J} \qquad \text{(S.I.)}.$$

Substituting for $B_{J_u \to J}$, $\tau_{J_u,J}$ becomes:

$$\tau_{J_u,J} = \text{TAU}\ g_{J_u} (n_J - n_{J_u}) \qquad \text{(S.I.)}$$

where

$$\text{TAU} = \frac{2\pi^2 c \mu^2 RN}{3hV} \frac{1}{4\pi\varepsilon_0} \qquad \text{(S.I.)}$$

In equation (1), T is the kinetic temperature of the molecular cloud, T_{BB} is the cosmic black-body radiation temperature, (2.7 K), and $A_{J_u,J}$ is the Einstein A-coefficient for spontaneous emission. For an asymmetric top it is expressed as (appendix 6):

$$A_{J_u \to J} = \frac{64\pi^4 \nu^3}{3hc^3} \frac{1}{4\pi\varepsilon_0} \frac{\mu^2 S}{g_{J_u}} \qquad \text{(S.I.)}$$

The formulation of the collisional excitation rates is difficult, due to little information given on the collision cross-sections. For simplication, it is assumed that all downward collision rates are equal. They hence can be expressed as:

$$C = N_{H_2} \langle \sigma V_T \rangle \frac{1}{Q}$$

where $\langle \sigma V_T \rangle$ is the total rate at which J-changing collisions occur. Assuming that hydrogen molecules are the principal colliding molecules, V_T takes the value of 1 km s^{-1} at 100 K. The probability that a transition will end in any particular final state (characterized by J, τ, M) must vary in inverse proportion to the total number of final states that can be

reached, and which are expressed by the rotational partition function Q_r (appendix 1):

$$Q_r = \left[\left(\frac{\pi}{ABC}\right)\left(\frac{kT}{h}\right)^3\right]^{1/2}$$

In terms of the previously defined notation the above equations of statistical equilibrium, formulated for an asymmetric top molecule (1) can be solved for $dn_J/dt = 0$, and accordingly to the selection rules.

CHAPTER 4

THE DETECTION OF INTERSTELLAR METHANOL

Methanol, CH_3OH, also named methyl alcohol, is an asymmetric molecule with a methyl internal top and a planar framework. Its rotational energy levels [1,2] are thus labelled according to the A and E-irreducible representations of the C_{3v} symmetry group. Energy level diagrams have already been drawn [17,3,2]. The torsionally degenerate pairs of the ($K \neq 0$) A-levels are slightly split by the molecular asymmetry and can be named, using the asymmetric top notation K_{-1}, K_{+1}. However they are usually sub-labelled with K only ($K > 0$), a plus or minus sign distinguishing the two levels of the doublet. The K doublets of the E-ladder are widely separated by torsion and are sub-labelled with K ($-J < K < J$).

Methanol is one of the most abundant and widespread molecules in the interstellar medium. Some of its transitions are seen with maser amplification. The ($J_K = 5_{-1} \rightarrow 4_0$ E) and ($J_K = 4_{-1} \rightarrow 3_0$ E) were predicted to be inverted. During this work, these two transitions have been searched in fourteen galactic and extra galactic sources, with declination from - 70° to + 62°. When detected, the ($J_K = 4_{-1} \rightarrow 3_0$ E) appeared almost always with maser emission and the ($J_K = 5_{-1} \rightarrow 4_0$ E) seemed very often to be inverted. The ($J_K = 3_1 \rightarrow 3_1$ A) has also been detected, for the first time, in maser emission from the galactic center and the ($J_K = 1_0 \rightarrow 0_0$ E) and ($J_K = 1_0 \rightarrow 0_0$ A^+) have been searched in eight sources without success. High resolution maps of the Ori A and Sgr B2 molecular clouds have been drawn with the ($J_K = 5_{-1} \rightarrow 4_0$ E) transition. The ($J_K = 4_{-1} \rightarrow 3_0$ E) has also been mapped in Ori A. A more detailed summary of the observations can be found at the start of each discussion on the methanol emission from individual sources. The last section reports a negative search of this methanol.

TABLE 4.1

Molecule and telescope parameters

transition	rest[a] frequency (MHz)	receiver front end-back end	telescope	HPBW	T_{syst} SSB (K)	date of observation
$4_{-1}\rightarrow 3_0$ E	36169.24 (10)	7 mm mixer-correlator	Parkes 16.7 m	90"[c]	1000	Feb. 1977 June 1978
$5_{-1}\rightarrow 4_0$ E	84521.21 (10)	3 mm mixer-filter banks	Kitt Peak 11.0 m	77"[d]	1700	April 1978
		3 mm mixer-correlator/AOS	Parkes 16.7 m	45"[c]	800	July 1978
$3_1\rightarrow 3_1$ A	5005.320 (10)[b]	6 cm parametric amplifier-correlator	Parkes 64.0 m	4'.3[c]	60	May 1979
$1_0\rightarrow 0_0$ A^+	48372.60 (50)	7 mm mixer-correlator	Parkes 16.7 m	85"[c]	1300	June 1978
$1_0\rightarrow 0_0$ E	48377.09 (50)	7 mm mixer-correlator	Parkes 16.7 m	85"[c]	1300	June 1978

a : Lees et al. [1], unless otherwise noted.

b : Measured in Monash laboratory.

c : Determined by measurements of the moon diameter.

d : Determined theoretically [32].

TABLE 4.2

Summary of methanol observations

source	transition	pointing position α (1950)	δ	V_{LSR} (km s^{-1})	T_A^* (K)	ΔV (km s^{-1})	ΔT_{rms} (K)	on-source time (S)	date of observation
Ori A	$4_{-1}\rightarrow 3_0$ E	$05^h 32^m 47^s.0$	-05°24'21"	7.6	2.70	1.7	0.66	10800	06/1978
M17(SW)	$4_{-1}\rightarrow 3_0$ E	18 17 27.0	-16 14 54	18.6	0.55	2.7	0.22	19500	06/1978
W51	$4_{-1}\rightarrow 3_0$ E	19 21 27.0	14 24 30	59	0.59	13	0.12	9600	06/1978
NGC 2264	$4_{-1}\rightarrow 3_0$ E	06 38 27.0	09 32 06	7.6	0.75	6.3	0.19	12000	06/1978
Sgr A (NH_3)	$4_{-1}\rightarrow 3_0$ E	17 42 28.0	-29 01 30	23.2	3.45	25	0.16	6000	06/1978
Sgr B2	$4_{-1}\rightarrow 3_0$ E	17 44 11.0	-28 22 30	62	8.79	27	0.05	1200	06/1978
N159(LMC)	$4_{-1}\rightarrow 3_0$ E	05 40 25.0	-69 46 00	235	...	...	0.14	18600	06/1978
Southern Coal Sack	$4_{-1}\rightarrow 3_0$ E	17 29 08.0	-63 28 12	-6	...	...	0.48	3900	06/1978
ρ Oph	$4_{-1}\rightarrow 3_0$ E	16 23 10.0	-24 18 20	3	...	...	0.70	3900	06/1978
CRL 3068 Planetary Nebula	$4_{-1}\rightarrow 3_0$ E	21 16 42.0	16 55 10	-28	...	...	0.11	7200	06/1978
Sgr B2	$5_{-1}\rightarrow 4_0$ E	17 44 11.0$_{map}$	-28 22 30	54	11.3	8.5	0.40	3600	07/1978
Ori A	$5_{-1}\rightarrow 4_0$ E	05 32 47.0$_{map}$	-05 24 21	8.0	5.0	1.6	0.20	3600	07/1978
IRC+10216	$5_{-1}\rightarrow 4_0$ E	09 45 14.8	13 30 38	-22	...	25	0.046	2880	04/1978
L134	$5_{-1}\rightarrow 4_0$ E	15 51 00.0	-04 26 57	3	...	0.8	0.15	3360	04/1978
L134N	$5_{-1}\rightarrow 4_0$ E	15 51 30.0	-02 43 31	3	...	0.5	0.11	4320	04/1978
W3(Mol)	$5_{-1}\rightarrow 4_0$ E	02 21 46.9	61 52 54	-40	...	7.0	0.048	5280	04/1978
NGC 2264	$5_{-1}\rightarrow 4_0$ E	06 38 28.4	09 32 12	7.4	0.69	3.0	0.16	2880	04/1978
Sgr A (NH_3)	$3_1\rightarrow 3_1$ A	17 42 28.0	-29 01 30	45	0.10	44	0.020	4500	05/1979
ρ Oph	$1_0\rightarrow 0_0$ E	16 23 10.0	-24 18 20	3	...	...	0.91	3900	06/1978
N159(LMC)	$1_0\rightarrow 0_0$ E	05 40 24.0	-69 46 00	235	...	...	0.57	4800	06/1978
IRC + 10011	$1_0\rightarrow 0_0$ A+	01 03 48.0	12 19 45	11	...	...	0.071	3300	06/1978
Sgr B2	$1_0\rightarrow 0_0$ A+	17 44 11.0	-28 22 30	62	...	...	0.061	9600	06/1978
N159(LMC)	$1_0\rightarrow 0_0$ A+	05 40 24.0	-69 46 00	235	...	...	0.13	3300	06/1978
M17(SW)	$1_0\rightarrow 0_0$ A+	18 17 27.0	-16 14 54	20	...	...	0.12	5700	06/1978
W51	$1_0\rightarrow 0_0$ A+	19 21 23.0	14 24 30	60	...	...	0.15	12000	06/1978
RCrA	$1_0\rightarrow 0_0$ A+	18 58 37.0	-37 02 26	6	...	...	0.095	6000	06/1978

4.1 OBSERVATIONS

The observations have been conducted at five different periods extended on more than two years, using the radiotelescopes at Parkes and Kitt Peak and in collaboration with R.D. Brown, P.D. Godfrey, B.J. Robinson and D.A. Winkler. The $4_{-1}\rightarrow 3_0$ E transition has first been detected in February 1977. More observations have then been recorded in April, June and July 1978 and then in May 1979. A summary is given in tables 4.1 and 4.2. The total power mode was adopted in Parkes and position switching in Kitt Peak.

4.2 DISCUSSIONS

4.2.1 Orion A

About thirty transitions of methanol have been detected towards Orion molecular cloud, but the searches for the $4_{-1}\rightarrow 3_0$ E and $5_{-1}\rightarrow 4_0$ E have always been unsuccessful. This was an anomaly considering first, that emission had been seen from higher-lying states (the 25 GHz lines for instance) and second, that predictions, based on infra-red emission rate coefficients, propose population inversions of the states involved in these transitions [2].

During this work the $4_{-1}\rightarrow 3_0$ E has been detected in maser emission and mapped around the 4.3 km s^{-1} OH position. This emission arises from within the outer 21 μ contour of the Kleinmann-Low nebula, perhaps from the OH maser sources or more probably from the 25 GHz maser methanol source.

The $5_{-1}\rightarrow 4_0$ E has also been detected with high antenna temperature and is probably inverted. A map of the $5_{-1}\rightarrow 4_0$ E locates the origin of this emission in a compact source, about 20" west from the OH positions, outside the IR Kleinmann-Low nebula.

transition	type	rest frequency (MHz)	pointing position α (1950)	δ	E_{lower}[a] (cm^{-1})	E_{upper}[a] (cm^{-1})	E_u/k (K)	$A\times10^7$ (s^{-1})	ΔV (km s^{-1})	T_A*(obs) (K)	$(2J_u+1)\times e^{-E_u/kT}\times A\times10^6$ (s^{-1})	T_A*(LTE) (K)	T_A*(obs)/T_A*(LTE)	HPBW (")	$N_T\times10^{-15}$ (cm^{-2})	ref
$5_0\rightarrow4_1$ E	b	76509.40 (200)	$5^h32^m47^s$	-5°24'21"	25.275	27.827	40.1	8.49	3.0	0.73	5.99	0.24	3	86	4.6	9
$2_{-1}\rightarrow1_{-1}$ E	a	96739.39 (10)	5 32 46.8	-5 24 24	0.000	3.227	4.6	24.7	4.1	1.55	11.73	0.47	3	67	11	10
$2_0\rightarrow1_0$ E	a	96744.58 (10)	5 32 46.8	-5 24 24	5.246	8.473	12.2	33.0	4.1	1.61	14.41	0.58	3	67	9.1	10
$2_1\rightarrow1_1$ E	a	96755.51 (10)	5 32 46.8	-5 24 24	10.751	13.979	20.1	24.8	4.1	1.12	9.91	0.40	3	67	9.2	10
$4_2\rightarrow4_1$ E	b	24933.468[b]	5 32 46.9	-5 24 18	25.275	26.106	37.6	0.78	4.5	3.5[c]	0.46	0.019	194	78	23	5
$2_2\rightarrow2_1$ E	b	24934.38 (10)	5 32 46.9	-5 24 18	13.979	14.811	21.3	0.58	3.5	0.35[c]	0.23	0.0092	38	78	7.3	5
$5_2\rightarrow5_1$ E	b	24959.080[b]	5 32 46.9	-5 24 18	33.343	34.175	49.2	0.81	3.5	4.5[c]	0.51	0.021	214	78	42	5
$6_2\rightarrow6_1$ E	b	25018.123[b]	5 32 46.9	-5 24 18	43.025	43.859	63.2	0.83	3.0	6.5[c]	0.53	0.022	309	78	50	5
$7_2\rightarrow7_1$ E	b	25124.873[b]	5 32 46.9	-5 24 18	54.320	55.158	79.4	0.85	3.0	5.5[c]	0.53	0.021	262	78	43	5
$8_2\rightarrow8_1$ E	b	25294.41 (10)	5 32 48	-5 24 20	57.229	68.072	98.3	0.88	3.0	0.70[c]	0.50	0.020	35	78	5.8	6
$3_2\rightarrow3_1$ E	b	24928.70 (10)	5 32 46.9	-5 24 18	18.820	19.651	28.3	0.72	3.0	1.20[c]	0.36	0.014	86	78	13	5
$1_0\rightarrow0_0$ E	a	48377.09 (50)	5 32 47.0	-5 24 21	3.632	5.246	7.5	3.44	4.7	0.29	0.95	0.038	8	135	7.3	11
$5_{-1}\rightarrow4_0$ E	b	84521.21 (10)	5 32 47.0	-5 24 21	19.765	22.584	32.5	18.7	1.6	5.95	14.33	0.58	10	45	10	this work
$6_{-2}\rightarrow7_{-1}$ E	b	85568.20 (100)	5 32 47	-5 24 21	43.546	46.400	66.8	12.0	4.0	0.30	7.42	0.30	1	76	2.5	12
$8_{-4}\rightarrow9_{-3}$ E	b	89505.80 (100)	5 32 47	-5 24 21	110.694	113.680	163.7	7.47	3.0	0.30	2.07	0.084	4	76	7.4	12
$8_3\rightarrow9_2$ E	b	94542.00 (1000)	5 32 47	-5 24 21	82.603	85.755	177.9	13.5	3.9	0.35	5.82	0.23	1	76	4.4	12
$10_1\rightarrow10_0$ E	b	169335.34 (10)	5 33 46.9	-5 24 11	92.235	97.886	141.0	253.0	8.0	0.70	110.9	4.48	.1	38	2.9	8
$3_0\rightarrow2_0$ E	a	145093.75 (10)	5 32 46.9	-5 24 26	8.473	13.313	19.2	119.0	4.5	1.25	67.3	2.72	1	60	3.6	3
$3_{-1}\rightarrow2_{-1}$ E	a	145097.47 (10)	5 32 46.9	-5 24 26	3.227	8.067	11.6	106.0	4.0	1.45	65.2	2.64	1	60	3.9	3
$4_{-1}\rightarrow3_0$ E	b	36169.24 (10)	5 32 47.0	-5 24 21	13.313	14.519	20.9	1.49	1.7	2.70	1.06	0.043	63	90	12	this work
$11_1\rightarrow10_2$ A^-	b	76247.60 (200)	5 32 47	-5 24 21	114.924	117.469	169.2	8.34	3.0	0.70	29.2	1.18	1	86	8.9	9
$2_0\rightarrow1_0$ A^+	a	96741.42 (10)	5 32 46.8	-5 24 24	1.614	4.840	7.0	33.0	4.1	1.87	15.3	0.62	3	67	10	10
$1_0\rightarrow0_0$ A^+	a	48372.60 (50)	5 32 47.0	-5 24 21	0.000	1.614	2.3	3.44	4.7	0.44	14.9	0.60	1	135	15	11
$7_2\rightarrow6_3$ A^-	b	86615.90 (100)	5 32 47	-5 24 21	68.493	71.382	102.8	6.73	3.5	0.60	3.22	0.13	5	76	10	12
$7_2\rightarrow6_3$ A^+	b	86902.90 (100)	5 32 47	-5 24 21	68.493	71.392	102.8	6.80	4.0	0.20	3.20	0.13	1	76	4.0	12
$8_0\rightarrow7_1$ A^+	b	95169.44 (10)	5 32 47	-5 24 21	54.887	58.062	83.6	40.8	3.9	0.85	27.4	1.11	1	76	2.3	12
$3_0\rightarrow2_0$ A^+	a	145103.23 (10)	5 32 46.9	-5 24 26	4.840	9.681	13.9	119.0	4.5	1.35	71.3	2.88	1	60	3.7	3

a : Lees et al. [1] unless otherwise noted.

b : Gaines et al. [4].

c : The (ΔJ = 0, K = 2→1) lines may be time variable; the J = 4, 5, 6 and 7 have been measured earlier with antenna temperature of 1.00 K, 1.10 K, 1.70 K and 1.50 K [6]. With these values, T_A*(obs)/T_A*(LTE) becomes 53, 52, 79 and 70. Another observation of the J = 6 and 7 [7] detected ∿ 40 K of T_A*; in this case, T_A*(obs)/T_A*(LTE) becomes ∿ 1800.

d : The column densities have been calculated using T_{ex} = 90 K

The $5_{-1}\rightarrow 4_0$ E and $4_{-1}\rightarrow 3_0$ E have been detected with high antenna temperatures as shown in table 4.3. In order to determine if they exhibit significant departures from LTE, a calculation of thermal intensities has been completed for all the lines reported in the literature, together with the new data reported here. The analysis has been made in the case of an optically thin cloud and assuming that the relative intensities are proportional to the product of the statistical weight of the upper level, the Einstein A-coefficient and the Boltzmann factor. A cloud kinetic temperature of 90 K has been used in the calculations. The spin weights of the A and E-states follow the ratio (2:1), but this is compensated by the double degeneracy of the E-states, hence the relative statistical weight of the J levels are proportional to (2J+1) only. The transition $6_{-2}\rightarrow 7_{-1}$ E at 85.6 GHz has its upper level not too high to be populated and the energy level scheme, showing spontaneous infra-red transitions with largest A-coefficients [2], does not predict inversion of population between the levels 6_{-2} E and 7_{-1} E. Hence the LTE antenna temperatures of all the observed lines have been evaluated using the intensity of the $6_{-2}\rightarrow 7_{-1}$ E as reference, and are listed in column 13 of the table 4.3.

The column 14 of the same table gives the calculated coefficients for departure from LTE. The highest deviations are observed in the lines ($\Delta J = 0$ $K = 2\rightarrow 1$) around 25 GHz, which are known to be masing. Another important departure is seen ffor the $4_{-1}\rightarrow 3_0$ E line which can thus be considered to emit with a maser action. The $5_{-1}\rightarrow 4_0$ E may be slightly inverted, as perhaps the $1_0\rightarrow 0_0$ E. Indeed, considering the energy level scheme [2], this last transition is also a candidate for nonthermal emission. Another slight anomaly seems to appear in the low observed intensity of the U 169336.1 (7) MHz, which had been tentatively assigned to the $10_1\rightarrow 10_0$ E transition of methanol [8]. This could be due to the high energy of the upper level (141 K). However higher levels seem to be

populated enough to produce thermal emission: 8_{-4} E, 8_{3} E and 11_{1} A^{-}. Another explanation could be, that this transition does not belong to the methanol spectrum; however the departure from LTE is not sufficient to definitely reject the identification.

A map of $5_{-1}\rightarrow 4_{0}$ E transition has been drawn and is shown on fig. 4.2. Fifteen different points have been recorded with, in some cases, several observations of the same position. The line observed at $\sim 3^{s}$ east of the OH positions is shown on fig. 4.1 together with its statistical analysis (via STATRED). The emission appears to be centered at the following position:

$$\alpha(1950) = 05^{h}\ 32^{m}\ 45^{s}.4 \qquad \delta(1950) = -\ 05^{\circ}\ 24'\ 20''$$

Since the half power beamwidth was only 45", it is possible to locate the source within a restrained area: the observations are in perfect agreement with a compact source smaller than 45" in diameter.

A map of the $4_{-1}\rightarrow 3_{0}$ E transition has also been drawn, with data obtained in February 1977, in an area of 1" around the OH position (fig. 4.3). The HPBW was 1.'5. The source does not appear to be bigger than 1' in diameter and could be centered at the 4.3 km s^{-1} OH position or within 20" south of it.

It would be interesting to compare the coordinates of the $5_{-1}\rightarrow 4_{0}$ E and $4_{-1}\rightarrow 3_{0}$ E sources with the position of the maser emission at 25 GHz. The (J = 6) and (J = 7) transitions have been detected [7] with a 35" HPBW. They show a peak emission at the (1950) position $\alpha = 05^{h}\ 32^{m}\ 46.^{s}4$ and $\delta = -\ 05^{\circ}\ 24'\ 30''$. VLBI observations [13] set a lower limit of 0.006" to the angular size of this source.

Since the $4_{-1}\rightarrow 3_{0}$ E is detected with a high antenna temperature at a position 1' south of the 4.3 km s^{-1} OH coordinates, it is possible that the emission originates in the same source than that of the 25 GHz maser lines (located $\sim$ 11" south of the 4.3 km s^{-1} OH source). At 1'

south of OH, the HPBW would not include the 25 GHz maser source, but the emission would be intense enough for the $4_{-1}\rightarrow 3_0$ E line to be observed. Another indication could have been given by the source distribution. Indeed, the (J = 6) and (J = 7 K = 2→1) lines of 3 km s^{-1} width have been seen composed of three 0.4 km s^{-1} components [7]. But, the resolution used in this work, during the observations of the $4_{-1}\rightarrow 3_0$ E, (0.16 km s^{-1} compare to 0.065 km s^{-1} for the 25 GHz lines) did not allow a subdivision of the line.

Hence it is not possible to associate definitely the $4_{-1}\rightarrow 3_0$ E maser source with the 25 GHz methanol position, but it is plausible that this new methanol maser source is situated south of the OH maser coordinates and certainly within the 21 μ contour of the Kleinmann-Low nebula [14]. The $5_{-1}\rightarrow 4_0$ E appears to arise from another methanol source outside this 21 μ contour. If the inversion of population in the levels of the $4_{-1}\rightarrow 3_0$ E transition is due to an infra-red excitation, it is thus understandable that the $5_{-1}\rightarrow 4_0$ E does not present a so strong anomalous behaviour.

Column densities of methanol have been calculated in the case of an optically thin cloud, in the approximation of the Boltzmann statistics, for a cloud temperature of 90 K and a beam filled at 100%. In the case of the $5_{-1}\rightarrow 4_0$ E, $4_{-1}\rightarrow 3_0$ E and (ΔJ = 0 K = 2→1) E-lines, these values are only lower limits, since the sizes of the sources are probably smaller than the beam. Details on the calculations are given in the appendix 5. Considering there is an equal number of A and E-levels, the total column density of methanol, reported in table 4.3, is twice the column density in the E or A-ladders.

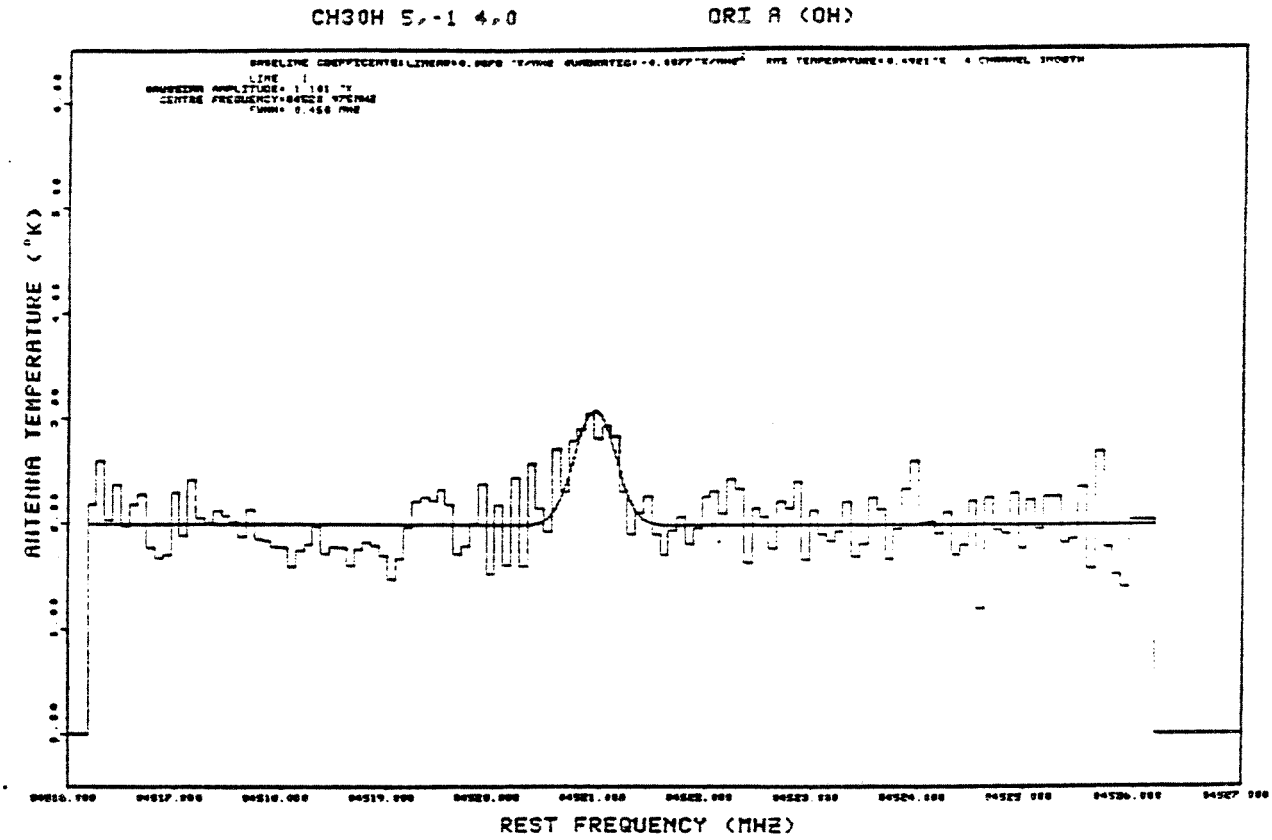

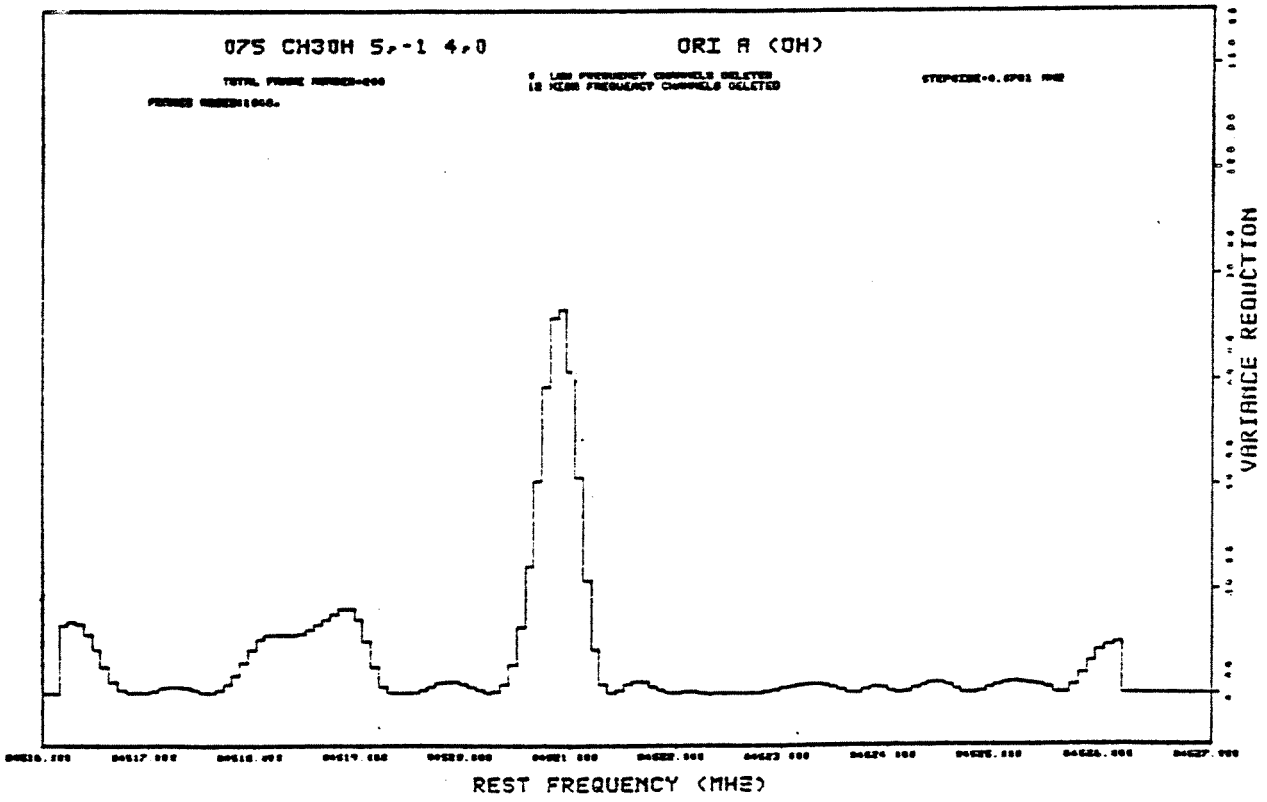

Fig. 4.1 The ($J_K = 5_{-1} - 4_0$ E) emission of methanol from Ori A and its statistical analysis. The (1950) pointing position was:
$\alpha = 05^h 32^m 43^s.0$ $\delta = -05°24'19''$.

Fig. 4.2 Map of the ($J_K = 5_{-1} \rightarrow 4_0$ E) emission of methanol from Ori A

Positions of several objects in Ori A

map label	object	pointing position α (1950)	δ	ref.
a	Becklin-Neugebauer			
	IR point source	$05^h\ 32^m\ 46^s.7$ (1)	-05° 24' 17" (1)	27
b	IR Kleinmann-Low	approximate contour of		
	nebula	the 21 μ emission		4
c	OH 4.0 - 4.5 km s^{-1}	$05^h\ 32^m\ 47^s.0$ (1)	-05° 24' 19" (2)	28
d	OH 6.8 - 7.9 km s^{-1}	$05^h\ 32^m\ 46^s.8$ (1)	-05° 24' 25" (3)	28
e	OH 17.6 - 23.7 km s^{-1}	$05^h\ 32^m\ 46^s.9$ (1)	-05° 24' 18" (2)	28
f	H_2O 2.4 km s^{-1} 06/1970	$05^h\ 32^m\ 45^s.90$ (15)	-05° 24' 12" (8)	29
g	H_2O 2.4 km s^{-1} 02/1971	$05^h\ 32^m\ 45^s.70$ (15)	-05° 24' 08" (5)	29
h	H_2O 2.4 km s^{-1} 03/1971	$05^h\ 32^m\ 45^s.90$ (15)	-05° 24' 07" (5)	29
i	H_2O 7.6 km s^{-1}	$05^h\ 32^m\ 46^s.8$ (2)	-05° 24' 26" (3)	30
j	H_2O 9.2 - 10.8 km s^{-1}	$05^h\ 32^m\ 47^s.8$ (2)	-05° 24' 8" (3)	30
k	H_2O .95 km s^{-1}	$05^h\ 32^m\ 47^s.7$ (2)	-05° 24' 0" (3)	30
l	HII	$05^h\ 32^m$ 48.9 (5)	-05° 25' 27" (8)	31
m	CH_3OH J = 6,7 K = 2→1	approximate position		
		$05^h\ 32^m\ 46^s.4$	-05° 24' 30"	7
n	$CH_3OH\ 5_{-1}-4_0$ E	$05^h\ 32^m\ 45^s.4$	-05° 24' 20"	this work
		diameter < 45"		
	$CH_3OH\ 4_{-1}-3_0$ E	probably at the position m		
		diameter < 1'		this work

Note: The numbers represent the antenna temperatures corrected for 20% dish efficiency (T_A^* K). The numbers within parentheses represent the rms noise (T_{rms} K).

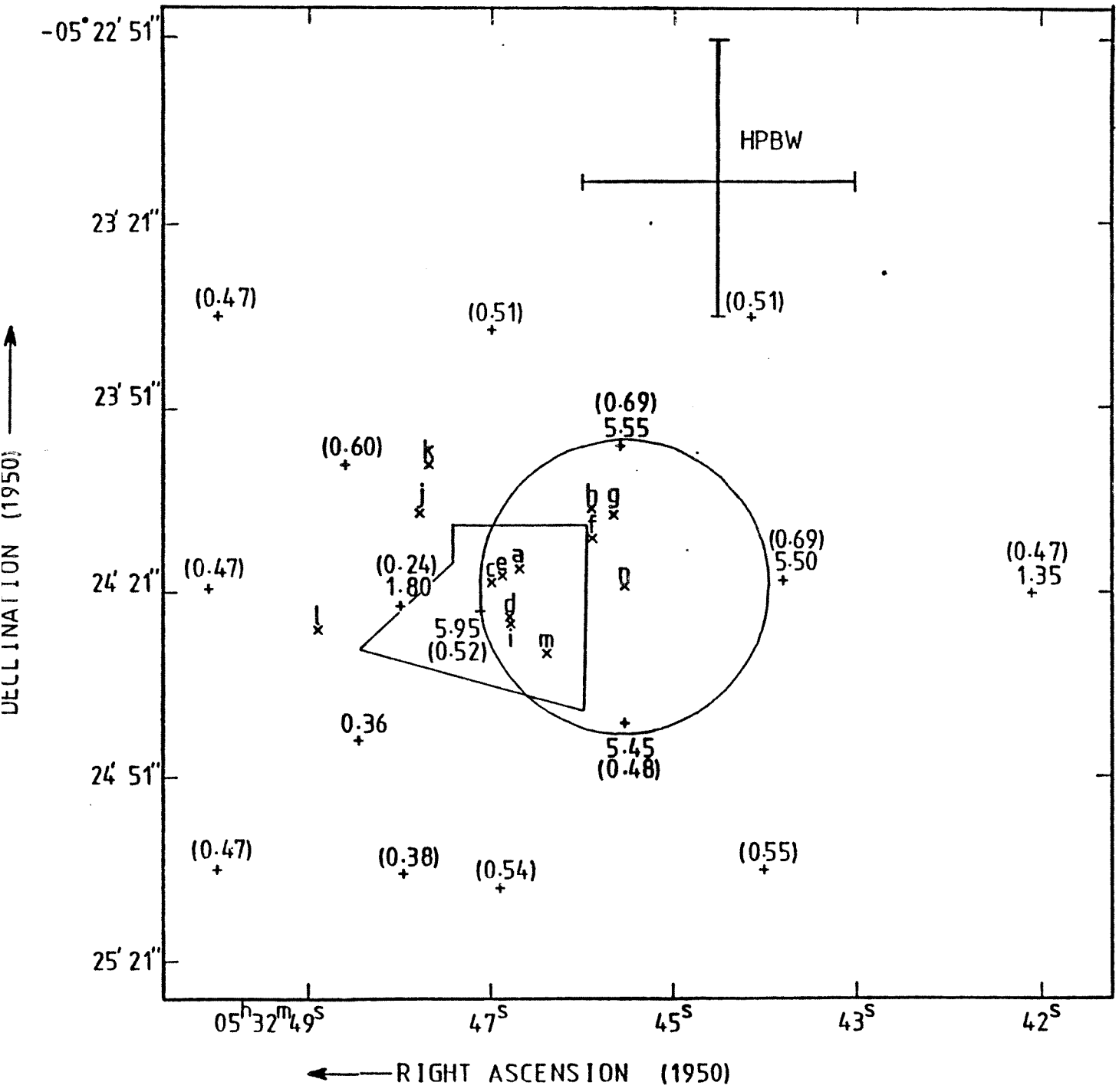
-05° 22' 51"
23' 21"
23' 51"
24' 21"
24' 51"
25' 21"
DECLINATION (1950)
HPBW
(0.47)
(0.51)
(0.51)
(0.69)
5.55
(0.60)
(0.69)
5.50
(0.47)
1.35
(0.47)
(0.24)
1.80
5.95
(0.52)
0.36
5.45
(0.48)
(0.47)
(0.38)
(0.54)
(0.55)
05h 32m 49s
47s
45s
43s
42s
RIGHT ASCENSION (1950)

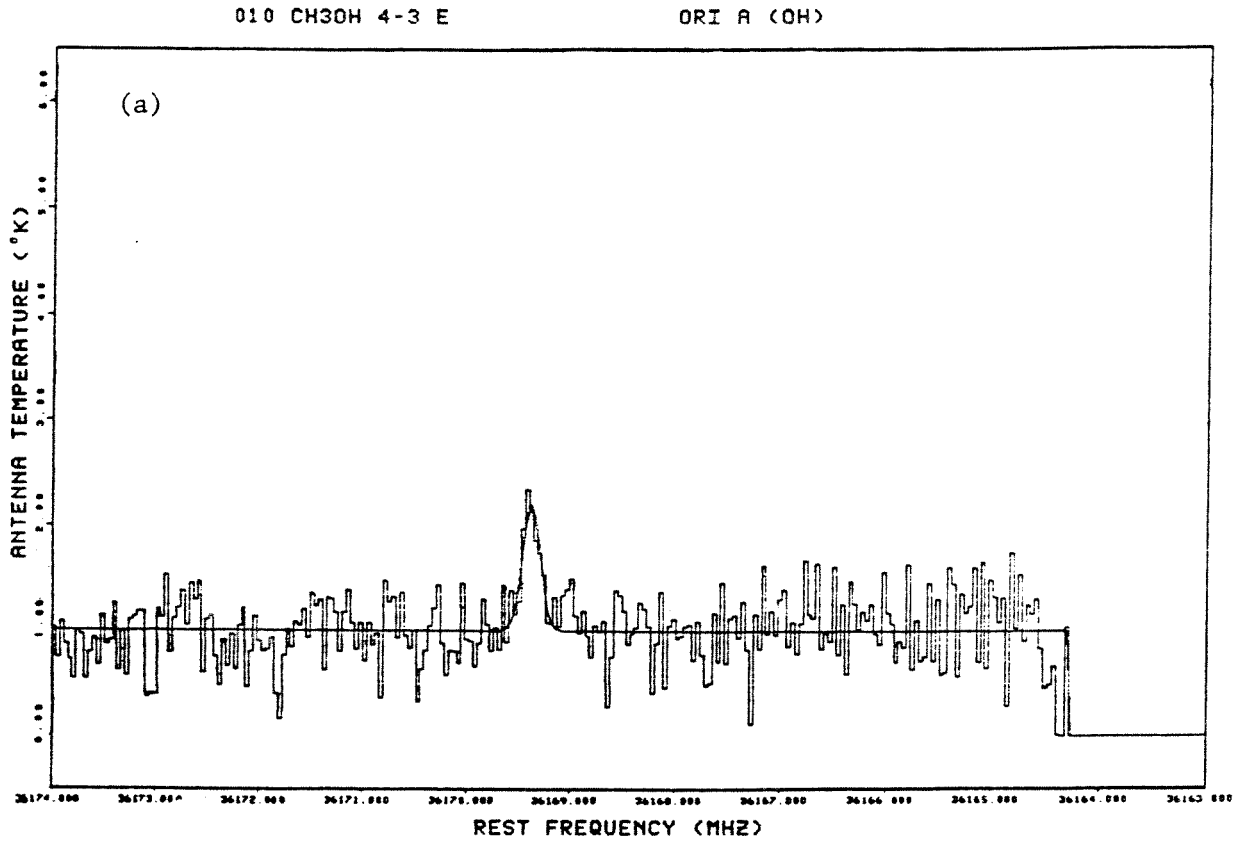

(b)

	$05^h32^m47^s.0$ -05°23'20" (T_A*=1.1 K) ΔT_{rms} = 0.62	
$05^h32^m51^s.0$ -05°24'20" T_A* = 1.6 K ΔT_{rms} = 0.53	$05^h32^m47^s.0$ -05°24'20" T_A* = 3.6 K ΔT_{rms}=0.57	$05^h32^m43^s.0$ -05°24'20" T_A* = 1.8 K ΔT_{rms} = 0.70
	$05^h32^m47^s.0$ -05°25'20" T_A* = 2.8 K ΔT_{rms} = 0.53	$05^h32^m51^s.0$ -05°23'20" T_A* = 1.8 K ΔT_{rms} = 0.62

Fig. 4.3 The ($J_K = 4_{-1} \rightarrow 3_0$ E) emission of methanol from Ori A.

(a) Line detected in June 1978 at the (1950) position $\alpha = 05^h32^m46^s.7$ δ = -05°24'21".

(b) Map drawn with the observations of February 1977. The antenna temperatures are corrected for 44% dish efficiency. The HPBW was 1!5.

4.2.2 *Sagittarius B2*

It is in Sgr B2 and Sgr A that methanol was first observed as interstellar molecule, with the detection of the $1_1 \rightarrow 1_1$ A transition at 834 MHz [15]. Since then, seven transitions have been found and are listed in table 4.4. During this work, a high resolution map of the central part of the methanol source has been drawn with the $5_{-1} \rightarrow 4_0$ E emission and two cloud velocities have been detected.

Column 12 of table 4.4 gives LTE antenna temperatures, calculated for a cloud kinetic temperature of 40 K and with reference to the $2_1 \rightarrow 1_1$ E transition. This transition has been chosen as reference since, within the seven listed, it is the only one for which the transition scheme [2] does not predict inversion of population. Very strong departure from LTE are seen in the two lowest frequency emission lines at 5 GHz and 834 MHz. The $5_{-1} \rightarrow 4_0$ E and especially the $4_{-1} \rightarrow 3_0$ E, which have been observed with a maser action in Orion, do not present here strong relative anomalous behaviour. They have been observed with antenna temperatures four times higher than in 1972 [16,17], and show some suggestion of inversion (if calibration errors have not been too important). Another support for the maser action of the $1_1 \rightarrow 1_1$ A, is the fact that this emission is seen against a high background temperature ($\sim$ 122 K [10]).

A possible maser emission in the three (K = 1) doublets (J = 1, 2, and 3) has been investigated by means of considerations on collisional de-excitation and radiative emission rates [20]. It can be noted that considerations, solely on infra-red de-excitation transitions, are not sufficient to explain the anomalous behaviour. Indeed it could be suggested that the lower level is depopulating in a fairly important way through the b-type transition $1_{1,1} \rightarrow 0_{0,0}$ and $1_{1,1} \rightarrow 2_{0,2}$, while the upper

TABLE 4.4

Methanol emission from Sgr B2

transition	type	rest frequency[a] (MHz)	E_{lower}[a] (cm^{-1})	E_{upper}[a] (cm^{-1})	E_u/k (K)	A (s^{-1})	ΔV (km s^{-1})	V_{LSR} (km s^{-1})	T_A^*(obs)[c] (K)	$(2J_u+1) \times e^{-E_u/kT} \times A$ (s^{-1})	T_A^*(LTE) (K)	$\frac{T_A^*(obs)}{T_A^*(LTE)}$	$N_T \times 10^{-16}$[g] (cm^{-2})	Ref
$5_{-1} \rightarrow 4_0$ E	b	84521.21 (10)	19.765	22.584	32.5	18.7×10^{-7}	24	63	2.8	9.1×10^{-6}	1.46	2	3.0	16
$4_{-1} \rightarrow 3_0$ E	b	36169.24 (10)	13.313	14.519	20.9	1.49×10^{-7}	27.6	62.1[d]	2.00	7.9×10^{-7}	1.26	2	5.6	17
$3_1 \rightarrow 3_1$ A	a	5005.320 (10)[b]	19.703	19.870	28.6	9.50×10^{-11}	27	57	0.05	3.2×10^{-11}	0.05×10^{-4}	10^4	6.6	18
$1_0 \rightarrow 0_0$ A^+	a	48372.60 (50)	0.000	1.614	2.3	3.44×10^{-7}	∿30 (1Q)	62[e]	1.50	9.7×10^{-7}	0.15	10	6.6	19
$1_0 \rightarrow 0_0$ E	a	48377.09 (50)	3.632	5.246	7.5	3.44×10^{-7}	∿30 (10)	62[e]	1.50	8.5×10^{-7}	0.14	10	4.4	19
$1_1 \rightarrow 1_1$ A	a	834.267 (2)	11.705	11.733	16.9	2.65×10^{-12}	35	66	0.3	5.2×10^{-12}	0.8×10^{-6}	$4\ 10^5$	90	15
$2_1 \rightarrow 1_1$ E	a	96755.5 (10)	10.751	13.979	20.1	24.8×10^{-7}	25	60	1.20	7.5×10^{-6}	1.20	1	2.2	10
$5_{-1} \rightarrow 4_0$ E	b	84521.21 (10)	19.765	22.584	32.5	18.7×10^{-7}	23	61.5[f]	11.3	9.1×10^{-6}	1.46	7	10.4	this work
$4_{-1} \rightarrow 3_0$ E	b	36169.24 (10)	13.313	14.519	20.9	1.49×10^{-7}	27.4	62	8.79	7.9×10^{-7}	1.41	6	24	this work

a : Lees et al. [1] unless otherwise noted.

b : Monash measurement.

c : For all observations the telescope was pointing at the OH position: $\alpha(1950) = 17^h44^m11^s$ $\delta(1950) = -28°22'30"$.

d : Two components are present at 53.9 and 70.3 km s^{-1} with FWHH ∿ 7 km s^{-1}.

e : The line is a blend of two components, formed by the A and E-transition or by two clouds radiating either in A or E.

f : Two components are present at V_{LSR} = 54 and 68 km s^{-1} with FWHH of 8.5 km s^{-1}.

g : The column densities have been calculated using T_{ex} = 40 K.

level is depopulating only through one b-type transition: the $1_{1,0} \rightarrow 1_{0,1}$ (using the asymmetric top notation). However calculations of the radiative coefficients rates of transitions into and out of the two levels do not lead to any inversion of population. Indeed the $^{b}P_{1-1}$ transition, $1_{1,1} \rightarrow 2_{0,2}$, has a coefficient rate ten times lower than the $^{b}R_{11}$ transition, $1_{1,1} \rightarrow 0_{0,0}$, and the $^{b}P_{1-1}$ transition from the $3_{1,3}$ level is hundred times slower than the $^{b}R_{11}$.

A map of the $5_{-1} \rightarrow 4_{0}$ E methanol source in Sgr B2 has been drawn using a 45" HPBW (fig. 4.4). Only seven different points could be recorded with in some cases, two observations of the same position. This map is extended on an area of $11.^{s}0 \times 140"$ around the OH (1950) position: $\alpha = 17^{h}\ 44^{m}\ 11.^{s}0$, $\delta = -\ 28°\ 22'\ 30"$. A contour map of Sgr B2 had been already drawn at 48 GHz, with fifteen points recorded on a $30^{s} \times 60'$ area around the OH position [19]. Two sites of peak emission were shown on the 48 GHz map: one 2'.5 north and one 2'.5 south of the OH position. Since the HPBW used for the observations in this earlier work, was 134", the map reported here gives a more detailed analysis of the central part of the cloud. A peak emission seems to be present around the position:

$\alpha(1950) = 17^{h}\ 14^{m}\ 8^{s}.1 \qquad \delta(1950) = -\ 28°\ 22'\ 42"$.

Two distinct velocity components appear at:

54 ± 1 km s^{-1} and 68 ± 1 km s^{-1} ,

with a predominance of the 54 km s^{-1} feature at about 45" north of the OH position.

The individual FWHH are 8.5 ± 0.5 km s^{-1} and

the overall FWHH is 23.0 ± 0.5 km s^{-1}.

These two velocity features had not been observed in an earlier detection of the $5_{-1} \rightarrow 4_{0}$ E transition [16]. The center velocity was then

Fig. 4.4 Map of the ($J_K = 5_{-1} \rightarrow 4_0$ E) emission of methanol from Sgr B2.

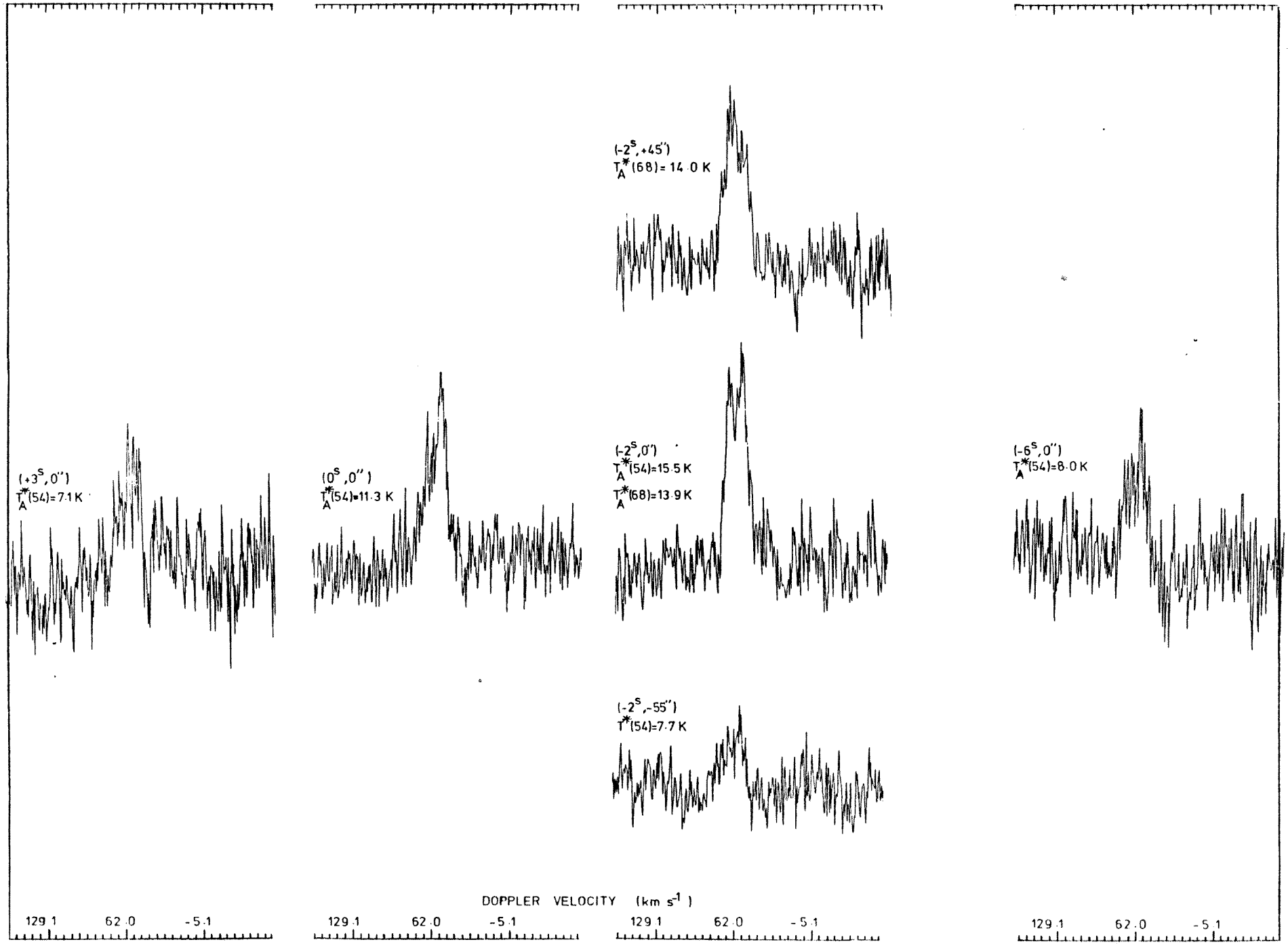
(+3S, 0")
T*A(54)=7.1 K
(0S, 0")
T*A(54)=11.3 K
(-2S, +45")
T*A(68)=14.0 K
(-2S, 0")
T*A(54)=15.5 K
T*A(68)=13.9 K
(-2S, -55")
T*(54)=7.7 K
(-6S, 0")
T*A(54)=8.0 K
DOPPLER VELOCITY (km s-1)
129.1
62.0
-5.1

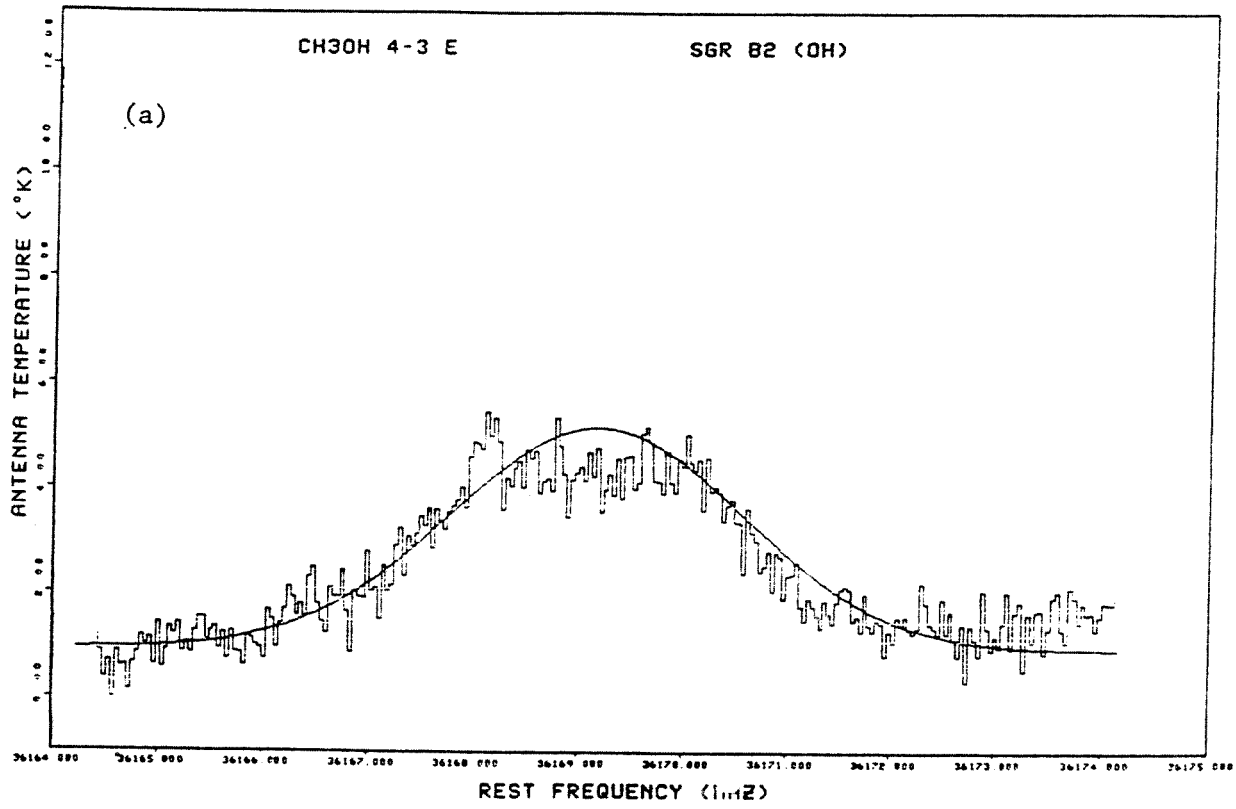

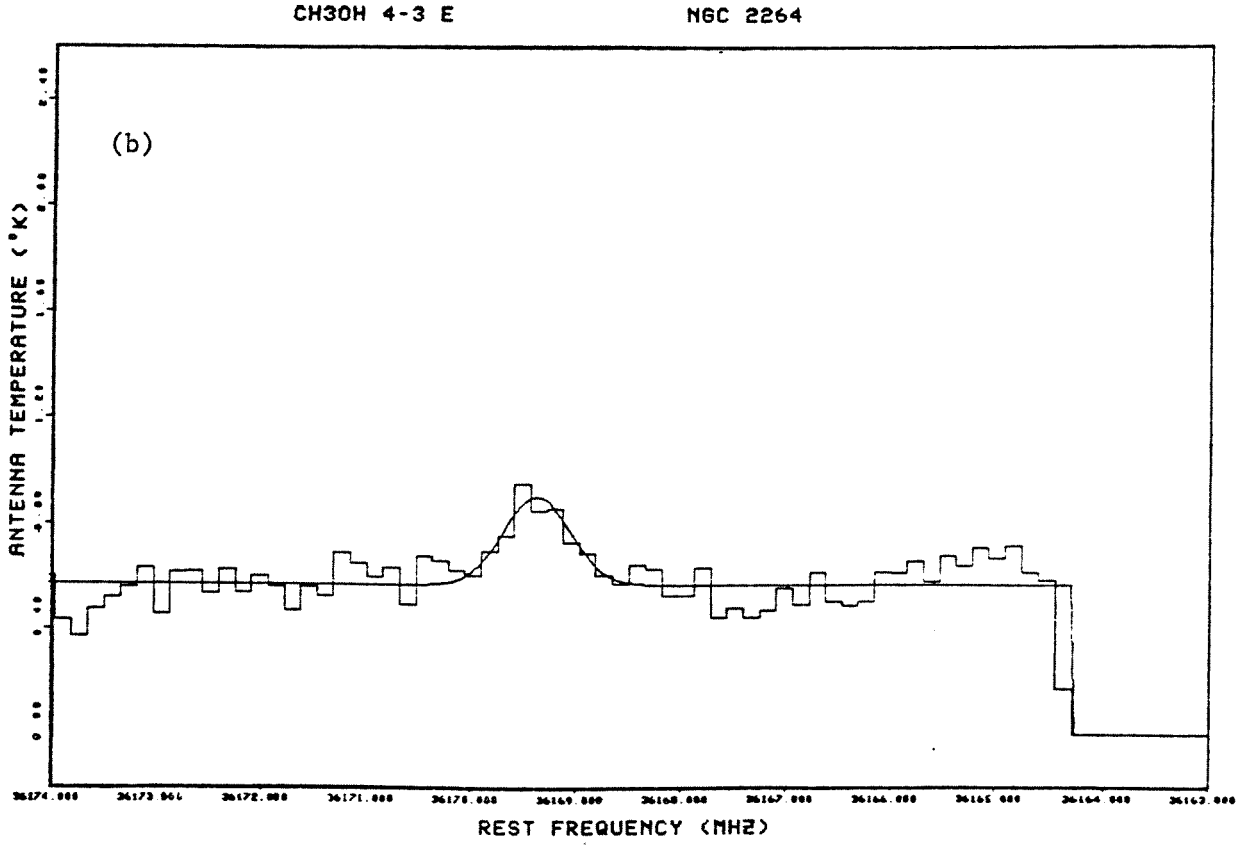

Fig. 4.5 The ($J_K = 4_{-1} \rightarrow 3_0$ E) emission of methanol
(a) from Sgr B2 (b) from NGC 2264.

63 (3) km s^{-1} and the FWHH 24 (3) km s^{-1}. The failure to detect the two components was probably due to a more limited spatial resolution (80", instead of 45" in this work) and a smaller signal to noise ratio. However the same source distribution is recognized in the observations of the $4_{-1}\rightarrow 3_0$ E line recorded at five points around the OH position and with a 54" HPBW. Two velocities were detected at 53.9 and 70.3 km s^{-1}, with about 7 km s^{-1} FWHH [17]. Several cloud velocities were also observed in the CO line, at about 56, 93 and possibly 78 km s^{-1} [21].

Column densities of methanol have been calculated for the case of an extended cloud, and thus a filled beam.

4.2.3 *Sagittarius A (NH_3)*

The observations made in Sgr A during this work led to the detection for the first time of the $4_{-1}\rightarrow 3_0$ E and the $3_1\rightarrow 3_1$ A transitions. The $4_{-1}\rightarrow 3_0$ E appears inverted and the $3_1\rightarrow 3_1$ A shows a maser emission.

Antenna temperatures have been calculated in the case of an LTE model, using the intensity of $1_0\rightarrow 0_0$ A^+ line as reference. This transition does not present any anomalous behaviour in Orion, but shows some departure from LTE when observed towards Sgr B2. Hence the calculated LTE antenna temperatures, given in column 12 of table 4.5, may be only lower limits. The coefficient for departure from LTE, given in column 13, shows that the $1_1\rightarrow 1_1$ A at 834 MHz and the $3_1\rightarrow 3_1$ A at 5 GHz are strong maser lines. The $4_{-1}\rightarrow 3_0$ E is probably showing some inversion of population and maser action too, but its anomalous behaviour is not so obvious.

The Doppler velocity of the $4_{-1}\rightarrow 3_0$ E line seems low, but it is the case of other molecules observed in Sgr A, such as: CO 17 to 60 km s^{-1} [15], NH_3 20.6 to 28.9 km s^{-1} [22], N_2H^+ 0 to 58 km s^{-1} [23], CS -10 to 110 km s^{-1} [24] and HCN 15 km s^{-1} [25]. These velocities

TABLE 4.5

Methanol emission from other sources

transition	type	rest[a] frequency (MHz)	E_{lower}[a] (cm^{-1})	E_{upper}[a] (cm^{-1})	E_u/k (K)	A (s^{-1})	ΔV ($km\ s^{-1}$)	V_{LSR} ($km\ s^{-1}$)	T_A^*(obs)[c] (K)	$(2J_u+1) \times e^{-E_u/kT} \times A$ (s^{-1})	T_A^*(LTE) (K)	$\frac{T_A^*(obs)}{T_A^*(LTE)}$	N_T[d] (cm^{-2})	Ref
						Sgr A (NH_3)								
$1_0 \rightarrow 0_0$ A$^+$	a	48372.60 (50)	0.000	1.614	2.3	3.44×10^{-7}	40	69	0.6	9.5×10^{-7}	0.6	1	2.2×10^{16}	19
$1_1 \rightarrow 1_1$ A	a	834.267 (2)	11.705	11.733	16.9	2.65×10^{-12}	40	51	0.58	4.5×10^{-13}	2.8×10^{-7}	10^6	1.5×10^{18}	15
$4_{-1} \rightarrow 3_0$ E	b	36169.24 (10)	13.313	14.519	20.9	1.49×10^{-7}	21.5	23.2	3.45	6.7×10^{-7}	0.42	8	5.8×10^{16}	this work
$3_1 \rightarrow 3_1$ A	a	5005.320[b] (10)	19.703	19.870	28.6	9.50×10^{-11}	44	45	0.10	2.6×10^{-10}	1.6×10^{-4}	62	1.8×10^{17}	this work
						W 51								
$2_{-1} \rightarrow 1_{-1}$ E	a	96739.39 (10)	0.000	3.227	4.6	24.7×10^{-7}	8.4	56.6	1.31	7.8×10^{-6}	1.3	1	6.8×10^{14}	10
$2_0 \rightarrow 1_0$ A$^+$	a	96741.42 (10)	1.614	4.840	7.0	33.0×10^{-7}	8.4	56.6	0.9	8.3×10^{-6}	1.4	1	4.4×10^{14}	10
$2_0 \rightarrow 1_0$ E	a	96744.58 (10)	5.246	8.473	12.2	33.0×10^{-7}	8.4	56.6	0.55	4.9×10^{-6}	0.82	1	4.6×10^{14}	10
$4_{-1} \rightarrow 3_0$ E	b	36169.24 (10)	13.313	14.519	20.9	1.49×10^{-7}	13.0	59	0.59	1.6×10^{-7}	0.027	22	4.2×10^{15}	this work

a : Lees et al. [1] unless otherwise noted.

b : Measured in Monash laboratory.

c : The (1950) pointing position was:

for Sgr A : $\alpha = 17^h42^m28^s.0$, $\delta = -29°01'30"$ ($-28°58'30"$ in the case of $1_1 \rightarrow 1_1$ A)

for W51 : $\alpha = 19^h21^m27^s.0$, $\delta = 14°24'39"$ ($30"$ in the case of $4_{-1} \rightarrow 3_0$ E)

d : The column densities have been calculated using T_{ex} = 30 K for Sgr A and 10 K for W51.

TABLE 4.5 continu'd

transition	type	rest[a] frequency (MHz)	E_{lower}[a] (cm^{-1})	E_{upper}[a] (cm^{-1})	E_u/k (K)	$A \times 10^7$ (s^{-1})	ΔV ($km\ s^{-1}$)	V ($km\ s^{-1}$)	T_A^*(obs)[b] (K)	$(2J_u+1) \times e^{-E_u/kT} \times A \times 10^6$ (s^{-1})	T_A^*(LTE) (K)	$\frac{T_A^*(obs)}{T_A^*(LTE)}$	N_{T_2}[c] (cm^{-2})	Ref.
						NGC 2264								
$2_{-1}\rightarrow1_{-1}$ E	a	96739.39 (10)	0.000	3.227	4.6	24.7	3.2	7.3	0.96	9.79	0.96	1	5.4×10^{14}	10
$2_0\rightarrow1_0$ A^+	a	96741.42 (10)	1.614	4.840	7.0	33.0	3.2	7.3	1.33	11.64	1.14	1	6.2×10^{14}	10
$5_{-1}\rightarrow4_0$ E	b	84521.21 (10)	19.765	22.584	32.5	18.7	3.0	7.4	0.69	4.04	0.39	2	6.8×10^{14}	this work
$4_{-1}\rightarrow3_0$ E	b	36169.24 (10)	13.313	14.519	20.9	1.49	6.3	7.6	0.75	0.47	0.046	16	2.8×10^{15}	this work
						M 17 (SW)								
$2_{-1}\rightarrow1_{-1}$ E	a	96739.39 (10)	0.000	3.227	4.6	24.7	3.5	20.3	0.44	10.99	0.44	1	7.6×10^{14}	10
$2_0\rightarrow1_0$ A^+	a	96741.42 (10)	1.614	4.840	7.0	33.0	3.5	20.3	0.70	13.86	0.55	1	9.4×10^{14}	10
$2_0\rightarrow1_0$ E	a	96744.58 (10)	10.751	13.979	12.2	33.0	3.5	20.3	0.29	9.97	0.40	1	4.4×10^{14}	10
$4_{-1}\rightarrow3_0$ E	b	36169.24 (10)	13.313	14.519	20.9	1.49	2.7	18.6	0.55	0.79	0.032	17	1.5×10^{15}	this work

a : Lees et al. [1].

b : The (1950) pointing position was:

for NGC 2264 : $\alpha = 6^h32^m28^s.0$, $\delta = 09°32'12"$ (06" in the case of $4_{-1}\rightarrow3_0$ E)

for M17SW : $\alpha = 18^h17^m28^s.0$, $\delta = -16°15'00"$ ($\alpha = 18^h27^m27^s.0$, $\delta = -16°14'54"$ in the case of $4_{-1}\rightarrow3_0$ E)

c : The column densities have been calculated using T_{ex} = 20 K for NGC 2264 and 40 K for M17(SW).

contrast with the velocity centroid of OH and H_2CO: $\sim$ 40 km s^{-1}. The 21.5 km s^{-1} linewidth of the $4_{-1}\rightarrow 3_0$ E transition appears also to be anomalously narrow. However hydrogen cyanide has been detected with a similar width: 20 km s^{-1} [25]. It is to be noted that if this line was in the upper side band, its frequency would correspond to the He 52α emission at 45472.25 MHz. However no He recombination line has ever been detected in Sgr A and a search for the H 52α has been unsuccessful during this work. Another factor which does not favor the attribution of this line to He, is the relatively high antenna temperature. Hence the line seen in Sgr A with a Doppler velocity of 23.2 km s^{-1} and a width of 21.5 km s^{-1} has been assigned to the methanol $4_{-1}\rightarrow 3_0$ E transition.

4.2.4 *Other sources*

During this work, the $4_{-1}\rightarrow 3_0$ F transition has been detected for the first time in NGC 2264, M17(SW) and W51. It has been seen, in all three sources, in maser emission. The $5_{-1}\rightarrow 4_0$ E has also been detected for the first time in NGC 2264 and its intensity seems to follow an LTE model. The results and analyses concerning the observations are shown on fig. 4.5 b, 4.7 and 4.8, and on table 4.5, together with the analysis of other transitions already detected in these sources.

4.3 A SEARCH FOR THIOMETHANOL

A search for CH_3SH has also been undertaken in several sources. Sulfur dioxide, SO_2, has been detected in emission from the direction of the OMC-1 and Sgr B2 molecular cloud [26]. The detection of thio--methanol would have gain some more information on the proposed circumstellar-type envelope associated with a late-type star in Orion.

Observations were made at Parkes in June 1978, in collaboration with R.D. Brown, P.D. Godfrey, B.J. Robinson and D.A. Winkler. The

7mm-mixer receiver was used. It was followed by a one-bit digital autocorrelator. Only negative results were obtained and are given in table 4.6.

TABLE 4.6

Negative searches of the (J = 2→1) transition of CH_3SH at 35857.4 MHz

source	pointing position α (1950)	pointing position δ	V_{LSR} km s^{-1}	on-source time (s)	ΔT_{rms}^{*} [a] (K)
Sgr B2	$17^h\ 44^m\ 11^s.0$	-28° 22' 30"	62	4800	0.16
CRL 3068 planetary nebula	$23^h\ 16^m\ 42^s.0$	16° 55' 10"	-28	7200	0.16
IRC+10011	$01^h\ 03^m\ 48^s.0$	12° 19' 45"	11	2400	0.23
OMC-1	$05^h\ 32^m\ 47^s.0$	-05° 24' 21"	8.5	14100	0.23

[a] ΔT_{rms}^{*} is corrected for 44% dish efficiency.

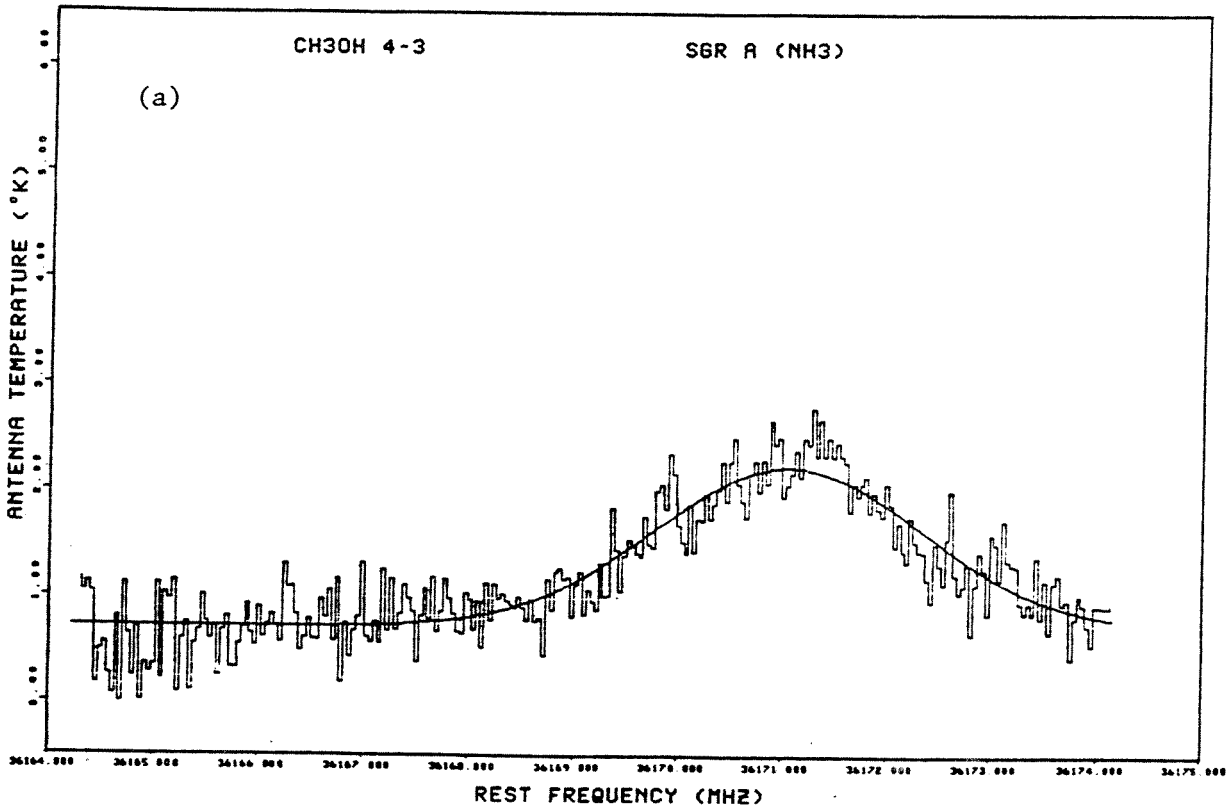

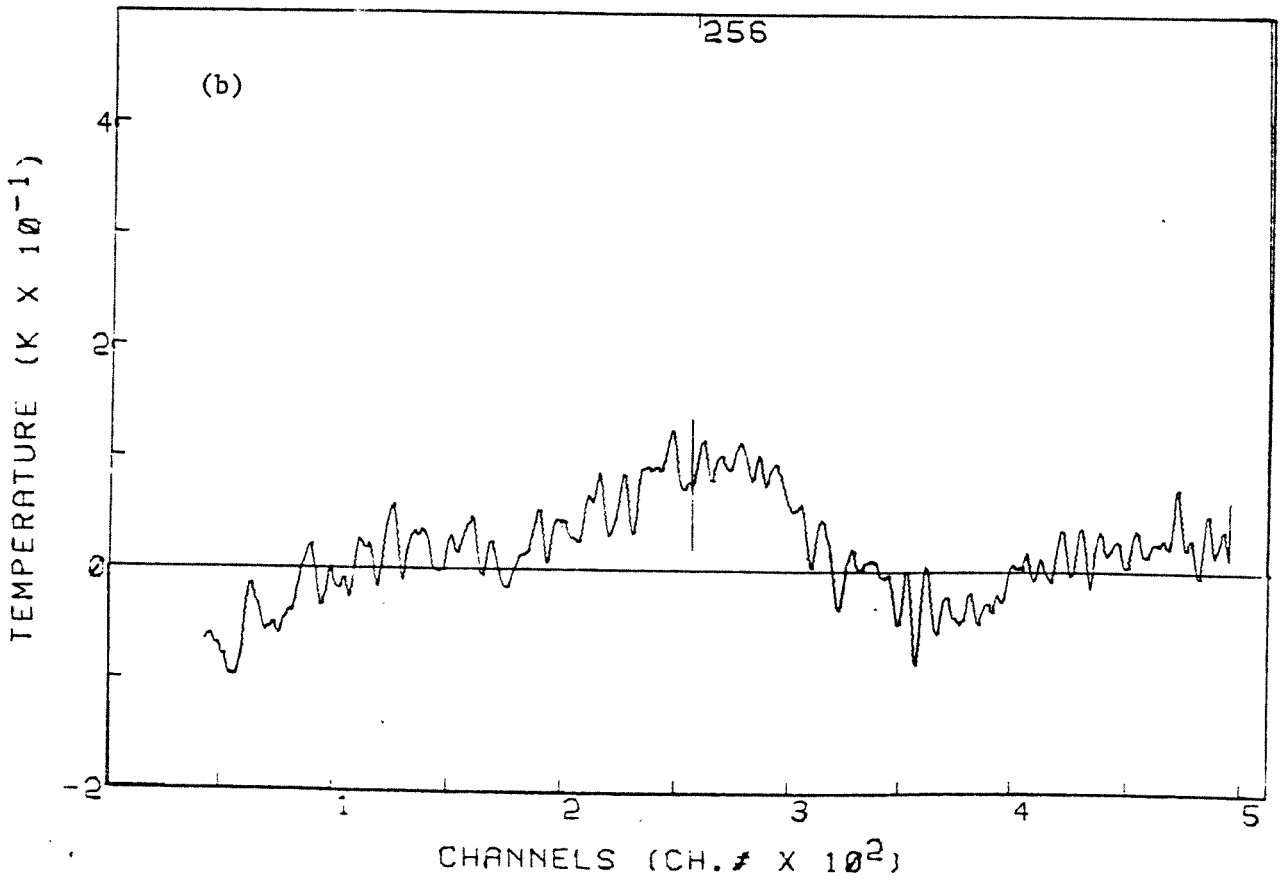

Fig. 4.6 Methanol emission from Sgr A

(a) The ($J_K = 4_{-1} \rightarrow 3_0$ E) transition (b) The ($J_K = 3_1 \rightarrow 3_1$ A) transition.

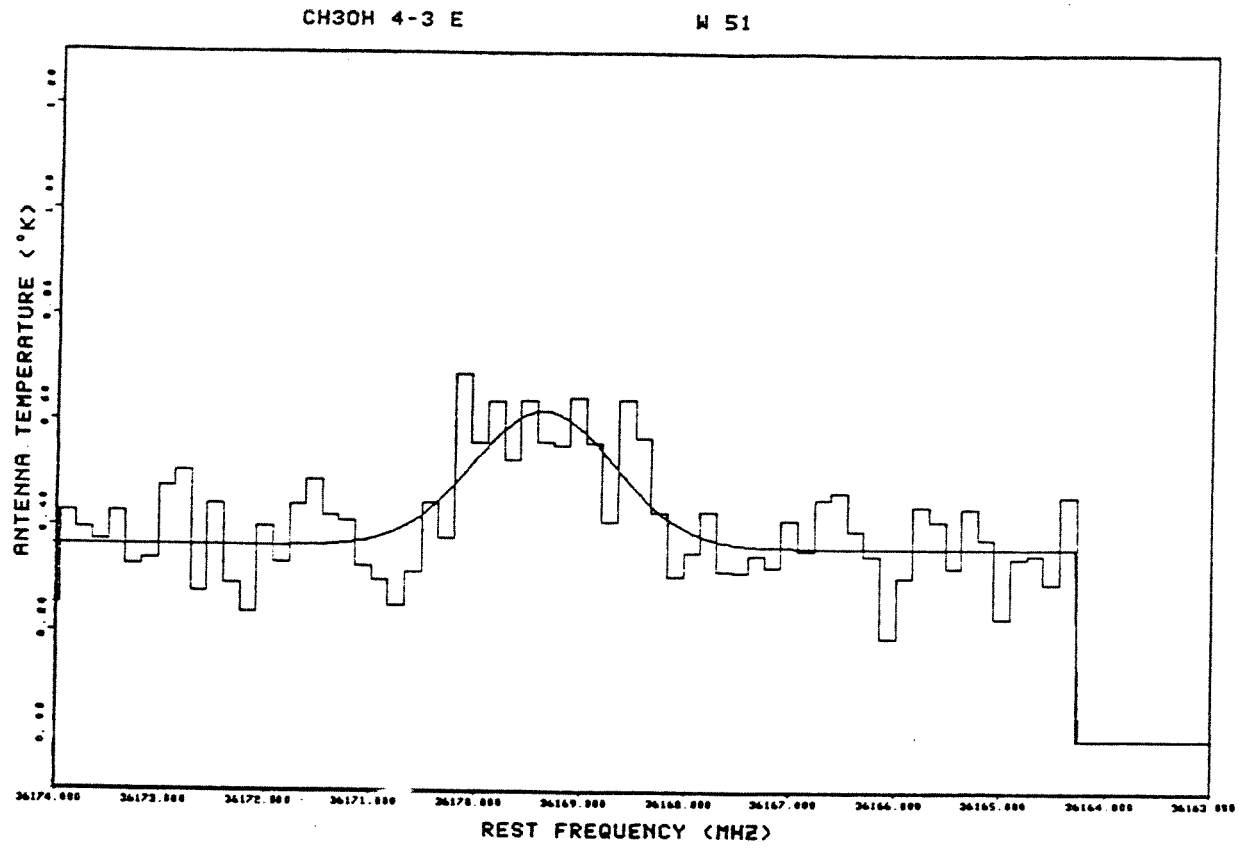

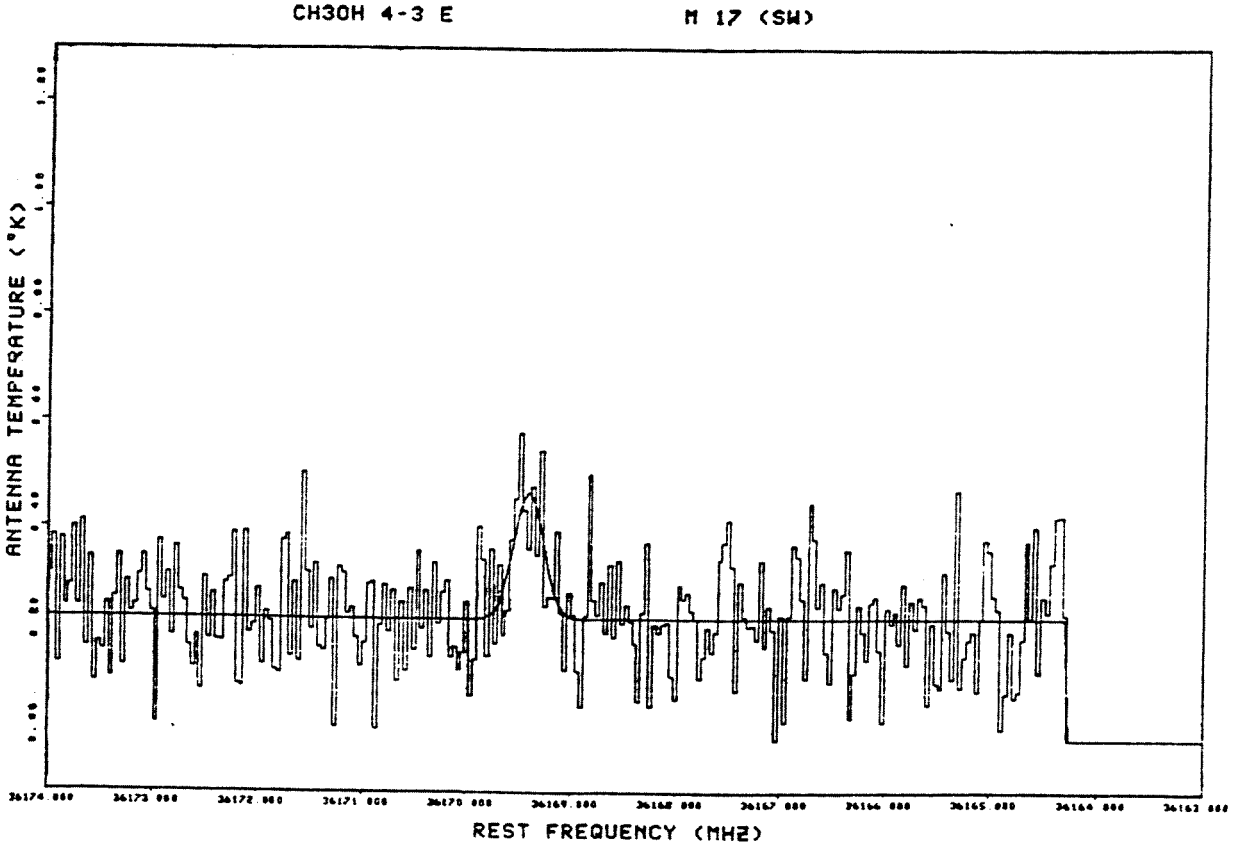

Fig. 4.7 The ($J_K = 4_{-1} \rightarrow 3_0$ E) emission of methanol from W51 and M17(SW).

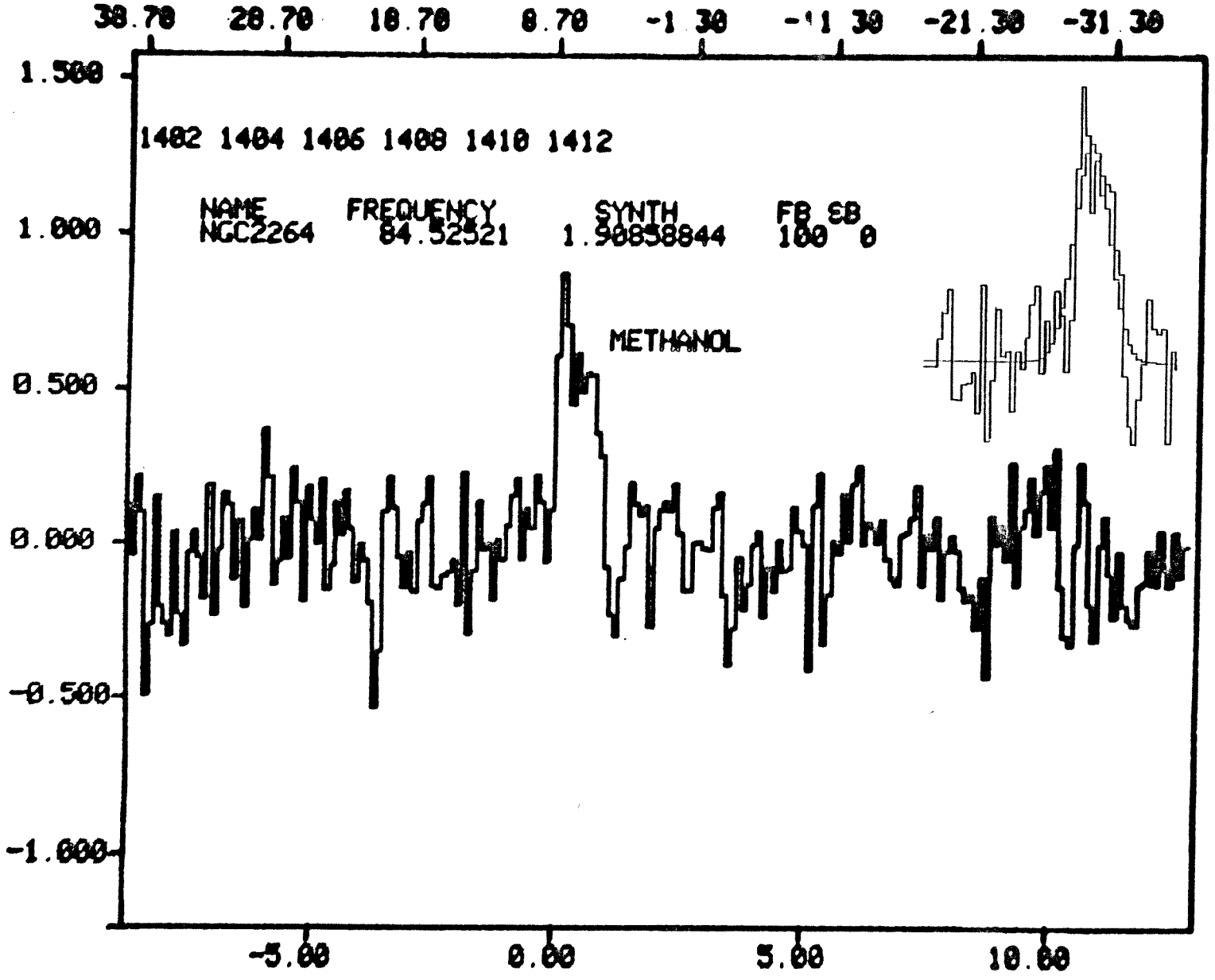

Fig. 4.8

The ($J_K=5_{-1}\rightarrow 4_0$ E) emission of methanol from NGC 2264. Enclosed is the statistical analysis of the line.

CHAPTER 5

THE DETECTION OF INTERSTELLAR METHYL CYANIDE

Methyl cyanide, CH_3CN, also named acetonitrile, is a symmetric top molecule which shows a rotational spectrum complicated by the centrifugal distorsion splitting of the K-levels and by the ^{14}N nuclear quadrupole hyperfine coupling. The microwave spectrum of this molecule has been studied in detail [1,2]. In the ground vibrational state, all K-levels except those for (K = 0) are doubly degenerate and the transitions occur according to the selection rules ($\Delta J = \pm 1$), ($\Delta K = 0$), ($\Delta I = 0$) and ($\Delta F = 0, \pm 1$). The lowest fundamental bending vibration $\nu_8(e)$ is doubly degenerate and gives rise to l-type doubling of the rotational levels. The levels are split into two due to the Coriolis interaction between vibration and rotation and are characterized by the quantum number of the vibrational angular momentum ($l = \pm 1$ when $V_8 = 1$) and ($l = 0, \pm 2$ when $V_8 = 2$).

Methyl cyanide has been classified as interstellar molecule with the detection, in 1971, of the 2.7 mm ($J = 6 \rightarrow 5$) transition in emission from the Sgr B2 and Sgr A molecular clouds [3,4]. The vibration--ally excited transitions ($V_8 = 1$) ($J = 6 \rightarrow 5$) ($K = 0$) and ($K = 3$) have also been detected in the comet Kohoutek [5,6]. No other positive detection has been recorded besides those undertaken by the Monash group and reported here (partly published [7,8]) and a transition observed approximately at the same time by the Monash group and F.J. Lovas et al. [9].

The ($J = 3 \rightarrow 2$) transition at 55 GHz is not accessible for observation, due to the large atmospheric oxygen absorption at this frequency. Searches have thus been undertaken for the ($J = 2 \rightarrow 1$), ($J = 4 \rightarrow 3$) and ($J = 5 \rightarrow 4$) transitions and are presented below. A summary

Summary of methyl cyanide observations

source	transition v	J	K	l	F[d]	pointing position α (1950)	δ	V_{LSR} (km s^{-1})	T_A^*[a] (K)	ΔV (km s^{-1})	ΔT_{rms}[a] (K)	on-source time (s)	date of obsv[t].	telescope-HPBW	receiver front end-back end	receiver configuration 1rst IF	observers
Sgr B2(2'S)	v=0	2→1				$17^h44^m11.^s0$	-28°24'30"	62	0.98(10)	28	0.10	8400	Jun. 1976	Parkes	7 mm mixer-	total	G.L. Blackman,
Ori A	v=0	2→1				05 32 47.0	-05 24 20	6.2	...	...	0.06	11400	Jun. 1976	16.7 m -	correlator	power -	R.D. Brown, P.D. Godfrey,
N159(LMC)	v=0	2→1				05 40 24.0	-69 46 00	235	(0.3)[f]	...	0.12	3300	Jun. 1976	90" at	.	4.5- 5.0 GHz	M.P. Bassez,
Sgr B2	v_8=1	2→1	±1	±1	3→2	17 44 11.0	-28 24 30	62	...	...	0.11	5400	Jun. 1976	36 GHz[b]	.	.	A.L. Ottrey, D. Winkler, B.J. Robinson
IRC+10216	v=0	2→1				09 45 14.0	13 30 40	-22	...	...	0.10	3000	Feb. 1977	.	.	.	R.D. Brown, P.D. Godfrey, M.P. Bassez, H.I. Gunn, A.P. Porter, D.A. Winkler, B.J. Robinson
RCW 38	v=0	2→1				08 57 24.0	-47 18 48	0.0	...	...	0.20	1500	Feb. 1977	.	.	.	
G333.6-0.2 Norma III	v=0	2	1			16 18 26.0	-49 58 48	-46[e]	...	...	0.40	900	Feb. 1977	.	.	.	
Ori A	v=0	4→3	0		5→4	05 32 47.0	-05 24 21	8.5	0.51	3	0.056	6300	Nov. 1976	Kitt Peak	3 mm mixer-	position	R.D. Brown, P.D. Godfrey, H.I. Gunn, J.W. Storey
Ori A	v=0	4→3	1		5→4	05 32 47.0	-05 24 21	8.5	0.38	3	0.056	6300	Nov. 1976	11.0 m -	filter	switching -	
Ori A	v=0	4→3	2		5→4 3→2	05 32 47.0	-05 24 21	8.5	0.15	3	0.056	6300	Nov. 1976	88" at	banks	4.75 GHz	
Ori A	v=0	4→3	2		4→3	05 32 47.0	-05 24 21	8.5	0.15	3	0.056	6300	Nov. 1976	74 GHz[c]	.	.	
Ori A	v=0	4→3	3		3→2	05 32 47.0	-05 24 21	8.5	0.13	3	0.056	6300	Nov. 1976	.	.	.	
Ori A	v=0	4→3	3		5→4	05 32 47.0	-05 24 21	8.5	0.13	3	0.056	6300	Nov. 1976	.	.	.	
Ori A	v=0	4→3	3		4→3	05 32 47.0	-05 24 21	8.5	0.08	3	0.056	6300	Nov. 1976	.	.	.	
NGC 2264	v=0	4→3				06 38 28.0	09 32 06	8.7	...	...	0.10	2880	Apr. 1978	.	.	.	R.D. Brown, P.D. Godfrey, M.P. Bassez
IRC+10216	v=0	4→3				09 45 14.8	13 30 40	-22	...	...	0.04	3840	Apr. 1978	.	.	.	
Ori A	v=0	5→4	0		6→5	05 32 47.0	-05 24 21	8.5	1.26	3	0.14	600	Mar./	Kitt Peak	3 mm mixer-	position	R.D. Brown, P.D. Godfrey, H.I. Gunn, J.W. Storey
Ori A	v=0	5→4	1		6→5	05 32 47.0	-05 24 21	8.5	0.94	3	0.14	600	Nov. 1976	11.0 m -	filter	switching -	
Ori A	v=0	5→4	2		6→5	05 32 47.0	-05 24 21	8.5	0.82	3	0.14	600	.	70" at	banks	4.75 GHz	
Ori A	v=0	5→4	3		6→5 4→3	05 32 47.0	-05 24 21	8.5	0.42	3	0.14	600	.	92 GHz[c]	.	.	
Ori A	v=0	5→4	3		5→4	05 32 47.0	-05 24 21	8.5	0.28	3	0.14	600	.	.	.	.	
Ori A	v=0	5→4	4		6→5 4→3	05 32 47.0	-05 24 21	8.5	0.19	3	0.14	600	.	.	.	.	
Ori A	v_8=1	5→4	±1	±1	6→5	05 32 47.0	-05 24 21	11.1	0.22	12.9	0.021	20000	Mar. 1976	.	.	.	F.D. Clark,
Sgr B2	v_8=1	5→4	±1	±1	6→5	17 44 11.0	-28 24 30	62	...	...	0.039	9540	Mar. 1976	.	.	.	R.D. Brown, P.D. Godfrey,
Ori A	v_8=1	5→4	±1	±2	6→5	05 32 47.0	-05 24 21	8.5	(0.065)	...	0.021	20000	Mar. 1976	.	.	.	J.W. Storey, D.R. Johnson
Sgr B2	v_8=1	5→4	±1	±2	6→5	17 44 11.0	-28 24 30	62	...	...	0.11	5400	Jun. 1976	.	.	.	see obs. for (J=2→1) Jun. 1976

a : T_A^* and ΔT_{rms} of the (J = 4→3) and (J = 5→4) observations made in March and Nov. 1976 are standardized as described in the text.

b : Determined by measurements on the moon diameter.

c : Determined theoretically [31].

d : When the quadrupole hyperfine splitting is negligible, only the strongest $F_u \rightarrow F_l$ component is nominated. However, in the calculations, it has been assumed that all components contribute to the intensity of the line.

e : Formaldehyde Doppler velocity.

f : The probability of presence of this line was 100%.

TABLE 5.2

Summary of observations related to methyl cyanide

molecule	source	transition	frequency (MHz)	pointing position α (1950)	pointing position δ	V_{LSR} (km s^{-1})	T_A^* (K)	ΔV (km s^{-1})	ΔT_{rms} (K)	on source time (s)	date of observation
H41α [a]	Ori A	n = 42→41	85688.4	$05^h32^m47^s.0$	-05°24'21	-1.4	0.50	20	0.14	600	Mar./Nov. 1976
U101951	Sgr B2		101951.0	17 44 11.0	-28 24 30	62	0.27	14.5	0.07	9540	Mar. 1976
U92363	Sgr B2		92363	17 44 11.0	-28 24 30	62	---	---	0.07	9540	Mar. 1976
CH_3NC	Sgr B2	J = 2→1	40210.9	17 44 11.0	-28 24 30	62	---	---	0.28	18600	Jun. 1976
CH_3NC	Ori A	J = 2→1	40210.9	05 32 47.0	-05 24 21	6	(0.50) [b]	---	0.59	3300	Feb. 1977

a : T_A^* and ΔT_{rms} are standardized as described in the text.

b : A statistical analysis on a Gaussian profile of the line showed a 95% confidence limit.

of the observations are presented at the start of the discussion on each of these transitions in individual sources.

5.1 OBSERVATIONS

The observations were conducted at five different periods, using the radiotelescopes at Parkes and Kitt Peak. A summary is given in tables 5.1 and 5.2.

5.2 DISCUSSION

5.2.1 Orion A

The ($J_K = 5_K \rightarrow 4_K$) and ($J_K = 4_K \rightarrow 3_K$) transitions of methyl cyanide have been detected towards Ori A molecular cloud with a Doppler velocity of 8.5 km s^{-1} and a velocity width of 3 km s^{-1}. Their intensities follow a Boltzmann distribution for a cloud kinetic temperature of 90 K. The column density of methyl cyanide in the direction of Ori A has been evaluated to $\sim 1 \times 10^{13}$ cm^{-2}. A discrepancy in intensity values obtained during different detections of the ($J_K = 5_K \rightarrow 4_K$) transitions led to a calibration of antenna temperatures by means of a hydrogen recombination line analysis. The detection of methyl cyanide in the vibrational excited state ν_8 is discussed.

a) The ($J_K = 5_K \rightarrow 4_K$) transitions

The ($J_K = 5_K \rightarrow 4_K$) transitions of methyl cyanide have been detected in March and November 1976. The same lines have been reported in the literature in November 1976 by F.J. Lovas et al. [9], with much lower antenna temperatures. Table 5.3 summarizes the data. The corresponding spectra, obtained by the Monash group, are shown in fig. 5.1 (a), (b), (c) and (d). The antenna temperatures which have been detected on the 17/11/1976 are consistent with those detected on the 19/11/1976, considering a dome attenuation of 58%. Those detected eight

Fig. 5.1 The (J = 5→4) emission of methyl cyanide from Ori A.

(a) Observations of March 1976.

Methyl cyanide is detected during a search for urea.

(b) Observations of November 1977.

Methyl cyanide is detected through the dome.

(c) Observations of November 1977.

Methyl cyanide is detected in good weather conditions.

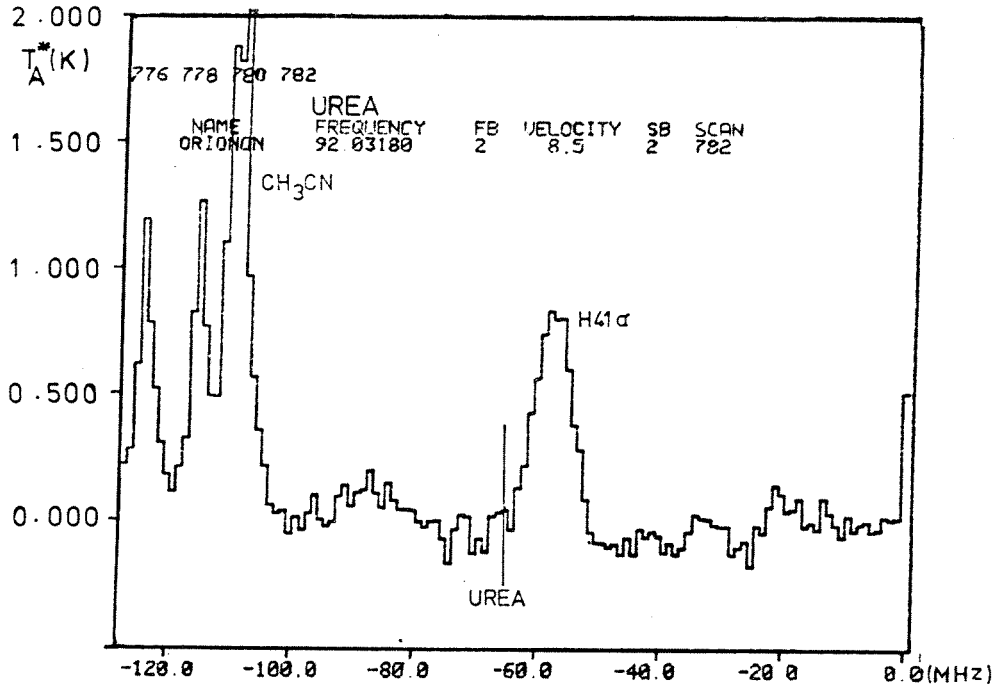
2.000
T_A^*(K)
776 778 780 782
UREA
NAME FREQUENCY FB VELOCITY SB SCAN
ORIONOH 92.03180 2 8.5 2 782
1.500
CH_3CN
1.000
H41α
0.500
0.000
UREA
-120.0 -100.0 -80.0 -60.0 -40.0 -20.0 0.0(MHz)

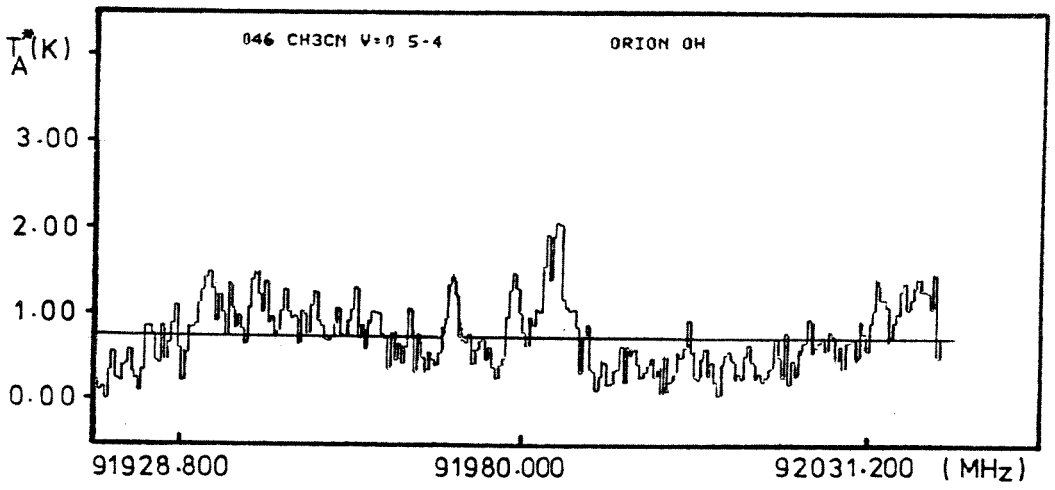
T_A^*(K)
046 CH3CN V=0 5-4
ORION OH
3.00
2.00
1.00
0.00
91928.800
91980.000
92031.200 (MHz)

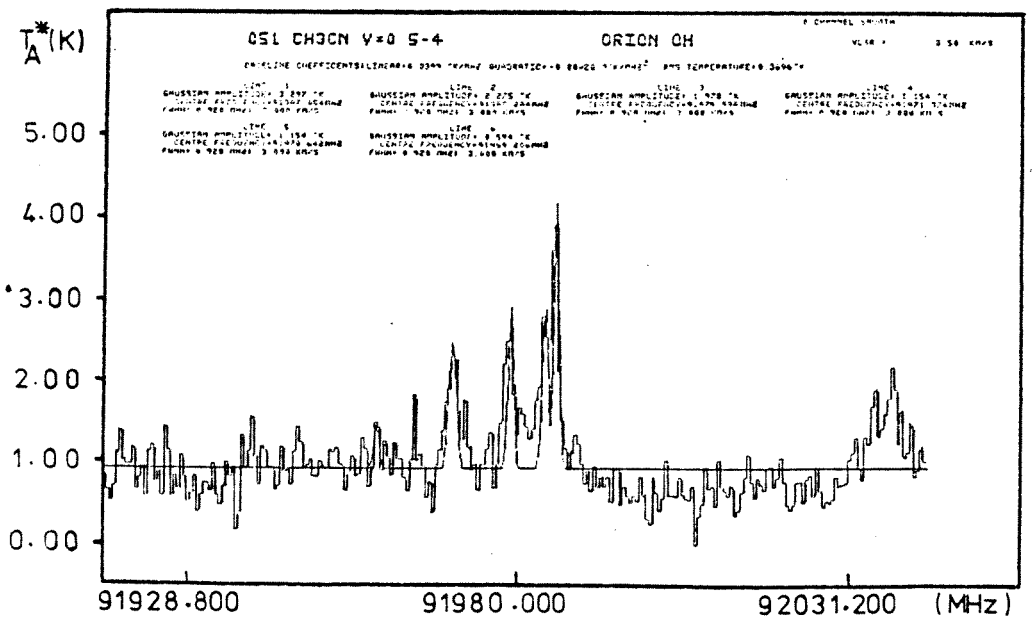
T_A^*(K)
051 CH3CN V=0 5-4
ORION OH
5.00
4.00
3.00
2.00
1.00
0.00
91928.800
91980.000
92031.200 (MHz)

Fig. 5.1 continu'd

(d) Observations of November 1977

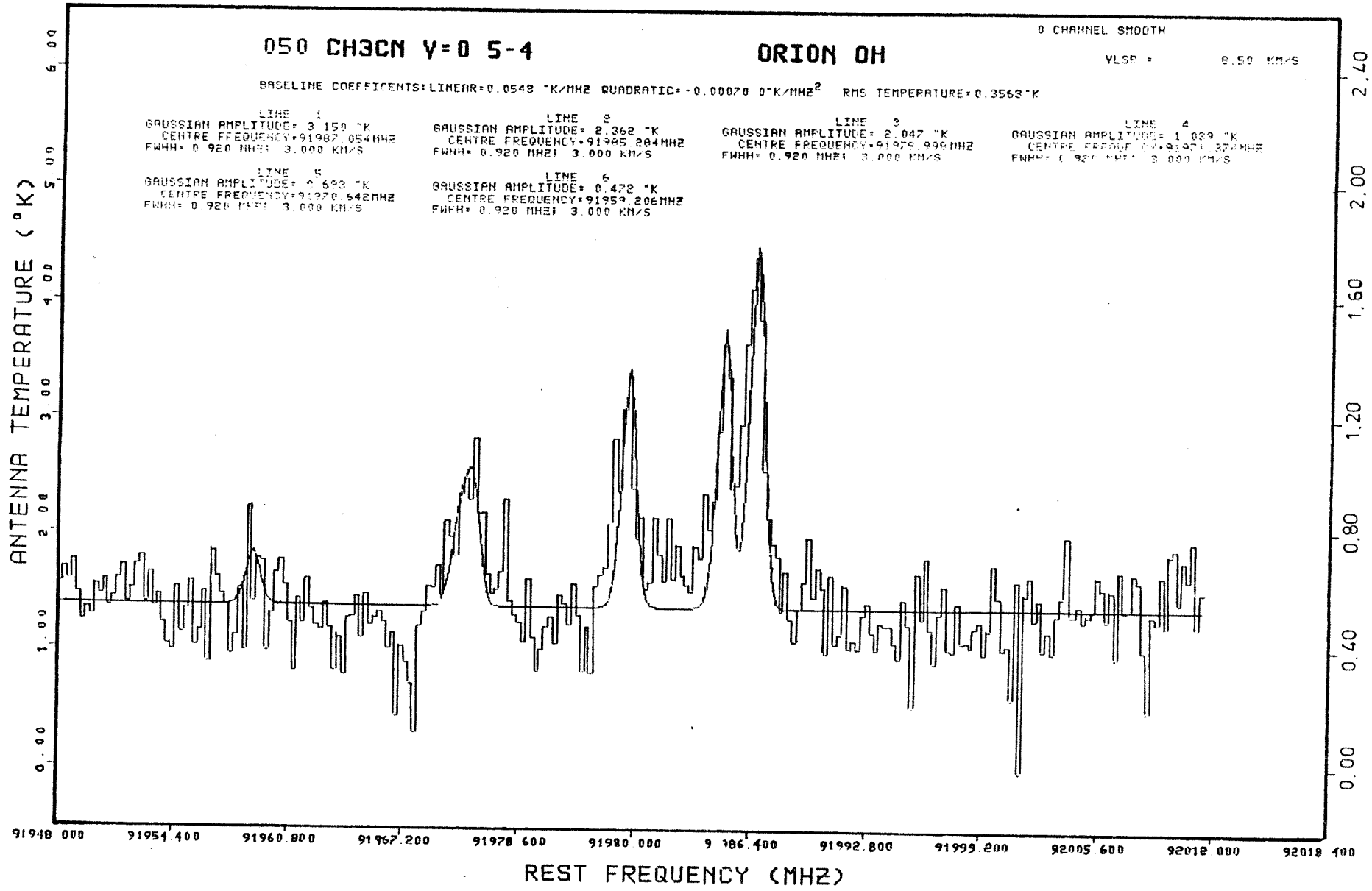
050 CH3CN V=0 5-4
ORION OH
0 CHANNEL SMOOTH
VLSR = 8.50 KM/S
BASELINE COEFFICIENTS:LINEAR=0.0548 °K/MHZ QUADRATIC=-0.00070 0°K/MHZ² RMS TEMPERATURE=0.3563°K
LINE 1
GAUSSIAN AMPLITUDE= 3.150 °K
CENTRE FREQUENCY=91987.054MHZ
FWHH= 0.920 MHZ; 3.000 KM/S
LINE 2
GAUSSIAN AMPLITUDE= 2.362 °K
CENTRE FREQUENCY=91985.284MHZ
FWHH= 0.920 MHZ; 3.000 KM/S
LINE 3
GAUSSIAN AMPLITUDE= 2.047 °K
CENTRE FREQUENCY=91979.998MHZ
FWHH= 0.920 MHZ; 3.000 KM/S
LINE 4
GAUSSIAN AMPLITUDE= 1.039 °K
LINE 5
GAUSSIAN AMPLITUDE= 0.693 °K
CENTRE FREQUENCY=91970.642MHZ
FWHH= 0.920 MHZ; 3.000 KM/S
LINE 6
GAUSSIAN AMPLITUDE= 0.472 °K
CENTRE FREQUENCY=91959.206MHZ
FWHH= 0.920 MHZ; 3.000 KM/S
ANTENNA TEMPERATURE (°K)
STANDARDIZED ANTENNA TEMPERATURE (K)
0.00
1.00
2.00
3.00
4.00
5.00
6.00
0.00
0.40
0.80
1.20
1.60
2.00
2.40
91948.000
91954.400
91960.800
91967.200
91973.600
91980.000
91986.400
91992.800
91999.200
92005.600
92012.000
92018.400
REST FREQUENCY (MHZ)

TABLE 5.3

The (J = 5→4) emission of methyl cyanide from Ori A

transition			date of obsv.[t]	on-source time (s)	filter 1			filter 2			T_{sys} (K)	comments	$\frac{I(H41\alpha)}{I(5_0)}$	ref.
J	K	F			resol. (kHz)	T_A^* (K)	ΔT_{rms} (K)	resol. (kHz)	T_A^* (K)	ΔT_{rms} (K)				
5→4	0	6→5	11-18	3600	1000	2.10	0.15							this
5→4	1	6→5	March	3600	1000	1.94	0.15							work
5→4	2	6→5	1976	3600	1000	1.33	0.15							·
5→4	3	6→5	⋮	3600	1000	1.25	0.15							·
H41α				3600	1000	0.90	0.15						0.43	·
5→4	0	6→5	17	2400	500	1.40	0.35				3730	observed		this
5→4	1	6→5	Nov.	2400	500	1.20	0.35				3730	through		work
5→4	2	6→5	1976	2400	500	0.78	0.35				3730	the		·
5→4	3	6→5	·	2400	500	0.72	0.35				3730	dome		·
H41α			·	2400	500	0.59	0.35				3730	⋮	0.42	·
5→4	0	6→5	19	600	500	3.30	0.27	250	3.15	0.36	2167			this
5→4	1	6→5	Nov.	600	500	2.27	0.27	250	2.36	0.36	2167			work
5→4	2	6→5	1976	600	500	1.98	0.27	250	2.05	0.36	2167			·
5→4	3	6→5 4→3	·	600	500	1.15	0.27	250	1.04	0.36	2167			·
5→4	3	5→4	·	600	500	1.15	0.27	250	0.69	0.36	2167			·
5→4	4	6→5 4→3	·	600	500	0.59	0.27	250	0.47	0.36	2167			·
H41α			·	600	500	1.24	0.27						0.37	·
5→4	0	6→5	10		1000	0.28					∿1000			9
5→4	1	6→5	Jan.		1000	...					∿1000			·
5→4	2	6→5	1975		1000	0.16					∿1000			·
5→4	3	6→5	(publ.		1000	0.20					∿1000			·
5→4	4	6→5 4→3	Nov.		1000	0.08					∿1000			·
H41α			1976)		1000	0.15					∿1000		0.53	·

months earlier appear to be lower by a factor of 1.5, while values reported by F.J. Lovas et al. are 12 times smaller. However, in all observations, the H41α recombination line is present and the ratio of its intensity to the intensity of the (K = 0) line of CH_3CN is 0.44 (9). This line could hence be used for calibration.

Several models (LTE and non-LTE [10,11]) are describing the behaviour of radio recombination lines. Using Lockman's curve [10] and a value of the continuum temperature at 3.5 mm, the intensities of the H42α and H41α lines have been predicted and are listed in table 5.4. The H42α calculated intensity agrees satisfactorily, within a factor of 0.8, with a recent detection of this line. The value of 0.56 K can thus be taken as an approximation of the antenna temperature of the H41α in Orion. This means that all four detections of the ($J_K = 5_K \rightarrow 4_K$) transitions of methyl cyanide, reported in table 5.4, are faulty. Calibrations errors may have occurred or incorrect scaling factors were computed. F.J. Lovas et al. reported an unbalanced sideband response of the receiver.

A standardization of the H41α antenna temperature at 0.50 K requires to decrease by factors of 1.8 and 2.5 the intensities reported by the Monash group for the observations made respectively in March and November 1976. The same standardization of the H41α requires to increase by a factor of 3.3 the values given by F.J. Lovas et al. The standardized intensities, reported in column 7 of table 5.5, have been obtained from the spectrum recorded with the highest resolution.

In order to verify if the 5_K and 4_K states are thermally populated, relative LTE intensities of the K-levels have been calculated, taking into account the statistical weight of the considered level, $(2J_u + 1)S(I,K)$, the Boltzmann factor and the A-Einstein coefficient for

TABLE 5.4

Millimetre-wave hydrogen recombination lines in Ori A

line	rest frequency (MHz)	$\frac{T_L}{T_C}\frac{100}{\nu(GHz)}$ Lockman's curve	T_c^* [a] at 3.5 mm (K)	T_L^* (K)	T_A^* (K)
H41α	85688.4	1.02 [10]	0.60 [12]	0.53	0.40 [13]
H42α	92034.45	1.02 [10]	0.60 [12]	0.56	

a : Y. Fukui et al. reported individual correcting values, for beam and aperture efficiencies, which seem in contradiction with their total correcting factor of 2.6. In order to verify this factor, the brightness temperature of Orion at 3.5 mm has been calculated using a value of the flux density deducted from a graph of S/ν [14], and the relation between flux density and antenna temperature [15]. This calculated temperature of the continuum (0.61 K) is in perfect agreement with the measured value corrected by 2.6 (0.60 K).

TABLE 5.5

Methyl cyanide emission from Ori A

transition					rest [a] frequency (MHz)	E_{upper} (cm^{-1})	E_u/k (K)	$A \times 10^5$ (s^{-1})	T_A^* obs (K)	T_A^* obs std (K)	$(2J_u+1)S(I,K)m \times e^{-E_u/kT} \times A \times 10^4$ (s^{-1})	$\frac{I_{J_K}}{I_{5_0}}$ [c] LTE	$\frac{I_{J_K}}{I_{5_0}}$ obs
v	J	K	l	F									
v =0	5→4	0		6→5	91987.054	9.20	13.2	6.32		1.26	24.1	1.00	1.00
v =0	5→4	1		6→5	91985.284	14.17	20.4	6.07		0.94	21.3	0.88	0.75
v =0	5→4	2		6→5	91979.978	29.10	41.9	5.31		0.82	14.6	0.61	0.65
v =0	5→4	3		6→5 4→3	91971.374	53.90	77.7	4.04		0.42	9.75	0.40	0.33
v =0	5→4	3		5→4	91970.642	53.90	77.7	4.04		0.28	4.80	0.20	0.22
v =0	5→4	4		6→5 4→3	91959.206	88.80	127.9	2.27		0.19	1.58	0.07	0.15
v_8=1	5→4	±1	±1	6→5	92353.516								
v_8=2	5→4	±1	±2	6→5	92538.810 [b]								
v=0	4→3	0		5→4	73590.207	6.13	8.8	3.16	1.29	0.51	10.3	0.43	0.41
v=0	4→3	1		5→4	73588.764	11.10	16.0	2.97	0.95	0.38	8.91	0.37	0.30
v=0	4→3	2		5→4 3→2	73584.748	26.02	37.5	2.37	0.39	0.15	3.62	0.15	0.12
v=0	4→3	2		4→3	73584.101	26.02	37.5	2.37	0.39	0.15	1.76	0.07	0.12
v=0	4→3	3		3→2	73578.256	50.89	73.3	1.38	0.32	0.13	1.05	0.04	0.10
v=0	4→3	3		5→4	73577.768	50.89	73.3	1.38	0.32	0.13	1.79	0.07	0.10
v=0	4→3	3		4→3	73576.501	50.89	73.3	1.38	0.19	0.08	1.38	0.06	0.06

a : A. Bauer et al. [1] unless otherwise noted.

b : A. Bauer [2].

c : Calculated for T_{ex} = 90 K.

spontaneous emission. The statistical weights S(I,K), of the K-levels, due to the hydrogen nuclear spin I, have been calculated using the Fermi-Dirac statistics for a symmetric top molecule with three identical nuclei [16], and considering that the level 5_0 is a lowest inversion level and the 4_0 an upper inversion one. The A-coefficients have been calculated using the dipole moment value of 3.918 D [17] and dipole moment matrix elements appropriate for a symmetric top [appendix 5]. The energies of the states have been calculated using the rotational parameters given by A. Bauer et al. [1] (B_0 = 9198.8970 MHz, D_J = 3.807 kHz, D_{JK} = 176.91 kHz) and a value of the rotational constant A (A = 158400 MHz), calculated from microwave structure obtained from B_0 values [18]. The Boltzmann factor has been determined for an Orion kinetic temperature of 90 K. In the case where the nuclear quadrupole hyperfine components are separated, the relative LTE intensities of these components have been calculated using the appropriate factors, m, [19].

The LTE relative intensities are listed in column 9 of table 5.5 and can be compared with the observed relative intensities given in column 10. The agreement is excellent, considering that the (K = 3) line is a convolution of hyperfine components and that errors up to 20% can be made on the evaluation of the intensities of the individual components. Uncertainties on the intensity of the (K = 4) line are also important since the signal to noise ratio of this line is about one. A comparison of the ($J_K = 5_K \rightarrow 4_K$) line intensity ratios with those of the ($J_K = 4_K \rightarrow 3_K$) lines is given below.

b) <u>The ($J_K = 4_K \rightarrow 3_K$) transitions</u>

The ($J_K = 4_K \rightarrow 3_K$) transitions of methyl cyanide has been detected, for the first time, towards Ori A in November 1976, by the Monash group. No report of detection of this transition has yet been

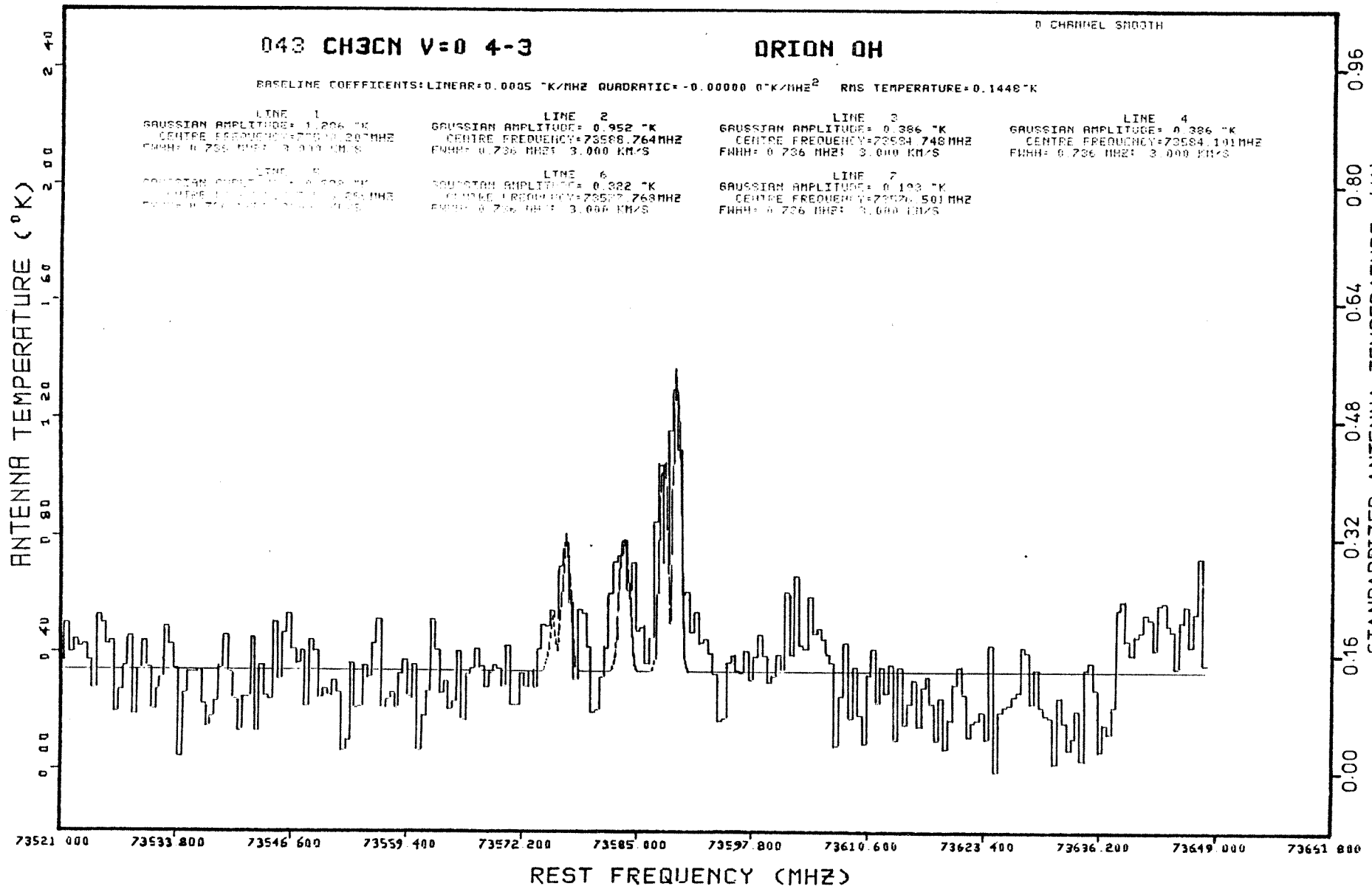

Fig. 5.2 The (J = 4→3) emission of methyl cyanide from Ori A.

given in the literature. The emission spectrum is shown in fig. 5.2 and the line characteristics are listed in table 5.5. In this case there is no evidence of calibration errors. However it is surprising how excellent is the agreement between LTE and observed intensity ratios when the antenna temperatures have been standardized with the same factor than which one used for the ($J_K = 5_K \rightarrow 4_K$) transitions. The error which occurred during the observations of November 1976 by the Monash group was probably on the temperature scaling factor, which was common to the observations of the ($J_K = 5_K \rightarrow 4_K$) and ($J_K = 4_K \rightarrow 3_K$) transitions.

c) Column density

A column density of $\sim 10^{13}$ cm^{-2} has been calculated for a cloud temperature of 90 K and using the conventional method (appendix 5). It appears that the abundance of methyl cyanide in the direction of Ori A is much less than which one of methanol.

d) Vibrationally excited transitions

A line detected in March 1976 by the observers listed in table 5.1 [7], has been during this work, submitted to a statistical analysis. A Gaussian fit indicated a width of 12.9 km s^{-1} and an intensity of 0.39 K. Considering that the observations at 92.35 GHz and at 92 GHz (for the V = 0 CH_3CN) have been made with the same receiver, it is highly probable that the scaling error of March 1976 was common to both detections. A standardization of the antenna temperature of the 92.35 GHz line requires a decrease of the observed intensity by a factor of 1.8 leading to a value of 0.22 K. This line has been assigned to one component of the pair of l-doublet ($V_8 = 1$) ($J = 5 \rightarrow 4$) ($K = \pm 1$) ($l = \pm 1$) transitions of the ν_8 vibrationally excited state of methyl cyanide (362 cm^{-1} above the ground state). The Doppler velocity is then 11.1 km s^{-1}.

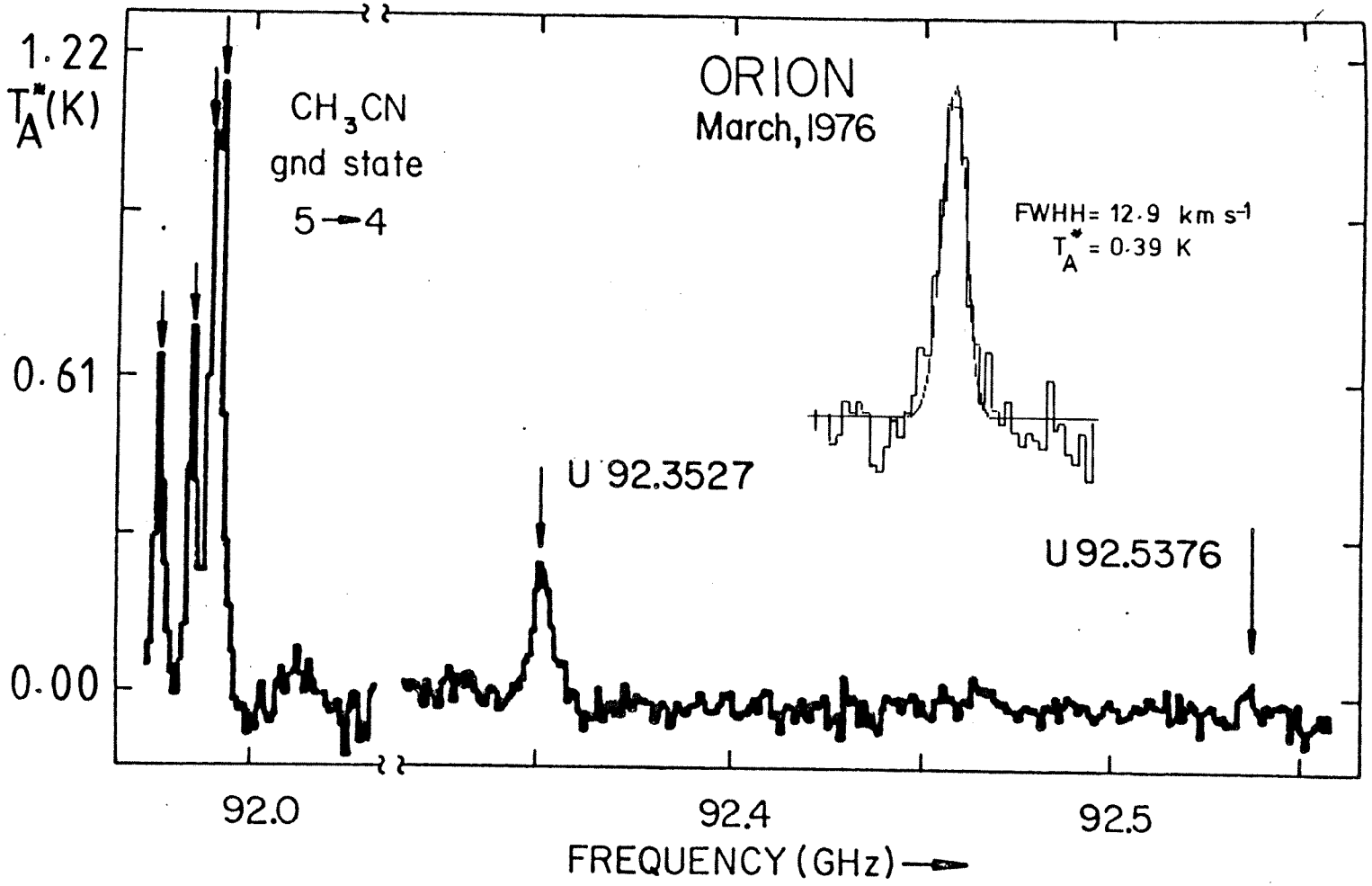

Fig. 5.3 The (v = 0) and (v_8 = 1) (J = 5→4) transitions of methyl cyanide from Ori A. A statistical analysis of the (v_8 = 1) line is enclosed.

Other emission lines from molecules in vibrationally excited states have already been detected from inside the 21 μ contour of the Kleinmann-Low nebula [20]. Such is cyanoacetylene, HC_3N, which emits a pair of (J = 10→9) l-doublet transitions in the ν_7 vibrationally excited state (224 cm^{-1} above the ground state [7]). Also the (V = 1→0) vibration rotation transitions of H_2 have been detected at ∿ 2 μ [26].

The detected velocities seem surprisingly high. However this feature is common to some molecules such as SO[23], SO_2[24], SiO[25], CO[21,26] which show a broad plateau of emission of ∿ 30 km s^{-1} width. Other molecules such as H_2S[22], H_2CO[27], CS[28], HC_3N[7] present a width of ∿ 9 km s^{-1}. Some authors suggest the presence of large magnetic fields [23] or large kinematic motions [29] or pre-main sequence objects [21] or of an expanding cloud resulting from an explosive event [26]. An association of HC_3N (ν_7) with the Kleinmann-Low nebula has been discussed [31]. It is plausible that the vibrationally excited CH_3CN emission is due to the same gas flows that are responsible for the emission of the cited inorganic and carbon molecules.

A suggestion of line has also been detected at the frequency of the transition (J = 5→4) (K = ±1) (l = ±2) of methyl cyanide in the vibrational excited state (V_8 = 2).

5.2.2 *Sagittarius B2*

The (J = 2→1) transition of methyl cyanide has been detected for the first time towards Sgr B2 molecular cloud with a Doppler velocity of 62 km s^{-1} and a velocity width of 28 km s^{-1}. Its intensity is anomalously high. The high K-components of the (J = 6→5) transition seem also to show some departure from LTE.

a) The (J = 2→1) transition

The (J = 2→1) transition of methyl cyanide has been detected during observations conducted at Parkes by the author and the other observers listed in table 5.1. In each of the pair of 5 mm integrations there was evidence of a broad line of about 3 MHz width. The sum of twenty eight integrations is shown in fig. 5.4. The optimum Gaussian profile is at a position corresponding to a Doppler velocity of 62 km s^{-1}, relative to the LSR, and a velocity width of 28 km s^{-1}. The solid curve in fig. 5.3 b is the laboratory spectrum convoluted with a Lorentzian function of 3.1 MHz FWHH, which corresponds to the velocity spread previously deduced for Sgr B2 (25 km s^{-1}). The detection of this line was confirmed by further observations in February 1977.

Fig. 5.3 (c) shows the high resolution laboratory spectrum recorded in Monash as a preliminary to the observations. In order to achieve a satisfactory experimental profile, the (K = 0) and (K = 1) lines have been observed separately under conditions of moderate resolution in an L-band Stark-modulated absorption spectrometer. The (K = 1) spectrum shows a linear Stark effect and was easily modulated at 25 V cm^{-1}. The (K = 0) spectrum exhibits quadratic field dependence and was modulated at 500 V cm^{-1}. In the later case, a DC bias corresponding to a field of 25 V cm^{-1} was applied to the square-wave modulation in order to shift the (K = 1) line from the region of interest. The (K = 0) and (K = 1) spectra were individually digitized and stored in a Varian V72 computer where they were later added to give the composite spectrum shown in fig. 5.3 (c). The theoretical stick spectrum calculated from the measured molecular constants is also shown. The components (F = 1→2) have not been drawn because of their low intensity (∿ 1.2% of the (F = 3→2)).

The overall multiplet is only 4 MHz wide, compared to 14 MHz

Fig. 5.4 The (J = 2→1) emission of methyl cyanide from Sgr B2

(a) The observed line with the optimum Gaussian profile superimposed.

(b) The laboratory spectrum convoluted with a Lorentzian function of 25 km s^{-1} FWHH (3.1 MHz at 37 GHz).

(c) The high resolution laboratory spectrum with quadrupole hyperfine structure shown.

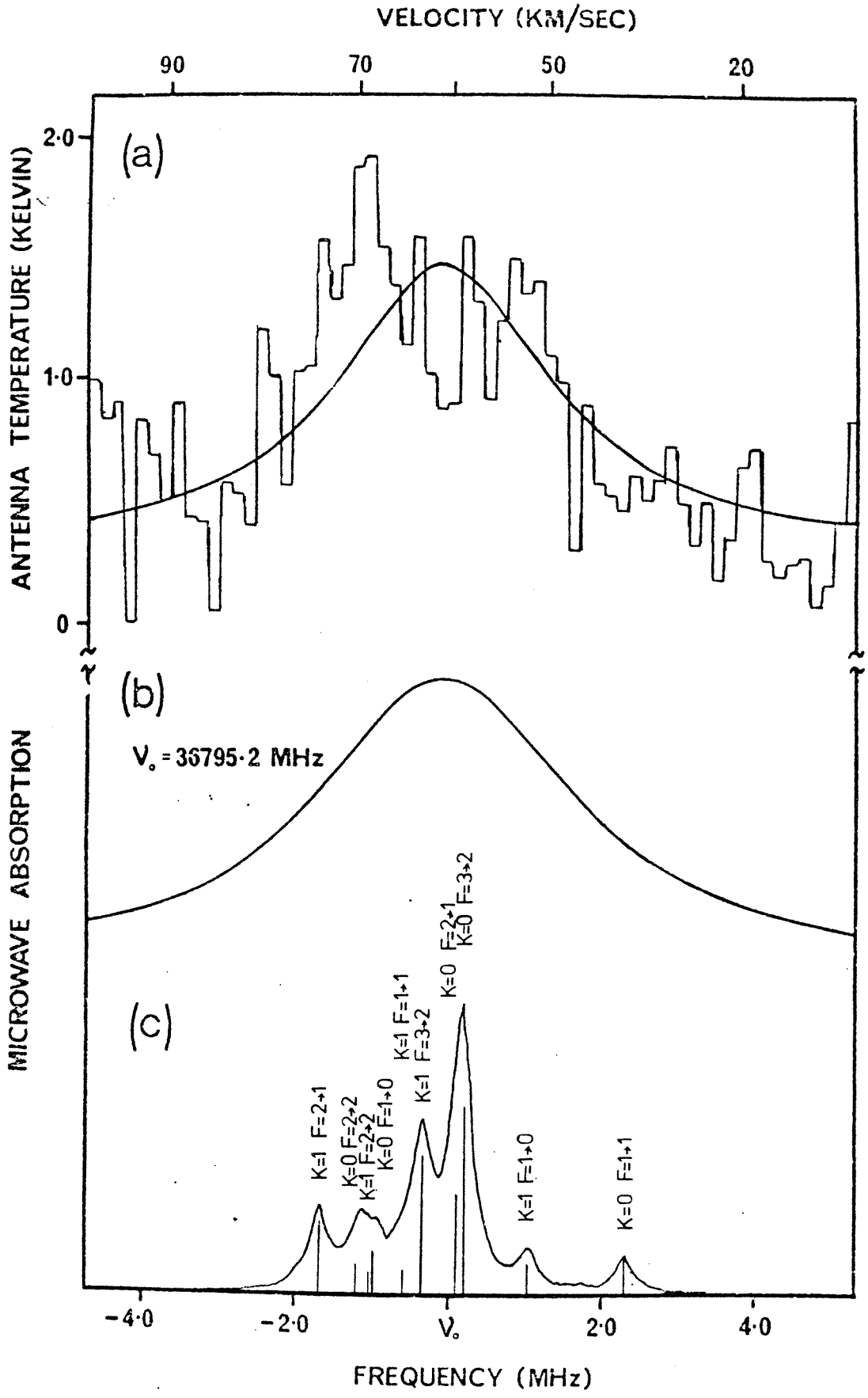
VELOCITY (KM/SEC)
90
70
50
20
ANTENNA TEMPERATURE (KELVIN)
2·0
1·0
0
(a)
(b)
V₀ = 36795·2 MHz
MICROWAVE ABSORPTION
(c)
K=1 F=2→1
K=0 F=2→2
K=1 F=2→2
K=0 F=1→0
K=1 F=1→1
K=1 F=3→2
K=0 F=2→1
K=0 F=3→2
K=1 F=1→0
K=0 F=1→1
-4·0
-2·0
V₀
2·0
4·0
FREQUENCY (MHz)

TABLE 5.6

Methyl cyanide emission from Sgr B2

transition J	K	F	rest[a] frequency (MHz)	E_u/k (K)	$A \times 10^5$ (s^{-1})	T_A^* obs. (K)	$(2J_u+1)S(I,K)m\ e^{-E_u/kT}$ $A \times 10^4$ (s^{-1})	$\frac{I_{J_K}}{I_{6_0}}$ LTE[e]	$\frac{I_{J_K}}{I_{6_0}}$ obs	ref.
6→5	0	7→6	110383.494	18.5	11.1	1.09	48.0	1.50	1.34	4
6→5	1	7→6	110381.362	25.7	10.8		43.4	1.36		4
6→5	2	7→6	110374.986	47.2	9.85	0.81	31.9	1.00	1.00	4
6→5	3	7→6 5→4	110364.490	83.0	8.31	0.31	24.9	0.77	0.38	4
6→5	4	7→6 5→4	110349.706	133.2	6.15	0.45	5.55	0.17	0.55	4
6→5	5	7→6 5→4	110330.728	197.6	3.38	0.30	1.60	0.05	∿0.37	3
2→1			36795.2[b]	2.65[c]	0.356[c]	0.98[d](10)	0.69	0.02	1.21	this work

a : A. Bauer et al. [1] unless otherwise noted.

b : Measured at Monash - [this work].

c : Calculated for the (K = 0, F = 2→1) component, the strongest of the multiplet.

d : Corrected for a telescope efficiency of 44%.

e : Calculated for T_{ex} = 100 K.

for the (J = 4→3), 29 MHz for the (J = 5→4) and 54 MHz for the (J = 6→5). The 25 km s^{-1} velocity width, characteristic of Sgr B2 is thus too big to separate the K-components.

b) The ($J_K = 6_K \rightarrow 5_K$) transition

The ($J_K = 6_K \rightarrow 5_K$) transitions have been detected towards Sgr B2 by P.M. Solomon et al. [3,4]. The data are listed in table 5.6 together with those of the (J = 2→1) observation. Even an excitation temperature of 100 K (instead of the usual value of ∿ 40 K) does not explain satisfactorily the relative intensities of the high K-components, especially for the (K = 5) component if present.

The 2→1 transition presents a strong anomalous behaviour.

c) Vibrationally excited state

A line detected in March 1976 by the observers listed in table 5.1 was reported with a frequency of 92352.7 MHz [7] and assigned to methyl cyanide in the first ν_8 vibrationally excited state. A second observation of this ($v_8 = 1$) (J = 5→4)(K = ±1)(l = ±1) transition at 92353.516 MHz has been undertaken by the author and the other observers listed in table 5.1 in June 1976. No positive detection of this line has been recorded.

The ($v_8 = 1$) (J = 2→1) transition at 36942.15 MHz has also been searched in June 1976 without success.

The detection of the vibrationally excited states of methyl cyanide in Ori A solely can be justified by the fact that the Kleinmann-Low nebula in Orion is an intense infra red source in the opposite to Sgr B2.

d) Column density

For levels which would be populated at a kinetic temperature of 100 K, the column density of methyl cyanide in the direction of Sgr B2 would be of the order of 5×10^{13} molecules cm^{-2}.

5.2.3 *Other sources*

The (v = 0) (J = 2→1) and (J = 4→3) transitions have been searched in other sources without success, with the possible exception of N 159. An apparent emission line of the (J = 2→1) transition of amplitude 0.3 K and of Doppler velocity 262 km s^{-1} has been seen towards the edge of the 10 MHz bandwidth at low signal to noise ratio. These negative searches are listed in table 5.1.

5.3 *A SEARCH FOR METHYL ISOCYANIDE*

CH_3NC has been searched towards Ori A and Sgr B2 by the author and the observers of June 1976 and February 1977 (table 5.1). No line has been detected, and the results are summarized in table 5.2.

CHAPTER 6

NEGATIVE SEARCHES AND SOME OTHER SUCCESSFUL RADIOASTRONOMICAL OBSERVATIONS

The author participated in some other observations of inter-stellar molecular lines. The following tables and figures summarize the results. The session of April 1978 was conducted at Kitt Peak and the other ones at Parkes.

TABLE 6.1

Negatives searches and some other successful observations

source	pointing position α (1950) δ	T_A^* [a] (K)	ΔT_{rms} (K)	ΔV km s^{-1}
$H^{15}NC$	J = 1→0 ν_{rest} = 88865.715 MHz		Apr. 1978	[1]
NGC 2264	$06^h\ 38^m\ 28^s.0$ 09° 32' 06"	...	0.051	...
L134N	15 51 30.0 -02 43 31	...	0.062	...
DR21(OH)	20 37 14.0 42 12 00	0.061	0.029	5.0
DNC	J = 1→0 ν_{rest} = 76305.727 MHz		Apr. 1978	[1]
L134N	$15^h\ 51^m\ 30^s.0$ -02° 43' 31"	0.59	0.083	0.79
W3(MOL)	02 21 47.0 61 52 54	...	0.043	...
DNC	J = 1→0 ν_{rest} = 76305.727 MHz		July 1978	[1]
R Cr A	$18^h\ 58^m\ 29^s.3$ -37° 01' 10"	...	0.35	...
RCW 36CC	08 58 20.0 -43 48 24	...	0.15	...
Chamaeleon	12 41 14.5 -28 32 00	...	0.30	...
IRC+10011	01 03 48.0 12 19 45	...	0.20	...
Coal Sack (CO)	12 28 51.0 -63 30 00	...	0.20	...
CRL 3068	23 16 42.4 16 55 10	...	0.30	...
HCN	J = 1→0 ν_{rest} = 88631.6024 MHz		July 1978	[1]
IRC+10011	$01^h\ 03^m\ 48^s.0$ 12° 19' 45"	...	0.25	...
HCO^+	J = 1→0 ν_{rest} = 89188.545 MHz		July 1978	[1]
CRL 3068	$23^h\ 16^m\ 42^s.4$ 16° 55' 09"	...	0.21	...
M17	18 17 26.5 -16 14 54	3.5	0.050	∿3.4
Mon R2	06 05 20.0 -06 22 30	5.0	0.25	∿3.0
Ori A	05 32 47.0 -05 24 21	13.0	0.35	3.5
	05 32 45.5 -05 24 11	17.5	0.35	3.5
	05 34 41.0 -05 24 21	11.0	0.35	3.5
	05 32 44.0 -05 24 21	20.0	0.35	3.5
	05 32 44.5 -05 24 31	15.0	0.35	3.5
Chamaeleon	12 41 14.5 -28 32 00	...	0.30	...
RCW 36CC	08 58 20.0 -43 48 24	...	0.30	...
Coal Sack (CO)	12 28 51.0 -63 30 00	...	0.20	...
N159(LMC)(CO)	05 40 24.0 -69 46 00	...	0.15	...

TABLE 6.1 cont'd

source	pointing position α (1950) δ	T_A^* [a] (K)	ΔT_{rms} (K)	ΔV km s^{-1}
HC_3N	J = 9→8 ν_{rest} = 81881.46 MHz		July 1978	[2]
Ori A	$05^h\ 32^m\ 47^s.0$ -05° 24' 21"	3.5	0.10	3.5
	05 32 51.0 -05 24 21	...	0.15	...
	05 32 41.0 -05 24 21	...	0.20	...
	05 32 47.0 -05 25 05	...	0.20	...
	05 32 47.0 -05 23 36	...	0.20	...
	05 32 47.1 -05 24 23	2.5	0.10	3.5
	05 32 38.0 -05 24 21	...	0.25	...
	05 32 43.8 -05 23 31	...	0.20	...
Eta Carina	10 43 06.9 -59 25 16	...	0.20	...
Chamaeleon	12 41 14.5 -78 32 00	...	0.50	...
	Formaldehyde absorption in cometary globules			[3,4]
H_2CO	$J_{K_-K_+} = 1_{1,0} \leftarrow 1_{1,1}$ ν_{rest} = 4829.6599 MHz		May 1979	
CG 13	$07^h\ 12^m\ 58^s.0$ -48° 25' 04"	0.20	0.019	0.5
CG 2 (center)	07 14 30.0 -43 52 00	0.17	0.017	1.0
CG 1 (star)	07 17 42.0 -44 29 00	0.20	0.028	1.5
CG 15	07 31 00.0 -50 39 15	...	0.017	...
CG 14	07 37 13.0 -49 44 07	0.13	0.017	0.8
CG 31 A (tail)	08 06 55.0 -35 44 44	0.32	0.033	1.0
CG 31 (center)	08 07 00.0 -35 48 36	0.55	0.036	1.0
CG 30 (center)	08 07 39.0 -33 55 53	0.082	0.019	2.0
CG 22 (center)	08 26 47.0 -33 35 26	0.28	0.036	1.3
CG 17	08 51 04.0 -51 40 32	...	0.016	...
CG 7 (head)	09 12 14.0 -43 17 35	...	0.020	...
CG 12-2 (dust cloud)	13 54 35.0 -39 41 19	0.25	0.031	1.3
CG 12-1	13 54 42.0 -39 44 25	0.20	0.026	1.3
CG 12-8	13 54 57.0 -39 49 37	...	0.025	...
Scorpius Teardrop 277-2B	16 43 09.0 -44 25 24	0.50	0.030	1.0
Scorpius Elephant Trunk	16 47 45.0 -43 36 01	(0.17)	0.030	(1.7)
277-2D Sco.E.T.	16 49 21.0 -43 27 31	(0.18)	0.043	(2.5)
277-2C Sco.E.T.	16 49 32.0 -43 31 45	...	0.040	...
277-2A Sco.E.T.	16 49 58.0 -43 40 15	(0.078)	0.020	(2.0)
C110α	n = 111→110 ν_{rest} = 4876.589 MHz		May 1979	
NGC 2024	$05^h\ 39^m\ 12^s.0$ -01° 57' 40"	0.216	0.010	3.7

a : when present, the formaldehyde line has always been detected with $V_{LSR} < 1$ km s^{-1}.

The antenna temperatures of the 5 GHz lines are corrected for 60% telescope efficiency; those of HCO^+ are corrected for 20% telescope efficiency.

TABLE 6.1 continu'd

Negative searches and some other positive detections

molecule	transition	source	pointing position α (1950)	δ	V_{LSR} (km s^{-1})	ΔV (km s^{-1})	on-source time (s)	ΔT_{rms} (K)	T_A^* (K)	date of obs$_t$
isocyanic acid	$J_{K\,K_+}=2_{1,1}\rightarrow 1_{1,0}$	Ori A	05 32 47.0	-05 24 21	6.1	...	14700	0.30	...	Jun. 1976
HNCO [5]	43$\bar{1}$9.879 MHz	IRC+10216	09 45 15.0	13 30 40	-22	...	7200	0.46	...	Jun. 1976
		Sgr B2	17 44 11.0	-28 24 30	62	...	20400	0.22	...	Jun. 1976
fulminic acid	J = 2→1	G311.6+0.3	14 01 17.0	-61 05 35	-54	...	6000	0.38	...	Jun. 1976
HNCO	45876.21 MHz	Sgr B2	17 44 11.0	-28 24 30	62	...	20400	0.20	...	Jun. 1976
		Ori A	05 32 47.0	-05 24 21	6.1	...	18000	0.24	...	Jun. 1976
ketene	$J_{K\,K_+}=2_{0,2}\rightarrow 1_{0,1}$	G328.2-0.5	15 54 13.0	- 3 54 00	-42.4	...	3000	0.82	...	Jun. 1976
CH_2CO	40$\bar{4}$17.90 MHz	Sgr B2 [a]	17 44 11.0	-28 24 30	62	...	22800	0.24	...	Jun. 1976
		Ori A	05 32 47.0	-05 24 21	6.1	...	11400	0.49	...	Jun. 1976
		N159(LMC)	05 40 24.0	-69 46 00	235	...	1500	0.87	...	Jun. 1976
		G311.6+0.3	14 01 17.0	-61 05 35	-54	...	7800	0.42	...	Jun. 1976
sulfur monoxide	$J_K = 2_3\rightarrow 2_2$	IRC+10216	09 45 15.0	13 30 40	-22	...	900	1.1	...	Jun. 1976
SO [6]	36201.942 MHz	W 51	19 21 27.0	14 24 30	60	...	5700	0.45	...	Jun. 1976
		Ori A	05 32 47.0	-05 24 21	6	23	31500	0.10	0.40	Feb. 1977
		Sgr B2(OH)	17 44 11.0	-28 22 30	62	...	21000	0.38	0.22	Feb. 1977
		Sgr B2(2'S)	17 44 11.0	-28 24 30	62	...	24000	0.40	...	Feb. 1977
		M 17 (SW)	18 17 27.0	-16 14 54	20.0	...	5100	0.46	...	Feb. 1977
		NGC 2264	06 38 27.0	09 32 04	8.6	...	7440	0.53	...	Feb. 1977
methylene ketene	$J_{K\,K_+}=4_{0,4}\rightarrow 3_{0,3}$	Sgr B2	17 44 11.0	-28 22 30	62	...	12000	0.25	...	Feb. 1977
CH_2CCO [7]	34$\bar{5}$79.3 MHz									
acetaldehyde	$J_{K\,K_+}=2_{1,2}\,^1\!1_{1,1}$ A	Sgr B2	17 44 11.0	-28 22 30	62	...	22800	0.21	...	Feb. 1977
CH_3CHO [8]	37$\bar{4}$64.168 MHz									
	$J_{K\,K_+}=2_{0,2}\rightarrow 1_{0,1}$ A	Sgr B2	17 44 11.0	-28 22 30	62	...	6600	0.34	...	Feb. 1977
	38$\bar{5}$12.113 MHz									
hydrogen cyanide	$v_2^1 = 1^1$, J = 14→14	M 17	18 17 27.0	-16 14 54	20	...	8400	0.37	...	Feb. 1977
HCN	47023.2 MHz	Ori A	05 32 47.0	-05 24 21	6.1	...	18300	0.22	...	Feb. 1977
		IRC+10216	09 45 15.0	13 30 40	-22	...	6000	0.42	...	Feb. 1977
cyanoacetylene	$v_7^1 = 1^1$, J = 5→4	Ori A	05 32 47.0	-05 24 21	6.1	...	22200	0.19	...	Feb. 1977
HC_3N [2]	45667.519 MHz									
methyl cyanoacetylene	J = 9→8	Sgr B2	17 44 11.0	-28 22 30	62	...	5400	0.36	...	Feb. 1977
CH_3C_3N	36309.63 MHz									
thioformaldehyde	$J_{K\,K_+}=1_{0,1}\rightarrow 0_{0,0}$	Ori A	05 32 47.0	-05 24 21	6.1	...	6600	0.30	...	Feb. 1977
H_2CS [4]	34$\bar{3}$51.43 MHz	IRC+10216	09 45 15.0	13 30 40	-22	...	2400	0.53	...	Feb. 1977

molecule	transition	pointing	position α (1950)	position δ (1950)	V_{LSR} (km s^{-1})	ΔV (km s^{-1})	on-source time (s)	ΔT_{rms} (K)	T_A^* (K)	date of obs^t
hydroxyl	$^2\pi_{3/2}$ J=11/2 F=5→5	G309.9+0.5	13 47 12.5	-61 19 58	-60	...	1800	0.47	...	Feb. 1977
OH [9]	36983.47 MHz									
carbon monosulfide	J = 1→0	W 51	19 21 22.0	14 24 36	60	...	900	...	3.2	Feb. 1977
CS	48991.00 MHz									
deutero formaldehyde	$J_{K\ K_+}=1_{1,0}\rightarrow1_{1,1}$	G333.3-0.4	16 17 47.0	-50 19 09	-53.9	...	7200	0.70	...	May 1977
HDCO [10]	5$\bar{3}$46.142 MHz	N159(LMC)	15 40 25.0	-69 46 01	235	...	5400	0.10	...	May 1977
		W 33	18 11 19.0	-17 56 54	34.1	...	1800	0.15	...	May 1977
		NGC 2024	05 39 12.0	-01 55 40	8.65	...	10500	0.20	...	May 1977
		NGC 2264	06 38 27.0	09 32 04	8.6	...	8100	0.40	...	May 1977
		G326.5+0.9	15 38 34.0	-53 48 58	-40.1	...	14400	0.30	...	May 1977
		G311.6+0.3	14 01 17.0	-61 05 35	-54.0	...	900	0.30	...	May 1977
		S. Coal Sack 2A	12 29 08.0	-63 28 12	- 6.5	...	8100	0.40	...	May 1977
		S. Coal Sack 2E	12 28 07.0	-63 25 00	- 6.5	...	8100	0.05	...	May 1977
		L134	15 51 00.0	-04 26 57	3	...	11400	0.06	...	May 1977
		Sgr B2	17 44 11.0	-28 22 30	62	...	4800	0.10	...	May 1977
methanimine	$J_{K\ K_+}=1_{1,0}\rightarrow1_{1,1}$	Sgr B2(OH)	17 44 11.0	-28 22 30	60	24	2400	0.046	0.303	May 1977
CH_2NH [11]	52$\bar{9}$0.124 MHz	Sgr B2(2'N)	17 44 11.0	-28 20 30	60	24	2400	...	0.30	May 1977
		Sgr B2(4'N)	17 44 11.0	-28 18 30	60	...	2400	0.08	...	May 1977
		Sgr B2(2'E)	17 44 19.0	-28 22 28	60	24	2400	...	0.32	May 1977
		Sgr B2(4'E)	17 44 27.0	-28 22 28	60	24	2400	...	0.08	May 1977
		Sgr B2(2'W)	17 44 03.0	-28 22 31	60	24	2400	...	0.30	May 1977
		Sgr B2(4'W)	17 43 55.0	-28 22 26	60	24	2400	...	0.13	May 1977
		W 51	19 21 23.0	14 24 28	57	...	9600	0.026	...	May 1977
		N159(LMC)	04 40 24.0	-69 46 00	235	..	18000	0.010	...	May 1977
		NGC 2264	06 38 28.0	09 32 11	8.3	...	6000	0.023	...	May 1977
	$J_{K\ K_+}=3_{0,3}\rightarrow2_{1,2}$	Sgr B2	17 44 11.0	-28 22 30	62	23	19200	0.050	0.450	Jun. 1978
	350$\bar{6}\bar{5}$.723 MHz	ρ Oph.	16 23 15.0	-24 19 30	3	...	2400	1.4	...	Jun. 1978
		Sgr A(4'N)	17 42 28.0	-28 [illegible]7 30	40	...	3300	0.18	...	Jun. 1978
		CRL 3068 planet. nebula	21 16 42.0	16 5[illegible] 10	-28	...	5100	0.19	...	Jun. 1978
HCN dimer [11]	J = 10→9	Sgr B2	17 44 11.0	-28 22 30	62	...	4800	0.07	...	Jun. 1978
	35753.94 MHz	CRL 3068 planet. nebula	21 16 42.0	16 55 10	-28	...	7200	0.07	...	Jun. 1978
		IRC+10011	01 03 48.0	12 19 45	11	...	2400	0.10	...	Jun. 1978
		Ori A	05 32 47.0	-05 24 21	8.5	...	14100	0.10	...	Jun. 1978
cis-thionylimide	$J_{K\ K_+}=2_{0,2}\rightarrow1_{0,1}$	ρ Oph.	16 23 09.0	-24 18 18	3	...	3600	0.40	...	Jun. 1978
HNSO	360$\bar{9}$8.34 MHz	Sgr B2	17 44 11.0	-28 22 30	62	...	22800	0.02	...	Jun. 1978
		Ori A	05 32 47.0	-05 24 21	8.6	...	13500	0.05	...	Jun. 1978

a : On statistical analysis, a weak ketene line was detected at V_{LSR} = 47 km s^{-1}.

Fig. 6.1 The ($J = 1 \rightarrow 0$) emission of HCO^+ from M17, Mon R2 and Ori A

WED 19/ 7/78 SEQUENCE NO. 1503.A.2

SOURCE: M17

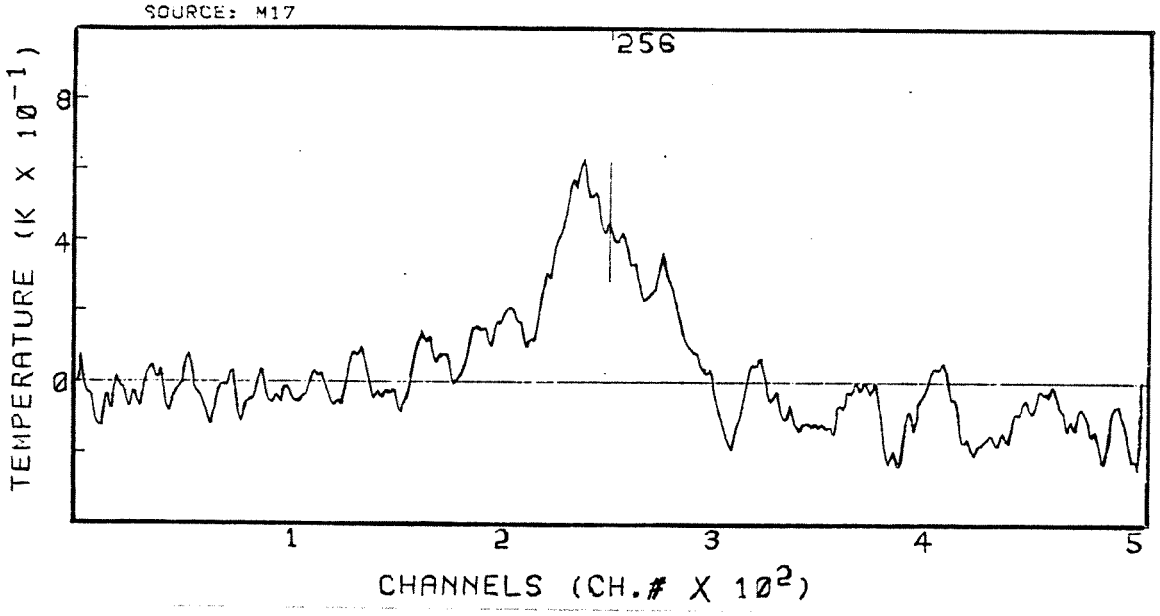

MON 17/ 7/78 SEQUENCE NO. 1436.A.2

SOURCE: MON R2

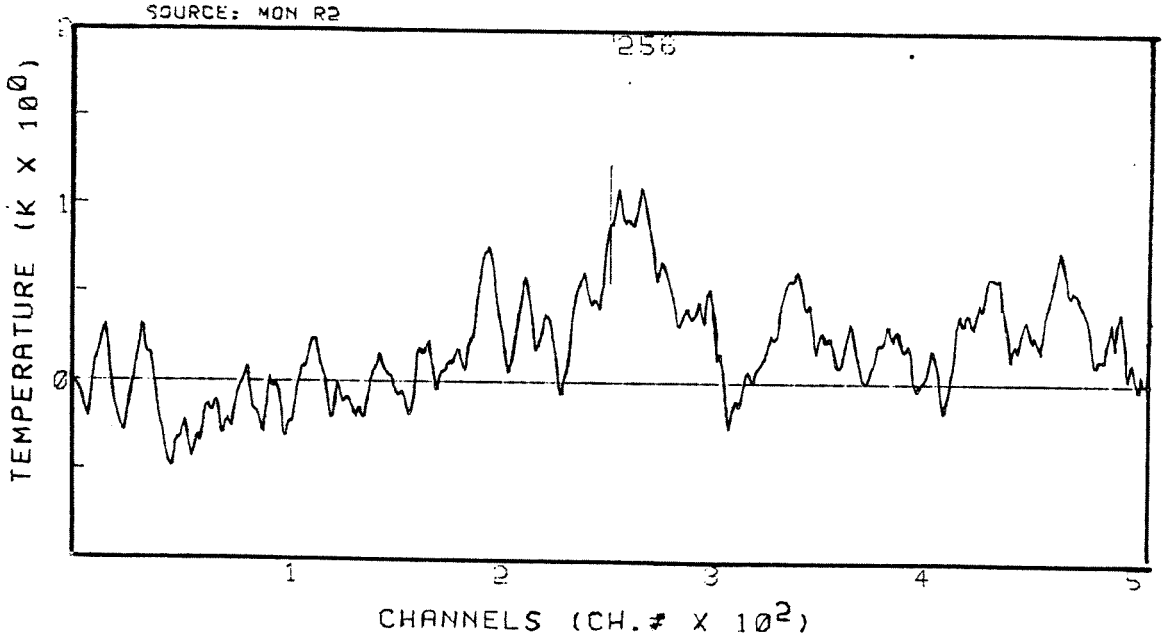

MON 17/ 7/78 SEQUENCE NO. 1424.A.2

SOURCE: ORION A

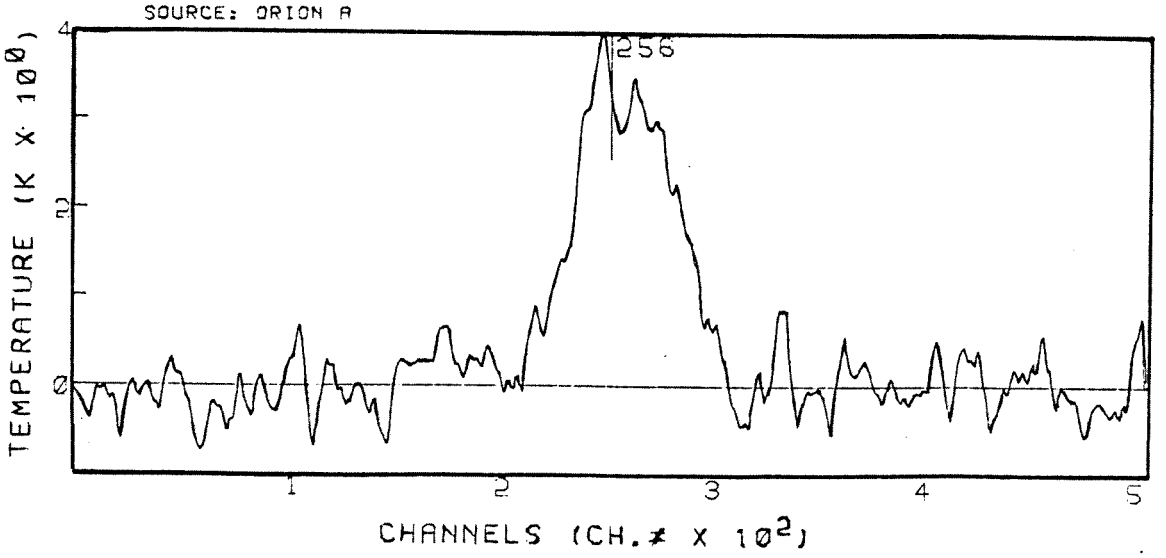

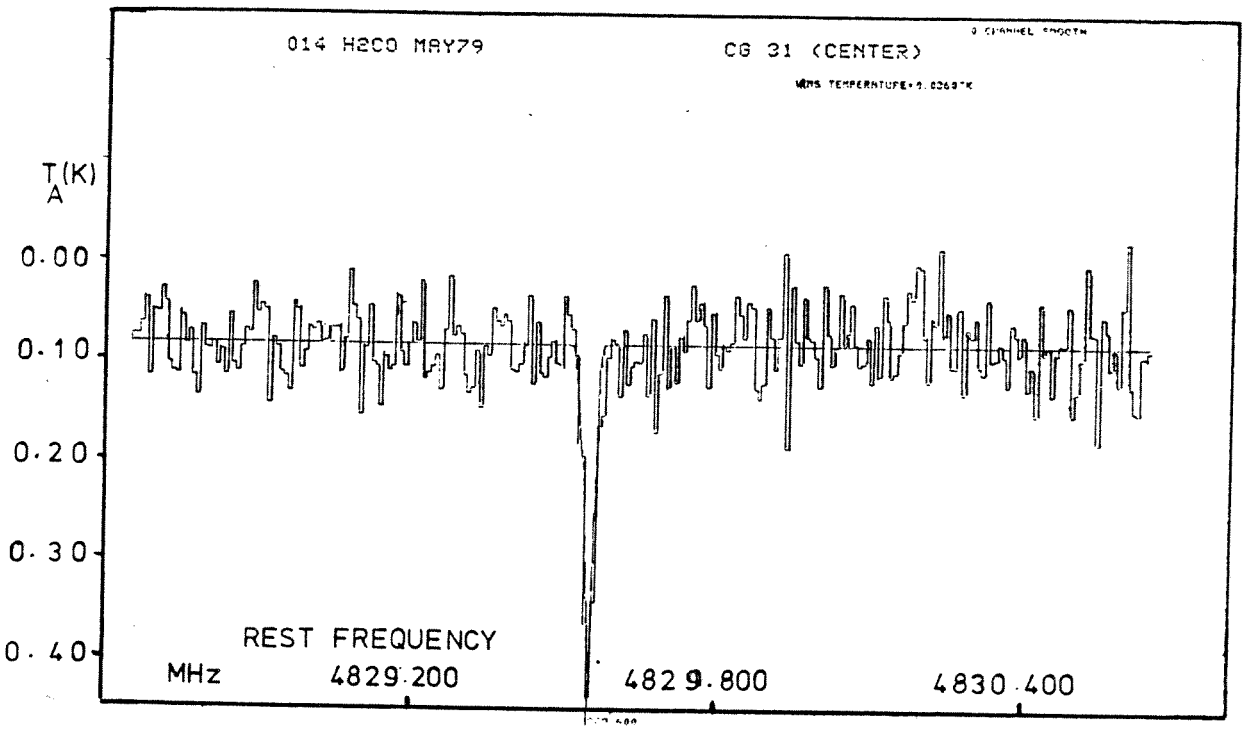

Fig. 6.2 The ($J_{K_aK_c} = 1_{1,0} \leftarrow 1_{1,1}$) absorption of formaldehyde in cometary globules.

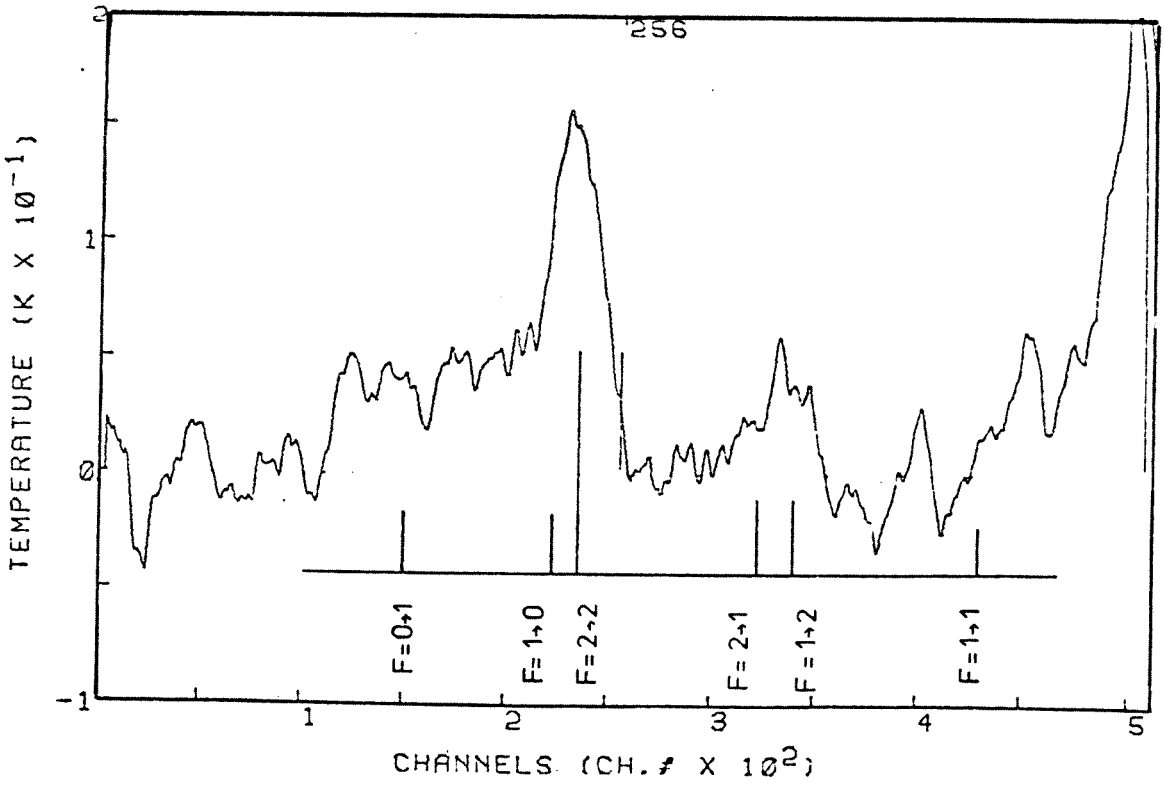

Fig. 6.3 The ($J_{K_aK_c} = 1_{1,0} \rightarrow 1_{1,1}$) emission of methanimine from Sgr B2.

APPENDIX 1

MOLECULAR ROTATION THEORY

In this appendix is presented a brief summary of the molecular rotation theory which has been the basis of the computer programs WANGLY-WASCAN and SFIT.

In the general case, the Hamiltonian may be formulated as follows:

$$\mathcal{H} = \mathcal{H}_R + \mathcal{H}_D + \mathcal{H}_Q + \mathcal{H}_E + \mathcal{H}_{SR} + \mathcal{H}_{IR}$$

where $\mathcal{H}_R$ is the rigid rotor Hamiltonian

$\mathcal{H}_D$ is the centrifugal distortion contribution to the rotational energy. This is usually expressed as an expansion in even powers of angular momentum operators

$\mathcal{H}_Q$ is the nuclear electric quadrupole Hamiltonian which describes the effect of the coupling of the nuclear spin to the molecular rotation

$\mathcal{H}_E$ is the Stark effect Hamiltonian which describes the interaction of a polar molecule with an external electric field

$\mathcal{H}_{SR}$ describes the effect of the interaction of a nuclear magnetic dipole moment with the induced molecular magnetic field

$\mathcal{H}_{IR}$ describes the contribution to the rotational energy due to the interaction of a molecular hindered internal rotor with the overall rotation.

The spin-rotation and internal rotation interaction have not been involved in the development of the programs and are not described here.

Semi-rigid rotor Hamiltonian

The glycine rotor is an asymmetric top, whose states can be specified by the quantum numbers J and M which describe the two constants of the motion:

$\vec{J}$ the total rotational angular momentum, and

$\vec{M}$ its projection on a space-fixed axis.

However $J_{K-1,K+1}$, J_{K_a,K_c}, are more significant representations; they make use of the state label K which is related to:

$\vec{K}$, projection of $\vec{J}$ along the molecule-fixed unique axis of the limiting oblate or prolate symmetric top.

Each state $J_{K-1,K+1}$ may be described by an asymmetric rotor wavefunction, as a linear combination of symmetric rotor basis functions of the same quantum number J:

$$|J,\tau> = \sum_K a_{J,K} |J,K> \quad ,$$

where τ is a pseudo-quantum number distinguishing the (2J+1) rotational states of the asymmetric rotor. The rotational energy levels of glycine are obtained by diagonalization of the Hamiltonian matrix, $[\mathcal{H}_R]$, set up in these basis functions. If I_a, I_b and I_c are the principal moments of inertia, then:

$$A = \frac{h}{8\pi^2 I_a} , \quad B = \frac{h}{8\pi^2 I_b} , \quad C = \frac{h}{8\pi^2 I_c} ,$$

and $$\mathcal{H}_R = A\, J_a^{\,2} + B\, J_b^{\,2} + C\, J_c^{\,2} \quad .$$

J_a, J_b and J_c are the operators representing the projections of the total angular momentum along each of the molecule-fixed principal axes.

In WANGLY, the rotational Hamiltonian includes the effects of centrifugal distortion for a symmetric top, and a simplification in the calculation of the energy levels is obtained by using the Wang basis. The Wang symmetrizing matrix transforms the symmetric rotor basis functions into a new set of functions:

$$|J,K,\gamma\rangle$$

where the label γ is used to distinguish the symmetric and antisymmetric Wang basis functions.

The asymmetric rotor wavefunctions are then formed in a linear combination of the Wang functions:

$$|J,\tau\rangle = \sum_{K,\gamma} a_{J,K,\gamma} |J,K,\gamma\rangle \ .$$

The Hamiltonian matrix may be reblocked into four independent sub-matrices, for each J value:

$$[\mathcal{H}_{E^+}], \ [\mathcal{H}_{E^-}], \ [\mathcal{H}_{O^+}], \ [\mathcal{H}_{O^-}]$$

where even and odd values of K are grouped respectively in the E and O sub-matrices, which are themselves subdivided with respect to the symmetry denoted by γ. The nearly degenerate states appear in separate sub-blocks and hence accurate calculations of their eigenvectors are facilitated.

The program WANGLY also forms the transitions accordingly to the selection rules and calculates line strengths and peak absorption coefficients using the following theoretical concepts.

Intensities of absorption lines are governed by the transition probabilities, $W_{u \leftarrow l}$, which are proportional to the square of the dipole moment matrix elements with reference to the space-fixed axes (F = X,Y,Z):

$$W_{u\leftarrow l} = g_u \, \rho(\nu/\omega) \, B_{u\leftarrow l}(\nu/\omega)$$

where $W_{u\leftarrow l}$ is the absorption probability per unit of time,

g_u is the degeneracy of the final state,

$\rho(\nu/\omega)$ is the intensity of the photon beam expressed as a function of the frequency (ν) or the angular frequency (ω) and as the energy density (ρ) or the specific intensity (I) (see appendix 6),

$B_{u\leftarrow l}(\nu/\omega)$ is the corresponding Einstein coefficient of absorption:

$$B_{J',\tau'\leftarrow J,\tau}(\nu/\omega) = k|\mu_{J',\tau';\ J,\tau}|^2 = k \sum_{F,M'} |\langle J',\tau',M'|\mu_F|J,\tau,M\rangle|^2$$

(S.I.).

Since the dipole moment is defined with respect to the principal inertia molecule-fixed axes (g = a,b,c), the line intensities are proportional to the square of the direction cosine matrix elements, $|\langle J',\tau',M'|\phi_{F,g}|J,\tau,M\rangle|^2$, where $\phi_{F,g}$ is the cosine of the angle between the two systems of axes. Defining the line strength of the transition as:

$$S(J,\tau;J',\tau') = \sum_{F,M,M'} |\langle J',\tau',M'|\phi_{F,g}|J,\tau,M\rangle|^2 \ ,$$

and the dipole moment matrix elements as:

$$\sum_{F,M'} |\langle J',\tau',M'|\mu_F|J,\tau,M\rangle|^2 = [\mu_g{}^2 S(J,\tau;\ J',\tau')]$$

the intensity of a Lorentzian line can be expressed by a peak absorption coefficient:

$$\alpha_{max} = \frac{1}{(4\pi\varepsilon_0)} \frac{8\pi^2 N F_{J,\tau} \nu_0^2}{3c\ kT\ (\Delta\nu)} \left(1 - \frac{1}{2}\frac{h\nu_0}{kT}\right) |\langle J',\tau'|\mu_F|J,\tau\rangle|^2 \qquad \text{(S.I.)}.$$

$F_{J,\tau}$ is the fractional population of the lower rotational state $|J,\tau\rangle$; in the case of glycine, it is expressed as:

$$F_{J,\tau} = \frac{N_{J,\tau}}{N} = \frac{F_v(2J+1)e^{-E_{J,\tau}/kT}}{Q_r}$$

where F_v is the fractional population in the vibrational state considered, and

Q_r is the rotational partition function:

$$Q_r = \left[\left(\frac{\pi}{ABC}\right)\left(\frac{kT}{h}\right)^3\right]^{\frac{1}{2}} = 5.34\ 10^6 \left(\frac{T^3}{ABC}\right)^{\frac{1}{2}} \quad \text{(A,B,C in MHz)}\ .$$

The peak absorption coefficient can hence be expressed as:

$$\alpha_{max}(cm^{-1}) = 3.85\ 10^{-14}\ F_v (ABC)^{\frac{1}{2}} \mu_g^2\ S\ (J',\tau';\ J,\tau)\ \frac{\nu_0^2}{(\Delta\nu)T^{5/2}}\ e^{-E_{J,\tau}/kT}$$

with A, B, C, ν_0, $\Delta\nu$ in MHz and μ in D.

Nuclear quadrupole coupling

The ^{14}N nucleus of spin angular momentum (I = 1), has a non spherical charge distribution and consequently an electric quadrupole moment. This moment, described by the second rank tensor $Q_{ij}^{(2)}$, interacts with the electric field gradient at the nucleus, $\nabla E_{ij}^{(2)}$, which is created by the electron charge distribution averaged over the rotational motion of the molecule. The Hamiltonian for this orientation dependent interaction is written as a scalar product of the two tensors:

$$\mathcal{H}_Q = -\frac{1}{6} \nabla E_{ij}^{(2)} : Q_{ij}^{(2)} .$$

With Q expressed as a function of I, V as a function of J and F the total angular momentum as (F = I+J), the quadrupole interaction energy may be written as:

$$\langle J,I,F|\mathcal{H}_Q|J,I,F\rangle = E_Q(J,I,F) = eQq_J \frac{2J+3}{J} Y(J,I,F)$$

where $$Y(J,I,F) = \frac{\frac{3}{4}C(C+1) - I(I+1)J(J+1)}{2I(2I-1)(2J-1)(2J+3)}$$

is the Casimir's function

with $$C = F(F+1) - I(I+1) - J(J+1).$$

q_J is defined as the molecular field gradient in the Z direction of the space-fixed system, averaged over the state $|J,M_J=J\rangle$:

$$q_J = \langle J,M_J=J|V_{ZZ}|J,M_J=J\rangle .$$

Q is defined as the nuclear quadrupole moment in the Z direction of the space-fixed system, averaged over the state $|I,M_I=I\rangle$.

In the case of an asymmetric rotor q_J may be expressed as a function of $\langle J_g^2\rangle$, which is the expectation value of the square of the molecule-fixed component J_g averaged over the asymmetric rotational state $|J,\tau\rangle$:

$$q_J = \frac{2}{(J+1)(2J+3)} \sum_{g=a,b,c} q_{gg} \langle J_g^2 \rangle$$

With the quadrupole coupling constant, $\chi_{gg} = eQq_{gg}$, the quadrupole energy may be written:

$$E_Q(J,I,F) = (D_1\chi_{aa} + D_2\chi_{bb})Y(J,I,F)$$

where

$$D_1 = \frac{2}{J(J+1)} (\langle J_a^2 \rangle - \langle J_c^2 \rangle)$$

$$D_2 = \frac{2}{J(J+1)} (\langle J_b^2 \rangle - \langle J_c^2 \rangle) \quad .$$

WAD1D2 calculates these D parameters, using the energy file written on disc partition by WANGLY.

Stark effect

The perturbing Hamiltonian operator describing the interaction energy between a dipole moment fixed in the molecule $\vec{\mu}_g$ and a static electric field, fixed along the Z space axis $\vec{E}_Z$, may be written as the following electric-dipole interaction:

$$\mathcal{H}_E = - E_Z \sum_{g=a,b,c} \mu_g \phi_{Zg}$$

where ϕ_{Zg} are the direction cosines of the principal axes of inertia with reference to the direction of the applied field Z.

In the case of no nearby degeneracy of the interacting levels, the conventional perturbation theory leads to a Stark energy which may be written:

$$E_S(J,\tau,M_J) = \sum_{g=a,b,c} (\alpha_g + \beta_g M_J^2)\mu_g^2 E^2$$

M_J is the quantum number which represents the projection of the angular momentum vector $\vec{J}$ along the applied electric field $\vec{E}_Z$;

α_g and β_g are coefficients dependent in J, in λ_g, and in the energies of

the levels involved in the transition.

WASTAR performs the above calculation and also treats, for each level, a case of near degeneracy by diagonalizing the 2×2 matrix for the nearest interacting level. This energy expressed below, is added to the Stark contribution from the remaining levels which are treated by the non degenerate formula.

$$E'_S(J,\tau,M_J) = (E_l + E_u)/2 \pm \sqrt{(E_l - E_u)^2/4 + \mu^2E^2(\gamma + \delta M_J^2)}$$

The plus or minus sign depends if the interacting level is the upper or the lower one.

Wastar calculates the Stark coefficients α_g, β_g, γ_g and δ_g for each dipole moment component along the principal axes and for each transition of the WANGLY transition file.

The hyperfine multiplet of the Stark structure is calculated in WASCAN in the following way:
Since the nuclear quadrupole coupling of the nitrogen atom is small, the Stark energies of glycine are expected to be much larger than the quadrupole coupling energies, and the approximation of the strong field case is used. Upon input of the nuclear quadrupole hyperfine constants χ_{aa} and χ_{bb}, and of the nuclear spin angular momentum I, the quadrupole perturbation energies are determined by:

$$E_{QS} = \langle J,\tau,M_J,I,M_I|\mathcal{H}_Q|J,\tau,M_J,I,M_I\rangle$$

$$E_{QS} = eQq_J \frac{[3M_J^2 - J(J+1)][3M_I^2 - I(I+1)]}{4J(2J+1)I(2I-1)}$$

with, as for the hyperfine multiplet of the line,

$$eQq_J = \frac{J}{2J+3}(D_1\chi_{aa} + D_2\chi_{bb}) \ .$$

The quadrupole-Stark transitions are formed according to the selection rules:

$$J = 0, \pm 1, \quad \Delta M_I = 0, \quad \Delta M_J = 0$$

In the case of the parallel plate spectrometer used in this experiment, where the microwave electric vector is parallel to the Stark field, the transition $\Delta M_J = \pm 1$ have not been observed.

APPENDIX 2

WAVEGUIDE BANDS

The nominal frequency range and internal dimensions of the rectangular waveguides used at Monash, are listed below.

Waveguide Designation	Nominal Frequency Range (GHz)	Internal Waveguide Dimensions (mm)	Cut-off frequency (GHz)
L	1.14 - 1.73	165.10 × 82.55	0.908
LS	1.72 - 2.61	109.22 × 54.61	1.372
S	2.60 - 3.95	72.14 × 34.04	2.078
G	3.94 - 5.99	47.55 × 22.149	3.152
J	5.38 - 9.18	34.85 × 15.799	4.301
X	8.20 - 12.5	22.860 × 10.160	6.557
P	11.9 - 18.0	15.799 × 7.899	9.486
K	17.6 - 26.7	10.668 × 4.318	14.047
R	26.4 - 40.1	7.112 × 3.556	21.081
F	39.3 - 59.7	4.775 × 2.388	31.357
V	49.9 - 75.8	3.759 × 1.880	39.863
E	60.5 - 92.0	3.099 × 1.549	48.350
N	92.3 - 140	2.032 × 1.016	73.6

APPENDIX 3

DATA ACQUISITION

Fig. 2.6 shows the block diagram of the computer interfaced spectrometer. The analog signal is digitized by a voltage to frequency converter and a counter. The analog input is first transformed into a pulse stream whose rate is proportional to the instantaneous input voltage. These pulses are then converted in a frequency divider to be acceptable by the counting register, and counted during a time interval determined by the sample control unit via the computer. The number of counts N is thus proportional to the integrated voltage input over the sampling period T:

$$N = k \int_{k=0}^{T} V \, dt$$

A voltage up to ± 0.5 V is transformed into a 12 bit data word, with an upper value of 2^{11}. The scaling factor k is determined by a spectroscopist control. One of the four remaining bits of the 16 bit Varian word is used as indicator of sweep direction via an interrupt sent by the sample control unit. In a later stage of the work, a second bit has been used as indicator of phase-lock stability via interrupt sent by the upper frequency phase-lock controller, and a third bit as indicator of heating cut-off via the heating controller.

The sampling rate is determined by the spectroscopist. A sample control unit recognizes the wanted digits on the frequency counter and sends interrupts to the computer via the bus line to initiate sampling procedures. Each channel point in the digitized spectrum thus represents a number of counts N registered during a sampling time T which corresponds to the frequency interval between two successive sampling digits of the counter. The sampling digits on the frequency counter have

to be chosen to adequately cater the expected width of the line, i.e. must satisfy the criteria that a line is observed if at least five points are distributed on its full contour. The scan speed of the function generator is then adjusted to satisfy a correct reading of the digits by the sample control unit.

The current scan and two averages, stored on disc, may be displayed on two 256 points traces of a visual display unit. The VDU push button allows erase of one average and smoothing action on the displayed spectrum.

The amplitude coordinate of a channel point is in fact a normalized value of N:

$$EIV_i = N_i/(T_i/T_1)$$

where i represents a channel with frequency interval ν, and with amplitude corresponding to the number of counts N_i, registered during the sampling time T_i. Since the frequency counter shows variable time intervals for equal frequency intervals, the sampling time of channel 1 is different: T_1. Unfortunately since T_1 is different from one scan to the next one, the amplitude points of different spectra are not normalized and it has not been possible to compare, with this method, the line intensities, observed for different vibrational states.

The signal averaging procedure, where the spectrum is scanned n times, stored and then averaged corresponds to an alternative smoothing procedure equivalent to the use of a filter circuit with high time constant τ and the signal-to-noise ratio is proportional to the square root of τ or n:

$$S/N \propto \sqrt{\tau} \quad \text{or} \quad S/N \propto \sqrt{n} \ .$$

APPENDIX 4

ELECTROFORMING PROCESS

Impurities content of the aluminium alloy.

The type 5083 available from ALCAN CLAYTON AUSTRALIA, is similar to the european AG 5 grade.

	AG 5		5083
Mg	4.5 - 5.8%	Mg	4.0 - 4.9%
Mn	.05 - .7%	Mn	.5 - .1%
Cr	.05 - .3%	Cr	.05 - .25%
Si	< .3%	Si	< .04%
Fe	< .4%	Fe	< .4%
Ti	< .1%	Ti	< .15%

The magnesium content of these alloys facilitates the polishing of the mandrel faces.

Mandrel

The mandrel has been cut in the 5083 Al alloy, centered at one extremity on a supporting bar, polished, cleaned with trichloro--ethylene and a concentrated sulfo-nitric mixture. Before transfer in the electroforming bath the open ends are covered with silicon rubber to avoid copper deposit.

The electroforming bath

As recommended, the bath should have

a high conductivity,

a high concentration in copper ions,

a good stability and

a pH less than 1 or 2 in order to obtain a strong and uniform copper deposit.

The solution was made as follows:

deionized water	1000 cm^3
copper sulfate	250 g
sulfuric acid	35 g
gelatine	.002 g

APPENDIX 5

MOLECULAR LINE RADIOASTRONOMY

In this appendix are described some fundamental theoretical concepts which have been used in the development of the work. A full treatment of the subject can be found elsewhere [1].

The observed antenna temperature of a molecular line is proportional to the column density of molecules along the line of sight of the source:

$$N_l = \frac{4\pi^{3/2}}{(\ln 2)^{1/2}} \frac{k\nu}{hc^2} \frac{g_l}{g_u} \frac{1}{A_{ul}} \int T_B \, d\nu$$

where N_l is the column density of molecules in the lower state of the transition,

A_{ul} is the Einstein A-coefficient for emission as given in the appendix 6 and

T_B is the brightness temperature, $T_B = (\theta_A/\theta_S)^2 T_A$,

where θ_A and θ_S are the angular diameters of the beam and the source respectively,

and T_A is the antenna temperature of the line.

If the levels of the molecule are in thermal equilibrium, then the total column density is obtained from:

$$N_T = N_l \, Q_r \frac{1}{g_l} \exp\left(\frac{E_l}{kT}\right) .$$

where Q_r is the rotational partition function (appendix 1).

The numerical expression is:

$$N_l = 619.0948841 \; \nu \; \Delta\nu \; T_B \frac{g_l}{g_u} \frac{1}{A_{ul}} \; cm^{-2}$$

with ν, $\Delta\nu$ in MHz, T_B in K and A_{ul} in s^{-1}.

The column density of molecules in the upper state can also be calculated:

$$N_u = 2.068804 \times 10^{-3} \frac{\nu^2}{A_{ul}} \frac{T_{ex}}{T_{ex} - T_c} T_A \Delta V \ cm^{-2}$$

with ν in MHz, ΔV in km s^{-1}, T_A in K and A_{ul} in s^{-1}.

In the last case, the total column density is expressed by:

$$N_T = N_u Q_r \frac{1}{g_u} \exp\left(\frac{E_u}{kT}\right) .$$

The Einstein A-coefficient is expressed as a function of the dipole moment matrix elements of the transition. In the case of a symmetric top molecule in emission from an upper level (J,K) to a lower level (J-1,K), these matrix elements are formulated as [2]:

$$|\mu_{lu}|^2 = \sum_{F,M'} |\langle J-1,K,M'|\mu_F|J,K,M\rangle|^2 = \mu^2 \frac{J^2 - K^2}{J(2J+1)}$$

This expression has been used in the evaluation of the Einstein A-coefficient of methyl cyanide.

In the case of an asymmetric top, these matrix elements are expressed as a function of the line strength (appendix 6).

APPENDIX 6

EINSTEIN COEFFICIENTS OF EMISSION AND ABSORPTION

	Formulation, in (S.I.) units, of the Einstein coefficients when the photon intensity per unit solid angle is expressed as the:			
	energy density per unit angular frequency ($\rho(\omega) = I(\omega)/c$, $J.m^{-3}.s$)	energy density per unit frequency ($\rho(\nu) = I(\nu)/c$, $J.m^{-3}.s$)	specific intensity per unit angular frequency ($I(\omega)$, $J.m^{-2}$)	specific intensity per unit frequency ($I(\nu)$, $J.m^{-2}$)
$B_{u\leftarrow 1}$	$\frac{16\pi^4}{3h^2}\frac{1}{4\pi\epsilon_0}\lvert\mu_{u1}\rvert^2$	$\frac{8\pi^3}{3h^2}\frac{1}{4\pi\epsilon_0}\lvert\mu_{u1}\rvert^2$	$\frac{16\pi^4}{3h^2c}\frac{1}{4\pi\epsilon_0}\lvert\mu_{u1}\rvert^2$	$\frac{8\pi^3}{3h^2c}\frac{1}{4\pi\epsilon_0}\lvert\mu_{u1}\rvert^2$
$B_{u\rightarrow 1}$	$\frac{16\pi^4}{3h^2}\frac{1}{4\pi\epsilon_0}\lvert\mu_{1u}\rvert^2$	$\frac{8\pi^3}{3h^2}\frac{1}{4\pi\epsilon_0}\lvert\mu_{1u}\rvert^2$	$\frac{16\pi^4}{3h^2c}\frac{1}{4\pi\epsilon_0}\lvert\mu_{1u}\rvert^2$	$\frac{8\pi^3}{3h^2c}\frac{1}{4\pi\epsilon_0}\lvert\mu_{1u}\rvert^2$
$A_{u\rightarrow 1}$	$\frac{8\pi\omega^3}{3hc^3}\frac{1}{4\pi\epsilon_0}\lvert\mu_{1u}\rvert^2$	$\frac{64\pi^4\nu^3}{3hc^3}\frac{1}{4\pi\epsilon_0}\lvert\mu_{1u}\rvert^2$	$\frac{8\pi\omega^3}{3hc^3}\frac{1}{4\pi\epsilon_0}\lvert\mu_{1u}\rvert^2$	$\frac{64\pi^4\nu^3}{3hc^3}\frac{1}{4\pi\epsilon_0}\lvert\mu_{1u}\rvert^2$
relations	$A_{u\rightarrow 1} = \frac{\hbar\omega^3}{2\pi^3c^3}B_{u\rightarrow 1}$	$A_{u\rightarrow 1} = \frac{8\pi h\nu^3}{c^3}B_{u\rightarrow 1}$	$A_{u\rightarrow 1} = \frac{\hbar\omega^3}{2\pi^3c^2}B_{u\rightarrow 1}$	$A_{u\rightarrow 1} = \frac{8\pi h\nu^3}{c^2}B_{u\rightarrow 1}$

When the states (u) and (1) are degenerate, the dipole moment matrix elements are expressed as a function of the line strength and of the degeneracy of the initial state:

$$\lvert\mu_{u1}\rvert^2 = \frac{\mu^2 S}{g_1} \quad \text{and} \quad \lvert\mu_{1u}\rvert^2 = \frac{\mu^2 S}{g_u} .$$

The relations between the coefficients become:

$$A_{u\rightarrow 1} = k\,B_{u\rightarrow 1},\ g_u B_{u\rightarrow 1} = g_1 B_{u\leftarrow 1} \quad \text{and} \quad A_{u\rightarrow 1} = k\frac{g_1}{g_u}B_{u\leftarrow 1} \qquad \text{(S.I.) (C.G.S.).}$$

APPENDIX 7

COMPUTER SOFTWARE LISTINGS

WASCAN

SFIT

```
      TITLE WANGSCAN
C       SCANS TRANSITION FILE ON TAPE PREPARED BY 'WANGLY' SUITE
C       AND COMPUTES STARK-MODULATED HYPERFINE MULTIPLET LINE
C       SHAPES FOR A GIVEN SINGLE COMPONENT LINEWIDTH.
C       THE QUADRUPOLE HYPERFINE STRUCTURE OF THE STARK COMPONENTS
C       IS CALCULATED IN THE STRONG FIELD CASE APPROXIMATION .

C       ORIGINAL VERSION WRITTEN BY P.D.GODFREY AND M.P.BASSEZ
C       ON 05/1977,      MODIFIED FOR CORRECT STARK HYPERFINE
C       STRUCTURE,BY M.P.BASSEZ ON 23/11/1979

        REAL LORENZ
        COMMON/S/LUN
        COMMON IFIL(212),IU
        DOUBLE PRECISION B(6),BI(3),DMU(3),FMIN1,FMAX1,FMIN,FMAX
       *,ABSMIN,TEMP,DDUMY,FREQ,STR,ENLO,ENL1,ENL2,ENR1,ENR2
        DIMENSION TEXT(20),RMU(3),IAXSYM(3),ALPHA(3),BETA(3),JD1(8)
       *,JD2(8),DUMMY(4),VFREQ(10),IVDEG(10)
       *,COMPON(200,2),HYPCOM(16,2),STARCM(20,2),PROFIL(514)
       *,LINE(64),IP(2),EQS1(30,36),EQS2(30,36)
        DIMENSION COVAR(6,6),FDERIV(6)
C       DIMENSION IFCB(13)
        INTEGER TAP,ANS4
        DATA IAXSYM(1),IAXSYM(2),IAXSYM(3)/2H A,2H B,2H C/
C       DATA IFCB(3),IFCB(8),IFCB(9),IFCB(10)/0,2HWS,2H  ,2H  /
        DATA IYES/2HYE/
        DATA (IP(I),I=1,2)/1H7,1H9/
        EQS(D1,D2,CA,CB,MJ,J,S,RMI)=(D1*CA+D2*CB)*(3.*(FLOAT(MJ)
       *-1.)**2.-FLOAT(J)*(FLOAT(J)+1.))*(3.*RMI**2.-S*(S+1.))/(4.*
       *FLOAT(J)*(2.*FLOAT(J)-1.)*S*(2.*S-1.))
        LUN=IU
        KB=IU
C       CALL V$OPEN(8,8,IFCB,0)
C       CALL V$OPEN(8,8,IFCB,0)
        WRITE(LUN,7463)
 7463 FORMAT(1X,'IS YOUR TAPE 7 TR OR 9 TR?
       *',/,1X,'ANSWER 7 OR 9')
        READ(LUN,1010)ANS4
 1010 FORMAT(A1)
        IF(ANS4.EQ.IP(1))TAP=14
        IF(ANS4.EQ.IP(2))TAP=19
        NFOUND=0
        READ(TAP)(TEXT(I),I=1,20)
        READ(TAP)NTRANS,JMIN,JMAX,I1,I2,I3,I4,(B(I),I=1,6)
       *,TEMP,(DMU(I),I=1,3),FMIN,FMAX,ABSMIN
  900 FORMAT(1X,'WASCAN V1 OUTPUT',10X,4A2,/
       *,1X,'WANGLY CALCULATION DONE ON',5X,3A2,'/',1A2,/
       *,1X,'WASCAN VERSION WRITTEN ON    23/11/79'//
       *,1X,'STARK-MODULATED LINE SHAPE AND INTENSITY CALCULATION',//
       *,1X,'THIS RUN IS FOR ',//,1X,20A4,//)
        CALL DATE(I5,I6,I7,I8)
        WRITE(LUN,900)I5,I6,I7,I8,I2,I3,I1,I4,(TEXT(I),I=1,20)
      1 WRITE(LUN,901)
  901 FORMAT(1X,'JMIN,JMAX = ')
        READ(LUN,902)JMIN1,JMAX1
  902 FORMAT(2I3)
        JMX=JMAX-1
        IF(JMIN1.GE.JMIN.AND.JMAX1.LE.JMX)GO TO 2
        WRITE(LUN,913)JMIN,JMX
  913 FORMAT(1X,'RANGE EXCEEDS LIMITS ON FILE: ',I5,' TO ',
       *I5)
        GO TO 1
    2 CONTINUE
    4 WRITE(LUN,910)
  910 FORMAT(1X,'FREQUENCY REGION OF INTEREST: FMIN,FMAX = ')
        READ(LUN,911)FMIN1,FMAX1
  911 FORMAT(2D15.3)
        IF(FMIN1.GE.FMIN.AND.FMAX1.LE.FMAX)GO TO 5
        WRITE(LUN,912)FMIN,FMAX
  912 FORMAT(1X,'RANGE EXCEEDS LIMITS USED IN FORMING FILE',
       *1X,': ',1F15.3,' TO ',1F15.3)
        GO TO 4
    5 CONTINUE
        WRITE(LUN,903)
  903 FORMAT(1X,'SPECTROMETER SENSITIVITY LIMIT',1X
       *,/,1X,'I.E. MINIMUM DETECTABLE PEAK ABSORPTION COEFFI',
       *'CIENT = ')
        READ(LUN,904)ABSMN
  904 FORMAT(6E12.6)
  225 WRITE(LUN,905)
  905 FORMAT(1X,'DIPOLE MOMENT COMPONENTS,MU(A),MU(B),MU(C) =')
        READ(LUN,906)(RMU(I),I=1,3)
        DO 3 I=1,3
        IF(DMU(I).EQ.0.0D00.AND.RMU(I).NE.0.0)GO TO 6
    3 CONTINUE
        GO TO 7
    6 WRITE(LUN,919)IAXSYM(I)
  919 FORMAT(1X,'WARNING! THE ',1A2,'-AXIS DIPOLE MOMENT',/,
       *' WAS ASSUMED TO BE EQUAL TO ZERO BY SYMMETRY WHEN',/,
       *' THIS TRANSITION TAPE FILE WAS CALCULATED, SO NO TRANSITIONS',
       */,1X,'OR STARK COEFFICIENTS OF THIS TYPE APPEAR.')
        GO TO 225
    7 CONTINUE
  906 FORMAT(6F12.6)
        WRITE(LUN,907)
  907 FORMAT(1X,'NUCLEAR SPIN, CHIAA, CHIBB = ')
        READ(LUN,906)SPIN,CHIAA,CHIBB
        ISPIN=SPIN
        LM=JMAX1*(ISPIN+1)
        IF(LM.LT.36) GO TO 3003
        WRITE(KB,3004)
 3004 FORMAT(1X,'STIFF LUCK MATE,J IS TOO LARGE SO YOU ARE NOT'/
       *,1X,'GOING TO GET ANY STARK HYPERFINE   ')
 3003 WRITE(LUN,908)
  908 FORMAT(/,1X,'PRESSURE OR DOPPLER-BROADENED LINEWIDTH (FWHM) = ')
        READ(LUN,906)FWHM
```

```
      WRITE(LUN,915)
  915 FORMAT(1X,'SAMPLE TEMPERATURE = ')
      READ(LUN,906)TEMP1
      WRITE(LUN,916)
  916 FORMAT(1X,'FREQUENCY (CM-1), IDEGENERACY;',/
     *,1X,'FOR ANY LOW FREQUENCY VIBRATIONS:',/
     *,1X,'SIGNIFY END OF LIST WITH A BLANK RECORD.')
      I=0
   33 I=I+1
      READ(LUN,917)VFREQ(I),IVDEG(I)
      IF(VFREQ(I).GT.0.0)GO TO 33
      NMODES=I-1
      WRITE(LUN,918)
  917 FORMAT(1F8.2,1I1)
  918 FORMAT(1X,'MOLE FRACTION OF COMPOUND OF INTEREST IN SAMPLE = ')
      READ(LUN,906)FMOLE
      WRITE(LUN,909)
  909 FORMAT(1X,'STARK VOLTAGE, ELECTRODE SPACING (CM) = ')
      READ(LUN,906)VOLTS,SPACE
      IFREQL=0
      WRITE(LUN,747)
  747 FORMAT(1X,'DO YOU WISH TO SET YOUR OWN FREQUENCY'
     *,/,1X,'RANGE FOR THE WASCAN OUTPUT',
     */,1X,'IF YOUR ANSWER IS "NO" ,THE FREQUENCYLIMITS WILL BE',
     */,1X,'SET AUTOMATICALLY TO INCLUDE ALL STARK LOBES',)
      READ(LUN,9941)IANSS
      IF(IANSS.NE.IYES)GO TO 746
      IFREQL=1
      WRITE(LUN,745)
  745 FORMAT(1X,'LOWER RANGE LIMIT,UPPER RANGE LIMIT = ',/,
     *1X,'NOTE :LOWER LIMIT MUST BE +VE',
     */,7X,'UPPER LIMIT MUST BE -VE',)
      READ(LUN,744)FLOW,FHIGH
  744 FORMAT(2F10.3)
  746 CONTINUE
      WRITE(LUN,940)
  940 FORMAT(1X,'DO YOU WISH TO READ IN THE COVARIANCE MATRIX',
     */,1X,'FOR THE ROTATIONAL CONSTANTS AND THE C.D. CONSTANTS',
     */,1X,'OF THE SYMMETRIC TOP TYPE; I.E. DJ, DJK, DK  ?',
     */,1X,'IF YOU ANSWER "YES", INPUT IS EXPECTED ON SIX CARDS,',
     */,1X,'AND ONLY THE LOWER HALF-TRIANGLE OF THE MATRIX IS NEEDED.')
      READ(LUN,9941)IANS
 9941 FORMAT(1A2)
      IF(IANS.EQ.IYES)READ(23,941)(((COVAR(I,J),J=1,6),I=1,6)
  941 FORMAT(5(6E13.6,/),6E13.6)
      IF(IANS.NE.IYES)GO TO 9876
      WRITE(LUN,942)
  942 FORMAT(1X,'MAXIMUM ACCEPTABLE 99% RANGE FOR SEARCHING',/
     *,1X,' I.E. + OR - 2.55 STD. DEVIATIONS (MHZ) =')
      READ(LUN,941)SRANGE
      DO 3142 I=1,6
      DO 3142 J=1,I
      COVAR(J,I)=COVAR(I,J)
 3142 CONTINUE
C      REFLECT COVARIANCE MATRIX ABOUT DIAGONAL
 9876 CONTINUE
      VPARTF=1.0
      IF(NMODES.LT.1)GO TO 31
      DO 30 I=1,NMODES
      VPARTF=VPARTF*(1.0-EXP(-VFREQ(I)/(0.695*TEMP1)))**IVDEG(I)
   30 CONTINUE
      VPARTF=1.0/VPARTF
   31 CONTINUE
      WRITE(22,900)I5,I6,I7,I8,I2,I3,I1,I4,(TEXT(I),I=1,20)
      WRITE(22,914)(B(I),I=1,6),(RMU(I),I=1,3),JMIN1,JMAX1,FMIN1,FMAX1
     *,TEMP1,ABSMN
  914 FORMAT(1X,'A=',F12.4,' MHZ',7X,'B=',F12.4,' MHZ',7X,'C=',
     *F12.4,' MHZ',//,1X,'DJ=',F12.8,' MHZ',7X,'DJK=',F12.8,
     *' MHZ',7X,'DK=',F12.8,
     *' MHZ',//,1X,'U(A)=',F8.3,' D',10X,'U(B)=',F8.3,' D',
     *10X,'U(C)=',F8.3,' D',///,1X,'THIS CALCULATION FOR:',//,19X,
     *'J=',I3,'   TO   J=',I3,//,19X,'FREQUENCY RANGE=',F14.3,
     *' MHZ   TO',F14.3,' MHZ',//,19X,'TEMPERATURE=',F9.1,' K',
     *//,19X,'MINIMUM INTENSITY=',4X,1PE8.2,' (CM)-1',/)
      EFIELD=VOLTS/SPACE
      WRITE(22,920)SPIN,CHIAA,CHIBB,FWHM,VOLTS,SPACE,EFIELD
  920 FORMAT(//,1X,'NUCLEAR QUADRUPOLE COUPLING PARAMETERS:'/,5X
     *,'SPIN = ',1F5.1,5X,'CHI(AA) = ',F9.3,' IHZ',5X
     *,'CHI(BB) = ',1F9.3,' MHZ',//
     *,1X,'PRESSURE OR DOPPLER BROADENED LINE WIDTH = ',1F6.3
     *,  MHZ FWHM',//
     *,1X,'STARK-MODULATION: VOLTAGE = ',1F9.1,' VOLTS, ELECTRODE SPACIN
     *G',
     *1X,'=',1F8.4,'CM ',/,20X,'ELECTRIC FIELD = ',
     *1F9.2,' V/CM',//)
      WRITE(22,921)FMOLE
  921 FORMAT(//,1X,'MOLE FRACTION OF COMPOUND OF INTEREST IN SAMPLE = ',
     *1F8.5,//)
      IF(NMODES.LT.1)GO TO 200
      WRITE(22,9211)(VFREQ(I),IVDEG(I),I=1,NMODES)
 9211 FORMAT(1X,'LOWEST VIBRATIONAL FREQUENCIES AND DEGENERACIES:',
     */,10(1X,1F8.1,5X,1I2,/))
      WRITE(22,922)VPARTF
  922 FORMAT(//,1X,'VIBRATIONAL PARTITION FUNCTION = ',
     *1F10.2)
  200 CONTINUE
      ISTATO=0
      IF(IANS.NE.IYES)GO TO 9877
      WRITE(22,944)(((COVAR(I,J),J=1,6),I=1,6)
  944 FORMAT(//1X,'VARIANCE-COVARIANCE MATRIX FOR ROTATIONAL/',
     *1X,'CENTRIFUGAL DISTORTION CONSTANTS',
     */,1X,'IN THE ORDER: A, B, C, DJ, DJK, DK',/,6(
     */,6(5X,E12.6)))
      WRITE(22,952)SRANGE
  952 FORMAT(//,1X,'MAXIMUM ACCEPTABLE 99% CONFIDENCE RANGE = ',F9.2,
     *1X,'MHZ')
```

```
C     WRITE(22,932)
C     WRITE(22,932)
      CALL PUMPOF
 9877 CONTINUE
      DO 100 ITRANS=1,NTRANS
      READ(TAP)J1,KM1,KP1,J2,KM2,KP2,FREQ,STR,ENLO
     *,D1U,D2U,D1L,D2L,(ALPHA(I),BETA(I),I=1,3),IDEG,JDEG
     *,(JD1(I),I=1,6),ENL1,ENR1,DDUMY,(DUMMY(I),I=1,4)
     *,GAMMA1,DELTA1,(DUMMY(I),I=1,4),IDEG1,JDEG1
     *,(JD2(I),I=1,6),ENL2,ENR2,DDUMY,(DUMMY(I),I=1,4)
     *,GAMMA2,DELTA2,(DUMMY(I),I=1,4),IDEG2,JDEG2
      IF(ISTATO.EQ.0)GO TO 2005
      CALL TIME(MIN2,MILLI)
      IF(MIN2-MIN1.LT.2)GO TO 2005
      ISTATO=0
C     WRITE(22,932)
C     WRITE(22,932)
      CALL PUMPOF
 2005 CONTINUE
      IF(FREQ.GT.FMAX1)GO TO 100
      IF(FREQ.LT.FMIN1)GO TO 100
      IXY=MAXO(J1,J2)
      IXZ=MINO(J1,J2)
      IF(IXY.GT.JMAX1)GO TO 100
      IF(IXZ.LT.JMIN1)GO TO 100
      PU2=FLOAT(J1*(J1+1))
      PL2=FLOAT(J2*(J2+1))
      DEUDC=PU2*(1.-(D1U+D2U)*.5)/3.
      DEUDA=PU2*D1U*.5+DEUDC
      DEUDB=PU2-DEUDA-DEUDC
      DELDC=PL2*(1.-(D1L+D2L)*.5)/3.
      DELDA=PL2*D1L*.5+DELDC
      DELDB=PL2-DELDA-DELDC
      RKAPPA=(2.*B(2)-B(1)-B(3))/(B(1)-B(3))
      KUGOOD=KM1
      IF(RKAPPA.GT.0.)KUGOOD=KP1
      KLGOOD=KM2
      IF(RKAPPA.GT.0.)KLGOOD=KP2
      JJP1U=J1*(J1+1)
      JJP1L=J2*(J2+1)
      DUPDJ=-(FLOAT(JJP1U))**2
      DLODJ=-(FLOAT(JJP1L))**2
      DUPDJK=-FLOAT(JJP1U)*(FLOAT(KUGOOD))**2
      DLODJK=-FLOAT(JJP1L)*(FLOAT(KLGOOD))**2
      DUPDK=-(FLOAT(KUGOOD))**4
      DLODK=-(FLOAT(KLGOOD))**4
      DNUDA=DEUDA-DELDA
      DNUDB=DEUDB-DELDB
      DNUDC=DEUDC-DELDC
      IF(IANS.NE.IYES)GO TO 9878
      FDERIV(1)=DNUDA
      FDERIV(2)=DNUDB
      FDERIV(3)=DNUDC
      FDERIV(4)=DUPDJ-DLODJ
      FDERIV(5)=DUPDJK-DLODJK
      FDERIV(6)=DUPDK-DLODK
      VARNU=PROVAR(COVAR,FDERIV,6)
      RANG99=2.55*2.*SQRT(VARNU)
      IF(RANG99.GT.SRANGE)GO TO 100
 9878 CONTINUE
      IAX=MUTYPE(KM1,KP1,KM2,KP2)
      IF(RMU(IAX).EQ.0.0)GO TO 100
      GAMMAX=FGAMMA(B,RMU(IAX),STR,FREQ,ENLO,TEMP1)
      GAMMAX=GAMMAX*FMOLE/VPARTF
      IF(GAMMAX.LT.ABSMN)GO TO 100
      HYPCOM(1,1)=0.
      HYPCOM(1,2)=1.
      NHYPCM=1
      IF(SPIN.GT.0.5)CALL QUAD1(J1,D1U,D2U,J2,D1L,D2L
     *,CHIAA,CHIBB,HYPCOM,NHYPCM,SPIN)
C
C          NOW CALCULATE THE STARK SHIFT
X      DO 301 I=1,NHYPCM
X     WRITE(LUN,9301)HYPCOM(I,1),HYPCOM(I,2)
X 301 CONTINUE
X9301 FORMAT(1X,2F12.8)
X      WRITE(LUN,9302)
X9302 FORMAT(//)
      SCONST=.50348
      I=0
      RM=0.
      RMAX=AMINO(J1,J2)
  101 I=I+1
      SHIFT=0.
      DO 102 IAX=1,3
      SHIFT=SHIFT+((EFIELD*RMU(IAX)*SCONST)**2)*(ALPHA(IAX)
     *+BETA(IAX)*RM**2)
X     WRITE(LUN,9305)EFIELD,RMU(IAX),ALPHA(IAX),BETA(IAX),RM
X     *,SHIFT
X9305 FORMAT(1X,6E15.6)
  102 CONTINUE
      IF(IDEG.GT.0)SHIFT=SHIFT+DSHIFT(JD1,ENR1,ENL1,GAMMA1,DELTA1
     *,IDEG1,JDEG1,RMU,RM,SCONST,EFIELD)
      IF(IDEG.GT.1)SHIFT=SHIFT+DSHIFT(JD2,ENR2,ENL2,GAMMA2,DELTA2
     *,IDEG2,JDEG2,RMU,RM,SCONST,EFIELD)
X      WRITE(LUN,9305)GAMMA1,DELTA1,GAMMA2,DELTA2,SHIFT
X      WRITE(LUN,9306)ENR1,ENL1,ENR2,ENL2
X9306 FORMAT(1X,6D15.8)
      STARCM(I,1)=SHIFT
      STARCM(I,2)=RINTEN(J1,J2,RM)
      RM=RM+1.
      IF(RM.LE.RMAX)GO TO 101
      NSTACM=I
      SUM=0.0
      DO 103 I=1,NSTACM
      SUM=SUM+STARCM(I,2)
```

```
  103 CONTINUE
      DO 104 I=1,NSTACM
      STARCM(I,2)=STARCM(I,2)/SUM
  104 CONTINUE
X      DO 303 I=1,NSTACM
X      WRITE(LUN,9304)STARCM(I,1),STARCM(I,2)
X 303 CONTINUE
X      WRITE(LUN,9302)
      DO 105 I=1,NHYPCM
      COMPON(I,1)=HYPCOM(I,1)
      COMPON(I,2)=HYPCOM(I,2)
 105  CONTINUE
C        NOW CALCULATE THE QUADRUPOLE HYPERFINE STRUCTURE OF THE
C             STARK COMPONENTS
      IF(SPIN.NE.0.)GO TO 3010
 3005 K=NHYPCM
      DO 3006 I=1,NSTACM
      K=K+1
      COMPON(K,1)=STARCM(I,1)
      COMPON(K,2)=-STARCM(I,2)
 3006 CONTINUE
      GO TO 3011
 3010 IF(LM.GT.36)GO TO 3005
      N=0
      MJMX1=J1+1
      MJMX2=J2+1
      DO 20 MJ1=1,MJMX1
      RMI1=SPIN
   21 IRMI1=RMI1+1
      EQS1(MJ1,IRMI1)=EQS(D1U,D2U,CHIAA,CHIBB,MJ1,J1,SPIN,RMI1)
      RMI1=RMI1-1.
      IF (RMI1.GE.0.) GO TO 21
   20 CONTINUE
      DO 22 MJ2=1,MJMX2
      RMI2=SPIN
   23 IRMI2=RMI2+1
      EQS2(MJ2,IRMI2)=EQS(D1L,D2L,CHIAA,CHIBB,MJ2,J2,SPIN,RMI2)
      RMI2=RMI2-1.
      IF(RMI2.GE.0.) GO TO 23
   22 CONTINUE
      JF=0
      K=NHYPCM
      DO 24 MJ2=1,MJMX2
      MJ1=MJ2
      JF=JF+1
      STCM=STARCM(JF,1)
      STCM2=STARCM(JF,2)
      RMI1=SPIN
 3025 IRMI1=RMI1+1
      K=K+1
      COMPON(K,1)=EQS1(MJ1,IRMI1)-EQS2(MJ2,IRMI1)+STCM
      RMI1=RMI1-1.
      IF(RMI1.GE.0.)GO TO 3025
      IX=INT(SPIN+.5)
      Y=SPIN/FLOAT(IX)
      IF(Y.EQ.1.)GO TO 26
      COMPON(K,2)=-STCM2/FLOAT(IX)
   26 IF(RMI1.NE.0.)COMPON(K,2)=-STCM2/(SPIN+.5)
      IF(RMI1.EQ.0.) COMPON(K,2)=-STCM2/((SPIN+.5)*2.)
      CONTINUE
   24 CONTINUE
 3011 KMAX=K
      NCOMP=KMAX
      K=NHYPCM
      K=K+1
      SUM=0.0
      DO 27 J=K,NCOMP
      SUM=SUM+COMPON(J,2)
   27 CONTINUE
      DO 28 J =K,NCOMP
      COMPON(J,2)=-COMPON(J,2)/SUM
   28 CONTINUE
      FMN=100.
      FMX=-100.
      DO 108 I=1,NCOMP
      IF(COMPON(I,1).GT.FMX)FMX=COMPON(I,1)
      IF(COMPON(I,1).LT.FMN)FMN=COMPON(I,1)
  108 CONTINUE
X      WRITE(LUN,9304)NHYPCM,NSTACM,NCOMP
X9304 FORMAT(1X,5I10,///)
X      DO 305 I=1,NCOMP
X      WRITE(LUN,9304)COMPON(I,1),COMPON(I,2)
X 305 CONTINUE
X      WRITE(LUN,9302)
      FSTART=FMN-3.0*FWHM
      FSTOP=FMX+3.0*FWHM
      IF(IFREQL.EQ.0)GO TO 742
      FSTART=FLOW
      FSTOP=FHIGH
  742 CONTINUE
      NPTS=512
      FINCR=(FSTOP-FSTART)/FLOAT(NPTS)
      SMIN=0.
      SMAX=0.
      DO 109 I=1,NPTS
      F=FSTART+FLOAT(I-1)*FINCR
      PROFIL(I)=0.
      DO 110 J=1,NCOMP
      PROFIL(I)=PROFIL(I)+COMPON(J,2)*LORENZ(COMPON(J,1),F,FWHM)
  110 CONTINUE
  109 CONTINUE
      PMIN=1.
      PMAX=-1.
      DO 111 I=1,NPTS
      IF(PROFIL(I).LT.PMIN)PMIN=PROFIL(I)
      IF(PROFIL(I).GT.PMAX)PMAX=PROFIL(I)
```

```
  111 CONTINUE
      PGAMMX=(PMAX-PMIN)*GAMMAX/2.
      IF(PGAMMX.LT.ABSMN)GO TO 100
      ISTATO=1
      CALL TIME(MIN1,MILLI)
C     WRITE(8)(TEXT(I),I=1,20),J1,KM1,KP1,J2,KP1,KP2
C     *,NPTS
C     *,FREQ,FSTART,FSTOP,CHIAA,CHIBB,(RMU(I),I=1,3),EFIELD
C     *,(B(I),I=1,6),FWHM,PGAMMX,PMAX,PMIN,IS,I6,I7,I8
C     *,TEMP1,SPIN,NMODES,(VFREQ(I),I=1,10),(IVDEG(I),I=1,10)
C     *,TEMP1,SPIN,NMODES,(VFREQ(I),I=1,10),(IVDEG(I),I=1,10)
C     *,FMOLE
C       WRITE(8)(PROFIL(I),I=1,NPTS)
      WRITE(22,930)IS,I6,I7,I8,(TEXT(I),I=1,20)
     *,J1,KM1,KP1,J2,KM2,KP2,PGAMMX,FREQ,FSTART,FSTOP
      WRITE(22,953)D1U,D2U,D1L,D2L
  953 FORMAT(2X,'D-PARAMETERS ',//,2X,'D1(UPPER) = ',F14.12,
     *5X,'D2(UPPER) = ',F14.12,10X,'D1(LOWER) = ',F14.12,
     *5X,'D2(LOWER) = ',F14.12,//)
      WRITE(22,946)DNUDA,DNUDB,DNUDC
  946 FORMAT(2X,'FREQUENCY DERIVATIVES',//,2X,'DF/DA = ',1F9.5,
     *5X,'DF/DB = ',1F9.5,5X,'DF/DC = ',1F9.5,//)
      IF(IANS.NE.IYES)GO TO 9879
      IF(VARNU.GE.0.)GO TO 9880
      WRITE(22,949)
  949 FORMAT(//2X,'DATA ERROR? CHECK VARIANCE-COVARIANCE MATRIX.',/
     *,2X,'THE VARIANCE FOR THIS TRANSITION APPEARS TO BE NEGATIVE!')
C     GO TO 9881
 9880 FMIN=FREQ-DBLE(RANG99/2.)
      FMAX=FREQ+DBLE(RANG99/2.)
      WRITE(22,947)RANG99,FMIN,FMAX
  947 FORMAT(2X,'99% PROBABILITY SEARCH RANGE = ',1F9.2,
     *//,5X,'SCAN FROM ',1F12.2,' TO ',1F12.2,' MHZ'/)
 9879 WRITE(22,950)
  950 FORMAT(///)
      NFOUND=NFOUND+1
      IFILL=ICHAR(255,255)
      IBLANK=ICHAR(160,160)
      NCOL2=64
      ILEFT=ICHAR(255,160)
      IRIGHT=ICHAR(160,255)
      DO 113 L=1,40
      DO 114 I=1,NCOL2
      LINE(I)=IBLANK
  114 CONTINUE
      PLIM=PMAX-((PMAX-PMIN)/40.)*FLOAT(L)
      DO 112 I=1,NCOL2
      KMIN=8*I-7
      KMAX=KMIN+3
      SUM2=0.0
      SUM=0.0
      DO 115 K=KMIN,KMAX
      SUM=SUM+PROFIL(K)
      SUM2=SUM2+PROFIL(K+4)
  115 CONTINUE
      SUM=SUM/4.
      SUM2=SUM2/4.
      IF(FWHM.GT.8.*FINCR)GO TO 116
      EXTREM=0.
      EXTRM2=0.
      DO 117 K=KMIN,KMAX
      IF(ABS(SUM-PROFIL(K)).GT.EXTREM)EXTREM=PROFIL(K)
      IF(ABS(SUM-PROFIL(K+4)).GT.EXTRM2)EXTRM2=PROFIL(K+4)
  117 CONTINUE
      SUM=EXTREM
      SUM2=EXTRM2
  116 IF(SUM.LE.PLIM.AND.SUM2.LE.PLIM)GO TO 2004
      IF(SUM.GT.PLIM.AND.SUM2.GT.PLIM)GO TO 2001
      IF(SUM.GT.PLIM.AND.SUM2.LE.PLIM)GO TO 2002
      IF(SUM.LE.PLIM.AND.SUM2.GT.PLIM)GO TO 2003
      GO TO 2004
 2001 LINE(I)=IFILL
      GO TO 2004
 2002 LINE(I)=ILEFT
      GO TO 2004
 2003 LINE(I)=IRIGHT
 2004 CONTINUE
  112 CONTINUE
      WRITE(22,931)(LINE(I),I=1,NCOL2)
  113 CONTINUE
      CALL PUMPOF
  930 FORMAT(1H1,2X,4A2,//,2X,20A4,//,2X,1I3,'(',1I3
     *,' , ',1I3,') -  ',1I3,'(',1I3,' , ',1I3,')',
     *10X,'OF AMPLITUDE ',1PE8.2
     *,' (CM)-1',//,10X,'CENTERED AT ',0P1F14.3,' MHZ',//
     *,10X,'AND PLOTTED FROM AN OFFSET OF ',1F8.3,'  TO  ',1F8.3
     *,' MHZ',//)
  931 FORMAT(1X,64A2)
  932 FORMAT(1H1)
  100 CONTINUE
C     WRITE(22,932)
C     WRITE(22,932)
      CALL PUMPOF
 9881 CONTINUE
      WRITE(24,933)NFOUND
  933 FORMAT(/,1X,'WANGSCAN: END OF SCAN',/,1X,1I5,2X,'DETECTABLE',
     *1X,'TRANSITIONS FOUND',//)
C     CALL V$CLOS(8,0)
      CALL EXIT
      END



      FUNCTION MUTYPE(KM1,KP1,KM2,KP2)
      COMMON/S/LUN
      I=MOD(KM1-KM2,2)
```

```
      J=MOD(KP1-KP2,2)
      IF(I.EQ.0)GO TO 1
      MUTYPE=3
      IF(J.NE.0)MUTYPE=2
      RETURN
    1 MUTYPE=1
      IF(J.NE.0)RETURN
      WRITE(LUN,900)KM1,KP1,KM2,KP2
      CALL EXIT
  900 FORMAT(1X,'FUNCTION MUTYPE IMPOSSIBLE TRANSITION:',2I5,5X,2I5,/)
      END



      SUBROUTINE QUAD1(J3,D1U,D2U,J2,D1L,D2L,CHIAA,CHIBB,HYPCOM,
     *NCOM,I)
      DIMENSION HYPCOM(16,2),QENER1(10),QENER2(10),A(10),B(10)
     *,TCOM(16,2)
      REAL I
      J1=J3
      FMAX1=I+FLOAT(J1)
      FMIN1=ABS(I-FLOAT(J1))
      IF(I.GT.FLOAT(J1)) R=2.*FLOAT(J1)+1.1
      IF(I.LE.FLOAT(J1)) R=2.*I+1.1
      N=IFIX(R)
      II=1
      A(II)=FMIN1
      DO 1 II=1,N
      IF(II.GT.1) A(II)=A(II-1)+1.
      F1=A(II)
      QENER1(II)=EQ(F1,I,J1,D1U,CHIAA,D2U,CHIBB)
    1 CONTINUE
      FMIN2=ABS(I-FLOAT(J2))
      FMAX2=I+FLOAT(J2)
      IF(I.GT.FLOAT(J2)) P=2.*FLOAT(J2)+1.1
      IF(I.LE.FLOAT(J2)) P=2.*I+1.1
      M=IFIX(P)
      II=1
      B(II)=FMIN2
      DO 2 II=1,M
      IF(II.GT.1) B(II)=B(II-1)+1.
      F2=B(II)
      QENER2(II)=EQ(F2,I,J2,D1L,CHIAA,D2L,CHIBB)
    2 CONTINUE
      NCOM=0
      SUM=0.
      L=1
      LL=1
      B(LL)=FMIN2
      DO 3 LL=1,M
      A(L)=FMIN1
      IF(LL.GT.1) B(LL)=B(LL-1)+1.
      DO 4 L=1,N
      IF(L.GT.1) A(L)=A(L-1)+1.
      IF(ABS(A(L)-B(LL)).GT.1.1) GO TO 4
      NCOM=NCOM+1
      HYPCOM(NCOM,1)=QENER1(L)-QENER2(LL)
      IF(J3.EQ.J2) GO TO 5
      IF(J3.LT.J2) GO TO 20
      F1=A(L)
      F2=B(LL)
      IF(F1.GT.F2) GO TO 7
      IF(F1.EQ.F2) GO TO 8
   21 TCOM(NCOM,2)=(FLOAT(J1)-F1+I)*(FLOAT(J1)-F1+I-1.)*(FLOAT(J1)
     *-F1-I-1.)*(FLOAT(J1)-F1-I-2.)/(F1+1.)
      GO TO 40
    7 TCOM(NCOM,2)=(FLOAT(J1)+F1+I+1.)*(FLOAT(J1)+F1+I)*(FLOAT(J1)
     *+F1-I)*(FLOAT(J1)+F1-I-1.)/F1
      GO TO 40
    8 TCOM(NCOM,2)=-(FLOAT(J1)+F1+I+1.)*(FLOAT(J1)+F1-I)*(FLOAT(J1)
     *-F1+1.)*(FLOAT(J1)-F1-I-1.)*(2.*F1+1.)/(F1*(F1+1.))
      GO TO 40
   20 J1=J3+1
      F1=B(LL)
      F2=A(L)
      IF(F1.EQ.F2) GO TO 8
      IF(F1.LT.F2) GO TO 21
      IF(F1.GT.F2) GO TO 7
    5 F1=A(L)
      F2=B(LL)
      IF(F1.GT.F2) GO TO 9
      IF(F1.EQ.0..AND.F2.EQ.0.) GO TO 11
      IF(F1.EQ.F2) GO TO 10
      TCOM(NCOM,2)=-(FLOAT(J1)+F1+I+2.)*(FLOAT(J1)+F1-I+1.)*(FLOAT(J1)
     *-F1+I)*(FLOAT(J1)-F1-I-1.)/(F1+1.)
      GO TO 40
    9 TCOM(NCOM,2)=-(FLOAT(J1)+F1+I+1.)*(FLOAT(J1)+F1-I)*(FLOAT(J1
     *)-F1+I+1.)*(FLOAT(J1)-F1-I)/F1
      GO TO 40
   10 TCOM(NCOM,2)=((FLOAT(J1)*(FLOAT(J1)+1.)+F1*(F1+1.)
     *-I*(I+1.))**2.)*(2.*F1+1.)/(F1*(F1+1.))
      GO TO 40
   11 TCOM(NCOM,2)=0.
   40 SUM=SUM+TCOM(NCOM,2)
    4 CONTINUE
    3 CONTINUE
      DO 15 L=1,NCOM
      HYPCOM(L,2)=TCOM(L,2)/SUM
   15 CONTINUE
      RETURN
      END



      FUNCTION CAS(F,I,J)
      REAL I
```

```
      CAS=F*(F+1.)-I*(I+1.)-FLOAT(J)*(FLOAT(J)+1.)
      RETURN
      END



      FUNCTION FCAS(F,I,J)
      REAL I
      FCAS=((3./4.)*CAS(F,I,J)*(CAS(F,I,J)+1.)-I*(I+1.)*FLOAT(J)*(FLOAT(
     *J)+1.))/(2.*I*(2.*I-1.)*(2.*FLOAT(J)-1.)*(2.*FLOAT(J)+3.))
      RETURN
      END



      FUNCTION EQ(F,I,J,D1,CHIAA,D2,CHIBB)
      REAL I
      EQ=(D1*CHIAA+D2*CHIBB)*FCAS(F,I,J)
      RETURN
      END



      FUNCTION FGAMMA(B,DIP,S,F,E,T)
      DOUBLE PRECISION B(6),S,F,E
      FGAMMA=2.46E-20*SNGL(DSQRT(B(1)*B(2)*B(3)))
      F1=SNGL(F)
      E1=SNGL(E)
      FGAMMA=FGAMMA*EXP(-E1/(20836.*T))
      S1=SNGL(S)
      FGAMMA=FGAMMA*(DIP**2)*S1*(F1**2)/30.
      T1=T/300.0
      FGAMMA=FGAMMA/(T1**2.5)
      RETURN
      END



      FUNCTION DSHIFT(J,WU,WL,G,D,ID,JD,DIP,RM,SC,EF)
      DIMENSION J(6),DIP(3)
      DOUBLE PRECISION WU,WL
C      ID=1   MEANS DEGENERACY IS IN UPPER LEVEL OF TRANSITION
C      ID=-1                "          LOWER LEVEL      "
C
C      JD=1   MEANS THAT LEVEL IS UPPER OF DEGENERATE PAIR.
C      JD=-1             "         LOWER        "
C
      IAX=MUTYPE(J(2),J(3),J(5),J(6))
      PERT=(SC*DIP(IAX)*EF)
      WDIFF=-DABS(WL-WU)/2.0D00
      DSHIFT=WDIFF+SQRT((WDIFF**2)+(PERT**2)*(G+D*(RM**2)))
      DSHIFT=DSHIFT*FLOAT(JD)*FLOAT(ID)
      RETURN
      END



      FUNCTION RINTEN(J1,J2,RM)
      IF(J1-J2.NE.0)GO TO 2
      RINTEN=RM**2
      RETURN
    2 RINTEN=(AMAX0(J1,J2))**2-RM**2
      RETURN
      END



      REAL FUNCTION LORENZ(F0,F,W)
      LORENZ=1./(1.+4.*((F-F0)/W)**2)
      RETURN
      END



      FUNCTION ICHAR(I,J)
      A=I
      B=J
      AIJ=A*256.+B
      AIJ=-(65536.-AIJ)-0.2
      ICHAR=AIJ
      RETURN
      END



      SUBROUTINE TOPFRM
      RETURN
      END



      FUNCTION PROVAR(COV,DERIV,N)
C      CALCULATES VARIANCE OF A QUANTITY FROM THE COVARIANCES
C      OF ITS PARAMETERS AND THE DERIVATIVES WITH RESPECT
C      TO ITS PARAMETERS.
      DIMENSION DERIV(N),COV(N,N)
      PROVAR=0.0
      DO 1 I=1,N
      K=I+1
      PROVAR=PROVAR+COV(I,I)*DERIV(I)**2
      DO 1 J=K,N
      PROVAR=PROVAR+2.*DERIV(I)*DERIV(J)*COV(I,J)
    1 CONTINUE
      RETURN
      END
```

```
C   "STARFIT" CONTROL ROUTINE

C            THIS PROGRAM CALCULATES THE STARK AND HYPERFINE
C     SPECTRUM,OF TRANSITIONS WITH J LESS THAN 30 FOR
C     MOLECULES,WITH ONE NUCLEAR SPIN INTERACTION.
C     THE HYPERFINE STRUCTURE OF THE STARK COMPONENTS IS
C     APPROXIMATED IN THE STRONG FIELD CASE.
C     THE QUAD ANALOG UNIT ALLOWS VARIATIONS OF THE THREE
C     DIPOLE MOMENT COMPONENTS AND OF THE APPLIED STARK VOLTAGE.
C     THE CALCULATED AND EXPERIMENTAL SPECTRA ARE
C     DISPLAYED ON A SCREEN.THEY CAN BE PLOTTED WITH HEADING.
C     ADAPTED FROM Q2FIT.
C     WRITTEN BY M.-P. BASSEZ ON 29/12/1978.


C     INSTRUCTIONS
C     ============
C     *A    THE PARAMETERS OF A NOMINATED TRANSITION ARE READ
C           EITHER FROM TAPE OR FROM DISC.A FIRST STARK STRUCTURE
C           IS CALCULATED.
C     *B    THE EXPERIMENTAL AND CALCULATED SPECTRA ARE DISPLAYED.
C           ADJUSTMENT OF THE LINE PARAMETERS (FREQUENCY,FWHH,
C           BASE,SCALE FACTOR)CAN BE ACHIEVED BY CHANGING
C           THE POSITION OF THE ANALOG UNIT KNOBS UNTIL
C           SUPERPOSITION OF THE MAIN LINE OF EACH SPECTRUM.
C     *C    ADJUSTMENT OF THE VALUES OF THE DIPOLE MOMENT
C           COMPONENTS AND OF THE STARK VOLTAGE CAN BE
C           ACHIEVED BY CHANGING THE POSITION OF THE
C           KNOBS UNTIL SUPERPOSITION OF THE CALCULATED
C           AND EXPERIMENTAL STARK MULTIPLETS.
C     *D    THE  CALCULATED AND EXPERIMENTAL SPECTRA
C           ARE PLOTTED.
C     *E    THE PROGRAM ENDS.
C     *F    THE EXPERIMENTAL DATA ARE READ FROM DISC.
C     *G    NOMINATED CHANNELS ARE DELETED.
C     *H    THE EXPERIMENTAL SPECTRUM IS DISPAYED AND A HEADING
C           CAN BE ADDED.
C     *I    THE SCREEN PARAMETERS ARE CHANGED.



      COMMON /TEX/ITEXAS(16)
      COMMON/KEYB/KB
      COMMON IFIL(242),IU
      COMMON/QRED/IGO,IDSPLY,IAUTO,ICALL,OFMIN,OFMAX,IRCHAN,ILCHAN,
     *OSPEC(1000),IANS,
     *NCHAN,FWHH,RFREQ,OMAX,OMIN,BASE,SCALER,ID(4),ICHAR(16)
     *,NSTICK,NCOMP,ZMU
      COMMON/Q1/VOLTS,ISTOP,IA,COMPON(200,2),CC(4),DC(4)
     *,SPACE,RMUQ(3)
      COMMON/Q/SPIN,CHIAA,CHIBB,D1U,D2U,D1L,D2L,TEMP1,FMOLE,J1,KM1,KP1,
     *J2,KM2,KP2,IDEG,JDEG,IDEG1,JDEG1,JDEG2,IDEG2
      COMMON/SCREEN/IOUT
      COMMON/ZOO/B,BI,DMU,FMIN1,FMAX1,FMIN,FMAX
     *,ABSMIN,TEMP,DDUMY,FREQ,STR,ENLO,ENL1,ENL2,ENR1,ENR2,
     *TEXT,RMU,IAXSYM,ALPHA,BETA,JD1,GAMMA1,DELTA1,GAMMA2,DELTA2,
     *JD2,DUMMY,VFREQ,IVDEG,PROFIL,LINE
      DIMENSION IOUT(256)
      DOUBLE PRECISION OFMIN,OFMAX,RFREQ
      DIMENSION TEXT(20),RMU(3),IAXSYM(3),ALPHA(3),BETA(3),JD1(6),
     *JD2(6),DUMMY(4),VFREQ(10),IVDEG(10),
     *HYPCOM(16,2),STARCM(20,2),PROFIL(514),LINE(64),
     *IFCB(13),ZMU(4)
      REAL LORENZ
      DOUBLE PRECISION B(6),BI(3),DMU(3),FMIN1,FMAX1,FMIN,FMAX,
     *ABSMIN,TEMP,DDUMY,FREQ,STR,ENLO,ENL1,ENL2,ENR1,ENR2

C*********************************************************************

C     THIS IS THE DIMENSIONS AND INSTRUCTIONS BLOCK TO BE CHANGED IF
C     THE INSTRUCTION SET IS TO BE EXTENDED.................

      DIMENSION ITEXT(9)
      DATA (ITEXT(I),I=1,9)/2H*A,2H*B,2H*C,2H*D,2H*E,2H*F,2H*G,2H*H,2H*I
     */
      KB=IU
      NSTRN=9


C*********************************************************************


      ID(1)=20
      ID(2)=253
      ID(3)=216
      ID(4)=14
      SCALER=1.
      BASE=ID(4)
      WRITE(KB,103)
      READ(KB,104)IDSPLY
    1 CALL OVLAY(0,0,6HGETDAT)
      RFREQ=(OFMAX+OFMIN)/2.00D+00
    2 WRITE(KB,100)
      READ(KB,101)INSTRN
      DO 3 IGO=1,NSTRN
      J=ITEXT(IGO)
      IF(INSTRN.EQ.J)GO TO 4
    3 CONTINUE
      WRITE(KB,102)
      GO TO 2
    4 GO TO (5,6,6,7,8,1,6,6,6),IGO
    5 CALL OVLAY(0,0,6HCSPECT)
      GO TO 2
```

```
      6     CALL OVLAY(0,0,6HRKNOBS)
            GO TO 10
        7   CALL OVLAY(0,0,6HPLOTTR)
            CONTINUE
            GO TO 2
     10     IF(ISTOP.NE.-1)GO TO 11
            CALL OVLAY(0,0,6HCSPECT)
            CALL OVLAY(0,0,6HRKNOBS)
            GO TO 10
     11     IA=0
            GO TO 2
      8     CALL EXIT
     100    FORMAT(1X,'?')
     101    FORMAT(A2)
     102    FORMAT(1X,'INVALID INSTRUCTION')
     103    FORMAT(1X,'DISPLAY NUMBER= ?')
     104    FORMAT(I1)
            END
```

```
C    "STARFIT"  GETDAT OVERLAY
      SUBROUTINE GETDAT
      COMMON/KEYB/KB
      COMMON/01/VOLTS,ISTOP,IA,COMPON(200,2),CC(4),DC(4)
     *,SPACE,RMUO(3)
      COMMON/QRED/IGO,IDSPLY,IAUTO,ICALL,OFMIN,OFMAX,IRCHAN,ILCHAN,
     *OSPEC(1000),IANS,
     *NCHAN,FWHH,RFREQ,OMAX,OMIN,BASE,SCALER,ID(4),ICHAR(16)
     *,NSTICK,NCOMP,ZMU
      COMMON/0/SPIN,CHIAA,CHIBB,D1U,D2U,D1L,D2L,TEMP1,FMOLE,J1,KM1,KP1,
     *J2,KM2,KP2,IDEG,JDEG,IDEG1,JDEG1,JDEG2,IDEG2
      COMMON/ZOO/B,BI,DMU,FMIN1,FMAX1,FMIN,FMAX
     *,ABSMIN,TEMP,DDUMY,FREQ,STR,ENLO,ENL1,ENL2,ENR1,ENR2,
     *TEXT,RMU,IAXSYM,ALPHA,BETA,JD1,GAMMA1,DELTA1,GAMMA2,DELTA2,
     *JD2,DUMMY,VFREQ,IVDEG,PROFIL,LINE
      DIMENSION TEXT(20),RMU(3),IAXSYM(3),ALPHA(3),BETA(3),JD1(6),
     *JD2(6),DUMMY(4),VFREQ(10),IVDEG(10),
     *HYPCOM(16,2),STARCM(20,2),PROFIL(514),LINE(64),
     *IFCB(13),ZMU(4)
      REAL LORENZ
      DOUBLE PRECISION B(6),BI(3),DMU(3),FMIN1,FMAX1,FMIN,FMAX,
     *ABSMIN,TEMP,DDUMY,FREQ,STR,ENLO,ENL1,ENL2,ENR1,ENR2
      DOUBLE PRECISION OFMIN,OFMAX,RFREQ
      DIMENSION ICAT(3),IRED(3),IOBS(13),ITEXT(40)
      DATA IOBS(3),ICAT(1),ICAT(2),ICAT(3),IRED(1),IRED(2),IRED(3)
     */2H C,2HCA,2HTO,2HOO,2HRE,2HDB,2HUF/
      DATA IFILE,IMA,ISA,IPA/1HR,2HMA,2HSA,2HPA/
      IOBS(8)=ICAT(1)
      IOBS(9)=ICAT(2)
      IOBS(10)=ICAT(3)
      WRITE(KB,100)
      READ(KB,101)ISPECT
      IF(ISPECT.NE.IFILE)GO TO 102
      IOBS(8)=IRED(1)
      IOBS(9)=IRED(2)
      IOBS(10)=IRED(3)
      GO TO 103
  102 DO 104 I=13,16
  104 CALL BITSET(I,0,ISPECT)
      ISPECT=ISPECT/256
      IOBS(10)=IOBS(10)+ISPECT
  103 CALL V$OPEN(16,16,IOBS,0)
      ILCHAN=1
      READ(16)(ITEXT(I),I=1,40),(IDUM,I=1,54),NCHAN,
     *(IDUM,I=1,2),INTERP,(IDUM,I=1,12),OFMIN,OFMAX
      WRITE(KB,113)(ITEXT(I),I=1,40)
      ICHAN=NCHAN*(INTERP+1)-INTERP
      IF(NCHAN.EQ.1)ICHAN=INTERP
      NCHAN=ICHAN
      WRITE(KB,999)NCHAN,OFMIN,OFMAX
  999 FORMAT(1X,'NCHAN = ',I4,4X,'OFMIN = ',F10.3,4X,'OFMAX = ',F10.3)
      IF(ISPECT)108,105,105
  105 WRITE(KB,106)
      READ(KB,107)ISPECT
      IF(ISPECT.EQ.IMA)GO TO 112
      IF(ISPECT.EQ.ISA)GO TO 111
      IF(ISPECT.EQ.IPA)GO TO 110
      WRITE(KB,109)
      GO TO 105
  110 IOBS(4)=IOBS(4)+18
  111 IOBS(4)=IOBS(4)+18
  112 IOBS(4)=IOBS(4)+8
  108 IOBS(4)=IOBS(4)+1
      READ(16)(OSPEC(I),I=1,NCHAN)
      IRCHAN=NCHAN
      CALL V$CLOS(16,0)
      RETURN
  100 FORMAT(1X,'NOMINATE SPECTROMETER BY  CATN  OR  CATRED')
  101 FORMAT(3X,A1)
  106 FORMAT(1X,'MA  ,PA  ,OR  SA ?')
  107 FORMAT(A2)
  109 FORMAT(1X,'INVALID INSTRUCTION')
  113 FORMAT(1X,'DATA FROM DISC IS',5X,20A2,/,23X,20A2)
      END
```

```
C      "STARFIT"  OVERLAY CSPECT
       SUBROUTINE CSPECT
       COMMON/KEYB/KB
       COMMON/ORED/IGO,IDSPLY,IAUTO,ICALL,OFMIN,OFMAX,IRCHAN,ILCHAN,
      *OSPEC(1000),IANS,
      *NCHAN,FWHH,RFREQ,OMAX,OMIN,BASE,SCALER,ID(4),ICHAR(16)
      *,NSTICK,NCOMP,ZMU
       COMMON/Q1/VOLTS,ISTOP,IA,COMPON(200,2),CC(4),DC(4)
      *,SPACE,RMUO(3)
       COMMON/Q/SPIN,CHIAA,CHIBB,D1U,D2U,D1L,D2L,TEMP1,FMOLE,J1,KM1,KP1,
      *J2,KM2,KP2,IDEG,JDEG,IDEG1,JDEG1,JDEG2,IDEG2
       DIMENSION ZMU(4),EQS1(30,36),EQS2(30,36)
       DIMENSION NAME32(13)
       COMMON/ZOO/B,BI,DMU,FMIN1,FMAX1,FMIN,FMAX
      *,ABSMIN,TEMP,DDUMY,FREQ,STR,ENLO,ENL1,ENL2,ENR1,ENR2,
      *TEXT,RMU,IAXSYM,ALPHA,BETA,JD1,GAMMA1,DELTA1,GAMMA2,DELTA2,
      *JD2,DUMMY,VFREQ,IVDEG,PROFIL,LINE
       DIMENSION TEXT(20),RMU(3),IAXSYM(3),ALPHA(3),BETA(3),JD1(6),
      *JD2(6),DUMMY(4),VFREQ(10),IVDEG(10),
      *HYPCOM(16,2),STARCM(20,2),PROFIL(514),LINE(64),
      *IFCB(13),QENER1(10),QENER2(10),A(10),C(10),TCOM(16,2)
       DOUBLE PRECISION B(6),BI(3),DMU(3),FMIN1,FMAX1,FMIN,FMAX,
      *ABSMIN,TEMP,DDUMY,FREQ,STR,ENLO,ENL1,ENL2,ENR1,ENR2
       DOUBLE PRECISION OFMIN,OFMAX,RFREQ
       REAL LORENZ
       INTEGER YES
       DATA IYES,NO/1HY,1HN/
       DATA YES,NO/2HYE,2HNO/
       DATA (NAME32(I),I=8,10)/2HUI,2HY1,2H  /
       DATA NAME32(3)/2H  /
       EQS(D1,D2,CA,CB,MJ,J,S,RMI)=(D1*CA+D2*CB)*(3.*FLOAT(MJ)**2.
      *-FLOAT(J)*(FLOAT(J)+1.))*(3.*RMI**2.-S*(S+1.))/(4.*
      *FLOAT(J)*(2.*FLOAT(J)-1.)*S*(2.*S-1.))
       LUN=IU




       IF (IA.EQ.1) GO TO 6430
       CALL WORKSP(KB,IFCB,LUND)

C       DO 6420 I=1,13
C 6420 IFCB(I)=NAME32(I)
C       LUND=21
       WRITE(KB,6015)
 6015 FORMAT(1X,'MINIMUM VALUES OF DIPOLES MOMENTS:MUA,MUB,MUC =?')
       READ(KB,6016)(RMUO(I),I=1,3)
 6016 FORMAT(3F5.3)
       WRITE(KB,6017)
 6017 FORMAT(1X,'NUCLEAR SPIN,CHIAA,CHIBB =?')
       READ(KB,6018)SPIN,CHIAA,CHIBB
 6018 FORMAT(3F12.6)
       ISPIN=SPIN
       LM=JMAX1*(ISPIN+1)
       IF(LM.LT.36)GO TO 3003
       WRITE(KB,3004)
 3004 FORMAT(1X,'OH LA LA, J IS TOO LARGE ,YOU WILL NOT GET
      *ANY STARK HYPERFINE')
 3003 WRITE(KB,6019)
 6019 FORMAT(1X,'PRESSURE OR DOPPLER BROADENED LINEWIDTH (MHZ) =?')
       READ(KB,6018)FWHH
       WRITE(KB,6020)
 6020 FORMAT(1X,'SAMPLE TEMPERATURE =?')
       READ(KB,6018)TEMP1
       WRITE(KB,6022)
 6022 FORMAT(1X,'MOLE FRACTION OF MOLECULE OF INTEREST IN SAMPLE =?')
       READ(KB,6018)FMOLE
       WRITE(KB,6023)
 6023 FORMAT(1X,'STARK VOLTAGE (V),ELECTRODE SPACING (CM) =?')
       READ(KB,6018)VOLTS,SPACE
       WRITE(KB,6400)
 6400 FORMAT(1X,'IS INPUT FROM TAPE ?')
       READ(KB,6401)IIN
 6401 FORMAT(A2)
       IF(IIN.NE.YES) GO TO 6402
       WRITE(KB,6403)
 6403 FORMAT(1X,'INPUT MAG. TAPE LUN,AND NO. OF EOFS TO BE SKIPPED')
       READ(KB,6404)MLUN,NEOF
 6404 FORMAT(4I4)
       IF(MLUN.EQ.0)MLUN=14
       NEOFS=0
       IF(NEOF.EQ.0)GO TO 6405
 6406 READ(MLUN)
       IF(IOCHK(J))6406,6406,6507
 6507 NEOFS=NEOFS+1
       IF(NEOFS.LT.NEOF)GO TO 6406
 6405 READ(MLUN)(TEXT(I),I=1,20)
       READ(MLUN)NTRANS,JMIN,JMAX,I1,I2,I3,I4,(B(I),I=1,6)
      *,TEMP,(DMU(I),I=1,3),FMIN,FMAX,ABSMIN
       WRITE(KB,6025)I5,I6,I7,I8,I2,I3,I1,I4,(TEXT(I),I=1,20)
 6025 FORMAT(1X,'SFIT CALCULATION OF STARK THEORITICAL SPECTRUM',
      *10X,4A2,/,
      *1X,'WANGLY CALCULATION DONE ON',5X,4A2,/,
      *1X,'SFIT ORIGINAL VERSION WRITTEN ON 23/11/79',//,1X,20A4//)
       WRITE(KB,6027)
 6027 FORMAT(1X,'JU,KMU,KPU,JL,KML,KPL =?')
       READ(KB,6028)JU,KMU,KPU,JL,KML,KPL
 6028 FORMAT(6I3)
 6200 READ(MLUN)J1,KM1,KP1,J2,KM2,KP2,FREQ,STR,ENLO,
      *D1U,D2U,D1L,D2L,(ALPHA(I),BETA(I),I=1,3),IDEG,JDEG
      *,(JD1(I),I=1,6),ENL1,ENR1,DDUMY,(DUMMY(I),I=1,4)
      *,GAMMA1,DELTA1,(DUMMY(I),I=1,4),IDEG1,JDEG1,
      *(JD2(I),I=1,6),ENL2,ENR2,DDUMY,(DUMMY(I),I=1,4)
      *,GAMMA2,DELTA2,(DUMMY(I),I=1,4),IDEG2,JDEG2
```

```
      IF(JU.NE.J1.OR.KMU.NE.KM1.OR.KPU.NE.KP1
     *.OR.JL.NE.J2.OR.KML.NE.KM2.OR.KPL.NE.KP2)GO TO 6200
      WRITE(KB,6301)J1,KM1,KP1,J2,KM2,KP2
 6301 FORMAT(1X,'TRANSITION FOUND ',3I3,3X,3I3)
      CALL V$OPEN(99,LUND,IFCB,0)
      IFCB(4)=5
      WRITE(99)J1,KM1,KP1,J2,KM2,KP2,FREQ,STR,ENLO,
     *D1U,D2U,D1L,D2L,(ALPHA(I),BETA(I),I=1,3),IDEG,JDEG
     *,(JD1(I),I=1,6),ENL1,ENR1,DDUMY,(DUMMY(I),I=1,4)
     *,GAMMA1,DELTA1,(DUMMY(I),I=1,4),IDEG1,JDEG1,
     *(JD2(I),I=1,6),ENL2,ENR2,DDUMY,(DUMMY(I),I=1,4)
     *,GAMMA2,DELTA2,(DUMMY(I),I=1,4),IDEG2,JDEG2
      CALL V$CLOS(99,1)
 6402 CALL V$OPEN(99,LUND,IFCB,0)
      IFCB(4)=5
      READ(99)J1,KM1,KP1,J2,KM2,KP2,FREQ,STR,ENLO,
     *D1U,D2U,D1L,D2L,(ALPHA(I),BETA(I),I=1,3),IDEG,JDEG
     *,(JD1(I),I=1,6),ENL1,ENR1,DDUMY,(DUMMY(I),I=1,4)
     *,GAMMA1,DELTA1,(DUMMY(I),I=1,4),IDEG1,JDEG1,
     *(JD2(I),I=1,6),ENL2,ENR2,DDUMY,(DUMMY(I),I=1,4)
     *,GAMMA2,DELTA2,(DUMMY(I),I=1,4),IDEG2,JDEG2
      WRITE(KB,6410)J1,KM1,KP1,J2,KM2,KP2
 6410 FORMAT(3X,3I3,3X,3I3)
      CALL V$CLOS(99,0)
      IA=0
 6430 KGO=IA+1
      GO TO(20,21),KGO
  20  EFIELD=VOLTS/SPACE
      DO 24 I=1,3
      RMU(I)=RMUO(I)
   24 CONTINUE
      GO TO 6500
  21  EFIELD=ZMU(4)/SPACE
      DO 23 I=1,3
      RMU(I)=ZMU(I)
  23  CONTINUE
      GO TO 6500
 6500 IAX=MUTYPE(KM1,KP1,KM2,KP2)
      IF(RMU(IAX).EQ.0.0)GO TO 108
      HYPCOM(1,1)=0.
      HYPCOM(1,2)=1.
      NHYPCM=1
      IF(SPIN.GT.0.5)CALL QUAD1(J1,HYPCOM,NHYPCM)
C          NOW CALCULATE THE STARK SHIFT
X      DO 301 I=1,NHYPCM
X     WRITE(KB,9301)HYPCOM(I,1),HYPCOM(I,2)
X 301 CONTINUE
X9301 FORMAT(1X,2F12.3)
X      WRITE(KB,9302)
X9302 FORMAT(//)
      SCONST=.50348
      III=0
      RM=0.
      RMAX=AMINO(J1,J2)
  101 III=III+1
      SHIFT=0.
      DO 102 IAX=1,3
      SHIFT=SHIFT+((EFIELD*RMU(IAX)*SCONST)**2)*(ALPHA(IAX)
     *+BETA(IAX)*RM**2)
X     WRITE(KB,9305)EFIELD,RMU(IAX),ALPHA(IAX),BETA(IAX),RM
X    *,SHIFT
X9305 FORMAT(1X,6E15.6)
  102 CONTINUE
      IF(IDEG.GT.0)SHIFT=SHIFT+DSHIFT(JD1,ENR1,ENL1,GAMMA1,DELTA1
     *,IDEG1,JDEG1,RMU,RM,SCONST,EFIELD)
      IF(IDEG.GT.1)SHIFT=SHIFT+DSHIFT(JD2,ENR2,ENL2,GAMMA2,DELTA2
     *,IDEG2,JDEG2,RMU,RM,SCONST,EFIELD)
X      WRITE(KB,9305)GAMMA1,DELTA1,GAMMA2,DELTA2,SHIFT
X      WRITE(KB,9306)ENR1,ENL1,ENR2,ENL2
X9306 FORMAT(1X,6D15.8)
      STARCM(III,1)=SHIFT
      STARCM(III,2)=RINTEN(J1,J2,RM)
      RM=RM+1.
      IF(RM.LE.RMAX)GO TO 101
      NSTACM=III
      SUM=0.0
      DO 103 III=1,NSTACM
      SUM=SUM+STARCM(III,2)
  103 CONTINUE
      DO 104 III=1,NSTACM
      STARCM(III,2)=STARCM(III,2)/SUM
  104 CONTINUE
X      DO 303 III=1,NSTACM
X      WRITE(KB,9301)STARCM(III,1),STARCM(III,2)
X 303 CONTINUE
X      WRITE(KB,9302)
      DO 105 III=1,NHYPCM
      COMPON(III,1)=HYPCOM(III,1)
      COMPON(III,2)=HYPCOM(III,2)
  105 CONTINUE
      SUM=0.0
      DO 106 N=1,NHYPCM
      SUM=SUM+COMPON(N,2)
  106 CONTINUE
      DO 107 N=1,NHYPCM
      COMPON(N,2)=COMPON(N,2)/SUM
  107 CONTINUE
C        NOW CALCULATE THE QUADRUPOLE HYPERFINE STRUCTURE OF THE
C            STARK COMPONENTS
      IF(SPIN.NE.0.)GO TO 3021
 3005 K=NHYPCM
      DO 3006 I=1,NSTACM
      K=K+1
      COMPON(K,1)=STARCM(I,1)
      COMPON(K,2)=-STARCM(I,2)
 3006 CONTINUE
```

```
      GO TO 3011
 3021 IF(LM.GT.36)GO TO 3005
      N=0
      MJMX1=J1+1
      MJMX2=J2+1
      DO 220 MJ1=1,MJMX1
      RMI1=SPIN
  221 IRMI1=IRMI1+1
      EQS1(MJ1,IRMI1)=EQS(D1U,D2U,CHIAA,CHIBB,MJ1,J1,SPIN,RMI1)
      RMI1=RMI1-1.
      IF (RMI1.GE.0.) GO TO 221
  220 CONTINUE
      DO 222 MJ2=1,MJMX2
      RMI2=SPIN
  223 IRMI2=IRMI2+1
      EQS2(MJ2,IRMI2)=EQS(D1L,D2L,CHIAA,CHIBB,MJ2,J2,SPIN,RMI2)
      RMI2=RMI2-1.
      IF(RMI2.GE.0.) GO TO 223
  222 CONTINUE
      JF=0
      K=NHYPCM
      DO 224 MJ2=1,MJMX2
      MJ1=MJ2
      JF=JF+1
      STCM=STARCM(JF,1)
      STCM2=STARCM(JF,2)
      RMI1=SPIN
 3025 IRMI1=RMI1+1
      K=K+1
      COMPON(K,1)=EQS1(MJ1,IRMI1)-EQS2(MJ2,IRMI1)+STCM
      RMI1=RMI1-1.
      IF(RMI1.GE.0.)GO TO 3025
      IX=INT(SPIN+.5)
      Y=SPIN/FLOAT(IX)
      IF(Y.EQ.1.) GO TO 226
      COMPON(K,2)=-STCM2/FLOAT(IX)
  226 IF(RMI1.NE.0.)COMPON(K,2)=-STCM2/(SPIN+.5)
      IF(RMI1.EQ.0.)COMPON(K,2)=-STCM2/((SPIN+.5)*2.)
      CONTINUE
  224 CONTINUE
 3011 KMAX=K
      NCOMP=KMAX
      K=NHYPCM
      K=K+1
      SUM=0.0
      DO 227 J=K,NCOMP
      SUM=SUM+COMPON(J,2)
  227 CONTINUE
      DO 228 J=K,NCOMP
      COMPON(J,2)=-COMPON(J,2)/SUM
  228 CONTINUE

      FMN=100.
      FMX=-100.
      DO 108 III=1,NCOMP
      IF(COMPON(III,1).GT.FMX)FMX=COMPON(III,1)
      IF(COMPON(III,1).LT.FMN)FMN=COMPON(III,1)
X     WRITE(KB,6305)COMPON(III,1),COMPON(III,2),FMX,FMN
X6305 FORMAT(4F10.5)
  108 CONTINUE
      WRITE(KB,6303)
 6303 FORMAT(1X,'CALCULATION COMPLETED')
      RETURN
      END



      FUNCTION MUTYPE(KM1,KP1,KM2,KP2)
      I=MOD(KM1-KM2,2)
      J=MOD(KP1-KP2,2)
      IF(I.EQ.0)GO TO 1
      MUTYPE=3
      IF(J.NE.0)MUTYPE=2
      RETURN
    1 MUTYPE=1
      IF(J.NE.0)RETURN
      WRITE(KB,900)KM1,KP1,KM2,KP2
      CALL EXIT
  900 FORMAT(1X,'FUNCTION MUTYPE IMPOSSIBLE TRANSITION:',2I5,5X,2I5,/)
      END



      SUBROUTINE QUAD1(J3,HYPCOM,NCOM)
      COMMON/KEYB/KB
      COMMON/Q1/VOLTS,ISTOP,IA,COMPON(200,2),CC(4),DC(4)
     *,SPACE,RMUO(3)
      COMMON/QRED/IGO,IDSPLY,IAUTO,ICALL,OFMIN,OFMAX,IRCHAN,ILCHAN,
     *OSPEC(1000),IANS,
     *NCHAN,FWHH,RFREQ,OMAX,OMIN,BASE,SCALER,ID(4),ICHAR(16)
     *,NSTICK,NCOMP,ZMU
      COMMON/Q/SPIN,CHIAA,CHIBB,D1U,D2U,D1L,D2L,TEMP1,FMOLE,J1,KM1,KP1,
     *J2,KM2,KP2,IDEG,JDEG,IDEG1,JDEG1,JDEG2,IDEG2
      DIMENSION ZMU(4)
      COMMON/ZOO/B,BI,DMU,FMIN1,FMAX1,FMIN,FMAX
     *,ABSMIN,TEMP,DDUMY,FREQ,STR,ENLO,ENL1,ENL2,ENR1,ENR2,
     *TEXT,RMU,IAXSYM,ALPHA,BETA,JD1,GAMMA1,DELTA1,GAMMA2,DELTA2,
     *JD2,DUMMY,VFREQ,IVDEG,PROFIL,LINE
      DIMENSION TEXT(20),RMU(3),IAXSYM(3),ALPHA(3),BETA(3),JD1(6),
     *JD2(6),DUMMY(4),VFREQ(10),IVDEG(10),
     *HYPCOM(16,2),STARCM(20,2),PROFIL(514),LINE(64),
     *IFCB(13),QENER1(10),QENER2(10),A(10),C(10),TCOM(16,2)
      DOUBLE PRECISION B(6),BI(3),DMU(3),FMIN1,FMAX1,FMIN,FMAX,
     *ABSMIN,TEMP,DDUMY,FREQ,STR,ENLO,ENL1,ENL2,ENR1,ENR2
      DOUBLE PRECISION OFMIN,OFMAX,RFREQ
      REAL LORENZ
```

```
      DATA IYES,NO/1HY,1HN/

      S=SPIN
      J4=J3
      FMAX1=I+FLOAT(J4)
      FMIN1=ABS(I-FLOAT(J4))
      IF(S.GT.FLOAT(J4)) R=2.*FLOAT(J4)+1.1
      IF(S.LE.FLOAT(J4)) R=2.*S+1.1
      N=IFIX(R)
      II=1
      A(II)=FMIN1
      DO 1 II=1,N
      IF(II.GT.1) A(II)=A(II-1)+1.
      F1=A(II)
      QENER1(II)=EQ(F1,S,J4,D1U,CHIAA,D2U,CHIBB)
    1 CONTINUE
      FMIN2=ABS(S-FLOAT(J2))
      FMAX2=S+FLOAT(J2)
      IF(S.GT.FLOAT(J2)) P=2.*FLOAT(J2)+1.1
      IF(S.LE.FLOAT(J2)) P=2.*S+1.1
      M=IFIX(P)
      II=1
      C(II)=FMIN2
      DO 2 II=1,M
      IF(II.GT.1) C(II)=C(II-1)+1.
      F2=C(II)
      QENER2(II)=EQ(F2,S,J2,D1L,CHIAA,D2L,CHIBB)
    2 CONTINUE
      NCOM=0
      SUM=0.
      L=1
      LL=1
      C(LL)=FMIN2
      DO 3 LL=1,M
      A(L)=FMIN1
      IF(LL.GT.1) C(LL)=C(LL-1)+1.
      DO 4 L=1,N
      IF(L.GT.1) A(L)=A(L-1)+1.
      IF(ABS(A(L)-C(LL)).GT.1.1) GO TO 4
      NCOM=NCOM+1
      HYPCOM(NCOM,1)=QENER1(L)-QENER2(LL)
      IF(J3.EQ.J2) GO TO 5
      IF(J3.LT.J2) GO TO 20
      F1=A(L)
      F2=C(LL)
      IF(F1.GT.F2) GO TO 7
      IF(F1.EQ.F2) GO TO 8
   21 TCOM(NCOM,2)=(FLOAT(J4)-F1+S)*(FLOAT(J4)-F1+S-1.)*(FLOAT(J4)
     *-F1-S-1.)*(FLOAT(J4)-F1-S-2.)/(F1+1.)
      GO TO 40
    7 TCOM(NCOM,2)=(FLOAT(J4)+F1+S+1.)*(FLOAT(J4)+F1+S)*(FLOAT(J4)
     *+F1-S)*(FLOAT(J4)+F1-S-1.)/F1
      GO TO 40
    8 TCOM(NCOM,2)=-(FLOAT(J4)+F1+S+1.)*(FLOAT(J4)+F1-S)*(FLOAT(J4)
     *-F1+1.)*(FLOAT(J4)-F1-S-1.)*(2.*F1+1.)/(F1*(F1+1.))
      GO TO 40
   20 J4=J3+1
      F1=C(LL)
      F2=A(L)
      IF(F1.EQ.F2) GO TO 8
      IF(F1.LT.F2) GO TO 21
      IF(F1.GT.F2) GO TO 7
    5 F1=A(L)
      F2=C(LL)
      IF(F1.GT.F2) GO TO 9
      IF(F1.EQ.0..AND.F2.EQ.0.) GO TO 11
      IF(F1.EQ.F2) GO TO 10
      TCOM(NCOM,2)=-(FLOAT(J4)+F1+S+2.)*(FLOAT(J4)+F1-S+1.)*(FLOAT(J4)
     *-F1+S)*(FLOAT(J4)-F1-S-1.)/(F1+1.)
      GO TO 40
    9 TCOM(NCOM,2)=-(FLOAT(J4)+F1+S+1.)*(FLOAT(J4)+F1-S)*(FLOAT(J4
     *)-F1+S+1.)*(FLOAT(J4)-F1-S)/F1
      GO TO 40
   10 TCOM(NCOM,2)=((FLOAT(J4)*(FLOAT(J4)+1.)+F1*(F1+1.)
     *-S*(S+1.))**2.)*(2.*F1+1.)/(F1*(F1+1.))
      GO TO 40
   11 TCOM(NCOM,2)=0.
   40 SUM=SUM+TCOM(NCOM,2)
    4 CONTINUE
    3 CONTINUE
      DO 15 L=1,NCOM
      HYPCOM(L,2)=TCOM(L,2)/SUM
   15 CONTINUE
      RETURN
      END



      FUNCTION CAS(F,I,J)
      REAL I
      CAS=F*(F+1.)-I*(I+1.)-FLOAT(J)*(FLOAT(J)+1.)
      RETURN
      END



      FUNCTION FCAS(F,I,J)
      REAL I
      FCAS=((3./4.)*CAS(F,I,J)*(CAS(F,I,J)+1.)-I*(I+1.)*FLOAT(J)*(FLOAT(
     *J)+1.))/(2.*I*(2.*I-1.)*(2.*FLOAT(J)-1.)*(2.*FLOAT(J)+3.))
      RETURN
      END



      FUNCTION EQ(F,I,J,D1,CHIAA,D2,CHIBB)
```

```
      REAL I
      EQ=(D1*CHIAA+D2*CHIBB)*FCAS(F,I,J)
      RETURN
      END




      FUNCTION FGAMMA(B,DIP,S,F,E,T)
      DOUBLE PRECISION B(6),S,F,E
      FGAMMA=2.46E-20*SNGL(DSQRT(B(1)*B(2)*B(3)))
      F1=SNGL(F)
      E1=SNGL(E)
      FGAMMA=FGAMMA*EXP(-E1/(20836.*T))
      S1=SNGL(S)
      FGAMMA=FGAMMA*(DIP**2)*S1*(F1**2)/30.
      T1=T/300.0
      FGAMMA=FGAMMA/(T1**2.5)
      RETURN
      END



      FUNCTION DSHIFT(J,WU,WL,G,D,ID,JD,DIP,RM,SC,EF)
      DIMENSION J(6),DIP(3)
      DOUBLE PRECISION WU,WL
C      ID=1   MEANS DEGENERACY IS IN UPPER LEVEL OF TRANSITION
C      ID=-1                "          LOWER LEVEL      "
C
C      JD=1   MEANS THAT LEVEL IS UPPER OF DEGENERATE PAIR.
C      JD=-1                "          LOWER        "
C
      IAX=MUTYPE(J(2),J(3),J(5),J(6))
      PERT=(SC*DIP(IAX)*EF)
      WDIFF=-DABS(WL-WU)/2.0D00
      DSHIFT=WDIFF+SQRT((WDIFF**2)+(PERT**2)*(G+D*(RM**2)))
      DSHIFT=DSHIFT*FLOAT(JD)*FLOAT(ID)
      RETURN
      END



      FUNCTION RINTEN(J1,J2,RM)
      IF(J1-J2.NE.0)GO TO 2
      RINTEN=RM**2
      RETURN
    2 RINTEN=(AMAX0(J1,J2))**2-RM**2
      RETURN
      END
47

      REAL FUNCTION LORENZ(F0,F,W)
      LORENZ=1./(1.+4.*((F-F0)/W)**2)
      RETURN
      END



      FUNCTION ICHAR(I,J)
      A=I
      B=J
      AIJ=A*256.+B
      AIJ=-(65536.-AIJ)-0.2
      ICHAR=AIJ
      RETURN
      END



      SUBROUTINE WORKSP(KB,IFCB,LKB)
C     OPENS TO EDIT WORKSPACE FOR KEYBOARD IN USE
      DIMENSION IFCB(14),IFCB1(10),IFCDAT(10),LUN(10)
      INTEGER FUN
      DATA (LUN(I),I=1,8)/8,8,70,70,70,70,70,70/
      DATA (IFCDAT(I),I=1,8)/'SS','LG','UI','TR','T3','T4','T5','T6'/
      DATA IFCB1(3)/0/
      DATA IFCB1(9),IFCB1(10)/'C1','  '/
      DATA ISS/'SS'/
      DO 500 I=1,10
  500 IFCB(I)=IFCB1(I)
      IF(KB.EQ.24)GO TO 24
      IF(KB.EQ.32)GO TO 32
      IF(KB.EQ.40)GO TO 40

      IF(KB.EQ.41)GO TO 41
      IF(KB.EQ.42)GO TO 42
      IF(KB.EQ.43)GO TO 43
      IF(KB.EQ.44)GO TO 44
    8 WRITE(KB,900)
  900 FORMAT('  NO EDIT WORKSPACE AVAILABLE FOR THIS TERMINAL:',)

      GO TO 1001
   24 INDEX=2
      IFCB(9)=IFCDAT(1)
      GO TO 1000
   32 INDEX=3
      GO TO 1000
   40 INDEX=4
      GO TO 1000
   41 INDEX=5
      GO TO 1000
   42 INDEX=6
      GO TO 1000
   43 INDEX=7
      GO TO 1000
   44 INDEX=8
      GO TO 1000
 1000 IFCB(8)=IFCDAT(INDEX)
      LKB=LUN(INDEX)
 1001 RETURN
      END
```

```
C     *STARFIT  OVERLAY PLOTTR
      SUBROUTINE PLOTTR
      COMMON /TEX/ITITLE(16)
      COMMON/KEYB/KB
      COMMON/Q1/VOLTS,ISTOP,IA,COMPON(200,2),CC(4),DC(4)
     *,SPACE,RMUO(3)
      COMMON/QRED/IGO,IDSPLY,IAUTO,ICALL,OFMIN,OFMAX,IRCHAN,ILCHAN,
     *OSPEC(1000),IANS,
     *NCHAN,FWHH,RFREQ,OMAX,OMIN,BASE,SCALER,ID(4),ICHAR(16)
     *,NSTICK,NCOMP,ZMU
      COMMON/Q/SPIN,CHIAA,CHIBB,D1U,D2U,D1L,D2L,TEMP1,FMOLE,J1,KM1,KP1,
     *J2,KM2,KP2,IDEG,JDEG,IDEG1,JDEG1,JDEG2,IDEG2
      DIMENSION ZMU(4)
      COMMON/ZOO/B,BI,DMU,FMIN1,FMAX1,FMIN,FMAX
     *,ABSMIN,TEMP,DDUMY,FREQ,STR,ENLO,ENL1,ENL2,ENR1,ENR2,
     *TEXT,RMU,IAXSYM,ALPHA,BETA,JD1,GAMMA1,DELTA1,GAMMA2,DELTA2,
     *JD2,DUMMY,VFREQ,IVDEG,PROFIL,LINE
      DIMENSION TEXT(20),RMU(3),IAXSYM(3),ALPHA(3),BETA(3),JD1(6),
     *JD2(6),DUMMY(4),VFREQ(10),IVDEG(10),
     *HYPCOM(16,2),STARCM(20,2),PROFIL(514),LINE(64),
     *IFCB(13),GENER1(10),GENER2(10),A(10),C(10),TCOM(16,2)
      DOUBLE PRECISION B(6),BI(3),DMU(3),FMIN1,FMAX1,FMIN,FMAX,
     *ABSMIN,TEMP,DDUMY,FREQ,STR,ENLO,ENL1,ENL2,ENR1,ENR2
      REAL LORENZ
      INTEGER YE
      DOUBLE PRECISION OFMIN,OFMAX,RFREQ
      DIMENSION IBUF(2000),CONVOL(200),INUMBR(120)
     *,STICKH(200),STICKF(200)
      DOUBLE PRECISION FRANGE,TICFRE,FMIN,FMAX,TICGAP,FSFAC
     *,STICKF
      DATA YE/2HYE/
      UP=1.
      WRITE(KB,3200)
 3200 FORMAT(1X,'IS THE MAIN LINE POINTING UPWARDS? ')
      READ(KB,3201)IENS
 3201 FORMAT(A2)
      IF(IENS.EQ.YE) GO TO 3202
      UP=-1.
 3202 CONTINUE
      CALL V$OPNB(99,0,IFCB,3,5,INUMBR,0)
      IF(ICALL.EQ.6)GO TO 5679
      ICALL=6
 5679 DO 2222 I=1,NCOMP
      STICKH(I)=COMPON(I,2)
 2222 STICKF(I)=DBLE(COMPON(I,1))+RFREQ
      PAGEWD=8.25
      PAGEHT=10.25
      SPACEX=(11.-PAGEWD)/2.
      SPACEY=(14.875-PAGEHT)/2.
      ORIGX=SPACEX-0.75
      ORIGY=SPACEY-0.5
C      INITIALIZE DATAPLOT II
      CALL PLOTS(IBUF,2000,22)
      CALL MLTPLE(1)
C
C      SHIFT ORIGIN TO CORNER OF PAGE NEAREST TOP LHS OF PLOT RECT.
      CALL PLOT(ORIGX,ORIGY,-3)

C      WRITE A CROSS AT EACH CORNER OF THE PAGE.
      CALL CROSS(0.0,0.0)
      CALL CROSS(0.0,PAGEHT)
      CALL CROSS(PAGEWD,PAGEHT)
      CALL CROSS(PAGEWD,0.0)
C      CALCULATE THE PAGE BORDER WIDTHS.
      BORDUP=(PAGEWD-5.)/2.
      BORDLO=PAGEWD-BORDUP-3.5
      BORDSD=(PAGEHT-8.)/2.
C      DRAW A BORDER RECTANGLE, MOVING ORIGIN TO LOWER LH CORNER.
      CALL PLOT(PAGEWD-BORDLO,BORDSD,-3)
      CALL PLOT(-3.5,0.,2)
      CALL PLOT(-3.5,8.,2)
      CALL PLOT(0.,8.,2)
      CALL PLOT(0.,0.,2)
      FMAX=OFMAX-((OFMAX-OFMIN)/DBLE(FLOAT(NCHAN)))
     **DBLE(FLOAT(NCHAN-IRCHAN))
      FMIN=OFMIN+((OFMAX-OFMIN)/DBLE(FLOAT(NCHAN)))
     **DBLE(FLOAT(ILCHAN-1))
      FINC=(OFMAX-OFMIN)/DBLE(FLOAT(NCHAN))
      FRANGE =FMAX-FMIN
C      THERE WILL BE SIX LABELLED FREQUENCY 'TICS'.
      TICGAP=FRANGE/5.00D00
      FSFAC=8.00D00/FRANGE
C      FSFAC= INCHES / MHZ ON FREQ. AXIS.
      TICDIS=FSFAC*TICGAP
C      DRAW AND LABEL FREQUENCY MARKS
      TICPOS=0.
      TICFRE=FMIN
      DO 3 I=1,6
      CALL PLOT(0.,TICPOS,3)
      CALL PLOT(0.05,TICPOS,2)
      WRITE(99,902)TICFRE
  902 FORMAT(8F10.3)
      CALL SYMBOL(0.2,TICPOS-0.5,0.1,INUMBR,90.,10)
      TICPOS=TICPOS+TICDIS
      TICFRE=TICFRE+TICGAP
    3 CONTINUE
C      LABEL FREQUENCY SCALE
      CALL SYMBOL(0.5,3.,0.1,15HFREQUENCY (MHZ),90.,15)
C      LABEL ABSORPTION SCALE
      CALL SYMBOL(-2.75,-0.2,0.1,20HABSORPTION INTENSITY,0.,20)
C      SCAN STICK SPECTRUM TO CHECK FOR COINCIDENT STICKS.
C      ADD COINCIDENT STICKS TOGETHER.
      FSTEP=FRANGE/8.00D+02
      FNEAR=FSTEP/2.
      DO 4 I=1,NCOMP
      K=I+1
```

```
      DO 4 J=K,NCOMP
      FSTICK=STICKF(I)-STICKF(J)
      IF(ABS(FSTICK).GT.FNEAR)GO TO 4
      STICKH(I)=STICKH(I)+STICKH(J)
      STICKH(J)=0.0
    4 CONTINUE
C     INVERT CONVOLVED SPECTRUM IF MAIN LINE IS POINTING DOWNWARDS
      DO 1112 I=1,NCOMP
      STICKH(I)=UP*STICKH(I)
 1112 CONTINUE
C      FIND MAXIMUM POSITIVE AND NEGATIVE STICKS.
      POSSTK=0.
      RNGSTK=0.
      DO 5 I=1,NCOMP
      IF(STICKH(I).GT.POSSTK)POSSTK=STICKH(I)
      IF(STICKH(I).LT.RNGSTK)RNGSTK=STICKH(I)
    5 CONTINUE
      IF(FWHH.NE.0.)GO TO 1111
      WRITE(KB,1233)
 1233 FORMAT(1X,'FWHH (MHZ) = ?')
      READ (KB,902) FWHH
 1111 HW=FWHH/2.
      F=FMIN
      FOFF=0.
      POSCON=-100.
      RNGCON=100.
      DO 6 I=1,200
      CONV=0.
      DO 7 J=1,NCOMP
      IF(STICKH(J).EQ.0.) GO TO 7
      CONV=CONV+STICKH(J)/(1.+(SNGL(F-STICKF(J))/HW)**2)
    7 CONTINUE
      CONVOL(I)=CONV
      IF(CONVOL(I).GT.POSCON)POSCON=CONVOL(I)
      IF(CONVOL(I).LT.RNGCON)RNGCON=CONVOL(I)
      FOFF=FOFF+4.*FSTEP
      F=FMIN+DBLE(FOFF)
    6 CONTINUE
C      SCALE BOTH STICK AND CONVOLVED SPECTRUM TO THE SAME SCALE
C      SUCH THAT THEIR COMBINED EXTREMA COVER 3 INCHES.
C      POS=POSSTK
C      IF(POSCON.GT.POS)POS=POSCON
C      RNEG=RNGSTK
C      IF(RNGCON.LT.RNEG)RNEG=RNGCON
C      POS=POS
C      RNEG=RNEG
C      FACT=3./(POS-RNEG)
      FACT=3./(POSCON-RNGCON)
C      DEFINE BASELINE POSITION
C      BASE=RNEG*FACT
      BASE=RNGCON*FACT
C      PLOT SPECTRUM.
      FREQ=0.
      FDIS=0.
      DO 8 I=1,800
      DO 9 J=1,NCOMP
      IF(STICKH(J).EQ.0.)GO TO 9
      STICK=STICKF(J)-FMIN
      IF(ABS(FREQ-STICK).GT.FNEAR)GO TO 9
      ROD=BASE-STICKH(J)*FACT
      CALL PLOT(BASE,FDIS,3)
      CALL PLOT(ROD,FDIS,2)
      STICKH(J)=0.
    9 CONTINUE
      FDIS=FDIS+0.01
      FREQ=FREQ+FSTEP
    8 CONTINUE
C      PLOT CONVOLVED SPECTRUM.
      CALL PLOT(BASE,0.,3)
      FDIS=0.
      DO 10 I=1,200
      CONV=BASE-CONVOL(I)*FACT
      CALL PLOT(CONV,FDIS,2)
      FDIS=FDIS+0.04
   10 CONTINUE
      NOBS=IRCHAN-ILCHAN+1
      DO 11 I=1,NOBS
      ITEMPY=ILCHAN+I-1
   11 CONVOL(I)=OSPEC(ITEMPY)
C      SCALE OBSERVED SPECTRUM TO 3 INCHES
      CMIN=CONVOL(1)
      CMAX=CONVOL(1)
      DO 12 I=1,NOBS
      IF(CMAX.LT.CONVOL(I))CMAX=CONVOL(I)
      IF(CMIN.GT.CONVOL(I))CMIN=CONVOL(I)
   12 CONTINUE
      FACT=3./(CMAX-CMIN)
      DO 13 I=1,NOBS
      CONVOL(I)=(CONVOL(I)-CMIN)*FACT
   13 CONTINUE
C      PLOT OBSERVED SPECTRUM WITH A BROKEN LINE
      FSTEP=8./FLOAT(NOBS-1)
      FDIS=0.
      CALL PLOT(-CONVOL(1),0.,3)
      DO 14 I=1,NOBS
      CALL PLOT(-CONVOL(I),FDIS,2)
      CALL SQUARE(-CONVOL(I),FDIS,4)
      FDIS=FDIS+FSTEP
   14 CONTINUE
   15 CONTINUE
C      WRITE TITLE STARTING 1 INCH IN FROM TOP LH CORNER .375 BELOW TOP
C          MARGIN
      CALL SYMBOL(-3.13,1.,0.1,ITITLE,90.,32)
C      OVER AND OUT
      CALL PLOT(0.,0.,999)
      CALL V$CLSB(99,0)
```

```
      RETURN
      END



      SUBROUTINE CROSS(X,Y)
      CALL PLOT(X-0.05,Y,3)
      CALL PLOT(X+0.05,Y,2)
      CALL PLOT(X,Y-0.05,3)
      CALL PLOT(X,Y+0.05,2)
      RETURN
      END



      SUBROUTINE SQUARE(X,Y,N)
      SIDE=FLOAT(N)*0.01
      HSIDE=SIDE/2.
      Y1=Y-HSIDE
      DO 1 I=1,N
      CALL PLOT(X-HSIDE,Y1,3)
      CALL PLOT(X+HSIDE,Y1,2)
      Y1=Y1+0.01
    1 CONTINUE
      CALL PLOT(X,Y,3)
      RETURN
      END
```

```
C     "STARFIT"  OVERLAY RKNOBS
      SUBROUTINE RKNOBS
      COMMON /TEX/ITEXT(16)
      COMMON/KEYB/KB
      COMMON/ORED/IGO,IDSPLY,IAUTO,ICALL,OFMIN,OFMAX,IRCHAN,ILCHAN,
     *OSPEC(4000),IANS,
     *NCHAN,FWHH,RFREQ,OMAX,OMIN,BASE,SCALER,ID(4),ICHAR(16)
     *,NSTICK,NCOMP,ZMU
      COMMON/Q1/VOLTS,ISTOP,IA,COMPON(200,2),CC(4),DC(4)
     *,SPACE,RMUO(3)
      COMMON/Q/SPIN,CHIAA,CHIBB,D1U,D2U,D1L,D2L,TEMP1,FMOLE,J1,KM1,KP1,
     *J2,KM2,KP2,IDEG,JDEG,IDEG1,JDEG1,JDEG2,IDEG2
      DIMENSION ZMU(4)
      COMMON/ZOO/B,BI,DMU,FMIN1,FMAX1,FMIN,FMAX
     *,ABSMIN,TEMP,DDUMY,FREQ,STR,ENLO,ENL1,ENL2,ENR1,ENR2,
     *TEXT,RMU,IAXSYM,ALPHA,BETA,JD1,GAMMA1,DELTA1,GAMMA2,DELTA2,
     *JD2,DUMMY,VFREQ,IVDEG,PROFIL,LINE
      DIMENSION TEXT(20),RMU(3),IAXSYM(3),ALPHA(3),BETA(3),JD1(6),
      JD2(6),DUMMY(4),VFREQ(10),IVDEG(10),
     *TYPCOM(16,2),STARCM(20,2),PROFIL(514),LINE(64),
     *IFCB(13)
      DOUBLE PRECISION B(6),BI(3),DMU(3),FMIN1,FMAX1,FMIN,FMAX,
     *ABSMIN,TEMP,DDUMY,FREQ,STR,ENLO,ENL1,ENL2,ENR1,ENR2
      REAL LORENZ
      DOUBLE PRECISION OFMIN,OFMAX,RFREQ,FFMIN,FFMAX,FINC,ORFREQ
      DIMENSION IOUT(256),ISPOUT(512),CCHI(4)
      COMMON /SCREEN/IOUT
      DIMENSION A(4),JCHAR(16)

      ORFREQ=RFREQ
      IUPARR=-25958
      CC(1)=RMUO(1)
      CC(2)=RMUO(2)
      CC(3)=RMUO(3)
      CC(4)=VOLTS
      I1=0
      I2=0
      I3=0
      I4=0
      I11=1
      I22=1
      I33=1
      I44=1
      ISTOP=0
      OSPECX=OSPEC(ILCHAN)
      OSPECN=OSPECX
      DO 200 I=ILCHAN,IRCHAN
      IF(OSPECX.LT.OSPEC(I))OSPECX=OSPEC(I)
      IF(OSPECN.GT.OSPEC(I))OSPECN=OSPEC(I)
  200 CONTINUE
      IF (IA.EQ.1) GO TO 104
      GO TO(4,2,1,4,4,4,5,6,7),IGO
    1 WRITE(KB,102)
```

```
      READ(KB,101)(DC(I),I=1,4)
      WRITE(KB,103)
      IA=1
204   CALL DELAY(5,0,0)
  104 CALL LORENT(OSPECN,OSPECX)
      CALL DATIN(21,I1,0)
      CALL DATIN(21,I2,0)
302   CALL DATIN(21,I3,0)
      CALL DATIN(21,I4,0)
303   CALL DATIN(21,ISTOP,1)
      IF(ISTOP.NE.-1)GO TO 4
      IF(I1-I11)105,106,105
106   IF(I2-I22)105,107,105
107   IF(I3-I33)105,108,105
108   IF(I4-I44)105,204,105
105   I11=I1
      I22=I2
      I33=I3
      I44=I4
      A(1)=I1-24
      A(2)=I2-24
      A(3)=I3-24
      A(4)=I4-24
      DO 110 I=1,4
110   ZMU(I)=CC(I)+DC(I)*A(I)/1000.
      WRITE(KB,111)IUPARR
      WRITE(KB,112)(ZMU(I),I=1,4)
      RETURN
2     WRITE(KB,113)
      READ(KB,101)FWHHMX
      WRITE(KB,114)
215   CALL DELAY(5,0,0)
115   CALL DATIN(21,I1,0)
      CALL DATIN(21,I2,0)
      CALL DATIN(21,I3,0)
      CALL DATIN(21,I4,0)
      CALL DATIN(21,ISTOP,1)
      IF(ISTOP.NE.-1)GO TO 4
      IF(I1-I11)119,116,119
116   IF(I2-I22)119,117,119
117   IF(I3-I33)119,118,119
118   IF(I4-I44)119,215,119
119   I11=I1
      I22=I2
      I33=I3
      I44=I4
      A(1)=I1-524
      A(2)=I2-24
      A(3)=I3-524
      A(4)=I4-524
      RFREQ=ORFREQ+DBLE(A(1)/1000.)*(OFMAX-OFMIN)
      FWHH=FWHHMX*A(2)/1000.
      IF(FWHH)120,120,121
120   FWHH=0.001
121   BASE=A(3)/2.
      SCALER=A(4)/200.
      WRITE(KB,111)IUPARR
      WRITE(KB,122)RFREQ,FWHH,BASE,SCALER
      CALL LORENT(OSPECN,OSPECX)
      GO TO 115
5     FINC=(OFMAX-OFMIN)/DBLE(FLOAT(NCHAN))
      WRITE(KB,123)
224   CALL DELAY(5,0,0)
124   CALL DATIN(21,I1,0)
      CALL DATIN(21,I2,0)
      CALL DATIN(21,ISTOP,1)
      IF(ISTOP.NE.-1)GO TO 4
      IF(I1-I11)126,125,126
125   IF(I2-I22)126,224,126
126   I11=I1
      I22=I2
      J1=I1-40
      J2=I2-40
      IF(J1)127,128,128
127   J1=0
128   IF(J2)129,130,130
129   J2=0
130   FFMIN=OFMIN+FINC*DBLE(FLOAT(J1))
      FFMAX=OFMAX-FINC*DBLE(FLOAT(J2))
      IF(FFMIN-FFMAX)134,135,135
135   WRITE(KB,136)
      GO TO 4
134   IRCHAN=NCHAN-J2
      ILCHAN=J1+1
      WRITE(KB,111)IUPARR
      WRITE(KB,131)J1,J2,FFMIN,FFMAX
      CALL LORENT(OSPECN,OSPECX)
      GO TO 124
6     WRITE(KB,132)
      READ(KB,133)(JCHAR(I),I=1,35)
      IF(IOCHK(I))137,139,141
137   WRITE(KB,138)
      GO TO 4
139   DO 140 I=1,16
140   ITEXT(I)=JCHAR(I)
141   CALL LORENT(OSPECN,OSPECX)
      GO TO 4
7     WRITE(KB,142)(ID(I),I=1,4)
      READ(KB,143)(JCHAR(I),I=1,4)
      IF(IOCHK(I))137,144,146
144   DO 145 I=1,4
145   ID(I)=JCHAR(I)
146   CALL LORENT(OSPECN,OSPECX)
    4 IA=0
      RETURN
101   FORMAT(4F10.5)
```

```
  102   FORMAT(1X,'NOMINATE KNOB RANGES  : IN DEBYES FOR MUA,'
     */1X,'MUB,MUC,AND IN VOLTS FOR STARK VOLTAGE ')
  103 FORMAT(1X,'MUA MUB MUC V ')
  111   FORMAT(1X,A2)
  112   FORMAT(1X,4(F7.3,2X))
  113   FORMAT(1X,'NOMINATE MAX. FWHH(MHZ) ')
  114   FORMAT(1X,'ROT. FREQ(MHZ) FWHH(MHZ)   BASE    SCALE',/)
  122   FORMAT(1X,F12.3,3X,F7.3,2X,1PE7.1,2X,0PF7.3)
  123   FORMAT(1X,'CHANNEL NUMBERS            FREQUENCY(MHZ)',/,1X,
     *'LH.       RH.          MIN         MAX',/)
  136   FORMAT(1X,'NO SPECTRUM LEFT')
  131   FORMAT(1X,I4,6X,I4,F15.3,F11.3)
  132   FORMAT(1X,'ENTER HEADING .(35A2)')
  133   FORMAT(35A2)
  138   FORMAT(1X,'I/O ERROR DURING READ')
  142   FORMAT(1X,'DISPLAY PARAMETERS',/,1X,
     *'LH,RH,HI,LOW,=',I3,',',I3,',',I3,',',I3,',')
  143   FORMAT(4I5)
        END



        SUBROUTINE LORENT(OSPECN,OSPECX)
        COMMON/KEYB/KB
        COMMON/ORED/IGO,IDSPLY,IAUTO,ICALL,OFMIN,OFMAX,IRCHAN,ILCHAN,
     *OSPEC(1000),IANS,
     *NCHAN,FWHH,RFREQ,OMAX,OMIN,BASE,SCALER,ID(4),ICHAR(16)
     *,NSTICK,NCOMP,ZMU
        COMMON/Q1/VOLTS,ISTOP,IA,COMPON(200,2),CC(4),DC(4)
     *,SPACE,RMUO(3)
        COMMON/Q/SPIN,CHIAA,CHIBB,D1U,D2U,D1L,D2L,TEMP1,FMOLE,J1,KM1,KP1,
     *J2,KM2,KP2,IDEG,JDEG,IDEG1,JDEG1,JDEG2,IDEG2
        DIMENSION TEXT(20),RMU(3),IAXSYM(3),ALPHA(3),BETA(3),JD1(6),
     *JD2(6),DUMMY(4),VFREQ(10),IVDEG(10),
     *HYPCOM(16,2),STARCM(20,2),PROFIL(514),LINE(64),
     *IFCB(13)
        DOUBLE PRECISION OFMIN,OFMAX,RFREQ
        DIMENSION IOUT(256),GAMMA(256),ISPOUT(512),CCHI(4),ZMU(4)
        DIMENSION SPOUT(512)
        COMMON /SCREEN/IOUT
        IF(ICALL.EQ.6)GO TO 3
        ICALL=6
3       CONTINUE
        DO 1 I=1,512
        SPOUT(I)=0.
1       ISPOUT(I)=ID(4)
        I=1
5555    IFIN=I+20
        ISTART=I
        NOBS=IRCHAN-ILCHAN+1
        DO 3333 I=ISTART,IFIN
        IF(NOBS/I.LT.ID(2)-ID(1))GO TO 4444
3333    CONTINUE
        GO TO 5555
4444    KCHAN=NOBS/I
        M=MOD(NOBS,I)
        IF(M)8888,9999,8888
8888    KCHAN=KCHAN+1
9999    JJJ=0
        IF(I-1)100,100,101
100     JJJ=JJJ+1
        IF(KCHAN*JJJ.LT.ID(2)-ID(1))GO TO 100
        JJJ=JJJ-2
 101    MARG=(ID(2)-ID(1)-KCHAN*(JJJ+1))/2
        VERTSC=FLOAT(ID(3)-ID(4))/(OSPECX-OSPECN)
        K=ID(1)+256+MARG
        L=0
        DO 6666 J=1,NOBS
        L=L+1
        KK=J+ILCHAN-1
        SPOUT(K)=SPOUT(K)+(OSPEC(KK)-OSPECN)*VERTSC
        IF(I.NE.L)GO TO 6666
        ISPOUT(K)=SPOUT(K)/FLOAT(I)
        ISPOUT(K)=ISPOUT(K)+ID(4)
        K=K+1+JJJ
        L=0
        IF(J.EQ.NOBS)GO TO 7777
6666    CONTINUE
        ISPOUT(K)=SPOUT(K)/FLOAT(L)
        ISPOUT(K)=ISPOUT(K)+ID(4)
7777    CONTINUE
        FMIN=OFMIN-RFREQ+((OFMAX-OFMIN)/DBLE(FLOAT(NCHAN)))
     **DBLE(FLOAT(ILCHAN-1))
        FMAX=OFMAX-RFREQ-((OFMAX-OFMIN)/DBLE(FLOAT(NCHAN)))
     **DBLE(FLOAT(NCHAN-IRCHAN))
        IF(FWHH.NE.0.)GO TO 22222
        WRITE(KB,903)
        READ(KB,904)FWHH
22222   DELNU=FWHH/2.
        DELTF=(FMAX-FMIN)/FLOAT(KCHAN)
        GAMAX=0.
        DO 11 K=1,KCHAN
        GAMMA(K)=0.
        KJ=K-1
        FREK=FMIN+FLOAT(KJ)*DELTF
        DO 12 I=1,NCOMP
        DENOM=((FREK-COMPON(I,1))/DELNU)**2+1.
        SUM=COMPON(I,2)/DENOM
   12   GAMMA(K)=GAMMA(K)+SUM
        IF(GAMAX.LT.GAMMA(K)) GAMAX=GAMMA(K)
   11   CONTINUE
        VERTSC=ID(3)-ID(4)
        SCALE=(VERTSC/GAMAX)*SCALER
        DO 15 K=1,KCHAN
        GAMMA(K)=SCALE*GAMMA(K)+BASE
```

```
266           J=(K-1)*(JJJ+1)+ID(1)+MARG
267      15   ISPOUT(J)=IFIX(GAMMA(K))
268           DO 36 I=1,512,2
269           J=(I+1)/2
270           I1=ISPOUT(I)
271           I2=ISPOUT(I+1)
272           CALL ASSEM(J,IOUT,I1,I2)
273        36 CONTINUE
274           ITTT=ICHAR(1)
275           DO 9876 I=1,8
276           IOUT(I)=ICHAR(I)
277           IOUT(I+128)=ICHAR(I+8)
278     9876  CALL BITSET(I+8,0,ITTT)
279           IOUT(1)=IDSPLY*4096+ITTT
280           CALL OUTPUT(IOUT,256)
281           RETURN
282         901 FORMAT(8F10.4)
283         903 FORMAT(1X,'FULL WIDTH @ HALF HEIGHT = ?  (MHZ)')
284           END
```

SUPPORTING PUBLICATIONS

(1) "Detection of J = 2→1 Emission of Acentonitrile (CH_3CN) in Sgr B2". G.L. Blackman, R.D. Brown, P.D. Godfrey, M.P. Bassez, A.L. Ottrey D. Winkler and B.J. Robinson, Mon. Not. R. astr. Soc., 180, 1P (1977).

(2) "Microwave Spectrum and Conformation of Glycine". R.D. Brown, P.D. Godfrey, J.W.V. Storey and M.P. Bassez, J.C.S. Chem. Comm. 547 (1978).

(3) "A Search for Interstellar Glycine". R.D. Brown, P.D. Godfrey, J.W.V. Storey, M.P. Bassez, B.J. Robinson, R.A. Batchelor, M.G. McCulloch, O.E.H. Rydbeck and Å.C. Hjalmarson. Mon. Not. R. astr. Soc., 186, 5P (1979).

(4) The Detection of Interstellar Methanol.

(5) The Detection of Interstellar Methyl Cyanide.

REFERENCES

INTRODUCTION

1 C.H. TOWNES and A.L. SCHAWLOW — Microwave Spectroscopy.

McGraw-Hill (1955), Dover Publ. Inc. (1975).

W. GORDY and R.L. COOK, Wiley-Interscience (1956) (1970). — Microwave Molecular Spectra.

J.E. WOLLRAB, Academic Press (1967). — Rotational Spectra and Molecular Structure.

H.W. KROTO, Wiley-Interscience (1975). — Molecular Rotation Spectra.

D.G. LISTER, J.N. MACDONALD and N.L. OWEN, Academic Press (1978). — Internal Rotation and Inversion.

A.R. EDWARDS, Princeton Univ. Press N.J. (1960). — Angular Momentum in Quantum Mechanics.

C.C. LIN and J.D. SWALEN, Rev. Mod. Phys. 31, 841 (1959). — Internal rotation.

S. GOLDEN and E.B. WILSON, J. Chem. Phys. 16, 669 (1948). — Stark effect - asymmetric rotor.

2 R.D. BROWN, Aust. Sc. Teachers J. 21, 53 (1975). — Origin of life.

R.D. BROWN, Interdisciplinary Sc. Rev. 2, 124, (1977). — Interstellar molecules - origin of life.

3 M. KAUFMAN, Ap. J., 232, 707 (1979). — Star formation - galactic evolution.

J.H. HUNTER, Ap. J. 233, 946 (1979). — Velocity fields - star formation.

F.N. BASH, Ap. J. 233, 524 (1979). — Density wave - star formation.

B.G. ELMEGREEN and J.M. MORAN, Ap. J. 227, L 93 (1979). — Shock - star formation.

H.A. THRONSON, P.M. HARVEY and I. GATLEY, Ap. J. 229, L133 (1979). — Front - star formation.

CHAPTER 1

1 C.K. JOHNSON, (1965). ORNL-3794. Oak Ridge Nat. Lab. — ORTEP program.

Oak Ridge Tennessee.

2 R.H. SCHWENDEMAN, J. Mol. Spectrosc. 7, 280 (1961). — Direction cosines - Wang basis.

3 W.H. KIRCHOFF, J. Mol. Spectrosc. 41, 333 (1972). — Centrifugal distorsion constants.

4 J.M. HOLLIS, Computer division internal report no. 18 NRAO — Kitt-Peak - 36 Ft telescope manual.

Tucson Arizona, Oct. (1976).

5 W.G. COCHRAN, Annals of Eugenics 11, 47 (1941). — Largest of a set of variances.

CHAPTER 2

1 H. BRACONNOT, Ann. Chim. et Phys. 2, 13, 113 (1820). — Sucre de gélatine.

2 E.N. HOSFORD, Ann. Chem. Pharm. 60, 1 (1846). — Glycocoll - (leimzücker).

3 J. BERZELIUS, Fortschr. Chem. Mineral. 27, 654 (1848). — Glycine.

4 J.P. GREENSTEIN and M. WINITZ, — Chemistry of The Amino Acids.

J. Wiley & Sons, Inc., Vol. 2, chap. 10 (1961).

5 R. OSTWALD, P.T. ADAMS and B.M. TOLBERT, — Glycine sublimation.

J. Am. Chem. Soc. 74, 2425 (1952).

6 C.-O. ANDERSSON, Acta Chem. Scand. 12, 1353 (1958). — Amino acids - mass spectra.

7 K. BIEMANN, J. SEIBL and F. GAPP, J. Am. Chem. Soc. 83, 3795 (1961). — Ethylesters of amino acids - mass spectra.

8 D. GROSS and G. GRODSKY, J. Am. Chem. Soc. 77, 1678 (1955). — Amino acids - sublimation.

9 G. JUNK and H. SVEC, J. Am. Chem. Soc. 85, 839 (1963). — α-Amino acids - mass spectra.

10 K. BIEMANN and J.A. McCLOSKEY, J. Am. Chem. Soc. 84, 3192 (1962). — Amino acids - mass spectra.

11	G.W. MILNE, T. AXENROD and H.M. FALES J. Am. Chem. Soc. 92, 5170 (1970).	Amino acids - CI mass spectra.
12	P.A. LECLERCQ and D.M. DESIDERIO, Org. Mass Spectrom. 7, 515 (1972).	Amino acids - CI mass spectra.
13	S. TAKAGI, H. CHIHARA and S. SEKI, Bull. Chem. Soc. Japan 32, 84 (1959).	Glycine - vapour pressure.
14	H.J. SVEC and D.D. CLYDE, J. Chem. Eng. Data 10, 151 (1965).	α-Amino acids - vapour pressure.
15	J. STOREY, Ph.D. thesis, Monash (1976).	
16	R.E. MARSH, Acta Cryst. 11, 654 (1958).	α-Glycine - X-ray diffraction.
17	J. ALMLÖF, Å. KVICK and J.O. THOMAS, J. Chem. Phys. 59, 3901 (1973).	α-Glycine - electron density.
18	P.G. JÖNSSON and Å. KVICK, Acta Cryst. B28, 1827 (1972).	α-Glycine - neutron diffraction.
19	A. IMAMURA, H. FUJITA and C. NAGATA, Bull. Chem. Soc. Japan 42, 3118 (1969).	Glycine - CNDO.
20	W.R. OEGERLE and J.R. SABIN, J. Mol. Struct. 15, 131 (1973).	Glycine - CNDO.
21	K. CHUNG, R.M. HEDGES, R.D. McFARLANE, J. Am. Chem. Soc. 98, 7523 (1976),	Glycine protonation - INDO.
22	Y. GRENIE, J.C. LASSEGUES and C.G. LAGRANGE, J. Chem. Phys. 53, 2980 (1970).	Matrix isolated glycine - IR.
23	Y. GRENIE and C. GARRIGOU-LAGRANGE, J. Mol. Spectrosc. 41, 240 (1972).	Matrix isolated glycine - IR.
24	S. VISHVESHWARA and J.A. POPLE, J. Am. Chem. Soc. 99, 2422 (1977).	Glycine - ab initio.
25	K-M. MARSTOKK and H. MØLLENDAL, J. Mol. Struct. 18, 247 (1973).	Methoxyacetic acid - microwave spectrum.
26	I. CHRISTIANSEN, K-M. MARSTOKK and H. MØLLENDAL, J. Mol. Struct. 30, 137 (1976).	Glyoxylic acid - microwave spectrum.
27	C.E. DYLLICK-BRENZINGER, A. BAUDER and Hs. H. GÜNTHARD, Chem. Phys. 23, 195 (1977).	Pyruvic acid - microwave spectrum.
28	Z. NÁHLOVSKÁ, B. NÁHLOVSKÝ and T.G. STRAND, Acta Chem. Scand.24, 2617 (1970).	Oxalic acid - electron diffraction - IR.
29	K. BOLTON, D.G. LISTER, and J. SHERIDAN, J. Chem. Soc. Faraday. Trans. II 70, 113 (1974).	Acrylic acid - microwave spectrum.
30	O.L. STIEFVATER, J. Chem. Phys. 62, 233 (1975).	Cis-propionic acid - microwave spectrum.
31	R.E. PENN and R.F. CURL, JR., J. Chem. Phys. 55, 651 (1971).	2-Aminoethanol - microwave spectrum.
32	D.R. LIDE, J. Chem. Phys. 27, 343 (1957). K. TAKAGI, J. Phys. Soc. Japan 30, 1145 (1971).	Methylamine - microwave spectrum. Methylamine - microwave spectrum.
33	J.A. POPLE and D.L. BEVERIDGE, McGraw-Hill (1970).	Approximate Molecular Orbital Theory.
34	W. GORDY and R.L. COOK, see Introduction [1], p 55.	Fractional populations.
35	C.H. TOWNES and A.L. SCHAWLOW, see Introduction [1], p 86.	Asymmetric top - symmetric top energy levels.
36	D. WOLF, Proceedings of the fifth international conference on noise, Bad Nauheim, Fed. Rep. of Germany, March 13-16 (1978).	Noise in Physical Systems.
37	A. NARATH and W.D. GWINN, Rev. Sci. Instr. 33, 79 (1962). H.M. PICKETT, Rev. Sci. Instr. 48, 706 (1977). P.S. HENRY, Rev. Sci. Instr. 47, 1020 (1976).	Phase stabilized klystron. Locking mm-klystrons with a digitial phase-frequency detector. Frequency-agile mm-wave phase lock system.

38	F.K. MANASSE, Prentice-Hall, (1977).	Semiconductor Electronics Design.
	M.J. HOWES and D.V. MORGAN ed. Wiley-Interscience (1978).	Variable Impedance Devices.
39	A.F. HARVEY, Academic Press, (1963).	Microwave Engineering.
40	G.W. MOREY, Am. Chem. Soc. Monograph Series (1938).	The Properties of Glass.
41	J. STRONG, Prentice Hall (1938).	Procedures in Experimental Physics.
42	Ref. [40], p 269.	Deritrification of glass.
43	R.W. LANDEE, D.C. DAVIS and A.P. ALBRECHT ed. p 3-23, (1977).	Electronic's Designers Handbook - mica.
44	R.A. DUGDALE, Mills and Boon (1971).	Glow Discharge Material Processing.
	G.F. WESTON, London Iliffe books (1968).	Cold Cathode. Glow Discharge Tubes.
45	R.D. SUENRAM and F.J. LOVAS, J. Mol. Spectrosc. 72, 372 (1978).	Glycine - millimeter wave spectrum.
46	A.S. ESBITT and E.B. WILSON JR, Rev. Sci. Instr. 34, 901 (1963).	Intensity measurements in microwave spectroscopy.
47	T. OKA and Y. MORINO, J. Mol. Spectrosc. 6, 472 (1961).	Inertia defect.
	T. OKA and Y. MORINO, J. Mol. Spectrosc. 11, 349 (1963).	Inertia defect - planarity.
48	D.R. HERSHBACH and V.W. LAURIE, J. Chem. Phys. 40, 3142 (1964).	Influence of vibrations on molecular structure - inertia defect.
49	K.M. MARSTOKK and H. MØLLENDAL, J. Mol. Struct. 15, 137 (1973).	Glyoxylic acid - microwave spectrum.
50	B.P. VAN EIJCK, A.A.J. MAAGDENBERG and J. WANROOY, J. Mol. Struct. 22, 61 (1974).	Chloroacetic acid.
51	K.R. LINDFORS and L.D. CORNWELL, J. Chem. Phys. 42, 149 (1965).	Rate of growth technique - dipole moment.
52	H.L. SELLERS and L. SCHAEFFER, J. Am. Chem. Soc. 100, 7728 (1978).	Glycine - ab initio.
53	G.R. GUNTHER-MOHR, R.L. WHITE and A.L. SCHAWLOW, Phys. Rev. 94, 1184 (1954).	NH_3 - hyperfine structure.
54	S. DUSHMAN - (J.M. LAFFERTY ed.) p 80. John Wiley & Sons, Inc., 1962.	Scientific Foundations of Vacuum Technique. Flow of gases through tubes and orifices.
55	W.L. BARROW, Proc. IRE 27, 41 (1939).	Sectoral electromagnetic horn.
	W.L. BARROW and L.J. CHU, Proc. IRE 27, 51 (1939).	Electromagnetic horn - theory.
	A.R.G. OWEN and L.G. REYNOLDS, IEE. J. 93, 1528 (1946).	Radiation pattern of small horns - effect of flanges.
56	R. WERTHEIMER, B. MACKE and G. SEGARD, Laboratoire de Spectroscopie hertzienne Université des Sciences et Techniques Villeneuve d'Ascq. France.	Electroforming process.
57	A.T. VAGRAMYAN and Z.A. SOLOV'EVA, R. Draper Ltd. (1961).	Technology of Electrodeposition.
	F.A. LOWENHEIM ed. J. Wiley and Sons, (1942, 1974).	Modern Electroplating.
58	P. PALLA, C. PETRONGOLO and J. TOMASI, J. Phys. Chem. 84, 435 (1980).	Glycine - conformational maps.

CHAPTER 3

1 M. BALISTER, R.A. BATCHELOR, R.F. HAYNES, S.H. KNOWLES, M.G. McCULLOCH, B.J. ROBINSON, K.J. WELLINGTON and D.E. YASBLEY Mon. Not. R. astr. Soc. 180, 415 (1977). — Parkes - 16.7 m reflecting surface - SiO masers at 43 GHz.

2 M. BALISTER and R.A. BATCHELOR, IREE (Australian) Conv. Digest, p 276 (1975). — International Electronics Convention. Parkes - cooled mixer receiver.

3 J.G. ABLES, B.F.C. COOPER, A.J. HUNT, G.G. MORREY and J.W. BROOKS, Rev. Sci. Instr. 46, 284 (1975). — A 1024-channel digital correlator.

4 T.W. COLE, Optica Acta 22, 2, 83 (1975). — Electro-optical processing in radio astronomy.

T.W. COLE and D.K. MILNE, Proc. Astron. Soc. Australia 3, 108 (1977). — Acousto-optical spectrograph.

5 J. BLUM, C.R. Acad. Sci. Paris 250, 3279 (1960). — Mesures spectrales en radio astronomie.

M. BORN and E. WOLF, Pergamon Press, p 499 (1964). — Principles of Optics. Correlation functions of light beams.

6 J.W. GOODMAN, McGraw-Hill, Phys. and Quantum Electronics series chap. 5, 6, (1968). — Introduction to Fourier Optics.

7 P. DEBYE and F.W. SEARS, Proc. Nat. Acad. Sci. U.S.A. 18, 413 (1932). — Scattering of light by supersonic waves.

L. LAMBERT, IRE Natn. Conv. Rec. 10, 6, 69 (1962). — Instantaneous spectrum analyzers.

L.B. LAMBERT, A. MOSES and A.AIMETTE, M.I.T. Press, p 715 (1965). — Optical and Electro-Optical Information Processing.

K. PRESTON, McGraw-Hill (1972). — Coherent Optical Computers.

8 B.J. ROBINSON, Proc. IRE. Australia 119 (1963). — Parametric amplifiers.

C.L. CUCCIA, Academic Press N.Y. vol. 7 (1973). — Advances in Microwaves - ultra low noise parametric amplifiers.

J.C. DECROLY, L. LAURENT, J.C. LIENARD, G. MARECHAL, and J. VOROBEITCHIK, Philips Technical Library, The Macmillan Press (1973). — Parametric amplifiers.

A.J. CROFT, Plenum Press (1970). — Cryogenic Laboratory Equipment

H.A. WATSON, McGraw-Hill (1969). — Microwave Semi conductor Devices and Their Circuit Applications - mixers.

Y. ANAND and W.J. MORONEY, Proc. IEEE 59, 1182 (1971). — Microwave mixer and detector diodes.

S. WEINREB and A.R. KERR, IEEE J. Solid-State Circuits, Sc-8, 58 (1973). — Mixers - cryogenic cooling.

M.J. HOWES and D.V. MORGAN ed. John Wiley & Sons (1976). — Microwave Devices.

S. WEINREB, Tech. Rep. 412, Res. Lab. Electronics, M.I.T., Cambridge. — One-bit correlator.

B.F.C. COOPER, Australian J. Phys. 23, 521 (1970). — Correlators - two-bit quantization.

P. FOLDES (K. ENDRESSEN, ed.), Pergamon Press, p 319 (1962). — Low Noise Electronics - Cassegrain microwave optics.

A.A. PENZIAS and C.A. BURRUS, Ann. Rev. Astron. Astrophys. 11, 51 (1973). — mm - Wave Radio Astronomy Techniques.

E.E. REBER, R.L. MITCHELL and C.J. CARTER, IEEE Trans. Antennas and Propagation 18, 472 (1970). — Atmospheric attenuation - 48-72 GHz.

F.I. SHIMABUKURO and E.E. EPSTEIN, IEEE Trans. Antennas and Propagation 18, 485 (1970). — Atmospheric attenuation - 3 mm.

9	D. BUHL and L.E. SNYDER, Nature Phys. Sci. 232, 161 (1971).	Microwave receivers - Kitt Peak.
	A.R. KERR, IEEE Trans. Microwave Theory Techn. MTT-23, 781 (1975).	Low-noise mixers - Kitt Peak 80-120 GHz.
	D.N. HELD and A.R. KERR, IEEE Trans. Microwave Theory Techn. MTT-26, 49 (1978).	Mixers - noise.
10	P.G. WANNIER, J.A. ARNAUD, F.A. PELOW and A.A.M. SALEH, Rev. Sci. Instr. 47, 56 (1976).	Fabry-Perot rejection filter - 100 GHz.
11	O.E.H. RYDBECK, A. SUME, Å.G. HJALMARSON, J. ELLDÉR, B.O. RÖNNÄNG and E. KOLLBERG, Res. Rept. No. 128, Res. Lab. Electronics, Chalmers Univ. Tech., Gothenburg (1977).	20 m, mm-Wave telescope equipped with a traveling wave maser.
	D.H. MENZEL, Sky and Telesc. 52, 240 (1976).	20 m, mm-Dish - Onsala.
12	E.L. KOLLBERG and P.T. LEWIN, IEEE Trans. Microwave Theory Techn. MTT-24, 718 (1976).	Traveling-wave masers - 20-40 GHz.
13	J. WEBER (compiler), Gordon & Breach, 9 (1967).	Masers - collection of reprints.
14	J.D. KRAUS, McGraw-Hill, p 450 (1966).	Radio Astronomy - HPBW.
15	N. FOURIKIS, K. TAKAGI and M. MORIMOTO, Ap. J. 191, L139 (1974).	Interstellar methylamine.
16	N. KAIFU, M. MORIMOTO, K. NAGANE, K. AKABANE, T. IGUCHI and K. TAKAGI, Ap. J. 191, L135 (1974).	Interstellar methylamine.
17	B.E. TURNER, A.G. KISLYAKOV, H.S. LISZT and N. KAIFU, Ap. J. 201, L149 (1975).	Interstellar cyanamide.
18	P.M. SOLOMON, K.B. JEFFERTS, A.A. PENZIAS and R.W. WILSON, Ap. J. 168, L107 (1971).	Interstellar methyl cyanide.
19	D.R. JOHNSON, F.J. LOVAS, C.A. GOTTLIEB, E.W. GOTTLIEB, M.M. LITVAK, M. GUELIN and P. THADDEUS, Ap. J. 218, 370 (1977).	Interstellar ethyl cyanide.
20	B. ZUCKERMAN, B.E. TURNER, D.R. JOHNSON, F.O. CLARK, F.J. LOVAS, N. FOURIKIS, P. PALMER and M. MORRIS, Ap. J. 196, L99 (1975).	Interstellar trans-ethyl alcohol.
21	A.T. SOLDATENKOV and I.A. SYTINSKII, Russian Chem. Rev. 45 (2), 168 (1976).	Prebiotic amino acids - meteorites, lunar rocks.
22	J. ORO and H.B. SKEWES, Nature 207, 1042 (1965).	Amino acids contamination - human fingers.
	K. HARADA, P.E. HARE, C.R. WINDSOR and S.W. FOX, Science 173, 433 (1971).	Amino acids - Apollo 11 and 12 lunar fines.
23	J.L. BADA, J. Am. Chem. Soc. 94, 1371 (1972).	Amino acids racemization as a function of pH.
	R.A. SCHROEDER and J.L. BADA, Science 182, 479 (1973).	Aspartic acid racemization in fossil bones - glacial - post glacial temperature.
	F.B. REED, J. Theoret. Biol. 39, 683 (1973).	Racemization.
24	A. MEISTER, Academic Press, Vol. 1, p 57 (1965).	Biochemistry of The Amino Acids.
25	B. MASON, Space Sci. Rev. 1, 621 (1962).	Carbonaceous chondrites.
26	a: K. KVENVOLDEN, J. LAWLESS, K. PERING, E. PETERSON, J. FLORES, C. PONNAMPERUMA, I.R. KAPLAN and C.B. MOORE, Nature 228, 923 (1970).	Murchison meteorite - amino acids, hydrocarbons.
	b: K. KVENVOLDEN, J. LAWLESS and C. PONNAMPERUMA, Proc. Nat. Acad. Sci. U.S.A. 68, 486 (1971).	Murchison meteorite - non-protein amino acids.
	c: J.R. CRONIN and C.B. MOORE, Science 172, 1327 (1971).	Murchison meteorite - amino acids.
	J. ORÓ, J. GIBERT, H. LICHTENSTEIN, S. WIKSTROM and D.A. FLOREY, Nature 230, 105 (1971).	Murchison meteorite - amino acids.

27 S.W. FOX and K. HARADA, Proc. IVth Lunar Sci. Conf. Geochim. Cosmochim. Acta, Suppl. 4, 2, 2241 (1973).

28 D. RING, Y. WOLMAN, N. FRIEDMANN and S.L. MILLER, Proc. Nat. Acad. Sci. U.S.A. 69, 3, 765 (1972).
Y. WOLMAN, W.J. HAVERLAND and S.L. MILLER, Proc. Nat. Acad. Sci. U.S.A. 69, 4, 809 (1972).

29 S.L. MILLER, J. Am. Chem. Soc. 77, 2351 (1955).

30 E. ANDERS, R. HAYATSU and M.H. STUDIER, Science 182, 781 (1973).
S.L. MILLER, H.C. UREY and J. ORÓ, J. Mol. Evol. 9, 59 (1976).

31 J.W. LARIMER, Geochim. Cosmochim. Acta 31, 1215 (1967).
L. GROSSMAN, Geochim. Cosmochim. Acta 36, 597 (1972).
A.H. DELSEMME ed., Univ. Toledo, Toledo, Ohio (1977).

32 F.J. LOVAS, L.E. SNYDER and D.R. JOHNSON, Ap. J. Suppl. 41, 451 (1979).

33 E. HERBST and W. KLEMPERER, Ap. J. 185, 505 (1973).

P.A. AANNESTAD, Ap. J. Suppl. 25, 205 (1973).

M.D. WATSON and E.E. SALPETER, Ap. J. 174, 321 (1972).
M. ALLEN and G.W. ROBINSON, Ap. J. 212, 396 (1977).
S.S. PRASAD and W.T. HUNTRESS, Ap. J. Suppl. 42, (3) (1980).
D. HOLLENBACH and C.F. McKEE, Ap. J. Suppl. 41, 555 (1979).

E. IGLESIAS, Ap. J. 218, 697 (1977).
G.F. MITCHELL, J.L. GINSBURG and P.J. KVNTZ, Ap. J. Suppl. 38, 39 (1978).

34 M.H. BRIGGS and G. MAMIKUNIAN, Space Sci. Rev. 1, 647 (1962).

35 C.W. GEHRKE, R.W. ZUNWALT, K.C. KUO, C. PONNAMPERUMA, C.N. CHENG and A. SHIMOYAMA, Proc. IV Lunar Sci. Conf., Suppl. 4, Geochim. Cosmochim. Acta 2, 2249 (1973).

36 I.I. ERU, S.A. PESKOVATSKIY and A.N. CHERNETS, IEEE J. Quantum Electronics QE-4, 723 (1968).

37 A.G. CARDIASMENOS, J.F. SHANLEY and K.S. YNGVESSON, IEEE Trans. Microwave Theory Techn. MTT-24, 725 (1976).

38 P.L. RICHARDS, T.M. SHEN, R.E. HARRIS and F.L. LLOYD, Appl. Phys. Lett. 34, 345 (1979).
T.M. SHEN, P.L. RICHARDS, R.E. HARRIS and F.L. LLOYD, to be published.

Amino acids precursors - lunar samples.

Hydrophobic and protein amino acids - prebiotic synthesis.
Non-protein amino acids - spark discharges, Murchison meteorite.
Organic compounds - primitive earth conditions.
Organic compounds - meteorites.
Organic compounds - primitive earth, meteorites.
Chemical fractionations in meteorites.
Condensation in the primitive nebula.
Comets, Asteroids, Meteorites: Interrelations, Evolution and Origins.
Interstellar molecules - rest frequencies.
Molecule formation - dense interstellar clouds.
Molecule formation - normal HI clouds, interstellar shock waves.
Molecule formation - interstellar grains.
Molecules - dense interstellar clouds.
Gas phase chemistry - interstellar clouds.
Molecule formation, IR emission - fast interstellar shocks.
Chemical evolution - molecular clouds.
Molecules - interstellar clouds - steady state.
Carbonaceous chondrites.
Organic compounds - Apollo 15 and 16 lunar fines.

Microwave crystal - c-2-trivalent - iron-dopped andalusite.
Traveling-wave maser - 85-90 GHz.

SIS tunnel junctions.

mm-Wave quasiparticle heterodyne mixers - conversion gain.

39 E.R. CAPRIOTTI, Perkins observatory - Ohio - p 1101-1119 (1965). Mean escape probabilities of line photons - numerical methods.

J.T. JEFFERIES, Blaisdell Publ. (1968). Spectral Line Formation.

R.G. ATHAY, Reidel-Boston (1972). Radiation Transport in Spectral Lines.

M.M. LITVAK (ed. T.R. CARSON and M.J. ROBERTS) Academic Press - London p 201 (1972). Atoms and Molecules in Astrophysics - non-equilibrium processes in interstellar molecules.

N. PANAGIA and M. RANIERI, Astron. & Astrophys. 24, 219 (1973). Radiative transfer - Monte-Carlo techniques.

N.Z. SCOVILLE and P.M. SOLOMON, Ap. J. (Letters), 187, L67 (1974). Radiative transfer - CO, CS. large flow velocities.

P. GOLDREICH and J. KWAN, Ap. J. 189, 441 (1974). Collapsing molecular clouds.

H.S. LISZT, R.W. WILSON, A.A. PENZIAS, K.B. JEFFERTS, P.G. WANNIER and P.M. SOLOMON, Ap. J. 190, 557 (1974). CO, CS. Ori A - systematic radial velocity.

B. ZUCKERMAN and N.J. EVANS, Ap. J. (Letters), 192, L149 (1974). Local motions in molecular clouds.

J. ARONS and C.E. MAX, Ap. J. (Letters), 196, L77 (1975). Hydromagnetic waves - CO.

T. de JONG, S.I. SHU and A. DALGARNO, Ap. J. 199, 69 (1975). CO in collapsing clouds.

D.C. BLACK and P. BODENHEIMER, Ap. J. 199, 619 (1975). Radiative transfer - numerical procedure.

A.S. MILMAN, G.R. KNAPP, S.L. KNAPP and W.J. WILSON, Astron. J., 80, 101, (1975). CO in 34 dust clouds.

M.M. LITVAK, Ap. J. 202, 58 (1975). Radiative transfer - molecular alignment

R. ATHAY, Ap. J. 204, 160 (1976). Probabilistic radiative transfer.

C.A. HARVEL, Ap. J. 210, 862 (1976). Radiative transfer - numerical procedure.

R. LUCAS, Astron. & Astrophys. 46, 473 (1976). Line formation - turbulent clouds with small velocity gradient - CO.

R.E. WHITE, Ap. J. 211, 744 (1977). Line formation - microturbulence, systematic motions.

F. MARTI and P.D. NOERDLINGER, Ap. J. 215, 247 (1977). Radiative transfer - decelerating spherical flow.

L.H. AUER, J.N. HEASLEY and L.L. HOUSE, Ap. J. 216, 531 (1977). Radiative transfer - statistical equilibrium - magnetic field.

C. HUNTER, Ap. J. 218, 834 (1977). Collapsing spheres - numerical studies.

S. DEGUCHI and Y. FUKUI, Publ. Astron. Soc. Japan 29, 683 (1977). Radiative transfer - collapsing clouds.

T.B.H. KUIPER, E.N. RODRIGUEZ, KUIPER and B. ZUCKERMAN, Ap. J. 219, 129 (1978). Line shapes - spherically symmetric radially moving clouds.

P.F. GOLDSMITH and W.D. LANGER, Ap. J. 222, 881 (1978). Radiative transfer - molecular cooling.

C.M. LEUNG, Ap. J. 225, 427 (1978). Radiative transfer - line formation.

40 J.I. CASTOR, Mon. Not. R. Astr. Soc. 149, 111 (1970). Line formation - escape probability.

1	R.M. LEES, F.J. LOVAS, W.H. KIRCHOFF and D.R. JOHNSON, J. Phys. Chem. Ref. Data 2, 205 (1973).	CH_3OH - microwave spectrum.
2	R.M. LEES, Ap. J. 184, 763 (1973).	CH_3OH - E-energy levels.
3	M.L. KUTNER, P. THADDEUS, A.A. PENZIAS, R.W. WILSON and K.B. JEFFERTS, Ap. J. 183, L27 (1973).	Interstellar CH_3OH ($J = 3 \rightarrow 2$).
4	L. GAINES, K.H. CASLETON and S.G. KUKOLICH, Ap. J. (Letters) 191, L99 (1974).	CH_3OH - beam maser frequency measurements.
5	A.H. BARRETT, P. HO and R.N. MARTIN, Ap. J. 198, L119 (1975).	CH_3OH maser (1.2 cm) - Ori A.
6	A.H. BARRETT, P.R. SCHWARTZ and J.W. WATERS, Ap. J. 168, L101 (1971).	CH_3OH (1.2 cm) - Ori A.
	M.F. CHUI, A.C. CHEUNG, D. MATSAKIS and C.H. TOWNES, Ap. J. (Letters) 187, L19 (1974).	CH_3OH (1.2 cm) - Ori A.
7	R. HILLS, V. PANKONIN and T.L. LANDECKER, Astron. Astrophys. 39, 149 (1975).	CH_3OH (1.2 cm) - Ori A.
8	R.W. WILSON, A.A. PENZIAS, K.B. JEFFERTS, P. THADDEUS and M.L. KUTNER, Ap. J. 176, L77 (1972).	Interstellar ^{15}N and U169.3.
9	D.E. JENNINGS and K. FOX, Ap. J. 227, 433 (1979).	CH_3OH - Ori A.
10	C.A. GOTTLIEB, J.A. BALL, E.W. GOTTLIEB and D.F. DICKINSON, Ap. J. 227, 422 (1979).	Interstellar CH_3OH ($J = 2 \rightarrow 1$).
11	J.M. HOLLIS and B.L. ULICH, Ap. J. 214, 699 (1977).	Interstellar H, OCS, H_2CO, CH_3OH (1_0-0_0 E, A^+).
12	F.J. LOVAS, D.R. JOHNSON, D. DUHL and E.L. SNYDER, Ap. J. 209, 770 (1976).	mm - Emission lines - Ori A.
13	A.H. BARRETT, J.M. BOLOGNA, A.C. CHEUNG, M.F. CHUI, P.T.P. HO, K.J. JOHNSTON, R.N. MARTIN, D. MATSAKIS, J.M. MORAN and P.R. SCHWARTZ, Ap. Letters 18, 13 (1976).	CH_3OH (1.2 cm) - Ori A.
14	G.H. RIEKE, F.J. LOW, D.E. KLEINMANN, Ap. J. 186, L7 (1973).	KLEINMANN - LOW nebula - map.
15	J.A. BALL, C.A. GOTTLIEB and A.E. LILLEY, Ap. J. 162, L203 (1970).	CH_3OH (834 MHz) - Sgr A, B2.
16	B. ZUCKERMANN, B.E. TURNER, D.R. JOHNSON, P. PALMER and M. MORRIS, Ap. J. 177, 601 (1972).	CH_3OH ($5_{-1} \rightarrow 4_0$ E) - Sgr B2.
17	B.E. TURNER and M.A. GORDON, Ap. J. 177, 609 (1972).	CH_3OH ($4_{-1} \rightarrow 3_0$ E) - Sgr B2.
18	B.J. ROBINSON, J.W. BROOKS, P.D. GODFREY and R.D. BROWN, Aust. J. Phys. 27, 865 (1974).	CH_3OH (3_1-3_1 A) - Sgr B2.
19	A.H. BARRETT, R.N. MARTIN and P.C. MYERS, Ap. J. 178, L23 (1972).	CH_3OH (48 GHz) - Sgr A, B2.
20	M.M. LITVAK, ed. M.A. GORDON, L.E. SNYDER, J. Wiley & Sons, p. 282 (1973).	Molecules in the Galactic Environment - masers - optical pumping.
21	A.A. PENZIAS, K.B. JEFFERTS and R.W. WILSON, Ap. J. 165, 229 (1971).	Interstellar CO.
22	M. MORRIS, B. TUCKERMAN, P. PALMER and B.E. TURNER, Ap. J. 186, 501 (1973).	Interstellar NH_3.
23	B.E. TURNER, Ap. J. 193, L83 (1974).	U 93.174 - N_2H^+.
24	B.E. TURNER, B. ZUCKERMAN, P. PALMER and M. MORRIS, Ap. J. 186, 123 (1973).	Intetstellar CS.
25	L.E. SNYDER and D. BUHL, Ap. J. 163, L47 (1971).	Interstellar HCN.
26	L.E. SNYDER, J.M. HOLLIS, B.L. ULICH, F.J. LOVAS, D.R. JOHNSON and D. BUHL, Ap. J. 198, L81 (1975).	Interstellar SO_2.

27 E.E. BECKLIN and G. NEUGEBAUER, ed. Y. Terzian - W.A. Benjamin Inc., Amsterdam. p 1 (1968). — Interstellar Ionized Hydrogen - protostars, IR.

28 E. RAIMOND and B. ELIASSON, Ap. J. 155, 817 (1969). — OH sources - interferometry.

29 J.M. MORAN, G.D. PAPADOPOULOS, B.F. BURKE, K.Y. LO, P.R. SCHWARTZ, D.T. THACKER, K.J. JOHNSTON, S.H. KNOWLES, A.C. REISZ and I.I. SHAPIRO, Ap. J. 185, 535 (1973). — H_2O sources - VLBI.

30 R. HILLS, M.A. JANSSEN, D.D. THORNTON, W.J. WELCH, Ap. J. 175, L59 (1972). — H_2O sources in HII regions.

31 W.J. WEBSTER and W.J. ALTENHOFF, Ap. Letters 5, 233 (1970). J.D. KRAUS, chapter 3, ref. [14]. — Ori A - map at 2.695 GHz. HPBW.

CHAPTER 5

1 A. BAUER and S. MAES, Journal de Physique 30, 169 (1969). — $CH_3C^{14}N$, $CH_3C^{15}N$ - etudes en ondes millimetriques.

2 A. BAUER, J. Mol. Spectrosc. 40, 183 (1971). — $CH_3C^{14}N$, $CH_3C^{15}N$ - microwave spectrum ($V_8 = 2$).

3 P.M. SOLOMON, K.B. JEFFERTS, A.A. PENZIAS, Ap. J. 168, L107 (1971). — CH_3CN ($J = 6 \rightarrow 5$, 2.7 mm) - Sgr B, Sgr A.

4 P.M. SOLOMON, A.A. PENZIAS, K.B. JEFFERTS, Ap. J. 185, L63 (1973). — CH_3CN ($J = 6 \rightarrow 5$, 2.7 mm) - Sgr B2

5 B.L. ULICH, E.K. CONKLIN, Nature 248, 121 (1974). — CH_3CN ($J = 6 \rightarrow 5$), $V_8 = 1$) - comet Kohoutek.

6 W.F. HUEBNER, D. BUHL, L.E. SNYDER, Astron. J. 81, 671 (1976). — CH_3CN - comet Kohoutek.

7 F.O. CLARK, R.D. BROWN, P.D. GODFREY, J.W.V. STOREY and D.R. JOHNSON, Ap. J. 210, L139 (1976). — HC_3N ($v_7 = 1$) - CH_3CN ($v_8 = 1$) - Orion.

8 G.L. BLACKMAN, R.D. BROWN, P.D. GODFREY, M.P. BASSEZ, A.L. OTTREY, D. WINKLER and B.J. ROBINSON, Mon. Not. R. astr. Soc. 180, 1 (1977). — CH_3CN ($J = 2 \rightarrow 1$) - Sgr B2.

9 F.J. LOVAS, D.R. JOHNSON, D. BUHL and L.E. SNYDER, Ap. J. 209, 770 (1976). — mm-Emission lines - Ori A.

10 F.J. LOCKMAN and R.L. BROWN, Ap. J. 201, 134 (1975). — Radio recombination lines - Ori A.

11 D. HOANG-BINH, Ap. Letters 6, 151 (1970). — Radio recombination lines from galactic nebulae.

R.M. HJELLMING and M.A. GORDON, Ap. J. 164, 47 (1971). — Radio recombination lines - non-LTE theory.

E.B. WALTMAN and K.J. JOHNSTON, Ap. J. 182, 489 (1973). W.B. WALTMAN, E.B. WALTMAN, P.R. SCHWARTZ, K.J. JOHNSTON and W.J. WILSON, Ap. J. 185, L135 (1973). — H66α recombination line. H42α - Ori A.

F.J. LOCKMAN and R.L. BROWN, Ap. J. 207, 436 (1976). — Radio recombination lines - nebular electron temperatures.

J.K. HILL, Ap. J. 212, 692 (1977). — Radio recombination lines from ionization fronts.

E.J. CHAISSON and M.A. DOPITA, Astron. Astrophys. 56, 385 (1977). — Orion nebula - radio and optical domains.

12 Y. FUKUI, T. IGUCHI, Publ. Ast. Soc. Japan 29, 63 (1977). — M17, Ori A - radio brightness at 3.5 mm.

13 E.N.R. KUIPER, T.B.H. KUIPER, B. ZUCKERMAN and R.K. KAFAR, Ap. J. 214, 394 (1977). — H42α - Ori A.

14 C. GOUDIS, Ap. Sp. Sci. 36, 105 (1975). — Orion nebula - radio spectrum.

15 J.D. KRAUS, chap. 3, ref 14, p 99. — Flux density.

16 C.H. TOWNES et al., chapter 1, ref. 1, p. 75 (1975). — Statistical weights.

17 Y. BEERS and T.W. RUSSELL, IEEE Trans. on Instrumentation and Measurement IM-15, 380 (1966). — CH_3CN - dipole moment.

18 G. HERZBERG, D. Van Nostrand - Vol III, p 631 (1967). — Molecular Spectra and Molecular Structure - molecular constants.

19 C.H. TOWNES et al., chapter 1, ref 1, p 501 (1975). — Intensities of hyperfine transitions.

20 G.H. RIEKE et al., chapter 4, ref. 14. — Kleinmann-Low nebula - 21 μ.

21 B. ZUCKERMAN, T.B.H. KUIPER and E.N. RODRIGUEZ KUIPER, Ap. J. 209, L137 (1976). — Interstellar CO - Orion.

22 P. THADDEUS, M.L. KUTNER, A.A. PENZIAS, R.W. WILSON and K.B. JEFFERTS, Ap. J. 176, L73 (1972). — Interstellar H_2S.

23 C.A. GOTTLIEB and J.A. BALL, Ap. J. 184, L59 (1973). F.O. CLARK and D.R. JOHNSON, Ap. J. 191, L87 (1974). — Interstellar SO - Interstellar SO - Ori A.

24 L.E. SNYDER, J.M. HOLLIS, B.L. ULICH, F.J. LOVAS, D.R. JOHNSON and D. BUHL, Ap. J. 198, L81 (1975). — Interstellar SO_2.

25 D.F. DICKINSON, C.A. GOTTLIEB, E.W. GOTTLIEB and M.M. LITVAK, Ap. J. 206, 79 (1976). — Interstellar SiO.

26 J. KWAN and N. SCOVILLE, Ap. J. 210, L39 (1976). — Interstellar CO - Orion.

27 N.J. EVANS, B. ZUCKERMAN, T. SATO and G. MORRIS, Ap. J. 199, 383 (1975). — Interstellar H_2CO - Orion.

28 B.E. TURNER, B. ZUCKERMAN, P. PALMER and M. MORRIS, Ap. J. 186, 123 (1973). — Interstellar CS.

29 B. ZUCKERMAN, P. PALMER, Ap. J. 199, L35 (1975). — Orion -

30 S. DEGUCHI, Y. NAKADA and T. ONAKA, Publ. Astron. Soc. Japan 31, 105 (1979). — HC_3N (ν_7) - Ori A.

31 J.D. KRAUS, chapter 3, ref. 14, p. 450. — HPBW.

CHAPTER 6

1 E.F. PEARSON, R.A. CRESWELL, M. WINNEWISSER and G. WINNEWISSER, Z. Naturforsch. 31a, 1394 (1976). — HCN, HNC and isotopic species - molecular structures.

R.L. SNELL and ALWYN WOOTTEN, Ap. J. 228, 748 (1979). — Interstellar HNC, DNC, $HN^{13}C$.

A.A. PENZIAS, Ap. J. 288, 430 (1979). — Interstellar HCN, HCO^+, DCN, DCO^+.

W.D. WATSON, L.E. SNYDER and J.M. HOLLIS, 222, L145 (1978). — Interstellar DCO^+/HCO^+.

B.E. TURNER and B. ZUCKERMAN, Ap. J. 225, L75 (1978). — Interstellar DCO^+, N_2D^+, DCN, DNC, HCO^+, N_2H^+, HCN, HNC.

M. GUELIN, W.D. LANGER, R.L. SNELL and H. ALWYN WOTTEN, Ap. J. 217, L165 (1977). — Interstellar DCO^+/HCO^+.

	R.D. BROWN, P.D. GODFREY, H.I. GUNN, G.L. BLACKMAN and J.W.V. STOREY, Mon. Not. R. astr. Soc. 180, 87p (1977).	Interstellar $H^{15}NC$.
2	W.J. LAFFERTY and F.J. LOVAS, J. Phys. Chem. Ref. data, 7, 441 (1978).	HC_3N - microwave spectrum.
3	A. SANDQVIST, Mon. Not. R. Astron. Soc. 177, 69 (1976).	Cometary globules - Gum nebula.
4	D.R. JOHNSON, F.J. LOVAS and W.H. KIRCHHOFF, J. Phys. Chem. Ref. data, 1, 1011 (1972).	H_2CO - H_2CS - microwave spectra.
5	G. WINNEWISSER, W.H. HOCKING and M.C.L. GERRY, J. Phys. Chem. Ref. data, 5, 79 (1976).	HNCO - microwave spectrum.
6	R.D. BROWN, P.D. GODFREY and D.W. WINKLER, Mon. Not. R. Astr. Soc. 190, 1 (1980).	Intetstellar SO.
7	G.L. BLACKMAN, R.D. BROWN, R.F.C. BROWN, F.W. EASTWOOD and G.L. McMULLEN, J. Mol. Spectrosc. 68, 488 (1977).	CH_2C_2O - microwave spectrum.
8	A. BAUDER, F.J. LOVAS and D.R. JOHNSON, J. Phys. Chem. Ref. data, 5, 53 (1976).	CH_3CHO - microwave spectrum.
9	R.A. BEAUDET and R.L. POYNTER, J. Phys. Chem. Ref. data, 7, 311 (1978) J. Phys. Chem. Ref. data, 7, 311 (1978).	OH - microwave spectrum.
10	W.D. LANGER, M.A. FRERKING, R.A. LINKE and R.W. WILSON, Ap. J. 232, L169 (1979).	Interstellar HDCO - $(2_{0,2} \rightarrow 1_{0,1})$.
11	D.A. WINKLER, Ph.D. thesis, Monash University (1979).	CH_2NH, HCN dimer - frequency measurements.

APPENDICES

1	G.L. VERSCHURR and K.I. KELLERMANN - (ed.) Springer-Verlag-Berlin - New York (1974).	Galactic and Extra-Galactic Radio Astronomy.
	M.L. MEEKS (ed.). Vol. 12, part B and C. Academic Press - New York (1976).	Methods of Experimental Physics - Astrophysics.
	J.D. KRAUS, McGraw Hill - New York (1966).	Radio Astronomy.
	R. BALIAN, P. ENCRENAZ and L. LEQUEUX (ed.) North-Holland Publ. Amsterdam/American Elsevier Publ. (1975).	Atomic and Molecular Physics and the Interstellar Matter.
2	C.H. TOWNES et al., introduction, ref [1], p. 74.	Dipole moment matrix elements.